THE UNIVERSITY OF CHICAGO

EXISTENCE, COEXISTENCE AND COLLAPSE OF MODEL ECOSYSTEMS: FROM PAIRWISE TO HIGHER-ORDER INTERACTIONS

A DISSERTATION SUBMITTED TO
THE FACULTY OF THE DIVISION OF THE BIOLOGICAL SCIENCES
AND THE PRITZKER SCHOOL OF MEDICINE
IN CANDIDACY FOR THE DEGREE OF
DOCTOR OF PHILOSOPHY

DEPARTMENT OF ECOLOGY AND EVOLUTION

BY
PABLO LECHÓN ALONSO

CHICAGO, ILLINOIS
DECEMBER 2026

© 2026 by Pablo Lechón Alonso

ORCID iD: https://orcid.org/0000-0003-2229-4778

ABSTRACT

Anyone who has walked through nature has witnessed its complexity. In order to understand it, ecologists build mathematical models, and have spent a century trading the realism of these models for their tractability. We model an ecosystem as a set of differential equations for the abundances of its species, whose per-capita growth rates are polynomials in the abundances: truncated at first order this is the generalized Lotka–Volterra model, and the higher-order terms are the higher-order interactions of ecological theory. The coefficients of these polynomials describe the species and their interactions, and we say that an ecosystem exists, or is feasible, when its coefficients are compatible with an equilibrium at which all species have positive abundance. At the core of this dissertation lies a simple question: can an ecological community exist? Rather than focusing on a specifically parametrized ecosystem, we draw the coefficients at random from a chosen probability distribution. Each draw is one ecosystem, and many draws reveal the typical behavior induced by the distribution: the baseline intuition for what to expect from these systems in the absence of particular mechanisms. The feasibility problem is an inverse problem that requires the equilibrium itself, and with higher-order interactions the equilibria are the roots of a polynomial system, which cannot be found in closed form. Each chapter slices the problem at a different level of complexity and makes it tractable with a different mathematical technique.

Chapter 1 keeps only pairwise interactions and asks whether self-regulation—intraspecific competition, the negative effect of each species on its own growth—guarantees existence as May showed it guarantees stability, a question with a lineage going back to the first responses to his work in 1974. Using the resolvent of random matrices, we derive the probability of feasibility as a function of self-regulation, diversity and the statistics of the interactions, and show that a critical level of self-regulation guarantees feasibility, universally but not sharply. For large systems, the transition to stability precedes the transition to feasibility

with probability one: feasible equilibria are stable, and dynamics converge to a globally stable equilibrium whether or not every species in the pool survives.

Chapter 2 lets the order of the interactions grow. Mapping the model onto the Kostlan–Shub–Smale ensemble of random polynomial systems, we count the expected number of feasible equilibria exactly, without having to explicitly solve for them. The probability of feasibility becomes a race between the number of real equilibria and the number of sign patterns among which they scatter; above interaction order four the former wins, and the probability of feasibility increases with diversity instead of vanishing as in the pairwise case. Feasibility emerges from nonlinearity alone, with no mechanism and no fine-tuning, provided the interactions are balanced on average, and it is then stability, not feasibility, that limits coexistence.

Chapter 3 combines the self-regulation of Chapter 1 with the higher-order interactions of Chapter 2, and follows a feasible, stable state as the environment changes. Tracking equilibria with polynomial homotopy continuation, we find that with higher-order interactions coexistence is typically lost abruptly, at a fold bifurcation where two equilibria collide and vanish, rather than through the familiar gradual extinction (corresponding to a transcritical bifurcation) of pairwise theory. Folds come to dominate the boundary of the coexistence domain as nonlinearity strengthens, and they arise as well in published nonlinear models of mutualistic, competitive and consumer–resource communities. At a fold, species collapse from finite abundance, so monitoring abundances cannot be expected to anticipate collapse.

The three chapters ask three questions about one object, the domain of parameters compatible with coexistence: whether a community falls inside it, how many feasible equilibria it holds, and what its boundary is made of.

TABLE OF CONTENTS

LIST OF FIGURES ix

LIST OF TABLES xi

ACKNOWLEDGMENTS xii

INTRODUCTION 1

1 ROBUST COEXISTENCE IN COMPETITIVE ECOLOGICAL COMMUNITIES 8
- 1.1 Introduction 9
- 1.2 Stability and feasibility thresholds 10
- 1.3 Feasibility implies robust coexistence almost surely 13
- 1.4 Robust coexistence emerges through community dynamics 18
- 1.5 Discussion 20
- 1.6 Methods 22
  - 1.6.1 A canonical form for competitive systems 22
  - 1.6.2 Equivalence between α and σ 23
  - 1.6.3 Intraspecific competition guaranteeing global stability 23
  - 1.6.4 Intraspecific competition guaranteeing feasibility 24
  - 1.6.5 Distribution of $y^\star$ for systems with random parameters 25

2 EMERGENT FEASIBILITY IN RANDOM ECOLOGICAL SYSTEMS WITH HIGHER-ORDER INTERACTIONS 27
- 2.1 Introduction 28
- 2.2 Higher-order interactions promote feasibility 30
- 2.3 Robustness and the role of interaction mean 34
- 2.4 Discussion 36
- 2.5 Methods 38
  - 2.5.1 Augmentation and polynomial homogenization 38
  - 2.5.2 Root count and roots at infinity 39
  - 2.5.3 Symmetry argument 39
  - 2.5.4 Closed-form approximation for the probability of feasibility 40
  - 2.5.5 Variance schedule for the Taylor ensemble 41

3 TIPPING POINTS ARE TYPICAL IN ECOSYSTEMS WITH HIGHER-ORDER INTERACTIONS 43
- 3.1 Introduction 44
- 3.2 Two routes to coexistence loss 46
- 3.3 Higher-order effects reshape coexistence 49
- 3.4 Abrupt boundaries in pairwise models with nonlinearities 53

3.5 Discussion . . . 55
3.6 Materials and methods . . . 57
3.6.1 Polynomial Homotopy Continuation . . . 57
3.6.2 Parameter sampling protocol . . . 58
3.6.3 Boundary detection with homotopy continuation . . . 59
3.6.4 Computing the feasibility boundaries analytically for $n = 2$ . . . 59
3.6.5 Global stability rules out fold bifurcations . . . 61

CONCLUSION . . . 63

APPENDIX A SUPPLEMENTARY INFORMATION: ROBUST COEXISTENCE IN COMPETITIVE ECOLOGICAL COMMUNITIES . . . 68
A.1 Preliminaries: competitive Generalized Lotka-Volterra models . . . 68
A.1.1 Local stability . . . 69
A.1.2 Types of dynamics . . . 71
A.1.3 Global stability and saturated equilibria . . . 72
A.1.4 Assembly . . . 75
A.2 General systems . . . 75
A.2.1 Effect of average interaction strength . . . 76
A.2.2 A sufficiently large α ensures feasibility . . . 77
A.2.3 Transitions to and from feasibility . . . 79
A.2.4 Finding α_F via eigendecomposition . . . 82
A.3 Random systems . . . 83
A.3.1 Random systems with statistically equivalent populations . . . 85
A.3.2 Previous results . . . 86
A.3.3 Feasibility when $\alpha = 0$ . . . 88
A.3.4 Feasibility when $\alpha < \alpha_L$ . . . 90
A.3.5 A single transition to feasibility when $\alpha > \alpha_L$ . . . 91
A.3.6 Approximating the probability of feasibility using the theory of small-rank perturbations of random matrices . . . 93
A.3.7 More accurate approximations of the probability of feasibility . . . 98
A.3.8 Computing $\sigma_{y^\star}$ using resolvents . . . 103
A.3.9 Resolvent-based approximation for arbitrary correlation and low variability in self-regulation. . . . 124
A.3.10 Computing $\sigma_{y^\star}$ by iteration . . . 127
A.3.11 Consequences for dynamics . . . 131
A.3.12 Consequences for assembly . . . 133
A.4 Distribution of the coefficients B_{ij} . . . 134
A.4.1 Skew normal distribution . . . 134
A.4.2 Discrete distribution . . . 137
A.4.3 Beta distribution . . . 139
A.5 Calculation of $\sigma_{y^\star}$ . . . 140

A.5.1 Through iterative solutions of linear systems . . . 140
A.5.2 Using resolvents . . . 149

APPENDIX B SUPPLEMENTARY MATERIAL: EMERGENT FEASIBILITY IN RANDOM ECOLOGICAL SYSTEMS WITH HIGHER-ORDER INTERACTIONS 153
B.1 Definitions and notation . . . 153
B.1.1 Projective Space . . . 154
B.2 GLV with HOIs . . . 156
B.3 Traditional representation of GLV with HOIs . . . 157
B.4 Polynomial representation of GLV with HOIs . . . 161
B.5 KSS system of random polynomials . . . 163
B.6 From KSS to GLV . . . 165
B.7 Probability of feasibility . . . 170
B.8 An exact upper bound to P_f . . . 174
B.9 Integral Geometry . . . 177
B.10 Expected number of zeros of orthogonally invariant ensembles . . . 178
B.11 Other random ensembles . . . 181
B.12 Distribution of the Jacobian of a Kostlan system . . . 182
B.13 Supporting numerical experiments . . . 186

APPENDIX C SUPPLEMENTARY INFORMATION: TIPPING POINTS ARE TYPICAL IN ECOSYSTEMS WITH HIGHER-ORDER INTERACTIONS . . . 194
C.1 Model . . . 194
C.1.1 Feasibility and equilibrium tracking . . . 195
C.1.2 Local stability . . . 196
C.2 Boundary detection with homotopy continuation . . . 197
C.2.1 Post-boundary dynamics and reversibility . . . 200
C.3 Computing the feasibility boundaries analytically for $n = 2$ . . . 201
C.4 Parameter sampling protocol: construction, scaling, and constraints . . . 204
C.4.1 Purely competitive systems . . . 209
C.5 Global stability rules out fold bifurcations . . . 212
C.6 Robustness and generality of fold-mediated collapse . . . 215
C.6.1 Quantifying nonlinearity without α . . . 215
C.6.2 Robustness to alternative parameterizations . . . 220
C.6.3 Robustness to alternative functional forms . . . 223
C.6.4 Published model specifications and parameterizations . . . 227
C.7 Mean matrices of S_A and S_B . . . 238
C.8 Scaling of the spectral thresholds . . . 240
C.9 Derivation of α_{eff}^{Taylor} . . . 244
C.10 Regimes in Gibbs et. al (2024) . . . 245
C.11 Pseudocode of main pipeline . . . 246
C.12 Full simulation results figures . . . 252

REFERENCES 260

LIST OF FIGURES

1.1 Three dynamical scenarios arising in an example random competitive community with six species (see Fig. A.3 for an example with two populations) 12
1.2 Feasibility and stability thresholds as intraspecific competition grows 14
1.3 Probability of feasibility for a given level of intraspecific competition (we plot $\widetilde{\alpha} = \alpha/\sqrt{(n-1)}$, x-axis) for systems of size $n = 1000$ 16
1.4 Community dynamics lead to robust coexistence 19

2.1 Phase transition in feasibility at $d = 4$ 32
2.2 Robustness and the role of interaction mean 34

3.1 Two ways coexistence can be lost in a three-species community with higher-order interactions 47
3.2 Feasibility domain as HOI strength increases 48
3.3 The strength and sign of higher-order interactions controls tipping-point prevalence 51
3.4 Fold-mediated collapse is common in published multispecies ecological models . 52

A.1 Bifurcation diagram obtained by varying the growth rates for the three species system in Eq. (A.2) 71
A.2 The components of $y^\star(\alpha)$ as a function of $\alpha \geq 0$ 82
A.3 Three dynamical phases in the classic two–species Lotka–Volterra competition model 84
A.4 Probability of feasibility (i.e., $P(x^\star > \mathbb{0})$, y-axis) for a given level of intraspecific interaction α (x-axis) 88
A.5 Spectrum of $\widetilde{Q}_i = \mathbb{1}(b^{(i)})^T - \widetilde{B}^{(i)}$ for a given i, when B is a large random matrix following the circular law 92
A.6 Transitions in and out of feasibility as system size grows 93
A.7 Spectra of several $Q_i = \mathbb{1}(b^{(i)})^T - \widetilde{B}^{(i)}$ matrices 97
A.8 Small-rank approximation of the probability of feasibility 98
A.9 Resolvent approximation of the probability of feasibility 104
A.10 Approximate probability of feasibility for the two approximations presented in the text 123
A.11 Assembly graph for a simple competitive community 135
A.12 Bottom-up assembly of the main-text community 136
A.13 Distributions used to sample the interaction coefficients 136

B.1 The ith slice of T: T_i, of the tensor T for $d = 1$ (top), $d = 2$ (middle), and $d = 3$ (bottom) 158
B.2 Expected number of real roots and positive roots 165
B.3 Variance of the GLV coefficients 170
B.4 Distribution of the number of positive roots, and the probability of feasibility . . 171
B.5 Accuracy of the approximation, and an upper bound on P_f 173

B.6 Using linear programming to obtain an exact upper bound of P_f 176
B.7 Probability of feasibility for four relaxations of the KSS ensemble 187
B.8 Probability of feasibility P_f as a function of population number n across the 3×3 grid of sign restrictions 188
B.9 Probability of feasibility P_f as a function of population number n for the four coefficient distributions that separate a nonzero mean from a skew 189
B.10 Feasibility is not the binding constraint above the transition 190
B.11 The signs of the components of a root show no bias in any direction, and sign restriction removes that property 191
B.12 The signs of distinct roots are not independent, and the departure grows with population number 192
B.13 The closed form for P_f separates into three errors that partly cancel 193

C.1 Schematic of the three boundary types detected by the homotopy continuation algorithm 198
C.2 Spectral density of S_B across the three μ_B regimes 207
C.3 Fold-boundary prevalence across the (μ_A, μ_B) plane 210
C.4 Hull nonlinearity vs. Taylor nonlinearity for the three main-text banks 220
C.5 Probability of stability across the three Gibbs regimes, replicating the parameter sweeps of Gibbs et al. with $S = 20$ species 223
C.6 Boundary-type prevalence vs. effective nonlinearity strength in the Gibbs bank ($n = 20$) 224
C.7 Fraction of abrupt boundaries versus two alternative non-linearity metrics . . . 228
C.8 Numerical verification of the upper bounds on the spectral thresholds δ_A and δ_B 243
C.9 Boundary-type prevalence as a function of HOI strength across four simulation banks 252
C.10 Critical perturbation magnitude δ_c across HOI strength and four simulation banks 253
C.11 Minimum species abundance $x_{\min}$ at the boundary across HOI strength and four simulation banks 254
C.12 Hysteresis amount $(\delta_c - \delta_{\text{recover}})$ across HOI strength and four simulation banks 255
C.13 Gradual (negative-transcritical) boundary prevalence across the (μ_A, μ_B) plane . 256
C.14 Unstable-boundary prevalence across the (μ_A, μ_B) plane 257
C.15 Successful-direction prevalence across the (μ_A, μ_B) plane 258
C.16 Boundary-type prevalence under the purely competitive parameterization 259

LIST OF TABLES

C.1 Parameters of the plant–pollinator model (Lever et al., 2014) 231
C.2 Parameters of the resource–consumer food web (Karatayev et al., 2023) 233
C.3 Parameters of the ecosystem-engineering food web (Mougi, 2024) 234
C.4 Parameters of the facilitation–competition community (Aguadé-Gorgorió et al., 2024) 236
C.5 Parameters of the allometric trophic network (Stouffer & Bascompte, 2010) . . . 237

ACKNOWLEDGMENTS

I am deeply grateful to my advisor, Stefano Allesina, for his guidance, generosity and trust throughout my doctoral studies. I thank the members of my committee, Seppe Kuehn, Mercedes Pascual and Tim Wootton, for the questions and advice that shaped this work. Each chapter of this dissertation is the product of a collaboration, and I am indebted to my coauthors: Srilena Kundu, Paula Lemos-Costa and José A. Capitán (Chapter 1); Alexander Strang and Paul Breiding (Chapters 2 and 3); and Zachary R. Miller, Armun Liaghat, and Mercedes Pascual (Chapter 3). I also thank the members of the Allesina lab and the many colleagues named at the end of each chapter for discussions that improved this work, and Bonnie Brown, Audrey Aronowsky and Susan Hu for their support throughout the program. This research was supported in part by the NSF–Simons National Institute for Theory and Mathematics in Biology (NSF DMS-2235451; Simons Foundation MP-TMPS-00005320) and by the University of Chicago's Research Computing Center. Finally, I thank my friends and my family for their patience, encouragement and love.

INTRODUCTION

Anyone who has taken a stroll around nature has witnessed its complexity. Ecologists have spent a century dealing with the tradeoff between tractability and realism imposed by it, in their efforts to understand the basic principles organizing ecosystems [1, 2]. Our way through this tradeoff is to keep the models complex and the questions basic. We do not ask what a particular ecosystem will do, which would require knowing its parameters, but what should be expected of an ecosystem about which nothing in particular is known. This dissertation is concerned with a basic notion about ecosystems: their existence. By existence we mean that the configuration of the system–the properties of its species, such as their growth rates, and their interactions with other species–is compatible with a state, or states, in which all the species in the ecosystem coexist at positive densities. To make "compatible" precise, one needs a mathematical model that establishes a relationship between the configuration of the system and its positive states. We choose to model an ecosystem as a set of differential equations describing the dynamics of n species in time,

$$\dot{x}_i = x_i \, f_i(\mathbf{x}; \theta), \qquad i = 1, \ldots, n, \tag{1}$$

where $\mathbf{x} = (x_1, \ldots, x_n)$ is the vector of species abundances, and f_i is the per-capita growth rate of species i: a function of the abundances themselves and of a set of parameters θ describing the species and the interactions between them. This model ecosystem can be arbitrarily complex. If we impose that the per-capita growth rates are smooth, we can expand them around any point–we choose the origin–obtaining the following model ecosystem:

$$f_i(\mathbf{x}) = r_i + \sum_j A_{ij} \, x_j + \sum_{j,k} B_{ijk} \, x_j x_k + \cdots, \tag{2}$$

where $r_i = f_i(\mathbf{0})$, $A_{ij} = \partial f_i / \partial x_j$, $B_{ijk} = \frac{1}{2} \, \partial^2 f_i / \partial x_j \partial x_k$, and so on, with all derivatives

evaluated at the origin. Expanding around any other point yields the same form; only the values of the coefficients change. This formulation allows us to pinpoint specific parameters: the intrinsic growth rates r_i, and effective interactions involving two species (A_{ij}), three species (B_{ijk}), or more. Importantly, these are not necessarily "real" species interactions, but rather model terms that arise from the nonlinearity of the per-capita growth rates [3–5].

The expansion represents Eq. (1) faithfully only near the origin, and we make no claim of predicting the behavior of any particular ecosystem, or of describing real ones, away from it. Rather, we take Eq. (2) as a model in its own right: a formulation compatible with a large class of ecosystem models, whose truncation at first order is the generalized Lotka–Volterra model [6, 7], whose subsequent terms are the higher-order interactions of ecological theory [8, 9], and whose equilibria are the roots of a system of polynomial equations—an object with a long tradition of study in algebraic geometry, both analytical and numerical [10, 11]. We take this class as the object of study because of its generality and this tradition. If interesting results are found for the class, one can always go back to a model of interest and ask whether they hold there as well.

In the spirit of May [12], we model the parameters of Eq. (2) as random variables. We understand random ecosystems as constituting a baseline, or null model, against which hypotheses about specific systems, including realistic ecological mechanisms of interest, can be contrasted. In addition, the rich mathematical environment surrounding random matrices and, as the order of the expansion grows, random polynomial systems [13], can be imported to ecology to our advantage.

Existence is a much harder question than (local) stability for a structural reason. Stability is inherently a linear problem: given an equilibrium, the dynamics in its neighborhood are governed by the Jacobian matrix of Eq. (1) at that point, and the question reduces to the sign of the real parts of its eigenvalues [14, 15]. Indeed, May's argument [12] never required the equilibrium itself, only the matrix of interactions around it. Existence, on the other

hand, requires the equilibrium, so it is by nature an inverse problem: given the parameters, one must find the abundances at which every per-capita growth rate vanishes, and only if all of them are positive, the ecosystem is feasible [16, 17]. Even in the linear case, where the equilibrium is the solution of a linear system, $\mathbf{x}^\star = -A^{-1}\mathbf{r}$ with $\mathbf{r} = (r_1, \ldots, r_n)$, this is much harder than stability: it requires characterizing the inverse of a random matrix [18–20], a far less tractable object than its spectrum [21, 22]. In the nonlinear case, the equilibria are the roots of a system of polynomial equations, and the problem is, in its most general form, provably impossible to solve in closed form: by Abel's impossibility theorem [23, 24], there is no general algebraic formula for the roots of a polynomial of degree five or higher. Since n species with interactions truncated at degree d have up to d^n equilibria [25], and a general system of polynomial equations is no more solvable than a general polynomial with as many roots [26], the general case is out of reach almost immediately. We argue that, although both analytically and numerically challenging, answering questions about feasibility in the general setting of Eq. (1) is not only possible but also deeply enlightening.

The three chapters of this dissertation each fit one piece into the larger puzzle of feasibility in ecological models. Given the challenging nature of Eq. (1) in its most general form, each piece slices it at a different complexity level, and achieves tractability via novel applications of mathematical techniques. Chapter 1 keeps only the linear term, where the inverse problem is hard but tractable: rather than solving for the equilibrium of any one system, we characterize the distribution of the abundances across the ensemble, using the theory of resolvents of random matrices to compute their variance, and from it the probability that all of them are positive. Chapter 2 lets the order of the expansion grow without bound, and sidesteps Abel's impossibility by taking a statistical approach: mapping the model onto a well-studied ensemble of random polynomial systems, the Kostlan–Shub–Smale ensemble [10, 13], we count the expected number of feasible equilibria exactly, without the need of ever finding one. Chapter 3 returns to the first nonlinear term, but allows the environment to change,

and sidesteps impossibility from the other side: we plant an equilibrium in the parameters, so that its existence is guaranteed at the outset, and follow it numerically as the environment moves–until the equilibrium ceases to exist.

In Chapter 1, we truncate the model at first order, which yields the generalized Lotka–Volterra model, and study feasibility, and its relationship to stability, as intraspecific competition increases. Intraspecific competition–the negative effect of a population on its own growth, the diagonal of the interaction matrix A–is the oldest stabilizing mechanism in ecological theory: Darwin already recognized that competition is fiercest among conspecifics, and self-regulation underlies foundational concepts such as limiting similarity and niche differentiation [27, 28]. May [12] showed that a sufficiently strong level of intraspecific competition stabilizes an equilibrium and that, for large random systems, the transition to stability is universal (independent of the distribution of the interactions) and sharp (always attained at the same critical level). Whether the same holds for existence remained open, despite a lineage of results going back to the very first response to May's work [16, 17, 19, 29–31]. We show that it does, in part: a critical level of intraspecific competition guarantees the existence of a feasible equilibrium, and the transition is universal, as for stability, but not sharp. We derive a general expression for the probability of feasibility as a function of intraspecific competition, system size, and the statistics of the interactions. More importantly, we show that, for large systems, the transition to stability precedes the transition to feasibility with probability one. Consequently, in large random competitive communities feasible equilibria are stable, and they remain so even when the initial pool of species cannot coexist and extinctions ensue: dynamics converge to a globally stable equilibrium, and coexistence through limit cycles or chaos is not observed.

Real interactions are not pairwise, and any nonlinearity, expanded around an operating point, yields higher-order interactions, as in Eq. (1). This system of polynomials differs qualitatively from a linear system. Most notably, it has exponentially many more solutions.

With many possible states two questions arise, is feasibility easier or harder than linear models? And does it still buy stability?

In Chapter 2, we show that as the order of the interactions increases (that is, the term at which the expansion is truncated), the probability of finding a feasible equilibrium flips from decreasing to increasing with diversity. This transition has no counterpart in the linear case. The generalized Lotka–Volterra model has a single equilibrium and, when its parameters are drawn symmetrically about zero, the probability that it is feasible is $1/2^n$ [32]: it can only fall with diversity. With higher-order interactions, existence becomes a race between two exponentials–the expected number of real equilibria, $d^{n/2}$, against the 2^n sign patterns among which they are scattered, only one of which is feasible–and the two cross at $d = 4$. Above that order, diversity makes feasibility generic rather than rare. This result runs against the classic reading of random models: from May's stability argument [12] to the feasibility results that followed it, the recurring lesson of the random-ensemble tradition is that diversity works against coexistence, and the rarity of feasibility has been taken as evidence that it demands specific ecological mechanisms. Chapter 2 exhibits a route to feasibility that invokes none: with self-regulation removed, feasibility emerges from the proliferation of equilibria alone, provided the interactions are balanced on average. In Chapter 1, stability followed automatically once feasibility was achieved; here, feasible equilibria are plentiful, but the fraction of them that is stable falls with diversity at every order, so that above the transition it is stability, not existence, that limits coexistence.

Finally, feasibility is not a static property: environments change. While the first two chapters deal with states at a fixed environment, in Chapter 3, we follow one stable and feasible state as the environment moves.

In Chapter 3, we show that higher-order interactions change the way in which existence is lost. In the linear model, coexistence can only be lost gradually, through a species declining smoothly to zero abundance [33]; with higher-order interactions, the equilibrium supporting

coexistence typically disappears abruptly, at a fold bifurcation–a tipping point–where it collides with another equilibrium and both cease to exist. Tracking equilibria with polynomial homotopy continuation as growth rates change, we find that folds progressively dominate the boundary of the coexistence domain as nonlinearity strengthens, replacing the gradual extinctions of pairwise theory. Because higher-order interactions and nonlinearity are intimately linked, we additionally show that tipping points also arise generically in pairwise models with strong nonlinearity, from a canonical model of plant–pollinator collapse to published multispecies models spanning mutualistic, competitive and consumer–resource interactions. This mode of collapse has no counterpart in the linear case either, and the previous chapters explain why. A fold is the collision of two equilibria, and the generalized Lotka–Volterra model has only one, which can therefore leave the positive orthant only through its faces, where the abundance of a species vanishes. The proliferation of equilibria of Chapter 2 is thus a requisite for the tipping points of Chapter 3, and the global stability of Chapter 1, which leaves a single equilibrium in the orthant, is what rules them out. Robustness in the sense of Chapter 1 therefore also guarantees a gradual end. Beyond this dissertation, Chapter 3 offers critical-transition theory a baseline. The theory of tipping points was built on low-dimensional models with an explicit positive feedback [34, 35], and the evidence for them in species-rich communities comes from models with a specific feedback architecture [36, 37], so whether they should be expected in diverse communities in general has remained open [38, 39]. These results reframe the question from whether a given community can tip (we find that it typically does) to what prevents it from doing so. The chapter also joins two traditions that have so far developed quite independently: structural stability, which measures the size of the safe operating space [33, 40], and critical transitions, which describe what happens at its edge [41]. The same nonlinearity that reshapes the domain also changes the nature of its boundary, with a practical corollary: at a fold, species collapse from finite abundances, rather than approaching zero gradually. Therefore,

monitoring abundances alone cannot be expected to anticipate collapse.

CHAPTER 1

ROBUST COEXISTENCE IN COMPETITIVE ECOLOGICAL COMMUNITIES

This chapter has been published as: P. Lechón-Alonso, S. Kundu, P. Lemos-Costa, J. A. Capitán, and S. Allesina. Robust coexistence in competitive ecological communities. Nature Communications 17:2637 (2026). https://doi.org/10.1038/s41467-026-69151-3. Reproduced under a Creative Commons Attribution 4.0 International License. Supplementary Information is given in Appendix A.

Abstract

Darwin already recognized that competition would be the fiercest among conspecifics. In time, intraspecific competition has become a centerpiece of ecological theory, yielding, for example the notions of niche differentiation and limiting similarity. When considering the dynamics of ecological communities, one can show that a sufficiently strong level of intraspecific competition can buffer the effects of perturbations, such that populations stably coexist at a steady state—i.e., they return to it after disturbance. Here we analyze the effect of intraspecific competition on the very *existence* of a steady state (feasibility) in large random ecological communities where competition is the predominant mode of interaction. We show that, in analogy to stability, when a critical level of intraspecific competition is surpassed, the existence of a steady state is guaranteed. More importantly, we derive a general expression for the probability of feasibility and demonstrate that, asymptotically (for large systems), the transition to stability occurs before the transition to feasibility with probability 1. Consequently, in large random competitive communities feasible equilibria are stable. This result holds even when the initial pool of species cannot coexist, and therefore extinctions ensue. That is, as the dynamics unfold, species extinctions affect the stability and feasibility threshold values, but their ordering is maintained. This has profound consequences for ecological

dynamics: a subset of the species pool will coexist at a globally stable equilibrium, and out-of-equilibrium coexistence via limit cycles or chaos will not be observed—consistently with experimental results.

1.1 Introduction

The notions of intraspecific competition and population self-regulation play a central role in ecological theory, leading to foundational concepts such as limiting similarity and niche differentiation[27, 28, 42–45]. They also are crucial for coexistence: for example, May[12] showed that ecological dynamics can be stabilized by imposing sufficiently strong intraspecific competition, and that for large systems with random species interactions the stability transition is universal (independent of the probability distribution used to model interactions) and sharp (always achieved at the same critical value of intraspecific competition). Importantly, the existence of an equilibrium (feasibility) is a necessary condition for coexistence. Further, results on stability can dramatically change when accounting for feasibility. The first contribution to this problem can be traced back to a response to May's work on stability[16], showing that in competitive Lotka-Volterra models with random interactions the probability of stability, conditioned on the presence of a feasible equilibrium, does increase, rather than decrease with system size. Since then, significant advances have been gradually accumulating in the literature[17, 19, 29–31, 46, 47] (Appendix A.3.2). However, the progress on the study of feasibility has yet to match that reached for stability[12, 22, 48, 49]. Here we show that accounting for feasibility is key to determining the expected dynamics of large competitive systems.

We compute the probability that a system would display a feasible equilibrium given its level of intraspecific competition, size, and the statistics on the random distribution of species interactions. We show that the transition to feasibility is universal, as for stability,

but is not sharp—thereby extending, generalizing and refining previous results[16, 18–20, 30, 31, 50, 51]. More importantly, we show that, in large random competitive systems, when we increase the strength of intraspecific competition, the transition to stability precedes that to feasibility[16, 20, 30]. Therefore, in these large systems feasibility implies stability. This result holds even when the initial pool of species cannot coexist, and extinctions ensue. That is, during ecological dynamics, species extinctions will alter the values for the stability and feasibility thresholds, but not their ordering. Differently from May, who focused on local asymptotic stability of an equilibrium, here we consider the stronger criterion of global stability—robust coexistence in which populations rebound from any perturbation short of extinction.

Overall, these findings have far-reaching implications for the ecological dynamics of large random competitive ecosystems. They rule out coexistence through limit cycles or chaos[52, 53], and instead indicate that the community dynamics converge to a highly-robust equilibrium, such that (1) any perturbation short of extinction would be buffered, (2) the community resists invasions, and (3) it can be assembled from the ground up[14, 54].

1.2 Stability and feasibility thresholds

We consider the Generalized Lotka-Volterra[6, 7, 55, 56] (GLV) model for n interacting populations:

$$\dot{x}_i = x_i r_i \left(1 - \sum_j A_{ij} x_j\right) , \tag{1.1}$$

where intrinsic growth rates r_i are organized in the vector r, and interactions A_{ij} in the matrix A. We say that Eq. (1.1) has a *feasible* (i.e., biologically attainable) equilibrium whenever there is a $x^\star > \mathbb{0}$ such that $\dot{x}_i = 0$ for all populations, and that such a feasible equilibrium is asymptotically *stable* if dynamics return to it following a perturbation.

Following May[12], we model A as the sum of two matrices, $A = \alpha I + B$, where B collects the inter-specific interactions (B_{ij}, $i \neq j$). I is the identity matrix, and $\alpha \geq 0$ the intraspecific competition in the system, assumed to be the same for all species (relaxing this assumption does not change the results, Appendix A.3.9).

Now we consider increasing α from zero to an arbitrary large positive value, and track the effects of this change on coexistence. We denote α_S as the level of intraspecific competition that is sufficient to guarantee the (global) stability of an equilibrium (Methods, and Appendix A.1.3). Importantly, for any $\alpha \geq \alpha_S$ stability is maintained, i.e., once surpassed this threshold, dynamics always converge to a globally stable equilibrium. Here we ask whether, in analogy to stability, there exist a critical level α_F that a) guarantees the existence of a positive equilibrium, and b) further increasing $\alpha \geq \alpha_F$ retains the feasibility of the equilibrium. In particular, we want to probe the relationship between α_F and α_S.

We start with a toy example (Fig. 1.1, $n = 6$, see Fig. A.3 for an example with two populations), illustrating the effect of increasing α on feasibility and stability. We first sample a baseline interaction matrix B, and compute the thresholds for stability, α_S, and feasibility, α_F (Methods, and Appendix A.1.3 and A.2.4), marked in Fig. 1.1 with green and yellow triangles, respectively. We then construct three interaction matrices A that differ only in their intraspecific competition values, α_{I}, α_{II}, and α_{III} (Fig. 1.1). For each system, we integrate the dynamics in Eq. (1.1) from two different initial conditions (Fig. 1.1 bottom panels, solid vs. dashed lines), revealing three qualitatively distinct dynamical regimes. System I (Fig. 1.1, left) undergoes extinctions and displays alternative stable states, indicating that the coexistence equilibrium is not feasible, and the resulting sub-community equilibrium is not globally stable (indeed, neither stability nor feasibility thresholds have been surpassed, since $\alpha_{\mathrm{I}} < \alpha_S < \alpha_F$). System II (Fig. 1.1, middle), also displays extinctions (as there is no feasible equilibrium), but starting from different initial conditions no longer leads to different outcomes, because the equilibrium of the sub-community is globally stable

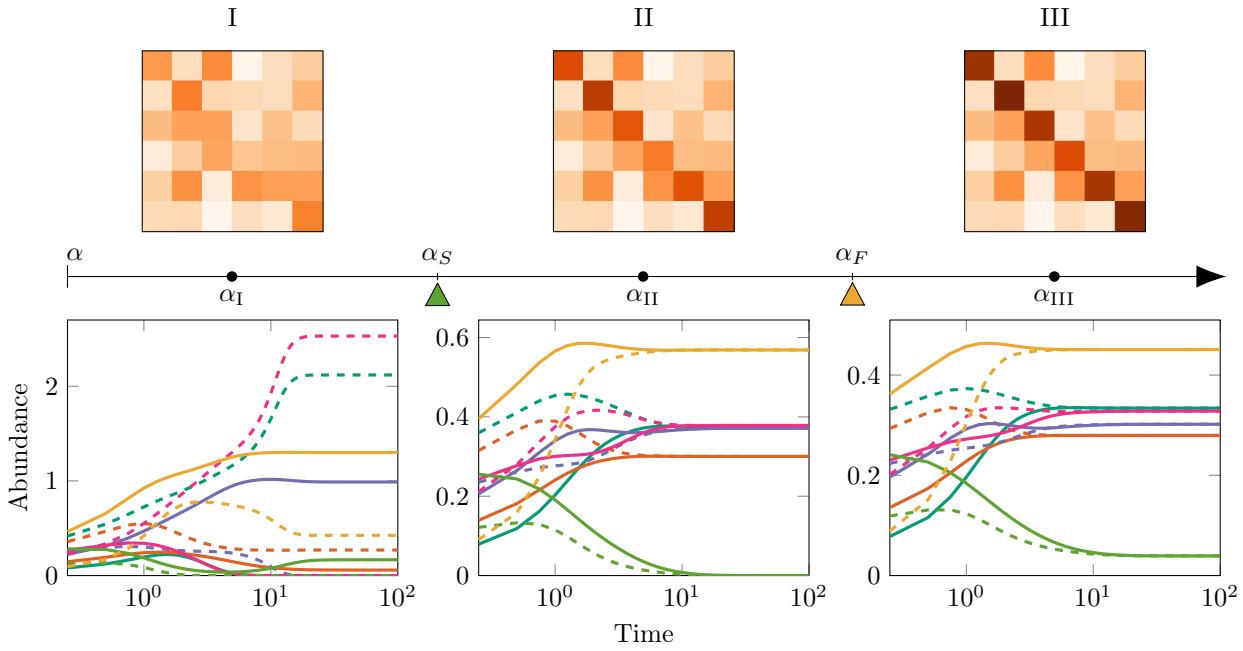

Figure 1.1: **Three dynamical scenarios arising in an example random competitive community with six species (see Fig. A.3 for an example with two populations).** We consider the dynamics for a GLV model with $A = \alpha I + B$ (Eq. 1.1), with B being the same across the three systems, and α taking three different values (α_{I}, α_{II}, and α_{III}). The three matrices, with the same off-diagonal coefficients and increasingly strong diagonal coefficients, are shown as tile plots above the arrow (darker colors reflect stronger competition). By increasing α from α_I to α_{III}, we observe distinct dynamical behaviors. First, when $\alpha_{\mathrm{I}} < \alpha_S < \alpha_F$, initializing the population densities (colors) at different values (linetypes) leads to extinctions, and a different set of coexisting populations (priority effects or alternative stable states): the equilibrium is not feasible and the set of surviving species depends on the initial conditions. Second, when $\alpha_S < \alpha_{\mathrm{II}} < \alpha_F$, the equilibrium is not feasible, but the same populations go extinct irrespective of initial conditions (in this case, the green population), while the remaining populations converge to a stable equilibrium (Appendix A.1.3). Third, when $\alpha_S < \alpha_F < \alpha_{\mathrm{III}}$, a feasible equilibrium exists, and is globally stable.

($\alpha_S < \alpha_{\text{II}} < \alpha_F$, and see Appendix A.1.3). Finally, system III (Fig. 1.1, right), exhibits all populations coexisting stably ($\alpha_S < \alpha_F < \alpha_{\text{III}}$). From this single realization, we can see that stability is achieved before feasibility. Next, we show that this is the case for large random ecological communities (but see Sec. A.2.3 for results on small or arbitrary competitive systems).

1.3 Feasibility implies robust coexistence almost surely

For each unstable matrix B, we can always find a critical level α_S such that for any $\alpha < \alpha_S$ the matrix $A = \alpha I + B$ is unstable, and for any value $\alpha \geq \alpha_S$ it is stable (Appendix A.1.3). Tracking the existence of an equilibrium as α increases is more complicated: for feasibility, we need $(\alpha I + B)x = \mathbb{1}$ to have a positive solution. As shown in Fig. 1.2**a**, when increasing α, a positive solution can appear or disappear several times; however, we prove that, for any B, a critical value α_F ensures a) that $(\alpha_F I + B)x = \mathbb{1}$ has a positive solution, and b) that further increasing $\alpha > \alpha_F$ maintains the positivity of the solution (Appendix A.2.3).

Moreover, Fig. 1.2**b** shows that, as the size of the community increases, the number of transitions in and out of feasibility converges to one; asymptotically (i.e., as $n \to \infty$), α_F behaves exactly as α_S, with feasibility precluded below α_F and guaranteed above it. Simulations can also give us a qualitative understanding of the behavior of α_F and α_S as the number of populations in the system increases: Fig. 1.2**c** shows that, once properly normalized to account for matrix size ($\widetilde{\alpha}_S = \alpha_S/\sqrt{n-1}$), the threshold for stability converges to a constant, while that for feasibility ($\widetilde{\alpha}_F = \alpha_F/\sqrt{n-1}$) keeps increasing with no saturation. Consequently (Fig. 1.2**d**), asymptotically we have $\alpha_F > \alpha_S$. Next, we show how these results can be derived mathematically.

In order to mathematically formalize the patterns from the toy example and auxiliary simulations (Figs. 1.1 and 1.2), we focus on the ensemble of large random ecosystems where

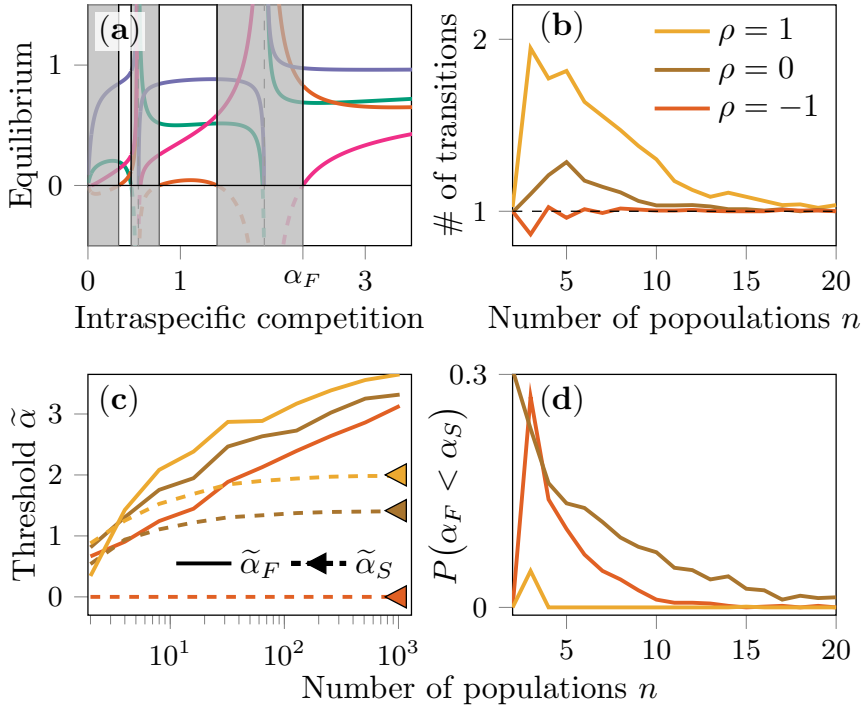

Figure 1.2: **Feasibility and stability thresholds as intraspecific competition grows.** **(a)** Bifurcation diagram of equilibrium abundances as a function of intraspecific competition α. Shaded regions correspond to parameter values where no feasible equilibrium exists, while unshaded regions mark feasibility. For a system with four populations (colors), we see that when $\alpha = 0$ no feasible solution of $(\alpha I + B)x = \mathbb{1}$ exists; as α increases, feasible equilibria can appear and disappear multiple times, but for sufficiently large $\alpha \geq \alpha_F$ feasibility is always guaranteed (see Sec.A.2.3). **(b)–(d)** Results from simulations across many system sizes. For each n, we sample many random interaction matrices with entries drawn in correlated pairs from a bivariate normal distribution with mean 0, unit variance, and correlation ρ (colors), and calculate both feasibility and stability thresholds. **(b)** The average number of transitions in and out of feasibility (y-axis) decreases with n and converges to one, indicating that for large systems feasibility is excluded below α_F and guaranteed above it. **(c)** Normalized thresholds $\widetilde{\alpha}_F = \alpha_F/\sqrt{n-1}$ and $\widetilde{\alpha}_S = \alpha_S/\sqrt{n-1}$ as a function of n. While $\widetilde{\alpha}_S$ converges to a constant, $\widetilde{\alpha}_F$ grows without bound. Triangles mark $\widetilde{\alpha}_S$ for $n = 10^3$, also shown in Fig. 1.3. **(d)** Probability that $\alpha_F < \alpha_S$ as a function of n, i.e. the chance that a feasible but unstable equilibrium exists. This probability decreases rapidly with system size.

each pair of interactions (B_{ij}, B_{ji}), with $i \neq j$ is sampled from *any* bivariate distribution with mean $\mu > 0$, variance σ^2, and correlation ρ (Appendix A.3.1); and the diagonal elements $B_{ii} = 0$. We call these systems *competitive* whenever $r > \mathbb{0}$ (i.e., all populations can grow in isolation), and $\sum_j B_{ij} > 0$ for every population i (i.e., each population has, on average, a negative effect on the growth of the other populations). We compute the probability p_F that one such random system of size n will have a feasible equilibrium as a function of α.

We begin by noting two simplifications that can be made without loss of generality (Methods). First, feasibility is unchanged if we subtract from each column of B its mean, obtaining a matrix C with zero column sums. This means that the absolute strength of competition is irrelevant: increasing the competitive effect of a given population on all others by the same amount does not alter whether the equilibrium is feasible. Thus, we may restrict attention to the canonical system

$$\dot{y}_i = y_i r_i \left(1 - \alpha y_i - \sum_j C_{ij} y_j\right), \tag{1.2}$$

with C centered in this way. Second, varying α is equivalent to rescaling the variance σ^2 of the distribution of species interactions, so we may fix $\sigma^2 = 1$ for convenience. Together, these reductions yield a simplified yet fully general representation of the competitive system, which we adopt for the analysis below.

For any model in which populations are *statistically equivalent* (i.e., there is no *a priori* structure making some populations behave differently from the rest), the distribution of the equilibrium values, $y^\star$, has always the same mean and correlation structure (Methods). Moreover, when n is large, we can assume the components of $y^\star$ to be approximately normally distributed[30] and uncorrelated (Methods, and Appendix A.3.7). Then, the probability of feasibility can be taken as the product of the probabilities that each component is positive, and can thus be written as the cumulative distribution function of a standard

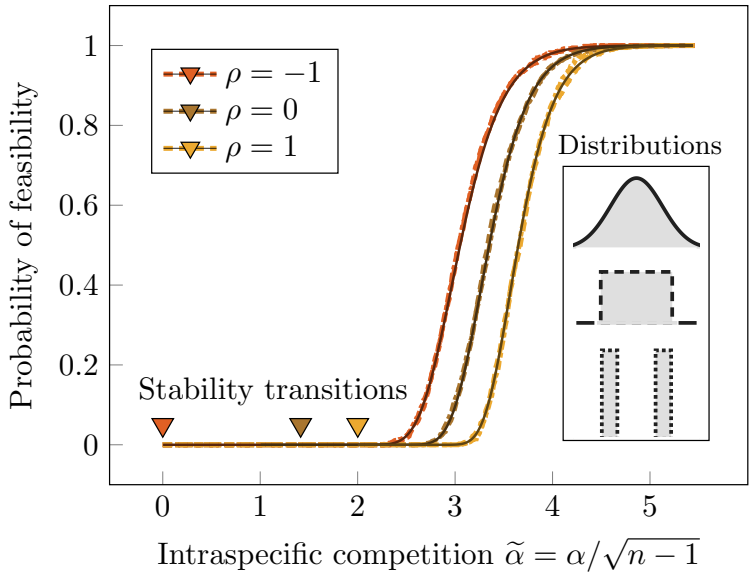

Figure 1.3: **Probability of feasibility for a given level of intraspecific competition (we plot $\widetilde{\alpha} = \alpha/\sqrt{(n-1)}$, x-axis) for systems of size $n = 1000$.** We sample entries from distributions (line types) whose marginals are either normal, uniform, or "discrete" (coefficients take positive or negative values with equal probability, Appendix A.4). The curves for different distributions collapse to the same curve, illustrating that results are asymptotically *universal* (i.e., the higher moments of the distribution have no effect). However, even for such large matrices, the effect of the correlation (line colors) is noticeable. For each choice of correlation, the value $\alpha = \alpha_S$ at which the stability of a feasible equilibrium is guaranteed is marked by a triangle: note that a negative ρ increases both the probability of feasibility and stability for any α, and a positive ρ decreases it[22]. Moreover the probability of feasibility at α_S is negligible. The black solid lines represent the analytical expectations obtained by approximating the variance using resolvents (Eqs. (1.3) and (1.4)).

normal distribution, raised to the nth power (Appendix A.3.7):

$$p_F(\alpha) \approx \Phi\left(\frac{1}{\alpha\sigma_{y^\star}}\right)^n . \tag{1.3}$$

As long as populations are statistically equivalent, more complex models, e.g., with higher-order correlations or network structure, will follow the same expression, but with a different $\sigma_{y^\star}$. Computing the variance $\sigma^2_{y^\star}$ (which in general depends on n, α, and ρ) is sufficient to approximate the probability of feasibility. In our case, we use the theory

of resolvents[57] (see Secs. A.3.8 and A.3.10 for an alternative method based on iterative solutions) to approximate the variance for any ρ, obtaining:

$$\frac{1}{(\alpha\sigma_{y^\star})^2} \approx \frac{\alpha^2 + \alpha\sqrt{\alpha^2 - 4\rho(n-1)}}{2(n-1)} - (1+\rho) \ . \tag{1.4}$$

Substituting this expression into Eq. (1.3), we obtain an extremely accurate analytical approximation of the probability of feasibility (Fig. 1.3, black curves): the probability $p_F(\alpha)$ is vanishingly small when $\alpha = 0$, (Appendix A.3.3) and increases smoothly to 1 with increasing α. Eq. (1.4) shows that the details of the distribution of interactions (Fig. 1.3, linetypes), once accounted for the correlation (Fig. 1.3, colors), are irrelevant when the system is large. This means that asymptotically, the curve describing the probability of feasibility is *universal*. Interestingly, exactly as a negative correlation between interaction strengths improves the chance of stability[22], it also increases the probability of feasibility[50]. Contrary to current expectations[19], the effect of the pairwise correlation ρ on the probability of feasibility remains significant for large systems ($n = 1000$ in Fig. 1.3). Additionally, the transition to feasibility also remains smooth compared to stability (Fig. 1.3, and Fig. A.10, see Sec. A.3.8 for a detailed discussion) for large systems.

Importantly, our calculations show that for large systems the amount of self-regulation required for feasibility is high enough (i.e., $\alpha_S < \alpha_F$) to yield global stability (as argued before[19, 20, 30, 58, 59]). Then, a feasible system will be stable with probability 1, and thus $p_F(\alpha)$ measures the *probability of coexistence* for a large, random competitive system. These results have profound implications for dynamics. Competitive GLV systems can give rise to any type of dynamics, including limit cycles (when $n \geq 3$) and chaos ($n \geq 4$)[52, 53]. Importantly, however, non-equilibrium coexistence still requires the existence of a feasible equilibrium[14]. But we have seen that feasibility generically implies global stability, and therefore non-equilibrium coexistence is precluded.

When the system is not feasible, extinctions will ensue, pruning the original pool of species to a subsystem with different thresholds for feasibility and stability (Fig. 1.2**c**). As such, in principle, any type of dynamics could be observed. Next, we show that, despite the change in values of α_S and α_F caused by extinctions, the ordering $\alpha_S < \alpha_F$ is maintained almost surely, provided that n is large. As a result, dynamics still converge to stable equilibria even when feasibility is not attained for the initial species pool.

1.4 Robust coexistence emerges through community dynamics

So far, we have investigated how coexistence is affected by increasing α. However, intraspecific competition models the effects of a species on itself. As such, when species are lost to extinction, the level of intraspecific competition should not be affected: the coefficients on the diagonal do not change when the matrix is pruned of the populations that have gone extinct. Thus, we turn our attention to a pool of n populations where we fix $\alpha < \alpha_S < \alpha_F$ (analogous to system I in Fig. 1.1), and consider "top-down assembly" (where all the species in the pool are introduced in the environment at the same time, Fig. 1.4**a**). Since we are below the feasibility threshold, some populations go extinct and, as a result, α_F and α_S changes (both values depend on n; Fig. 1.2**c**). We re-compute their values every time an extinction occurs (plotted in Fig. 1.4**b**), and find that their initial ordering is maintained throughout assembly. Consequently, the initial species pool traverses the dynamical states illustrated in Fig. 1.1: I $\rightarrow$ II $\rightarrow$ III, converging to a globally stable equilibrium after ecological dynamics have elapsed. Furthermore, we show (Appendix A.3.12) that the same equilibrium can be achieved via "bottom-up assembly", through successive invasions[54].

To confirm that these observations are a generic feature, we plot the ratio α_F/α_S when we run the same simulation in the previous example for many draws of random systems with the same characteristics (Fig. 1.4**c**). We see that the ratio is kept above one, implying that

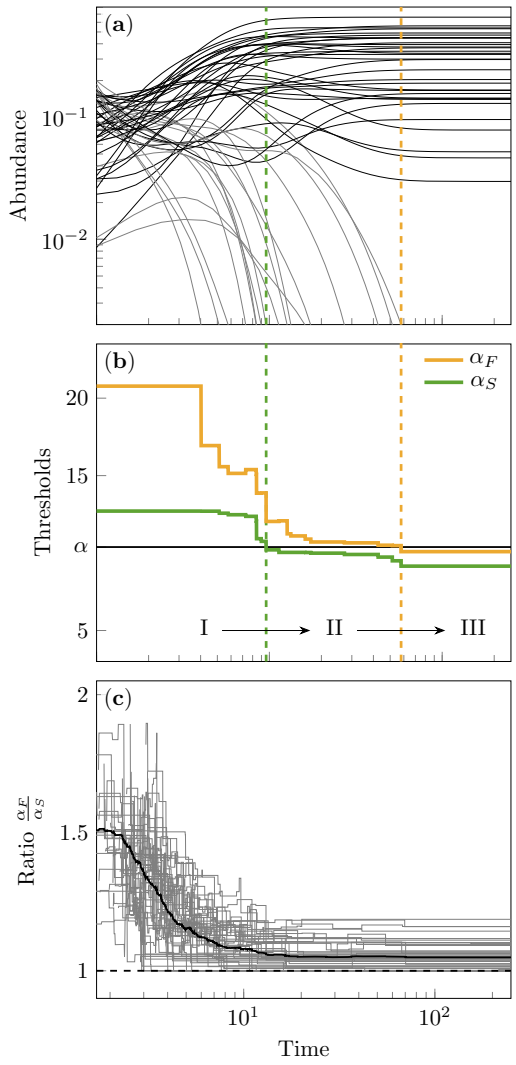

Figure 1.4: **Community dynamics lead to robust coexistence.(a)** We initialize a community with $n = 50$ populations and random interactions, setting $\alpha = \alpha_F/2$ (black line, middle panel); then, there is no feasible equilibrium, and extinctions are guaranteed (grey lines, top panel); note that for this simulation we also have $\alpha < \alpha_S < \alpha_F$, and thus we are in phase I of Fig. 1.4. **(b)** As populations are lost to extinction, the values of α_S and α_F (green and yellow lines respectively, middle panel) for the surviving sub-community change. As the number of extinctions mounts, α_S crosses α (dashed green line, top and middle panels), and thus the system transitions to case II. Extinctions continue until α_F falls below α (dashed yellow line), and the system transitions to phase III. The extant populations coexist at a globally stable equilibrium, and those that went extinct since during phase II cannot re-invade the system. **(c)** The ratio α_F/α_S is plotted as a function of time for many random realizations (individual trajectories in gray, average in black) of the communities with the same statistics as in the example. The ratio is always above 1, meaning that the relationship $\alpha_F > \alpha_S$ maintains through the dynamics in all simulations.

the relationship $\alpha_S < \alpha_F$ is maintained throughout the dynamics for all the simulations. This shows that, with high probability, the dynamical outcome of large random competitive systems is always the same: a sub-set of the species pool will coexist robustly at an equilibrium that is characterized by $\alpha_S < \alpha_F < \alpha$; the equilibrium is stable, and the last few populations to go extinct (if started in phase I), or all the extinct populations (if started in phase II) cannot re-invade the system.

1.5 Discussion

Ecological dynamics can be extremely complex, with populations' trajectories oscillating regularly or chaotically. The Generalized Lotka-Volterra model for multiple competitors embodies this complexity: for less than three competitors, trajectories always converge to steady states; for three or more species, one can observe cyclic dynamics; four or more competitors can coexist via nonperiodic, chaotic oscillations. Importantly, to ensure the long-term coexistence of the populations there must exist a *feasible* equilibrium: a choice of positive densities at which all populations, if unperturbed, could remain indefinitely. Here we ask what types of dynamics arise when the number of competitors is large and interactions are chosen at random: we derive the probability of feasibility, and in doing so, notice that as intraspecific interaction is increased, the transition to stability always precedes that for feasibility when the system is large. As a consequence, feasible systems will be stable. Importantly, all the results in this paper are true in probability. That is, while the probability of finding feasible but unstable systems is never exactly zero, it becomes vanishingly small with system size.

Intraspecific competition models the fact that each species has access to private resources or regulating factors that are species-specific; as such, it plays an important role in niche differentiation, and sets a limit to niche similarity[27, 28, 42–45]. Our results show that,

to ensure feasibility, one had to postulate a level of niche differentiation that is sufficient to guarantee stability. This observation reinforces the notion that, in competitive systems, feasibility is key for coexistence[16, 44, 51, 60]. This is in analogy with consumer-resource models[61], as well as in GLV models with symmetric interactions produced by niche overlap or species' similarity[62], for which stability is guaranteed, and thus feasibility determines coexistence[32, 54].

As a consequence, we have shown that, when the number of competitors is large, trajectories converge to stable steady states with high probability, ensuring the robust coexistence of the extant competitors. These findings are in line with empirical results: experimenting with organisms at the same trophic level (for which competition is believed to be the dominant mode of interaction) often results in equilibrium dynamics [63–68], while sustained cycles and chaos are typically associated with predator-prey systems and structured populations[69–74]. While direct empirical test of these patterns is out of the scope of this work, it is an exciting avenue for future research.

Recently, it has been shown[75] that a dynamical phase characteristic of persistent fluctuations can arise for the high-diversity, high-interaction strength limit in bacterial systems dominated by competitive interactions. Furthermore, this observation mirrors dynamical phases arising in a GLV model with dispersal. Crucially, these findings hinge on the presence of constant immigration—without it, irrespective of interaction strength, robust coexistence emerges for large communities (see Fig. S1 in[75] for results when $n = 50$). As such, our findings are not in contradiction with these previous results[75]—including constant immigration for all species precludes extinctions, thereby preventing the system from relaxing to the equilibria studied here. Therefore, the results presented can be used to form an expectation for isolated systems in which populations can go extinct, or systems in which immigration is rare. For open systems in which immigration is widespread, outcomes could depart severely from what presented here.

In summary, we have shown that, for large competitive communities with random coefficients following the GLV model, the probability of non-equilibrium coexistence is negligible—feasible systems are almost surely stable, and thus chaos or limit cycles will not be observed. Moreover, coexistence via stable equilibria emerges through community dynamics. In conclusion, when considering the subset of coexisting populations, we find that each population rebounds from perturbations, that the community cannot be invaded and can be built through successive invasions—the hallmark of robust coexistence [28, 45].

1.6 Methods

1.6.1 A canonical form for competitive systems

We consider the competitive GLV system in Eq. (1.1), with $r > \mathbb{0}$, $A = \alpha I + B$ and $B^T \mathbb{1} > \mathbb{0}$. We can further decompose the matrix $A = \alpha I + C + \mathbb{1} m^T$, where C is the matrix obtained by subtracting from each column of B its (positive) mean, and $m > \mathbb{0}$ is a vector containing the column means. We can write the solution of $(\alpha I + C + \mathbb{1} m^T) x^\star = \mathbb{1}$ as a function of the solution of the simpler system $(\alpha I + C) y^\star = \mathbb{1}$ (Appendix A.2.1), finding:

$$x^\star = \frac{1}{1 + m^T y^\star} y^\star \quad .$$

Thus, $x^\star$ is related to $y^\star$ through multiplication by the scalar $1/(1 + m^T y^\star)$. As such, we have a feasible equilibrium $x^\star > \mathbb{0}$ when either a) $y^\star > \mathbb{0}$ (i.e., $y^\star$ is feasible, and because $m^T y^\star = \sum_j m_j y_j^\star$ is the sum of products of nonnegative values, then the constant of proportionality is also positive), or, b) $y^\star < \mathbb{0}$ and $m^T y^\star < -1$ (i.e., all the components of $y^\star$ are negative, and sufficiently large to make the constant of proportionality negative as well). However, the average of $y^\star$ is positive (Appendix A.2.1) , thereby ruling out case b). We conclude that $x^\star$ is feasible if and only if $y^\star$ is feasible. Because infinitely many

competitive matrices B will map into the same C, we say that this is the *canonical* matrix of interactions for the competitive system. Although increasing the strength of competition μ does not affect feasibility, it decreases equilibrium abundance values. As such, increasing μ too much will result in very low abundances, which could lead to extinctions in real systems where stochasticity plays a factor.

1.6.2 Equivalence between α and σ

Consider a matrix of interactions C, such that the variance of C_{ij} is σ^2. We show that there exists a rescaled system with the same feasibility properties, a different α, and a scaled interaction matrix such that $\sigma^2 = 1$. The equilibrium for the system is

$$y^\star = (\alpha I + C)^{-1}\mathbb{1} = \left(\alpha I + \sigma\,\widetilde{C}\right)^{-1}\mathbb{1} = \frac{1}{\sigma}\left(\tilde{\alpha} I + \widetilde{C}\right)^{-1}\mathbb{1}.$$

Setting $z^\star = \sigma y^\star$ we have that $z^\star = \left(\tilde{\alpha} I + \widetilde{C}\right)^{-1}\mathbb{1}$, where $\tilde{\alpha} = \alpha/\sigma$ and $\widetilde{C}_{ij}$ have unit variance. Since $\sigma > 0$, then $z^\star > \mathbb{0} \Leftrightarrow y^\star > \mathbb{0}$. Therefore, varying σ (i.e., the variance of the interaction matrix) is equivalent to varying intraspecific competition α. Without loss of generality, we can fix $\sigma^2 = 1$ and study solely the effect of α.

1.6.3 Intraspecific competition guaranteeing global stability

The Wigner semicircular law for symmetric matrices with i.i.d. entries with mean zero and variance $1/n$, $Q_{ij} = Q_{ji} \sim Z(0, \frac{1}{n})$, states that, as $n \to \infty$, the eigenvalues of Q are contained in the semicircle centered at 0 with radius 2 almost surely. Because Q is symmetric, all its eigenvalues are real, and we can write

$$-2 \leq \lambda_{min}(Q) \leq \lambda_{max}(Q) \leq 2$$

We consider a random interaction matrix $B \in \mathbb{R}^{n\times n}$ with $\mathbb{E}[B_{ij}] = 0$, $\mathbb{V}(B_{ij}) = 1$, and $\mathbb{Cor}(B_{ij}, B_{ji}) = \rho$, and introduce intraspecific competition via $A = \alpha I + B$. A standard argument based on Lyapunov functions (see Appendix A.1.3) shows that global stability of the coexistence equilibrium is guaranteed by the positive definiteness of the symmetric part of A,

$$\frac{1}{2}\left(A + A^T\right) \succ 0 \iff \alpha I + \frac{B + B^T}{2} \succ 0.$$

Let $H := (B + B^T)$, then, $\mathbb{E}(H_{ij}) = 0$, and $\mathbb{V}(H_{ij}) = \frac{1}{2}(1 + \rho)$. As such, the eigenvalue

$$\lambda_{min}\left(\frac{H}{\sqrt{\frac{1}{2}n(1+\rho)}}\right) \geq -2 \iff \lambda_{min}(H) \geq -\sqrt{2n(1+\rho)}.$$

Therefore, positive definiteness of $A + A^T$ is guaranteed as long as intraspecific competition is above the threshold $\alpha_S = \sqrt{2n(1+\rho)}$.

1.6.4 Intraspecific competition guaranteeing feasibility

One can show that, in competitive systems, there exists a level of intraspecific competition at which the feasibility of the equilibrium is guaranteed, and further strengthening intraspecific competition retains feasibility (Appendix A.2.2). We denote this critical level as α_F. To find this value for a given matrix of interaction strengths B, we consider the eigenvalues of several matrices derived from B (or, equivalently, C, Appendix A.2.3). In particular, consider the real, positive eigenvalues of $-C = \mathbb{1}m^T - B$, and call α_0 the largest value such that the components of the solution $(\alpha_0 I + C)y^\star = \mathbb{1}$ diverge to $\pm\infty$ (if it exists, otherwise $\alpha_0 = 0$). Then, we form n matrices Q_i, each of size $n - 1$. Each Q_i is obtained as the sum of two matrices, $Q_i = \mathbb{1}(b^{(i)})^T - B^{(i)}$, where $b^{(i)}$ is the ith row of matrix B with the ith element removed, and $B^{(i)}$ is the matrix B with the ith row and the ith column removed. Denote as

α_i the maximum real eigenvalue of Q_i (if it exists, otherwise $\alpha_i = 0$). Finally, we have that the value α_F that guarantees the feasibility of the system is $\alpha_F = \max\{\alpha_0, \alpha_1, \alpha_2, \ldots, \alpha_n\}$.

Interestingly, the value of intraspecific competition sufficient to guarantee the global stability of any feasible equilibrium is also an eigenvalue, this time the largest positive eigenvalue of $-(B + B^T)/2$ (see above, and Appendix A.1.3).

1.6.5 Distribution of $y^\star$ for systems with random parameters

For random models in which populations are *statistically equivalent* (Appendix A.3.1), we have that the expectations $\mathbb{E}(y_i^\star) = \mathbb{E}(y_j^\star)$, the variances $\mathbb{V}(y_i^\star) = \mathbb{V}(y_j^\star) = \sigma^2_{y^\star}$, and the correlation $\mathbb{C}\mathtt{or}(y_i^\star, y_j^\star)$ is the same for all pairs. Note that the sum of the components of $y^\star$ is fixed: $\mathbb{1}^T y^\star = n/\alpha$, and therefore the mean correlation must be negative; because it has to be the same for all pairs, it is exactly $\mathbb{C}\mathtt{or}(y_i^\star, y_j^\star) = -1/(n-1)$, as shown also by calculating it explicitly (Appendix A.3.7). Moreover, if one approximates the distribution of $y^\star$ as a multivariate normal distribution, finding the unknown variance (which will depend on the exact definition of the model, the statistics of the distribution, etc.) is sufficient to approximate the probability, by either ignoring the correlation between the components (because for large n it is negligible), or by computing an integral over the positive orthant (Appendix A.3.7).

Acknowledgments: We thank A. Skwara, Z.R. Miller, and C. Serván for discussion. We acknowledge the University of Chicago's Research Computing Center for their support of this work.

Funding: This research was supported in part by grants from the NSF (DMS-2235451) and Simons Foundation (MPS-NITMB-00005320) to the NSF-Simons National Institute for Theory and Mathematics in Biology (NITMB). J.A.C. acknowledges financial support from grant PRIORITY (PID2021-127202NB-C22), funded by MCIN/AEI/10.13039/501100011033 and

"ERDF. A way of making Europe".

Author contributions: S.A. conceived and designed the study. P.L.A. and S.A. drafted the manuscript. P.L.A. drafted the code and the figures. S.A. and J.A.C. performed the derivations; J.A.C. derived the approximation using resolvents; S.A. derived those based on iterative solutions and small-rank perturbations. P.L.A., S.K., P.L.C., J.A.C. and S.A. contributed to the mathematical derivations, the implementation of the code, edited the manuscript, and discussed and interpreted the results.

Competing interests: The authors declare no competing interests.

Materials & Correspondence: All materials and correspondence requests should be addressed to plechon@uchicago.edu or sallesina@uchicago.edu.

Data & Code availability: No data was used in this work. Code to reproduce all findings is available at https://doi.org/10.5281/zenodo.17742734.

CHAPTER 2

EMERGENT FEASIBILITY IN RANDOM ECOLOGICAL SYSTEMS WITH HIGHER-ORDER INTERACTIONS

This chapter is in press in Journal of the Royal Society Interface *as: P. Lechón-Alonso, A. Strang, P. Breiding, and S. Allesina. Emergent feasibility in random ecological systems with higher-order interactions. Preprint: https://doi.org/10.64898/2026.06.11.728491. Supplementary Material is given in Appendix B.*

Abstract

A recurring lesson from random ecological models is that coexistence is hard to come by: in the Generalized Lotka-Volterra (GLV) model with pairwise interactions, the probability that randomly sampled parameters admit a positive (feasible) equilibrium – a necessary condition for coexistence – is exactly $1/2^n$ in n species, vanishing rapidly with diversity. This rarity is often read as evidence that feasibility demands specific ecological mechanisms. Real interactions, however, are rarely strictly pairwise: any nonlinear dependence of one species' growth rate on another's abundance, Taylor-expanded, generates higher-order interactions (HOIs) of increasing degree. Treating the interaction order d as a knob that indexes this nonlinearity, we map the random GLV with HOIs onto the Kostlan–Shub–Smale class of random polynomial systems, which gives the expected number of feasible equilibria exactly and the probability of feasibility (P_f) approximately. We find a phase transition at $d = 4$: below this threshold, P_f decays with diversity as in the pairwise case; above it, the exponential proliferation of equilibria outpaces the probability that any given equilibrium is feasible, and the probability of feasibility increases with n, approaching one. The transition is robust to changes in the coefficient distribution, but vanishes when interactions are on average competitive or mutualistic rather than balanced. This work uncovers a route by

which feasibility emerges from nonlinearity alone, with no fine-tuning of parameters and no appeal to specific ecological mechanisms.

2.1 Introduction

Ecological theory has long taken the species pair as its unit of analysis, and much of our intuition about the coexistence of many species descends from pairwise models – the Generalized Lotka-Volterra (GLV) model prominent among them. Drawing the parameters at random makes it possible to probe the typical behavior of a structureless community against which coexistence can be judged [76, 77] (Chapter 1). Randomly parametrized pairwise models share a common property: at high diversity they are very unlikely to admit equilibria in which all species are present at positive abundance [18, 19, 31–33, 50, 58, 78–83] (feasible equilibria). Feasibility is easily destroyed by adding species, because random pairwise models lack the ecological mechanisms (self-regulation, positive intrinsic growth rates, predator-prey structure, etc.) that are thought to prevent extinctions.

Species interactions, however, often involve complexities that cannot be captured through the lens of the species pair – spatial and structural complexity [84–86], behavior switching [87–90], habitat modification [91, 92], nonlinearities in prey consumption [93, 94], and evolution [95]. For example, two competitors of a focal annual plant depress its seed production more when they are interspersed than when they are clustered, with their number and identity held fixed: the effect of one competitor on the focal species is modulated by the position of the other [96]. Interactions shaped by these mechanisms are better understood through the lens of *higher-order interactions* (HOIs): the interaction between two species is modulated by a third (three-way interactions), which may itself be modulated by a fourth, and so on. Beyond such literal multi-species mechanisms, any smooth nonlinear interaction becomes a sum of higher-order terms after Taylor expansion around an operating point, rendering HOIs

a generic, agnostic representation of highly nonlinear systems [3, 4, 83] (Chapter 3).

Although their existence and relevance were initially debated [3, 8, 87, 97–100], HOIs are now an active area of research in both experimental [91–93, 101–110] and theoretical [111–116] ecology. Their analysis, however, is hard: explicit steady-state solutions of systems with HOIs do not exist in general [23], hindering the standard first step in analysis. As a result, existing feasibility results are confined to three- or four-way interactions, treated using mathematical heuristics [115], computer simulations [83, 111] (Chapter 3), or reduction to effective pairwise interactions [112].

AlAdwani and Saavedra delivered the first results on feasibility under generalized HOIs, showing numerically that at fixed diversity the probability of feasibility increases with interaction order [47, 113, 114]. That is one axis; the other – how feasibility scales with diversity at fixed interaction order, the limit in which pairwise models predict decline – has remained out of reach. Recent work [117] shows that a random replicator equation maps to a well-studied family of random polynomials, the Kostlan–Shub–Smale (KSS) ensemble [13, 118], reducing the counting of equilibria to the counting of polynomial zeros. Because replicator and GLV dynamics are formally equivalent [14, 119–121], this mapping carries over directly to GLV with HOIs, putting the tools of random polynomial theory [122, 123] also at the disposal of ecology, in analogy to how random matrix theory has shaped our thinking about pairwise systems [12, 22].

With this machinery, we ask: how does the probability of feasibility scale with diversity once interactions are allowed to be higher-order? We find that below a critical interaction order $d = 4$, the probability of feasibility decays exponentially with the number of species, recovering the familiar intuition from pairwise theory [124]. Strikingly, however, beyond $d = 4$ the probability of feasibility grows with diversity and rapidly approaches one. The first half of this transition follows from the expected number of feasible equilibria, which we compute exactly (Methods and Appendix B.5); the second is a numerical finding, reproduced

by a closed-form approximation. Simulations show the transition to be robust to the shape of the coefficient distribution, and to break down once interactions carry a nonzero mean – once the community is on average competitive or mutualistic rather than balanced. This work suggests that feasibility (a necessary condition for coexistence) can emerge without fine-tuned constraints, as a consequence of nonlinearity combined with a balance of interaction signs. What emerges is a supply of feasible equilibria, not coexistence itself: we find numerically that these equilibria are seldom stable, and that above the transition it is stability, not feasibility, that limits coexistence.

2.2 Higher-order interactions promote feasibility

We study the per-capita generalized Lotka-Volterra dynamics in which species interact through terms of increasing order [8],

$$\frac{1}{x_i}\frac{dx_i}{dt} \;=\; r_i \;+\; \sum_j A_{ij}\,x_j \;+\; \sum_{j,k} B_{ijk}\,x_j x_k \;+\; \cdots\,, \tag{2.1}$$

where r_i is the intrinsic growth rate of species i, A_{ij} the pairwise interaction coefficients, B_{ijk} the three-way (first higher-order) coefficients, and the ellipsis collects interactions of still higher order. We let d denote the highest degree appearing on the right-hand side – the largest number of abundances multiplied in any single term – so that $d = 1$ recovers the pairwise GLV, $d = 2$ adds three-way interactions, and general d collects all interactions up to degree d. We index a given interaction by its degree p, the number of abundances it multiplies: $p = 0$ for the growth rate, $p = 1$ for the pairwise couplings A_{ij}, $p = 2$ for the three-way terms $B_{ijk}\,x_j x_k$, and so on up to $p = d$. Equilibria are the zeros of the polynomial system in Eq. (2.1), $f_i(x) = 0$; feasible equilibria are those with $x_i > 0$ for all i.

We draw the interaction coefficients randomly, each an independent mean-zero Gaussian.

Intra- and interspecific coefficients are drawn alike, so the diagonal terms A_{ii}, B_{iii}, ... carry no negative mean and the model has no self-regulation. This is deliberate: self-regulation is among the mechanisms known to protect feasibility in pairwise models, and building it in would leave open whether any feasibility we find is due to it rather than to interaction order. Setting the variance of every degree-p coefficient to $\binom{d}{p}$ places the dynamics in the Kostlan–Shub–Smale (KSS) ensemble of random polynomial systems [13]: the per-capita rates are then equivalent to n homogeneous polynomials in $n+1$ variables of common degree d (see Methods and Appendix B.6 for the mapping, and [117] for the original argument in the context of multiplayer evolutionary games). This scaling is a theoretical baseline that makes the counting analytically tractable, and we relax the specific parameter choices below.

A degree-d system of this kind has d^n complex roots by Bézout's theorem; the expected number of these that are real is

$$\mathbb{E}[N_{\mathbb{R}}] = d^{n/2}, \tag{2.2}$$

the Kostlan–Shub–Smale–Edelman identity [13]. None of these roots sits at infinite abundance, so the count carries over to the real space $\mathbb{R}^n$ in which equilibria live (see Methods).

Every coefficient is drawn from a law symmetric about zero, so flipping the sign of any subset of species maps the ensemble onto itself and carries real roots in one orthant onto real roots in another. No orthant is therefore preferred: the real roots distribute uniformly across the 2^n orthants of $\mathbb{R}^n$ in expectation, and feasibility is not favoured by the ensemble but is one box in 2^n. Because of this, we show (see Methods, and [117]) that the expected number of feasible equilibria is exactly

$$\mathbb{E}[N_+] = \left(\frac{\sqrt{d}}{2}\right)^n. \tag{2.3}$$

As a function of diversity n, $\mathbb{E}[N_+]$ is monotonically decreasing for $d < 4$, identically equal

to one for $d = 4$, and monotonically increasing for $d > 4$ (Appendix B.5). The same counting applies when species carry different interaction orders d_i: the expected number of feasible equilibria becomes $(d_1 \cdots d_n)^{1/2}/2^n$, and feasibility still emerges whenever the product $d_1 \cdots d_n$ outgrows 4^n (Appendix B.10). Enumerating every real equilibrium of the sampled systems confirms the uniformity directly: no orthant is systematically preferred, and the measured $\mathbb{E}[N_+]$ reproduces Eq. (2.3) across the grid (Appendix B.13, Fig. B.11). The ecologically relevant quantity, however, is not the expected count of feasible equilibria

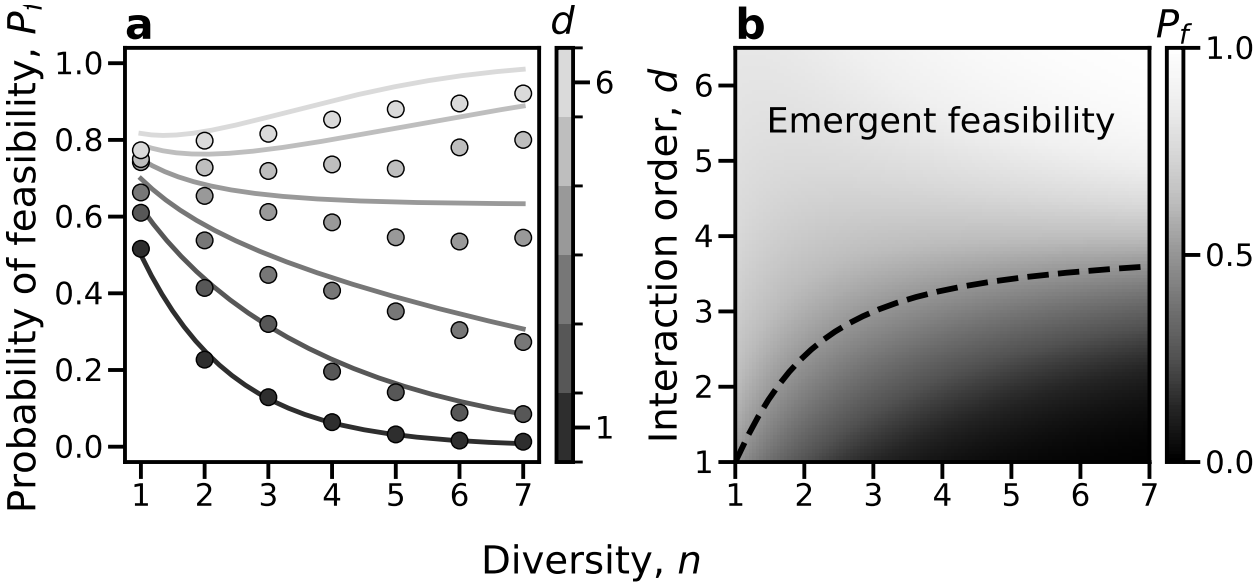

Figure 2.1: **Phase transition in feasibility at $d = 4$.** (**a**) Probability of feasibility P_f versus diversity n, from the independence approximation in Eq. (2.4) (curves, colored by interaction order d) and from homotopy continuation simulations of the random GLV+HOI system (points). P_f decays with n for $d < 4$ and grows with n for $d > 4$. (**b**) Phase diagram in the (n, d) plane: heatmap of the approximation in Eq. (2.4). The dashed line marks the contour line $P_f = 0.5$. Each simulation point is a Monte Carlo estimate from 10^3 independent realizations of the ensemble.

but the probability P_f that at least one exists, which Eq. (2.3) does not determine: a large expected count can be produced by rare systems carrying many feasible equilibria while P_f stays bounded away from one. Treating the orthants of distinct real roots as independent, so that a system with j real roots has none feasible with probability $(1 - 2^{-n})^j$, and applying

Jensen's inequality, we obtain (see Methods)

$$P_f \lessapprox 1 - \left(1 - \frac{1}{2^n}\right)^{d^{n/2}}. \tag{2.4}$$

Equation (2.4) is a Jensen upper bound on the independence approximation, not on P_f itself; empirically it tracks the simulated P_f closely (Fig. 2.1**a**). The independence step is exact only at $d = 1$, where a system has a single equilibrium and there is nothing to correlate; for $d > 1$ the equilibria of one community solve the same random system, and their sign patterns are not independent, in a direction that leaves Eq. (2.4) above the measured P_f (Appendix B.13, Figs. B.12 and B.13). At $d = 1$ this collapses to $P_f = 1/2^n$, the pairwise baseline of Serván et al. [32]. For $d < 4$ the exponent $d^{n/2}$ grows more slowly than 2^n and P_f vanishes exponentially in n; for $d > 4$ the exponent outruns 2^n and $P_f \to 1$. The line $d = 4$ is the phase boundary, on which the two rates are matched. Numerical simulations using homotopy continuation [83, 125] (the method is introduced in Chapter 3, Sec. 3.6.1) agree with Eq. (2.4) across n and d (Fig. 2.1**a**); the corresponding (n, d) phase diagram in Fig. 2.1**b** makes the transition visible at a glance, with feasibility collapsing under diversity below $d = 4$ and emerging from it above. One half of the transition does not depend on the approximation: maximizing P_f over all distributions of N_+ consistent with Eq. (2.3) is a linear program, and its optimum is the exact bound $P_f \leq (\sqrt{d}/2)^n$ (Appendix B.8), so P_f must vanish with n for $d < 4$. Above $d = 4$ that bound is vacuous, and the emergence claim rests instead on Eq. (2.4) and its agreement with simulations, which we probe further in the next section.

Feasibility is not coexistence: a feasible equilibrium must also be stable. Since $f(x^*) = 0$ at an equilibrium, the community matrix of Eq. (2.1) is $M = \mathrm{diag}(x^*)\, J(x^*)$ with $J = \partial f/\partial x$; enumerating every feasible equilibrium across the same grid, the fraction that is locally stable falls with n at every d, and shows no transition at $d = 4$ (Appendix B.13).

2.3 Robustness and the role of interaction mean

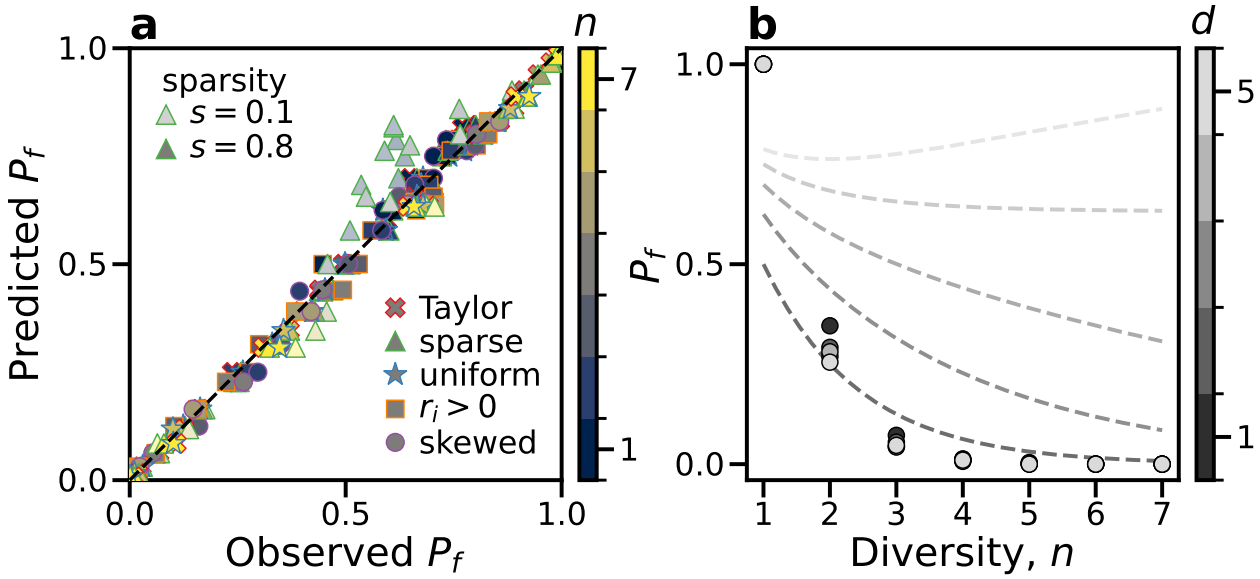

Figure 2.2: **Robustness and the role of interaction mean. (a)** Observed versus predicted P_f across the (n, d) grid for the Taylor (cross), sparse (triangle), uniform (star), positive growth rate (square; $r_i > 0$, interactions symmetric) and skewed (circle; interactions folded onto one sign and recentered at zero) ensembles. "Predicted" is the KSS independence approximation of Eq. (2.4); "observed" is the numerical estimate. Color encodes species count n; for the sparse markers, lightness encodes sparsity s. The dashed line is $y = x$. **(b)** Transition vanishes under a nonzero interaction mean. Same as in Fig. 2.1**a**, but for the sign-restricted (purely competitive) ensemble. The data depart sharply from the approximation. Every point in both panels is a Monte Carlo estimate from 10^3 independent realizations at that (n, d).

The KSS ensemble of the previous section served as a theoretical baseline, but as an ecological model it is unrealistic for several reasons. First, the coefficients A_{ij}, B_{ijk}, etc. have a binomial variance scaling $\binom{d}{p}$ that peaks at $p = d/2$, meaning that intermediate-order interactions are the most variable component of the dynamics. There is no biological reason higher-order terms should be amplified relative to growth rates and pairwise couplings. Second, the KSS ensemble is dense: every interaction coefficient is non-zero. In addition, this result rests on the assumption of gaussian distribution symmetrica round zero but the question of whether it holds for a broader family of distributions, and for different mean,

remains. We relax each property in turn and ask whether the transition at $d = 4$ is maintained. As we show below, the transition survives the first four relaxations, but breaks when relaxing the zero-mean assumption (Appendix B.13).

Reading Eq. (2.1) as a multivariate Taylor expansion of a smooth per-capita dynamics around an operating point, $f_i(x) = \sum_\ell a_\ell x^\ell$ with $a_\ell = (\partial^\ell f_i)(0)/\ell!$ and i.i.d. Gaussian derivatives $(\partial^\ell f_i)(0)$ yields the coefficient variance (see Methods)

$$\mathrm{Var}(a_\ell) \;=\; \frac{1}{(\ell_1! \cdots \ell_n!)^2}. \tag{2.5}$$

Higher-order monomials are further suppressed the higher the interaction order, encoding the intuition that nonlinearity is a perturbation of the linearized dynamics. Numerical estimates of P_f under this variance fall on the same side of $d = 4$ as the KSS baseline (crosses, Fig. 2.2**a**): P_f still decays with n for $d < 4$, and grows with n for $d > 4$.

To probe whether the transition survives the dense all-to-all property of the KSS ensemble, we impose sparsity on every higher-order coefficient – those on a monomial of total degree $|\ell| \geq 2$, that is, the three-way terms $B_{ijk}x_j x_k$ and above – by retaining each with probability s and zeroing it otherwise, while growth rates and pairwise couplings ($|\ell| \leq 1$) are kept intact. Across n and d, P_f is essentially independent of s. The sparse markers in Fig. 2.2**a** (triangles) are well-aligned with theory even with sparsity as low as $s = 0.1$.

Next, we relax the assumption of Gaussian entries by sampling interactions from a Uniform distribution with variance decaying according to Eq. (2.5) (Fig. 2.2**a**, stars). Again, we observe no change: at a fixed variance schedule, the transition does not depend on the coefficients being Gaussian.

Finally, we break the sign symmetry of the entries by restricting all interaction coefficients ($|\ell| \geq 1$) to the negative half-line while restricting the growth rates to be positive, yielding a purely competitive ensemble. Unlike the three previous relaxations, the transition does

not survive: P_f decays monotonically with n at every d we tested, and the $d = 4$ crossover vanishes (Fig. 2.2**b**).

The competitive ensemble changes two things at once – it makes the growth rates positive and the interactions negative – and the change in the interactions is itself two changes, giving their distribution both a negative mean and a skew. To separate which of the two drives the negative result, we compare four interaction distributions at fixed second moment: symmetric or folded onto one sign, each centred at zero or shifted off it (Appendix B.13). The mean carries the effect: a distribution skewed onto one sign but recentered at zero keeps the transition, threshold and all (Fig. 2.2**a**), while a symmetric distribution shifted off zero loses it. Consistent with this, restricting the growth rates to be positive shifts their mean as well, yet the transition is indifferent to it: P_f rises, but its trend in n does not change (Fig. 2.2**a** and Appendix B.13). The transition therefore requires that interactions be balanced on average, and depends neither on the sign of the growth rates nor on the variance decay, the sparsity, or the shape of the coefficient distribution.

2.4 Discussion

The transition at $d = 4$ – recall that d is the polynomial degree – is a counting race between two exponentials. Bézout's theorem caps the number of complex equilibria at d^n [121, 124, 126]; reflection symmetry of any sign-symmetric coefficient distribution sends each real root into one of 2^n orthants with equal weight. The expected number of feasible roots is therefore the real-root count $\sqrt{d^n}$ divided by the orthant count 2^n, and these two exponentials cross at $\sqrt{d} = 2$. As such, feasible equilibria proliferate whenever the rate at which a polynomial system produces real solutions overtakes the rate at which a symmetric distribution scatters them across orthants. The simulations show that P_f, the probability that at least one exists, turns at the same threshold. Monotonicity in d is the fixed-n slice of the same expression:

$\mathbb{E}[N_+]$ increases with interaction order at every diversity, which is what earlier numerical work reported [113, 114]. The transition lies on the other axis, where the sign of the effect is set by whether $\sqrt{d}/2$ exceeds one, and a threshold in n is invisible at fixed n.

The transition survives modifications relevant to ecological realism. Namely, (1) imposing a variance structure resembling the structure emerging from Taylor expansion of a nonlinear system; (2) sparsifying the higher-order coefficients; and (3) sampling interaction terms from a uniform rather than Gaussian distribution, or (4) from a skewed zero-mean rather than symmetric around zero distribution. Emergent feasibility disappeared, however, once the interactions carried a nonzero mean. If multiplicity of equilibria is what drives $P_f \to 1$ in real ecosystems, it does so where interaction strengths are balanced.

Independence of the coefficients is a convenience of the ensemble, not a requirement of the argument. Higher-order terms produced by a shared resource, a shared predator or a nonlinear functional response will be correlated with the pairwise terms they accompany. The count uses three properties: that each species' per-capita growth polynomial has a law unchanged by rotating the state space, which is what lets the expected number of equilibria factor into one number per species; that the same law is unchanged by flipping the sign of any one abundance, which is what makes the feasible orthant one box in 2^n; and that the n species' polynomials are independent of *each other*. Drawing every coefficient independently under the binomial variance schedule realizes the first two, but it is not the only law that does, and the rotation-invariant family includes ensembles whose coefficients are correlated (Appendices B.9 and B.10). Correlation between higher-order and pairwise terms therefore need not disturb the transition. Correlation between different species' equations however could disturb it, a case we leave open.

Feasibility is necessary for coexistence but not sufficient: a feasible equilibrium must also be dynamically stable. Recent results for pairwise competitive communities (Chapter 1) guarantee stability if feasibility is achieved [77]. Here we report the opposite: stability is

the limiting factor, not feasibility. The probability that a community has a stable feasible equilibrium falls with n at every d, even where P_f turns up (Appendix B.13, Fig. B.10).

Enough nonlinearity, together with interactions that are balanced on average, suffices to make feasibility generic at high diversity; no ecological mechanism – self-regulation (Chapter 1), intrinsic growth-rate sign structure, predator-prey architecture, modularity or niche partitioning [18, 33, 77, 78, 80] – need be invoked to recover it.

2.5 Methods

2.5.1 Augmentation and polynomial homogenization

We collect the growth rate, pairwise couplings, and higher-order coefficients of species i in Eq. (2.1) into a single order-d tensor $T^{(i)}$ and homogenize. Promoting the environment to an auxiliary $(n{+}1)$-th coordinate of fixed value $\tilde{x}_{n+1} \equiv 1$ and writing $\tilde{x} = (x_1, \ldots, x_n, 1)^\top$, the right-hand side of Eq. (2.1) becomes the degree-d form

$$f_i(\tilde{x}) \;=\; \sum_{l_1,\ldots,l_d=1}^{n+1} T^{(i)}_{l_1\cdots l_d}\, \tilde{x}_{l_1} \cdots \tilde{x}_{l_d}, \tag{2.6}$$

n homogeneous polynomials in the $n+1$ variables $\tilde{x}_1, \ldots, \tilde{x}_{n+1}$, all of common degree d. A monomial with all d indices equal to $n+1$ reproduces the growth rate r_i; one with a single index $j \neq n+1$ the pairwise term $A_{ij}x_j$; two the three-way term $B_{ijk}x_jx_k$; and so on [14, 117, 119, 120, 127].

Sampling every entry of $T^{(i)}$ as an independent mean-zero, unit-variance Gaussian places the system in the KSS ensemble, and indeed corresponds to ecological coefficients r_i, A_{ij}, etc. being sampled from mean-zero Gaussians with variance $\binom{d}{p}$. The full correspondence is given in Appendices B.2–B.4 and B.6.

2.5.2 Root count and roots at infinity

By Bézout's theorem, a generic degree-d system of n homogeneous polynomials in $n+1$ variables has exactly d^n complex roots, with probability one over the random coefficients. The expected number of these that are real is $\mathbb{E}[N_{\mathbb{R}}] = d^{n/2}$, the Kostlan–Shub–Smale–Edelman identity [13]. The ecologically relevant roots are those on the affine chart $\tilde{x}_{n+1} = 1$, i.e. in $\mathbb{R}^n$; any remaining roots would sit at infinite abundance, $\tilde{x}_{n+1} = 0$. Setting $\tilde{x}_{n+1} = 0$ collapses the system to n homogeneous polynomials in only n variables, an overdetermined system that generically has no solution, so with probability one none of the d^n roots escapes to infinity and the count carries over to $\mathbb{R}^n$. A self-contained treatment in projective space, the integral-geometry framework underlying the identity, and its extension to other random ensembles are given in Appendices B.1 and B.9–B.11.

2.5.3 Symmetry argument

The expected count of feasible equilibria in Eq. (2.3) differs from the real-root count of Eq. (2.2) by a factor 2^{-n}. This is the statement that, in expectation, real roots are distributed uniformly across orthants. We show this.

Index the 2^n orthants of $\mathbb{R}^n$ by o, and let N_o count the real roots falling in orthant o, so that $N_{\mathbb{R}} = \sum_o N_o$ and, by linearity of expectation, $\mathbb{E}[N_{\mathbb{R}}] = \sum_o \mathbb{E}[N_o]$. We claim every term in this sum is equal. Consider the reflection $(x_1, \ldots, x_n) \mapsto (-x_1, x_2, \ldots, x_n)$. Applied to a KSS system, it flips the sign of every coefficient attached to a monomial of odd degree in x_1; since these coefficients are sampled from a centered Gaussian, the reflected system has the same law as the original. The map is a bijection between the orthant with $x_1 > 0$ and its $x_1 < 0$ counterpart (remaining signs fixed), so the two carry equal expected root counts. Composing such reflections coordinate by coordinate connects any orthant to any

other, hence $\mathbb{E}[N_o]$ is independent of o and

$$\mathbb{E}[N_o] = \frac{1}{2^n}\,\mathbb{E}[N_{\mathbb{R}}]. \tag{2.7}$$

Taking o to be the positive orthant gives $\mathbb{E}[N_+] = 2^{-n}\,\mathbb{E}[N_{\mathbb{R}}]$, and substituting Eq. (2.2) recovers Eq. (2.3). The argument uses only that the coefficient law is symmetric about zero coordinate-wise; it is otherwise distribution-free.

2.5.4 Closed-form approximation for the probability of feasibility

Let $N_{\mathbb{R}}$ count the real zeros of the polynomial system and N_+ the subset of those zeros lying in the positive orthant. Feasibility is the event $\{N_+ \geq 1\}$, so

$$P_f \;=\; 1 - P(N_+ = 0). \tag{2.8}$$

By orthogonal invariance of the KSS measure, every real root is equally likely to land in any of the 2^n orthants of $\mathbb{R}^n$. Treating the orthant assignments of distinct real roots as independent (a working approximation that ignores correlations between sign patterns; Appendix B.13, Figs. B.12 and B.13), conditional on $N_{\mathbb{R}} = j$ the probability that none of the j real roots is positive is $(1 - 2^{-n})^j$. Averaging over the law of $N_{\mathbb{R}}$,

$$\begin{aligned} P(N_+ = 0) \;&\approx\; \mathbb{E}\Big[\big(1 - 2^{-n}\big)^{N_{\mathbb{R}}}\Big] \;=\; \mathbb{E}[f(N_{\mathbb{R}})], \\ f(j) &= \big(1 - 2^{-n}\big)^{j}. \end{aligned} \tag{2.9}$$

The function f is convex on $[0, \infty)$: its second derivative is $f(j)\,\log^2(1 - 2^{-n}) > 0$. Jensen's inequality for convex f then gives

$$\mathbb{E}[f(N_{\mathbb{R}})] \;\geq\; f(\mathbb{E}[N_{\mathbb{R}}])\,, \tag{2.10}$$

and combining (2.8)–(2.10) yields an upper bound on the independence approximation rather than on P_f itself,

$$P_f \;\lessapprox\; 1 - f(\mathbb{E}[N_{\mathbb{R}}]) \;=\; 1 - \left(1 - \frac{1}{2^n}\right)^{\mathbb{E}[N_{\mathbb{R}}]}. \tag{2.11}$$

Substituting the identity $\mathbb{E}[N_{\mathbb{R}}] = d^{n/2}$ from Eq. (2.2) into (2.11) recovers the approximation (2.4) used in the main text. The linear program of Appendix B.8, by contrast, bounds P_f itself: maximizing $P_f = P(N_+ \geq 1)$ over all distributions of N_+ on the nonnegative integers with $\mathbb{E}[N_+]$ fixed by Eq. (2.3) gives $P_f \leq \mathbb{E}[N_+] = (\sqrt{d}/2)^n$, with no assumption on how root signs are related.

2.5.5 Variance schedule for the Taylor ensemble

Write the per-capita growth rate $f_i : \mathbb{R}^n \to \mathbb{R}$ as a degree-d Taylor polynomial around the origin,

$$f_i(x) \;=\; \sum_{|\ell| \leq d} a_\ell \, x^\ell, \qquad a_\ell \;:=\; \frac{(\partial^\ell f_i)(0)}{\ell!}, \tag{2.12}$$

where $\ell = (\ell_1, \ldots, \ell_n)$ is a multi-index of total degree $|\ell| = \sum_j \ell_j$, $\ell! := \ell_1! \cdots \ell_n!$, and $x^\ell = \prod_j x_j^{\ell_j}$.

We postulate that the partial derivatives at the origin are i.i.d. standard Gaussians, $(\partial^\ell f_i)(0) \sim \mathcal{N}(0,1)$, independently across i and ℓ. This is the smooth-function analogue of the centered Gaussian prior used for the KSS baseline: a maximally agnostic, sign-symmetric law on the local jet of f_i. Because a_ℓ is a deterministic rescaling of $(\partial^\ell f_i)(0)$ by the constant $1/\ell!$, $\mathrm{Var}(cX) = c^2\mathrm{Var}(X)$ gives

$$\mathrm{Var}(a_\ell) \;=\; \frac{1}{(\ell!)^2} \;=\; \frac{1}{(\ell_1! \cdots \ell_n!)^2}, \tag{2.13}$$

recovering Eq. (2.5). The factorial suppression encodes the smoothness prior: higher-order partials are penalized geometrically through $\ell!$, so the typical magnitude of a degree-$|\ell|$

contribution to f_i decays as $1/\ell!$ at a fixed point in state space. Sign symmetry of the coefficient law is preserved, so the orthant-uniformity argument of Sec. 2.5.3 carries over.

Acknowledgments: P.L.A. acknowledges E. Alastrue De Asenjo, C. Améndola, M. Bogan, D. Costa, J. Hoskins, S. Kuehn, S. Kundu, K. Lee, P. Lemos-Costa, S. Li, A. Liaghat, J. Lindberg, M. Loschi, M. Pascual, J. I. Rodriguez, S. Sheik, M. Silber, A. Skwara, M.-Ş. Sorea, L. Souto Ferreira, H.-Y. Tsai, T. Wootton, and P. Y. Yu for helpful discussions. P.B. acknowledges A. Lerario for helpful discussions.

Funding: This research was supported in part by grants from the NSF (DMS-2235451) and Simons Foundation (MP-TMPS-00005320) to the NSF-Simons National Institute for Theory and Mathematics in Biology (NITMB). P.B. was supported by DFG, German Research Foundation – Projektnummer 445466444.

Author contributions: P.L.A. designed the study and performed the research, with advice from A.S., S.A. and P.B.; P.L.A. wrote the manuscript; P.L.A. developed the code; P.L.A., A.S., P.B., and S.A. performed the derivations. All authors edited the manuscript, discussed and interpreted the results.

Competing interests: The authors declare no competing interests.

Materials & Correspondence: All materials and correspondence requests should be addressed to plechon@uchicago.edu.

Data & Code availability: All code and data necessary to reproduce the paper are publicly available at https://github.com/pablolich/emergent_feasibility: the sampling and solver code, the test suite, the scripts that render every figure, and the tabulated output of the sweeps.

CHAPTER 3

TIPPING POINTS ARE TYPICAL IN ECOSYSTEMS WITH HIGHER-ORDER INTERACTIONS

This chapter is in revision as: P. Lechón-Alonso, Z. R. Miller, A. Liaghat, P. Breiding, M. Pascual, and S. Allesina. Tipping points are typical in ecosystems with higher-order interactions. Preprint: https://doi.org/10.64898/2026.04.24.720639. Supplementary Information is given in Appendix C.

Abstract

Whether species-rich communities gradually erode or collapse abruptly under environmental change is a central question in ecology [41]. Classical pairwise theory predicts that coexistence is always lost gradually, through smooth declines to extinction [33], yet real ecological interactions are often strongly state-dependent – shaped by nonlinearities that fixed pairwise coefficients cannot capture [9]. Here we show that higher-order (nonlinear) interactions make abrupt, irreversible loss of coexistence a typical route to community collapse: across diverse random communities, the equilibrium supporting coexistence disappears suddenly at a fold bifurcation. Using polynomial homotopy continuation [125] to track equilibria as environmental conditions change, we find that folds progressively dominate the boundary of the coexistence domain as nonlinearity strengthens, replacing the gradual extinctions of pairwise theory. Furthermore, the sign structure of higher-order interactions controls both the onset of tipping-points and whether biodiversity buffers or amplifies collapse. Because higher-order and nonlinear interactions are intimately linked, tipping points also arise generically in pairwise models with strong nonlinearity. Applying our continuation framework to a canonical model of plant–pollinator collapse [36], we formally resolve its bifurcation structure as fold-mediated and show that fold bifurcations are typical across published multispecies models

spanning mutualistic, competitive, and consumer-resource interactions. These results challenge the expectation that monitoring abundances suffices to anticipate collapse, and unify structural-stability theory, which delineates the safe operating space for coexistence, with critical transition theory, which characterizes the nature of its boundaries.

3.1 Introduction

Ecosystems around the world face environmental changes that will push communities of species beyond the conditions that support present-day coexistence. Understanding when and how coexistence will be lost are central questions for both ecological theory and conservation [41]. Structural-stability theory addresses the first of these questions by taking a geometric approach, characterizing the size and shape of the feasibility domain – the space of environmental conditions under which a community admits an equilibrium where all species have positive abundances [33, 40, 46, 79, 128]. In generalized Lotka–Volterra (GLV) models and related models that underpin this framework [129], interactions are pairwise and equilibrium conditions are linear in species abundances, making the feasibility domain analytically tractable. A key consequence of this linearity is that it also settles the second question: feasibility can only be lost through transcritical bifurcations, in which one or more species declines smoothly to zero abundance, a fundamentally gradual change [33].

Yet real ecological interactions are strongly state-dependent, shaped by saturating functional responses, context-dependent behaviors, environmental modification, and other nonlinearities that make per-capita interaction effects depend on community state [87, 89, 91–93, 130–132]. Such effects cannot be absorbed into fixed pairwise coefficients [5, 9]. The theory of critical transitions shows that nonlinear feedbacks can fundamentally alter how coexistence is lost, destroying stable states abruptly at fold bifurcations – tipping points – where the system shifts discontinuously and hysteretically to an alternative state [34, 35, 133–

136]. Analytical theory for critical transitions has been developed largely for low-dimensional models [39], while numerical studies have presented evidence for their occurrence in species-rich networks with specific feedback architectures [36, 37, 137, 138]. Whether tipping points arise generically across diverse communities with state-dependent interactions remains an open question [38].

Thus, structural-stability theory handles diversity but assumes linearity; critical-transitions theory handles nonlinearity but not diversity. This gap is a key barrier to characterizing resilience in realistic communities, where it is important to understand not only the size of the safe operating space for coexistence, but also how collapse unfolds once its boundary is crossed [39, 139, 140].

Here we address this question by extending the GLV model with quadratic higher-order interaction (HOI) terms as a minimal representation of state-dependent interaction effects [5]. The resulting equilibrium conditions are systems of coupled multivariate polynomials of degree two, for which no closed-form solution exists in general beyond small systems [24]. In addition, the exponential growth in the number of equilibria makes the study of feasibility boundaries challenging, even computationally [114]. We overcome these obstacles using polynomial homotopy continuation [125], a method from numerical algebraic geometry [11] that tracks all solutions of polynomial systems as parameters vary.

By subjecting model communities with HOIs to growth-rate perturbations and mapping their feasibility boundaries, we show that fold bifurcations progressively dominate the boundary as nonlinearity strengthens, replacing the gradual extinctions that characterize pairwise theory. The sign structure of HOIs controls tipping-point prevalence and whether biodiversity acts as a buffer or amplifier of abrupt collapse. Furthermore, because saturating functional responses generate effective higher-order interactions [3, 4], we use the same continuation framework to explore tipping points in pairwise models with nonlinear interactions. We formally resolve the bifurcation structure of a canonical model of ecosystem collapse in

plant-pollinator networks, confirming that it is fold-mediated. More broadly, we find that fold-mediated coexistence loss is common in other published multispecies models across interaction types and functional forms, and that it becomes more common as the nonlinearity of interactions increases.

3.2 Two routes to coexistence loss

We study coexistence under environmental perturbations in generalized Lotka-Volterra (GLV) models with higher-order interactions (HOIs),

$$\dot{x}_i \;=\; x_i\Big[r_i \;+\; (1-\alpha)\sum_j A_{ij}\,x_j \;+\; \alpha\sum_{j,k} B_{ijk}\,x_j x_k\Big], \tag{3.1}$$

where $\mathbf{x} = (x_i)$ are abundances, $\mathbf{r} = (r_i)$ are intrinsic growth rates, A_{ij} entries are pairwise interactions, B_{ijk} entries are three-way interactions (HOIs), and $\alpha \in [0, 1]$ controls the relative weight of higher-order vs. pairwise terms (recovering the classic pairwise GLV when $\alpha = 0$; see [141]). Throughout, we model environmental change by perturbing intrinsic growth rates along fixed directions:

$$\mathbf{r} = \mathbf{r_0} + \delta\,\mathbf{u}, \tag{3.2}$$

where $\mathbf{u}$ is the direction of the perturbation and δ is its magnitude. We explore the robustness of the coexistence equilibrium and how it is lost by tracking the long-term community state as δ varies (see Appendix C.2). In the pairwise model ($\alpha = 0$), the coexistence equilibrium $\mathbf{x}^*$ is mapped linearly to $\mathbf{r}$, so it shifts continuously under environmental forcing, and extinctions can only occur when species abundances are driven smoothly to zero. With HOIs, however, the same ecosystem can respond in fundamentally different ways depending on the perturbation direction (Appendix C.1), even from the same baseline coexistence state

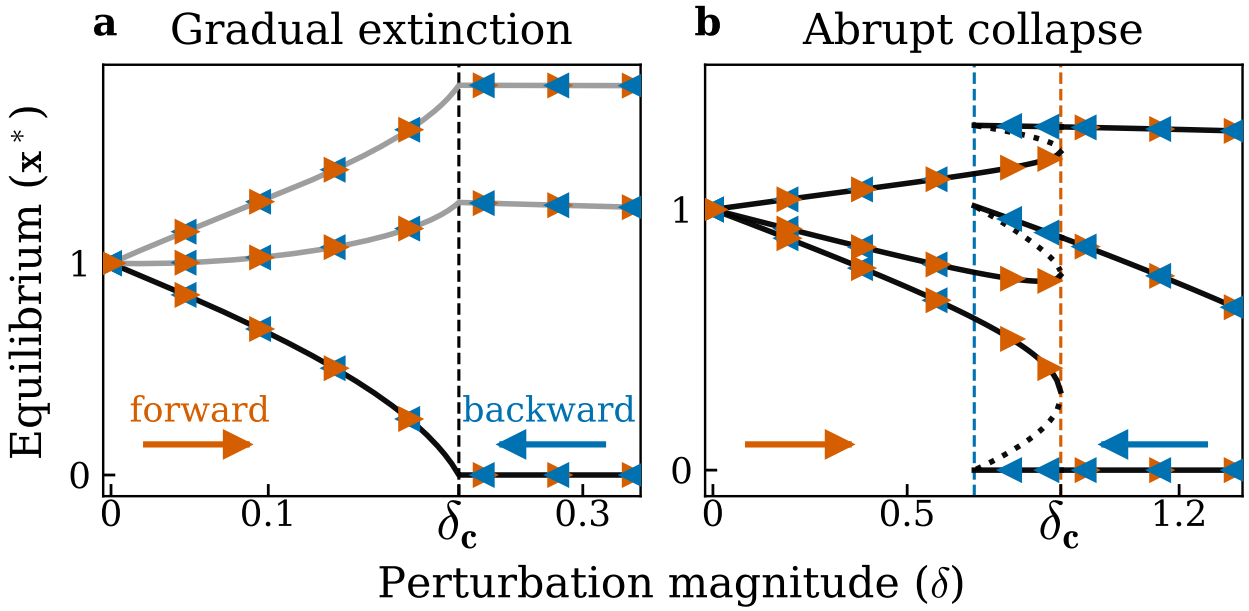

Figure 3.1: **Two ways coexistence can be lost in a three-species community with higher-order interactions.** Black/grey curves show the equilibrium abundances of each species computed using polynomial homotopy continuation ($\mathbf{x}^\star$, y-axis) as perturbation magnitude (δ, x-axis) varies along two fixed perturbation directions (panels). Line type indicates stability of the equilibrium (solid: stable; dotted: unstable). Triangles mark endpoints of numerical integrations of Eq. (3.1) that validate the continuation curves: in the forward sweep (orange right-pointing triangles), δ is increased in small steps from $\delta = 0$, with each integration initialized at the final state of the previous step; the backward sweep (blue left-pointing triangles) reverses the process from the post-collapse state, testing where coexistence is recovered. Vertical dashed lines mark critical perturbations where coexistence is lost/gained. Panel **a** shows gradual extinction: one species declines continuously to zero abundance at δ_c (where a transcritical bifurcation takes place), and the same threshold is recovered upon reversal of the perturbation (arrows). Panel **b** shows abrupt collapse: coexistence is lost at a fold bifurcation as the perturbation magnitude increases. When the perturbation is gradually reversed (backward sweep), recovery occurs at a different critical value, indicating hysteresis.

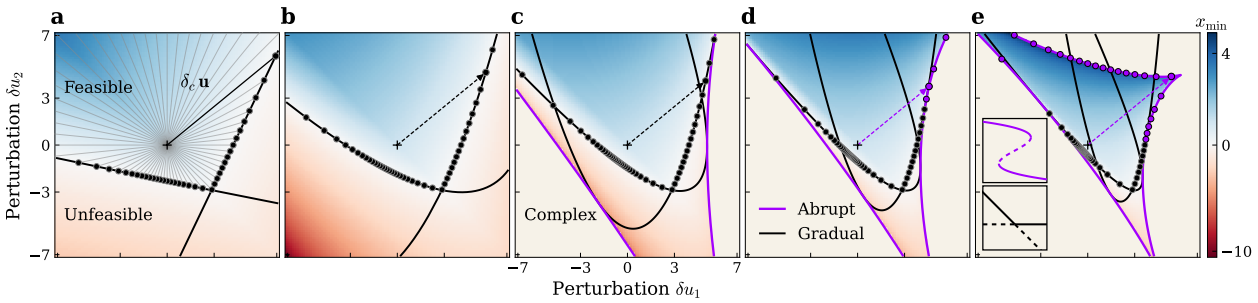

Figure 3.2: **Feasibility domain as HOI strength increases.** Shading shows $\min_i x_i^\star(r_1, r_2)$ along the focal coexistence equilibrium branch (where $r_i = r_i^0 + \delta u_i$). Blue indicates a positive equilibrium (feasible), red indicates at least one negative component (unfeasible), off-white background indicates regions where no real equilibrium exists (complex). Black curves are boundaries where a species gradually declines to zero at a transcritical bifurcation (gradual boundary, see bottom inset in panel **e**, and Fig 3.1**a**). Purple curves are boundaries where two equilibria collide and disappear from the real line at a fold bifurcation (abrupt boundary, see top inset of panel **e**, and Fig 3.1**b**). Left to right, stronger HOIs bend gradual boundaries (**a**, **b**) and generate abrupt boundaries (**c**-**e**) that ultimately truncate the feasible region. The baseline environmental state (cross) is plotted across all panels, and one perturbation direction **u** is highlighted (dashed segment). Along this direction, the distance to the gradual boundary (δ_c) varies as α increases (**a**-**c**), and eventually the gradual boundary is superseded by an abrupt one (**d**,**e**). Lines: analytic boundaries obtained using elimination theory; points: numerical boundary points obtained by polynomial homotopy continuation along a set of 100 perturbation directions (gray lines in panel **a**). Interior (semitransparent) black curves correspond to gradual boundaries of additional equilibria introduced by HOIs, which do not affect the focal branch.

(Fig. 3.1, $\delta = 0$). Along one direction (Fig. 3.1**a**), numerical integration of Eq. (3.1) (orange triangles) tracks the stable coexistence branch found by polynomial homotopy continuation (lines) until one species smoothly declines to zero abundance at a transcritical bifurcation (δ_c, vertical dashed line); reversing the perturbation (blue triangles) recovers coexistence at the same threshold. Along a different direction (Fig. 3.1**b**), we find instead a critical transition: trajectories follow the stable coexistence branch until it terminates at a fold (saddle-node) bifurcation, beyond which no nearby stable coexistence equilibrium exists and the system collapses to an alternative attractor where one species is absent. This transition exhibits hysteresis: coexistence is regained only after reversing the perturbation well past

the forward critical point.

3.3 Higher-order effects reshape coexistence

To connect the bifurcation picture in Fig. 3.1, which follows two specific perturbation directions, to a geometric, global notion of robustness, we next visualize coexistence geometry in a two-species system. With two species, interactions are necessarily pairwise, but they include nonlinear per capita terms. Figure 3.2 shows how the feasibility domain – the set of growth rates that admit a positive coexistence equilibrium – deforms as non-linearity (α) strengthens (panels **a**-**e**). For $\alpha = 0$ the domain is the classical feasibility cone [40, 46, 79, 128] whose boundaries are gradual transcritical bifurcations (Fig. 3.1**a**, black lines in Fig. 3.2). As α increases, these gradual boundaries bend (panel **b**), and for sufficiently strong HOIs, a new boundary type appears: the coexistence equilibrium abruptly disappears through the loss of real solutions to the equilibrium equations at a fold bifurcation (Fig. 3.2**c**-**e**, purple lines, and Fig. 3.1**b**). This abrupt boundary initially lies outside the feasibility domain for small α but ultimately truncates it. Throughout, we restrict our attention to the focal coexistence branch, which continues smoothly from the unique coexistence equilibrium at $\alpha = 0$. Other equilibria can be created by HOIs, generating additional interior boundaries (e.g., interior semitransparent curves in panels **c**-**e**).

In two dimensions, this geometric picture can be computed in closed form: gradual boundaries follow from the vanishing of a coordinate of the coexistence equilibrium, while abrupt boundaries correspond to the vanishing of the appropriate discriminant (a classical algebraic object called tact invariant [142]; see Methods and Appendix C.3). However, the resulting expressions are already unwieldy for $n = 2$ and become intractable in higher dimensions, motivating our computational approach. We use the analytic boundary in Fig. 3.2 (lines) as a ground-truth benchmark to validate the continuation-based numerical pipeline

used for larger communities: the numerical boundary points found using polynomial homotopy continuation along fixed perturbation directions (see Eq. (3.2)) coincide with the exact analytic curves.

We next apply this numerical boundary-tracking algorithm to HOI communities with $n > 2$ species (Fig. 3.3), systematically varying HOI strength α (x-axis), community size n (colors), and the mean of B_{ijk} μ_B (rows) to probe competitive, mixed, and facilitative HOI regimes (Fig. 3.3**g**). To isolate the effect of nonlinearity on robustness, we construct random communities that share the same locally stable baseline equilibrium across all α (Fig. 3.2 crosses, and see Methods), perturb growth rates along many directions (shown in gray in Fig. 3.2 **a**), and classify the first feasibility boundary encountered as gradual or abrupt. Loss of stability is also tracked (see Appendix C.2) but occurs before feasibility very rarely (Appendix C.12) and is omitted for clarity.

For all combinations of n and μ_B, abrupt boundaries become more likely as α increases. When HOI coefficients are drawn symmetrically around zero ($\mu_B = 0$; Fig. 3.3**c**,**d**), fold boundaries progressively replace transcritical extinctions as the typical mode of coexistence failure at moderate to high α. This basic pattern is robust to alternative parameterizations that relax our imposed controls, including the planted equilibrium, convex interpolation between pairwise and HOI terms, and the imposition of baseline stability via self-regulation (Methods, and Appendix C.6).

The shift from gradual to abrupt boundaries is greatest when HOI coefficients are biased toward positive (facilitative) values ($\mu_B = 0.1$; Fig. 3.3**e**,**f**): fold boundaries dominate even at moderate α, and the transition to the abrupt regime occurs earlier and more completely than in the purely mixed case ($\mu_B = 0$). Strikingly, the effect of biodiversity is reversed in this regime. Whereas increasing community size n reduces fold prevalence in the competitive and mixed regimes – diversity buffers against abrupt extinctions – facilitative HOIs cause richer communities to be more prone to tipping-point collapse (Fig. 3.3**f**). These three

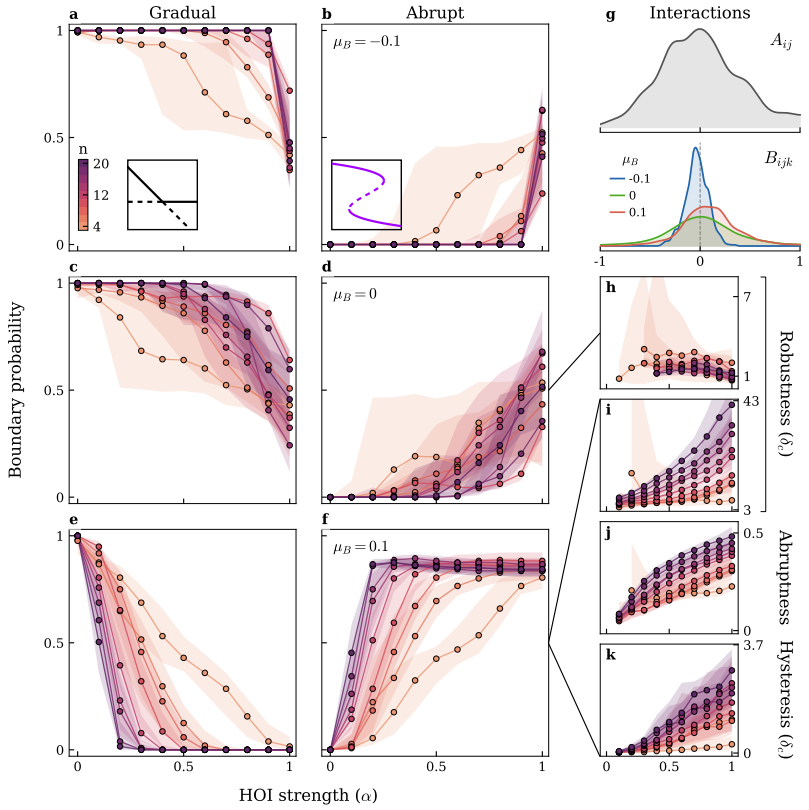

Figure 3.3: **The strength and sign of higher-order interactions controls tipping-point prevalence.** Panels show results for random multispecies communities ($\mu_A = 0$, $\sigma_A = \sigma_B = 1$) with three levels of HOI mean ($\mu_B \in \{-0.1, 0, 0.1\}$, rows). Panel **g** shows the empirical distributions of off-diagonal pairwise interactions A_{ij} (shared across μ_B, grey) and higher-order interactions B_{ijk} (coloured by μ_B) for communities of size $n = 4$. For each HOI strength (α, x-axis) and community size (n, colors), we perturb growth rates along 128 uniformly sampled directions and classify the first boundary encountered by the continued coexistence equilibrium. Panels **a-f** show the fraction of directions (y-axis) terminating at a gradual (left column) or abrupt (right column) boundary, for each value of μ_B (row); an estimator of boundary probability. Connected points give the median across replicates for each (n, α) condition. Panels **h-k** characterize the abrupt boundaries: (**h**, **i**) critical distance to the boundary δ_c for $\mu_B = 0$ (**h**) and $\mu_B = 0.1$ (**i**); (**j**) minimum species abundance at the equilibrium just before crossing the boundary ($x^{\star}_{\text{min}}$); (**k**) amount of δ that must be reversed before ecosystem recovery after collapse: zero indicates immediate recovery, values > 0 indicate hysteresis. (**j**) and (**k**) show results for $\mu_B = 0.1$. Note that in contrast to the competitive and mixed regimes (rows 1-2), increasing diversity in the facilitative regime (row 3) amplifies fold prevalence and community robustness as a function of α. Cases where no boundary was reached or where stability is lost before feasibility are infrequent for all α and n, and are omitted for clarity.

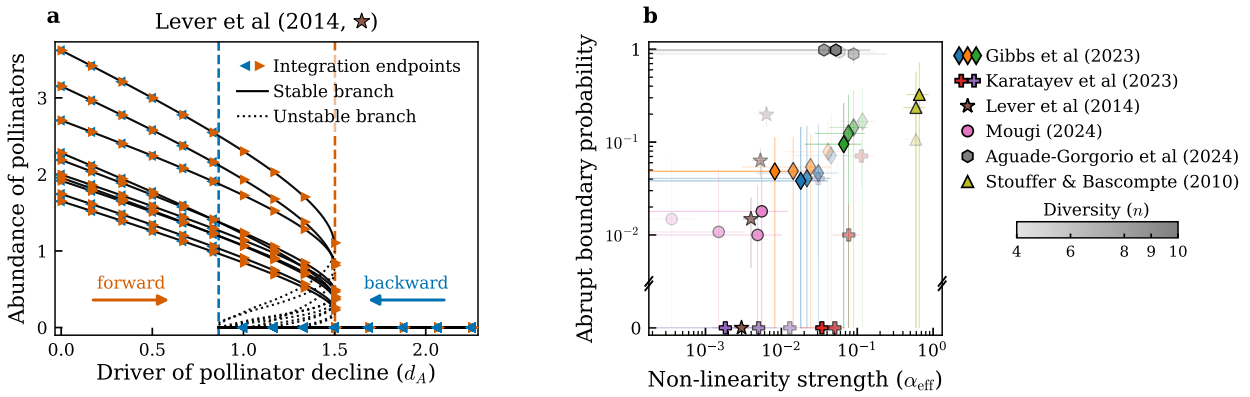

Figure 3.4: **Fold-mediated collapse is common in published multispecies ecological models. (a)** Bifurcation diagram for the canonical plant-pollinator model of Lever et al. (2014). Polynomial homotopy continuation tracks two equilibrium branches (stable, solid; unstable, dotted) as pollinator mortality d_A increases. The forward sweep (orange triangles) shows numerical integration endpoints confirming that the realized community state follows the stable branch until a fold bifurcation, where stable and unstable branches meet and annihilate (orange dashed vertical line). Beyond the fold, the system collapses to a zero-abundance state. The backward sweep (blue triangles) shows numerical integration from the collapsed state as the perturbation is gradually reduced, revealing hysteresis. **(b)** Fraction of perturbation directions terminating at a fold (abrupt) boundary versus effective nonlinearity strength α_{eff} across published multispecies ecological models (shapes). Shading indicates species richness. Diversity effects on fold prevalence are model-dependent: fold prevalence increases with richness in some systems (Aguadé-Gorgorió et al., Stouffer & Bascompte) but decreases in others (Lever et al.). Error bars show interquartile ranges across replicate parameterizations. Despite spanning different interaction types, functional forms, and parameterization schemes, models with stronger effective nonlinearity tend to exhibit a higher prevalence of fold-mediated coexistence loss, matching the pattern from our random HOI ensembles (Fig. 3.3).

qualitative patterns – the monotonic rise of fold prevalence with α, the earlier onset under facilitative HOIs, and the sign-reversal of the diversity effect across μ_B – persist when the mean pairwise interaction μ_A is also varied across competitive, mixed, and facilitative values (Appendix C.4, Fig. S3).

Panels **h-k** further characterize the abrupt boundaries in the $\mu_B \geq 0$ regime (results for all regimes in Appendix C.12). In the facilitative regime richer communities encounter more tipping point boundaries yet are farther from them in parameter space (panel **i**) – a tradeoff

between likelihood and imminence that is absent in the mixed regime (panel **h**), where δ_c is only weakly related to α for all community sizes. With increasing α, the species that goes extinct at the boundary retains higher abundance immediately before the tipping point is reached (panel **j**), indicating a more abrupt transition. Additionally, hysteresis strengthens (panel **k**): the perturbation must be reversed further before coexistence recovers.

When HOI coefficients are instead biased toward negative (competitive) values ($\mu_B = -0.1$; Fig. 3.3**a**,**b**), fold boundaries are largely suppressed: while abrupt extinctions occur, especially in small communities, coexistence is primarily lost through gradual extinctions even at high α. The suppression of folds in this regime raises a natural question: Are there conditions under which fold boundaries are ruled out entirely? A fold bifurcation requires two equilibria to collide and annihilate; if the coexistence equilibrium is globally asymptotically stable on the positive orthant, it is the only interior equilibrium and such collisions are precluded. Using a Lyapunov function [120, 143], we derive sufficient conditions on A and B that guarantee global stability and thereby rule out fold boundaries (Methods, and Appendix C.5). This result extends to the HOI setting a problem studied by Cenci and Saavedra [129] for nonlinear pairwise models: when do the equilibrium conditions remain topologically equivalent to the linear case, preserving uniqueness of the coexistence equilibrium (and precluding tipping points)?

3.4 Abrupt boundaries in pairwise models with nonlinearities

We used a random GLV+HOI model to explore whether fold bifurcations become typical when interactions are strongly state-dependent. Effective HOIs arise in any model with nonlinear interactions [3, 4, 144], with a non-random structure that reflects the underlying interaction mechanism(s). To test whether fold-mediated collapses also occur in such models, we applied our continuation framework to a canonical model of ecosystem collapse

in plant-pollinator networks [36], which features mutualistic interactions mediated by saturating functional responses. These saturating responses generate effective higher-order interactions (Appendix C.6), providing a concrete, mechanistic instance of the polynomial nonlinearity found in our GLV+HOI model. We implement the model for 10 plants and 10 pollinators following the original parameterization in [36] and apply our perturbation protocol. Using polynomial homotopy continuation, we map out the bifurcation where the system collapses (Fig. 3.4**a**; see Appendix C.6 for details), confirming that it encounters a fold bifurcation, with hysteresis delimited by the endpoints of the stable and unstable branches, as in Fig. 3.1**b**. This example illustrates the power of our homotopy continuation approach to resolve the structure of bifurcations in complex ecological models: the collapse in this model has long been conjectured to be a tipping point, but establishing this formally is challenging using only simulations of the model dynamics [139].

To test whether tipping points are typical across other nonlinear interaction models, we repeated our perturbation protocol on a range of published multispecies models spanning competitive HOIs [145], consumer-resource systems [138], food webs with ecosystem-engineering effects [146], mixed competitive-facilitative communities [147], and empirical trophic networks [148] (Fig. 3.4**b**, and Appendix C.6). Despite the diverse origins and interaction types in these models, the results are consistent with our random ensembles: models with stronger effective nonlinearity (α_{eff}, Appendix C.6) exhibit a high fraction of fold-mediated boundaries. In line with our finding that diversity can increase or decrease the prevalence of fold bifurcations depending on the sign of HOIs, the effect of diversity varies across models.

3.5 Discussion

Our results show that higher-order interactions make fold-mediated, tipping-point loss of coexistence a common route to community collapse. We find the same outcome using alternative HOI sampling approaches [145] and in other nonlinear models including: mutualistic plant-pollinator networks [36, 148], consumer-resource systems with nonlinear functional responses [138], and communities with adaptive foraging [146] or multiple interaction types [147]. This cross-model comparison suggests that tipping points are a widespread consequence of nonlinear state-dependent interactions in complex communities.

We further found that the mean HOI effect controls important features of the transition from gradual to abrupt extinctions. HOIs that are facilitative on average make fold boundaries dominant even at weak nonlinearity, whereas competitive HOIs largely suppress them. Tipping points in ecological models have often been associated with positive feedback loops, such as in mutualistic systems [35, 133]. The facilitative HOI regime mirrors this type of mechanism because HOIs tend to weaken antagonistic pairwise effects (and amplify mutualistic ones). HOIs contribute more strongly to net growth rates when most species are relatively abundant, while pairwise effects dominate when abundances are lower. This creates the conditions for multistability, driven by a diffuse positive feedback loop between abundances and growth rates: HOIs can rescue the community from extinctions driven by pairwise interactions, but only once abundances are sufficiently high. Consistent with this interpretation, we found that HOIs simultaneously increase the prevalence of tipping points and the distance to a coexistence boundary (Fig. 3.3**i**), postponing extinctions compared to the pairwise baseline (consistent with experimental evidence [149]). However, this difference in tipping-point prevalence is driven by subtle changes in the mean HOI effect (Fig. 3.3**g**). Even in the facilitative regime, many individual HOIs are negative, suggesting that specific interaction structures are not necessary for tipping points to become common. Furthermore,

restricting interactions to be only negative (purely competitive, Appendix C.4) does not change the increased prevalence of folds with α.

Our analysis focused throughout on the focal equilibrium that is continuous with the unique coexistence equilibrium in the pairwise GLV model, but HOIs generically create additional coexistence states [113–115]. This implies that a complete picture of community robustness must account for both the size and shape of the local feasibility domain around each equilibrium, but also the total number and distribution of equilibria. Accounting for this global picture, nonlinearities might make any particular community more prone to tipping abruptly but increase the chances that the community shifts to an alternative coexistence state.

We also focused on loss of equilibrium feasibility; however, coexistence can alternatively be lost via instability, mediated for example by delayed feedbacks [150] or explicit time delays [151]. Characterizing when each route dominates is an important open question (see Chapter 1 for the pairwise competitive case [77]).

Our analysis leveraged polynomial homotopy continuation to navigate the nonlinear feasibility domains that arise in large ecological communities with nonlinear and nonpairwise interactions. This numerical technique has significant potential to extend the structural-stability perspective beyond pairwise models and help unify our understanding of the regime shifts that occur in complex ecological models. We may also gain a deeper understanding of these systems by looking across fields: "explosive" discontinuous transitions [152] have been reported in higher-order network models of contagion [153, 154], synchronization [155], and social dynamics [156], typically derived from mean-field reductions. Whether these transitions share a formal connection with the species-resolved fold bifurcations we identify here is an intriguing parallel that warrants further investigation.

Taken together, our findings show that HOIs add more than quantitative corrections to pairwise coexistence theory. They qualitatively transform the geometry of coexistence,

replacing gradual erosion of coexistence with abrupt hysteretic collapse as the generic mode of community failure. This perspective provides a missing link between structural-stability theory, which quantifies how large the safe operating space is, and critical-transitions theory, which determines what happens when its boundary is crossed. By mapping how the strength and sign of nonlinear interactions govern tipping-point prevalence across diverse community types, our results establish a baseline expectation for when abrupt ecosystem collapse may become typical.

3.6 Materials and methods

3.6.1 Polynomial Homotopy Continuation

Following Eq. (3.1) we define the coexistence equilibrium as any real solution $\mathbf{x}^\star \in \mathbb{R}^n_{>0}$ of

$$r_i + (1-\alpha)\sum_{j=1}^{n} A_{ij}x_j^\star \;+\; \alpha \sum_{j,k=1}^{n} B_{jki}\, x_j^\star x_k^\star \;=\; 0, \tag{3.3}$$

for $1 \le i \le n$. When we perturb the growth-rate as $\mathbf{r}_0 + \delta\mathbf{u}$ (see Eq. (3.2)) we obtain from (3.3) the following system of polynomial equations depending on both $\mathbf{x}$ and δ:

$$H_i(\mathbf{x},\delta) = (r_i^0 + \delta u_i) + (1-\alpha)\sum_j A_{ij}\, x_j + \alpha \sum_{j,k} B_{ijk}\, x_j x_k,$$

The coexistence equilibrium $\mathbf{x}^\star$ corresponding to $H(\mathbf{x},\delta) = 0$ depends continuously on δ. Therefore, if we move δ in a continuous way, $\mathbf{x}^\star$ will move along. This observation is the basis of polynomial homotopy continuation [11].

If $\frac{\mathrm{d}}{\mathrm{d}\mathbf{x}}H$ is invertible at $(\mathbf{x},\delta)$, the implicit function theorem implies that $\mathbf{x} = \mathbf{x}(\delta)$ is

locally a differentiable function of δ. Implicit differentiation yields

$$\frac{\mathrm{d}H}{\mathrm{d}\mathbf{x}}\,\dot{\mathbf{x}} \;+\; \frac{\mathrm{d}H}{\mathrm{d}\delta} = 0. \tag{3.4}$$

We always have the initial equilibrium $\mathbf{x}^\star = \mathbf{1}$ corresponding to $\delta = 0$, by construction (see Parameter sampling protocol, below). Together with Eq. (3.4) this defines an initial value problem, which can be solved using numerical integration. All of this is implemented to be used out-of-the-box in the software `HomotopyContinuation.jl` [125], which we use in our work.

3.6.2 Parameter sampling protocol

To isolate the effect of HOI strength α on the geometry of feasibility boundaries, we construct random communities that share a common baseline coexistence state across all α. Off-diagonal pairwise entries are drawn as $A^0_{ij} \sim \mathcal{N}(\mu_A, n^{-1})$ and HOI entries as $B^0_{ijk} \sim \mathcal{N}(\mu_B, n^{-2})$, where the variance scalings ensure that both pairwise row sums and HOI slice sums contribute $O(1)$ to per-capita growth rates as community size grows. Diagonal entries are then set so that row sums of A and slice sums of B each equal -1, planting a coexistence equilibrium $\mathbf{x}^\star = \mathbf{1}$ corresponding to $\mathbf{r} = \mathbf{1}$ for every $\alpha \in [0, 1]$. Local stability is guaranteed by rescaling each matrix by its symmetrised spectral radius and subtracting a unit diagonal, so that the symmetrised pairwise and HOI sectors (S_A and S_B) are each negative definite (Appendix C.1). Because the Jacobian at $\mathbf{x}^\star$ is a convex combination of these two sectors, Hurwitz stability holds for all α. For each community realisation, the same bank of perturbation directions $\{\mathbf{u}_k\}$, sampled uniformly on the unit sphere, is used across all α, so that changes in boundary-type frequency reflect reshaping of the feasibility domain rather than a changing reference state or perturbation set. See Appendix C.4 for details.

3.6.3 Boundary detection with homotopy continuation

For each perturbation direction $\mathbf{u}$, we track the coexistence equilibrium from $\delta = 0$ to $\delta_{\max}$ using coefficient-parameter homotopy continuation implemented in [125]. At each continuation step we monitor the tracked solution for three boundary events: (i) a gradual boundary, where the minimum species abundance drops below $x_{tol} = 10^{-9}$, signalling a transcritical bifurcation; (ii) an abrupt boundary, where the tracker terminates before any component reaches x_{tol}, signalling a fold bifurcation at which the Jacobian $\frac{\mathrm{d}H}{\mathrm{d}\mathbf{x}}$ becomes singular and the real equilibrium branch ceases to exist; and (iii) an unstable boundary, where the leading eigenvalue of the community Jacobian $J = D(\mathbf{x}^\star)\, J_F$ crosses $\lambda_{\mathrm{tol}} = 10^{-9}$. Along each direction, we record the type of the boundary and the value δ_c. Complete details on the algorithmic approach are given in Appendix C.2.

3.6.4 Computing the feasibility boundaries analytically for $n = 2$

To compute the gradual and abrupt boundary analytically, we substitute in (3.3) $A'_{ij} = (1-\alpha)A_{ij}$ and $B'_{jki} = \alpha B_{jki}$, and obtain polynomials

$$f_i(\mathbf{x}, \mathbf{r}, \mathbf{A'}, \mathbf{B'}) = r_i + \sum_{j=1}^{n} A'_{ij} x_j \; + \; \sum_{j,k=1}^{n} B'_{jki}\, x_j x_k.$$

The gradual boundary consists of those parameters $\mathbf{r}, \mathbf{A'}, \mathbf{B'}$, such that there exists an $\mathbf{x}^\star$ with

$$\begin{aligned} &x_1^\star \cdot x_2^\star \cdots x_n^\star = 0 \quad \text{and} \\ &f_1(\mathbf{x}^\star, \mathbf{r}, \mathbf{A'}, \mathbf{B'}) = \cdots = f_n(\mathbf{x}^\star, \mathbf{r}, \mathbf{A'}, \mathbf{B'}) = 0\,. \end{aligned}$$

The first condition means that at least one entry of $\mathbf{x}^\star$ is zero, while the second line implies that $\mathbf{x}^\star$ is a solution of (3.3). The Tarski-Seidenberg theorem [157, Theorem 4.17] implies that the gradual boundary is a semialgebraic set (a set defined by polynomial equations and inequalities). While computing all equations and inequalities of a semialgebraic set is a challenging problem, computing only the equations is easier, using elimination theory [25, Chapter 3] and exact computer algebra [158]. The polynomials above generate a polynomial ideal [25]

$$I_{\text{gradual}} = \langle x_1 \cdot x_2 \cdots x_n, f_1, \cdots, f_n \rangle.$$

Eliminating $\mathbf{x}$ from the ideal I_{gradual} and substituting back $A'_{ij} = (1-\alpha)A_{ij}$ and $B'_{jki} = \alpha B_{jki}$ we obtain an ideal J_{gradual} generated by polynomials in $\mathbf{r}, \alpha, \mathbf{A}, \mathbf{B}$, that define the Zariski closure of the gradual boundary (i.e., the smallest algebraic variety – a set defined as the vanishing locus of finitely many polynomials – containing the gradual boundary). We find that J_{gradual} is generated by a single polynomial Δ_{gradual} (see Appendix C.3).

Similarly, for the abrupt boundary we can eliminate $\mathbf{x}$ from the ideal

$$I_{\text{abrupt}} = \langle \det \text{Jac}, f_1, \cdots, f_n \rangle,$$

where Jac denotes the Jacobian matrix of the polynomials in (3.3) (Appendix C.1). Eventually, we obtain the ideal J_{abrupt} generated by a single polynomial Δ_{abrupt} in $\mathbf{r}, \alpha, \mathbf{A}, \mathbf{B}$, that define the Zariski closure of the abrupt boundary (see Appendix C.3). This polynomial has 17,586 terms, underscoring the complexity of elimination. Recently, methods from numerical algebraic geometry have emerged to tackle elimination ideals [159] which are infeasible to compute using exact computer algebra.

3.6.5 Global stability rules out fold bifurcations

A fold bifurcation requires two equilibria to collide and annihilate; if the coexistence equilibrium $\mathbf{x}^\star$ is globally asymptotically stable on the positive orthant $\mathbb{R}^n_{>0}$, it is the only interior equilibrium and such collisions are precluded. We derive sufficient conditions for global stability using Goh's Lyapunov function [14, 120, 143]

$$V(\mathbf{x}) = \sum_{i=1}^{n} \Big(x_i - x_i^\star - x_i^\star \ln(x_i/x_i^\star) \Big), \tag{3.5}$$

which is non-negative on $\mathbb{R}^n_{>0}$ and vanishes only at $\mathbf{x}^\star$. Using $\dot{x}_i = x_i f_i(\mathbf{x})$ and $f(\mathbf{x}^\star) = 0$, together with the path integral $f(\mathbf{x}) - f(\mathbf{x}^\star) = [\int_0^1 \nabla f(\mathbf{x}^\star + t(\mathbf{x} - \mathbf{x}^\star))\, dt](\mathbf{x} - \mathbf{x}^\star)$, its derivative along trajectories takes the quadratic form

$$\dot{V} \;=\; (\mathbf{x} - \mathbf{x}^\star)^\top \left[(1-\alpha)\, S_A + \alpha \sum_{k=1}^{n} \tfrac{x_k + x_k^\star}{2}\, S_k \right] (\mathbf{x} - \mathbf{x}^\star), \tag{3.6}$$

where $S_A = (A + A^\top)/2$ and $(S_k)_{ij} = (B_{ijk} + B_{jik})/2$ (assuming $B_{ijk} = B_{ikj}$). Because each $(x_k + x_k^\star)/2 > 0$ on $\mathbb{R}^n_{>0}$, the bracketed matrix is a conic combination of S_A and the slice matrices $\{S_k\}_{k=1}^n$. A sufficient condition for $\dot{V} < 0$ everywhere, and hence for global stability, is therefore that $S_A \prec 0$ and $S_k \prec 0$ for every $k = 1, \ldots, n$ – the slice-wise negative-definiteness condition. An equivalent condition arises in the theory of nonlinear complementarity problems via strict monotonicity of $F = -f$ [160] (see Appendix C.5).

Acknowledgments: P.L.A. acknowledges helpful discussions with E. Alastrue de Asenjo, K. Lee, S. Pawar, S. Kuehn, S. Sheik, M. Tikhonov and T. Wootton.

Funding: P.B. was supported by DFG, German Research Foundation – Projektnummer 445466444.

Author contributions: P.L.A. designed the study and performed the research, with advice from Z.M. and M.P.; P.L.A. wrote the manuscript, with advice from Z.M. and M.P.; P.L.A.,

P.B., and A.L. developed the code; P.L.A, Z.M, P.B. and S.A. performed the derivations. All authors contributed to the mathematical derivations, the implementation of the code, edited the manuscript, and discussed and interpreted the results.

Competing interests: The authors declare no competing interests.

Materials & Correspondence: All materials and correspondence requests should be addressed to plechon@uchicago.edu or zachary.miller@yale.edu.

Data & Code availability: Simulations data needed to reproduce the figures is deposited at https://doi.org/10.5281/zenodo.19892157. Code to reproduce all findings can be found at https://github.com/pablolich/tipping_hoi.

CONCLUSION

Taken together, the three chapters yield an expectation about fundamental behaviors of the family of models in Eq. (2), by asking about existence as a function of self-regulation (Chapter 1), the amount of complexity in the form of interaction order (Chapter 2), and the strength of three-way interactions as the environment changes (Chapter 3). This is the sense in which random ecosystems are an expectation generator: whatever the ensemble produces generically needs no special explanation. The three questions are questions about one object, the domain of parameters compatible with coexistence: whether the parameters of a community fall inside it, how many feasible equilibria it holds, and what its boundary is made of. We thus return to the question with which this thesis began, whether the configuration of a system is compatible with a state in which all of its species coexist, and know that three things are not surprising: equilibrium dynamics in large competitive Lotka–Volterra communities, which converge to a globally stable equilibrium whether or not every species in the pool survives; the feasibility of many-species ecosystems with enough complexity and balanced interactions, which the proliferation of equilibria brings about on its own; and tipping points in diverse ecosystems with enough nonlinearity, which follow from the collision of equilibria that nonlinearity creates. We believe that the techniques and findings of this dissertation leave open promising questions, three of which we discuss next: coexistence away from equilibrium, the return to mechanistic models, and the multiplicity of stable states.

To begin with, this work has been concerned almost exclusively with equilibrium coexistence. Chapter 1 showed that in large competitive communities a feasible equilibrium is stable with a probability that approaches one with size; Chapter 2 counted the feasible equilibria that are unstable, but never asked what dynamics they support; and Chapter 3 followed a stable state, which rarely lost its stability before it lost its existence. There is,

however, a whole class of coexistence away from equilibrium, sustained cycles or chaos along which every species persists, which may be prevalent in systems whose interactions are not competitive on average, or which are strongly forced by noise. The notion suited to the study of non-equilibrium coexistence is permanence: every trajectory that starts in the interior of the positive orthant eventually stays bounded away from its boundary, whether or not it settles down [14, 161]. A permanent system must possess an interior equilibrium, stable or not [14], so feasibility is necessary not only for coexistence at equilibrium but for coexistence of (almost) any kind. The equilibrium-only coexistence results of Chapter 1 were derived for competitive communities. Whether feasibility precedes stability when a substantial fraction of the interactions is positive is not known, and it is there that the expectation of equilibrium dynamics could give way to persistent fluctuations [75, 162]. We return to the move promised in the introduction: results obtained for the class in Eq. (2) can be carried back to a model of interest and tested there. Chapter 3 took a first step by repeating its protocol on published models with nonlinear interactions [36, 138, 146, 147]. Consumer–resource models of microbial communities with cross-feeding, the class we used to study community coalescence [163], are the natural next stop, for two reasons. First, they are a class in which higher-order interactions can be derived: when resources equilibrate fast, eliminating them leaves a Lotka–Volterra model for the consumers whose higher-order terms are fixed by the metabolic wiring [61, 144, 164]. Second, their parameters have an experimental meaning: resource supply, leakage and yields are quantities one controls in a flask [165, 166].

Whether such communities tip is unresolved, and the literature points in two directions. In a structural model, in which a consumer persists only if every metabolite it requires is produced by someone else, cross-feeding creates folds, hysteresis and cascading losses of diversity as the connectivity of the metabolic network changes [167]. In a dynamical model of consumers exchanging essential resources, the equilibrium is unique and its stability changes continuously with supply [168]. The two differ in whether the dependence on a partner is

obligate: in the first, an unmet requirement is fatal; in the second, the essential resources are also supplied from outside. The classical two-species theory suggests that this is the axis that matters. Vandermeer and Boucher [169] separated facultative from obligate mutualists by the sign of the growth rate in the partner's absence, and showed that obligate mutualism with a saturating benefit produces a threshold: a saddle below which both partners go extinct and a node above it, which is the fold of Chapter 3 in its simplest form. The same fold appears for two cross-feeders in a chemostat, where the dilution rate moves the system across it [170], and it has been observed: the same pair of yeast strains behaves as an obligate mutualism, a facultative one, or a competition depending only on how much of the exchanged resources the medium supplies [166]. The question we would like to ask is therefore whether obligacy, the dependence on a partner with no alternative supply, is the quantity that decides if a many-species cross-feeding community can tip, and whether the prevalence of folds that Chapter 3 measured against the strength of higher-order interactions can be re-expressed in the coordinates that set obligacy in an experiment. This question is the subject of ongoing work.

The states that this dissertation has counted and followed are those in which every species is present, whereas a growing literature is concerned with communities that hold several stable states at once, most of them missing some of the species in the pool [147, 162, 171, 172]. The two questions are the same question asked on different faces of the positive orthant. The random pairwise model organizes these states into phases. For weak or homogeneous interactions the dynamics reach a single such state from any initial condition; beyond a critical heterogeneity the number of equilibria grows exponentially with diversity [162, 172, 173], the state reached depends on history, and, for symmetric interactions, the survivors of every assembled state sit at the edge of stability, with the spectrum of their stability matrix touching zero [174]. The same sequence of phases has been traversed experimentally by bacterial microcosms as diversity and interaction strength increase [75]. Chapter 1 locates

competitive communities on this diagram. The threshold α_S is a sufficient condition for the unique phase: above it, whichever species survive converge to one globally stable state that none of the others can invade, so alternative stable states require self-regulation below α_S; and since the transition to stability precedes the transition to feasibility with probability one, the whole region in which the full community can coexist lies inside the unique phase.

Similar phases exist when the interactions are nonlinear. The boundary at which the unique fixed point gives way to multiple attractors has recently been derived for Lotka–Volterra models with a saturating functional response (the class of pairwise nonlinearity that Chapter 3 showed to fold): by Zenari et al. [175] for random nonreciprocal interactions, and by Patil and Altieri [176] for the bipartite mutualistic networks (such as the plant–pollinator model). For a nonlinear model, that boundary is also a sufficient condition for tipping points to happen. A fold is the collision of two equilibria, so it cannot occur while the fixed point is unique. Whether the prevalence of folds measured in Chapter 3 switches on at that boundary, so that the fold region of the nonlinear model and the multiple-attractor phase of the disordered-systems literature are one region drawn on the same axes, is a question we are asking.

With this thesis we have illustrated that feasibility is more than a boring mathematical requirement, and that higher-order interactions are more than quantitative corrections to the Lotka–Volterra model. We have shown that, although challenging, the feasibility of these models is a tractable problem. In doing so, we have drawn from mathematical techniques like the theory of resolvents and numerical and random algebraic geometry, which are rarely used in the ecological literature. These techniques have allowed us to uncover generic behaviors about the ecological dynamics, coexistence, and collapse of complex, highly nonlinear, ecological models.

Feasibility entered the debate half a century ago, with Roberts's response to May [12, 16], and a lineage of work has since steadily carried that question forward until today [17–20, 29–

33, 40, 46, 47, 50, 51, 58, 60, 78–80, 82, 113–115, 129, 145]. This dissertation has followed that question from the single equilibrium of the linear model to the many equilibria of the nonlinear one, overturning some classic expectations from pairwise models along the way and opening the door to new research on highly nonlinear ones.

APPENDIX A

SUPPLEMENTARY INFORMATION: ROBUST COEXISTENCE IN COMPETITIVE ECOLOGICAL COMMUNITIES

A.1 Preliminaries: competitive Generalized Lotka-Volterra models

We consider the dynamics of ecological communities composed of n interacting populations, and following the Generalized Lotka-Volterra (GLV) model[6, 7, 56]:

$$\dot{x}_i = x_i r_i \left(1 - \sum_j A_{ij} x_j\right), \tag{A.1}$$

where $x_i(t) \equiv x_i$ is the density of population i at time t, $\dot{x}_i \equiv dx_i(t)/dt$ its time derivative, r_i is the intrinsic growth/death rate of population i, achieved when growing in isolation at low abundance, and A_{ij} is the amount by which population j depresses/enhances the growth of population i.

We analyze cases in which all populations can grow in isolation ($r > \mathbb{0}$), and, moreover, interactions are "mostly competitive" (defined below). Following May[12], we write A as the sum of two matrices:

$$A = \alpha I + B \quad ,$$

with $\alpha \geq 0$. Then, B collects all the inter-specific interactions, as well as the baseline levels of intraspecific interactions, and α can be interpreted as the "excess" intraspecific competition in the system.

We call the system *competitive* whenever $r > \mathbb{0}$, and $\frac{1}{n} B^T \mathbb{1} = m > \mathbb{0}$ (i.e., the column

means of B are all positive, and thus the columns of B sum to positive values). While not *every* interaction needs to be competitive, each population must, on average, depress the growth of the others.

An equilibrium $x^\star$ for this system is a point at which all the derivatives in Eq. (A.1) vanish. We say that the equilibrium is feasible if $x^\star > \mathbb{0}$. In this work, we analyze the effect of α on the existence of a feasible equilibrium for competitive GLV systems.

A.1.1 Local stability

The goal of this section is to show that there exists a level of $\alpha = \alpha_L$, corresponding to the celebrated May's bound[12], that guarantees that all the eigenvalues of A have positive real part, and discuss its implication for local stability.

The eigenvalues of A are related to the eigenvalues of B, which are generically complex numbers of the form $\lambda_j(B) = \gamma_j + i\beta_j$, with $i = \sqrt{-1}$. Because the matrix B is composed of real numbers, whenever $\lambda_j(B) = \gamma_j + i\beta_j$ is an eigenvalue, then $\lambda_k(B) = \gamma_j - i\beta_j = \lambda_j^*(B)$, i.e., its conjugate, is also an eigenvalue. Adding a constant diagonal αI to B results in a shift in the real part of all the eigenvalues: $\lambda_j(A) = \lambda_j(\alpha I + B) = \alpha + \gamma_j + i\beta_j$. Hence, whenever $\alpha > \alpha_L = \min\{0, \min_j \mathcal{R}\rceil(\lambda_j)\}$, all eigenvalues of $\alpha I + B$ are contained in the right half of the complex plane, and thus have positive real part.

This is important for the local stability of an equilibrium of the GLV system in Eq.(A.1). An equilibrium $x^\star$ is said to be *locally asymptotically stable* if trajectories originating arbitrarily close to it eventually converge to it. An equilibrium is locally stable if all the eigenvalues of the Jacobian matrix of the system of differential equations, evaluated at the equilibrium, have negative real part. The Jacobian for Eq.(A.1) evaluated at $x^\star > \mathbb{0}$ is simply:

$$J|_{x^\star} = -D(x^\star \circ r)A \quad ,$$

where $D(z)$ is a matrix with the vector z on the diagonal, and $\circ$ represents the Hadamard (element by element) product. Hence, if all the eigenvalues of A have positive real part, and we were to choose r such that $r_i = 1/x_i^\star$, the equilibrium would be locally asymptotically stable.

Whenever $A = \alpha I + B$, we have that both A and $x^\star$ depend on α, while the vector r does not. We can write:

$$J|_{x^\star} = D(r)(-D(x^\star)A) \quad ,$$

to stress the fact that only the part in parenthesis is influenced by α. Importantly, we could have that $-D(x^\star)A$ has only eigenvalues with a negative real part, while $J|_{x^\star}$ does not. For example, take the competitive GLV system with:

$$A = \begin{pmatrix} 1 & 2 & 3 \\ 2 & 3 & 0 \\ 0 & 3 & 1 \end{pmatrix} \qquad x^\star = \frac{1}{17}\begin{pmatrix} 1 \\ 5 \\ 2 \end{pmatrix} \quad . \tag{A.2}$$

The system is feasible (for any choice of $r > \mathbb{0}$). However, the local stability of the equilibrium depends on the choice of r. For $r = \mathbb{1}$, we have that the eigenvalues of $J|_{x^\star}$ are $(-1, -\frac{1}{34}(1 \pm i\sqrt{39}))$ and the equilibrium is thus locally stable. However, by increasing the value of r_1 we observe a bifurcation: the real part of the maximum eigenvalue becomes positive and the system loses stability, as shown in Figure A.1.

Thus, in general, the stability of a feasible equilibrium $x^\star > \mathbb{0}$ might depend on the choice of r. However, if A is "sufficiently" stable, then the stability of any *feasible* equilibrium is guaranteed for *any* choice of $r > \mathbb{0}$, as discussed below.

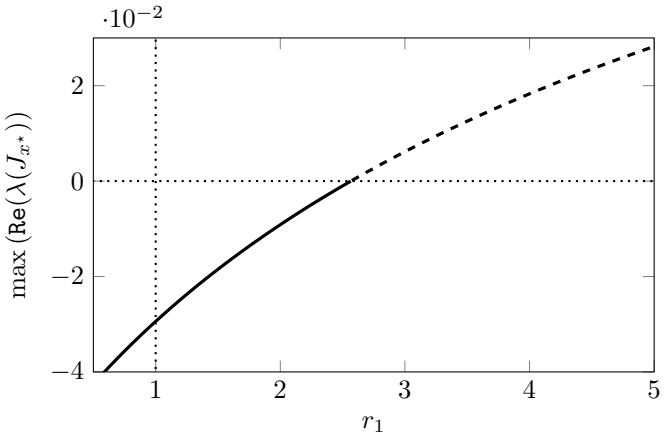

Figure A.1: **Bifurcation diagram obtained by varying the growth rates for the three species system in Eq.** (A.2)**.** When the growth rates are chosen as $r = (r_1, 1, 1)^T$, the system experiences a transition from stability to instability as the maximum of $\mathcal{R}](\lambda(J|_{x^\star}))$ changes sign from negative to positive. The bifurcation occurs at about $r_1 = 2.57$ as r_1 is varied in the range $[1/2, 5]$, but the system remains feasible throughout.

A.1.2 Types of dynamics

Despite its simplicity, the competitive GLV model can give rise to any type of dynamics, including limit cycles and chaos. For purely competitive systems with positive growth rates, when there is a single population, dynamics will always converge to an equilibrium; for two populations, dynamics will generically converge to an equilibrium at which point either population, or both, are present; for three or more populations, one can observe limit cycles, and chaos for four or more populations[52, 53].

Importantly, a necessary condition for the coexistence of all the populations is the existence of a feasible equilibrium $x^\star > \mathbb{0}$, which is also the time-average of the orbits[14]. When such a feasible equilibrium does not exist, trajectories can either reach the boundaries of $\mathbb{R}^n_+$ (i.e., populations undergo extinction), or escape to infinity. When interactions are purely competitive, populations limit each others' growth and divergences to infinity are precluded; therefore, in the absence of a feasible equilibrium, some populations will necessarily go extinct.

A.1.3 Global stability and saturated equilibria

The goal of this section is to show that there exists a further bound $\alpha = \alpha_S \geq \alpha_L$ that guarantees that a) any feasible equilibrium is locally asymptotically stable, i.e., whenever the densities are slightly perturbed away from the equilibrium, they will eventually return to it; b) the equilibrium is in fact *globally* stable, i.e., any perturbation short of extinction will eventually subside; c) dynamics are guaranteed to result in an equilibrium; d) this equilibrium is *saturated*: some of the populations coexist at a feasible, globally stable equilibrium, and the rest of the populations are extinct and cannot re-invade the system when introduced at low abundance.

In the section discussing local stability, we have shown that choosing $\alpha = \alpha_L$ guarantees local stability for a specific choice of r. However, whenever $A + A^T$ is positive definite (i.e., has only positive eigenvalues), then a) dynamics will always converge to an equilibrium, $\bar{x}$; b) the equilibrium $\bar{x}$ is saturated, meaning that if any population goes extinct, it cannot re-invade the system when starting from low abundance; c) $\bar{x}$ is globally stable (i.e., for any choice of $r > \mathbb{0}$ and initial conditions $x > \mathbb{0}$, dynamics asymptotically converge to $\bar{x}$).

We adapt the proof found for example in Hofbauer & Sigmund[14], because this result is important for our discussion on the dynamics of large competitive communities with random interactions.

We order the vector of densities of the populations in Eq. (A.1) as $x = (y, z)^T$, where y are the densities of the (unknown) set of the k populations that coexist at the saturated equilibrium, and z the densities of the $n - k$ populations that are extinct at the saturated equilibrium. Therefore $\bar{x} = (y^\star, \mathbb{0})^T$. We also consider a vector of positive weights $w > \mathbb{0}$, which we will use to prove stability. We partition the vector of growth rates, the vector of weights w, and the matrix of interactions according to whether the populations belong to

the set that coexists, or that that goes extinct:

$$w = \begin{pmatrix} u \\ v \end{pmatrix} > \mathbb{0} \quad r = \begin{pmatrix} a \\ b \end{pmatrix} > \mathbb{0} \quad A = \begin{pmatrix} \mathcal{A} & \mathcal{B} \\ \mathcal{C} & \mathcal{D} \end{pmatrix} \quad .$$

Next, we consider the candidate Lyapunov function[143]:

$$V(y,z) = \sum_i u_i \left(y_i - y_i{}^\star - y_i{}^\star \log \frac{y_i}{y_i{}^\star} \right) + \sum_l v_l z_l \quad .$$

The function is positive for any $y > \mathbb{0}$ and $z > \mathbb{0}$ (i.e., for any positive initial conditions), given that $u, v, y^\star$ are all positive. Moreover, the function is exactly zero at the saturated equilibrium $\bar{x} = (y^\star, \mathbb{0})^T$. We choose $u_i = 1/a_i$, and $v_l = 1/b_l$, and then differentiate with respect to time:

$$\begin{aligned} \frac{dV(y,z)}{dt} =& \sum_i (y_i - y_i{}^\star) \left(1 - \sum_j \mathcal{A}_{ij} y_j - \sum_k \mathcal{B}_{ik} z_k \right) \\ &+ \sum_l z_l \left(1 - \sum_j \mathcal{C}_{lj} y_j - \sum_k \mathcal{D}_{lk} z_k \right) \quad . \end{aligned}$$

We define $\Delta y_i = y_i - y_i{}^\star$; noticing that $1 = \sum_j \mathcal{A}_{ij} y_j{}^\star$ we can write:

$$\frac{dV(y,z)}{dt} = -\sum_{i,j} \Delta y_i \mathcal{A}_{ij} \Delta y_j - \sum_{i,k} \Delta y_i \mathcal{B}_{ik} z_k - \sum_{l,k} z_l \mathcal{D}_{lk} z_k + \sum_l z_l \left(1 - \sum_j \mathcal{C}_{lj} y_j \right) \quad .$$

Now we add and subtract $\sum_l z_l \sum_j \mathcal{C}_{lj} y_j{}^\star$, thereby obtaining:

$$\begin{aligned} \frac{dV(y,z)}{dt} =& -\sum_{i,j} \Delta y_i \mathcal{A}_{ij} \Delta y_j - \sum_{i,k} \Delta y_i \mathcal{B}_{ik} z_k - \sum_{l,j} z_l \mathcal{C}_{lj} \Delta y_j \\ &- \sum_{l,k} z_l \mathcal{D}_{lk} z_k + \sum_l z_l \left(1 - \sum_j \mathcal{C}_{lj} y_j{}^\star \right) \quad . \end{aligned}$$

Thus, $dV(y,z)/dt$ is the sum of two parts. The first part can be rewritten as a quadratic form:

$$-\sum_{i,j}\Delta y_i \mathcal{A}_{ij}\Delta y_j - \sum_{i,k}\Delta y_i \mathcal{B}_{ik} z_k - \sum_{l,j} z_l \mathcal{C}_{lj}\Delta y_j - \sum_{l,k} z_l \mathcal{D}_{lk} z_k = -\sum_{i,j}(x_i - \bar{x}_i)A_{ij}(x_j - \bar{x}_j) =$$
$$-(x-\bar{x})^T A(x-\bar{x}) = -\frac{1}{2}(x-\bar{x})^T\left(A + A^T\right)(x-\bar{x}) \quad ,$$

and is thus negative whenever $A + A^T$ is positive definite.

Finally, $(1 - \mathcal{C}y^\star)_j$ is positive only when population j can grow (and thus invade the system) when the system is resting at the saturated equilibrium. Hence, by the definition of a saturated equilibrium, this term is also negative, and the proof is complete.

Note that the real parts of the eigenvalues of A are bounded from above and below by those of $H = \frac{1}{2}(A + A^T)$, as stated by Bendixson's inequality; in particular, if we order the eigenvalues of H in ascending order, $\lambda_1(H) \leq \lambda_2(H) \leq \ldots \leq \lambda_n(H)$, we have

$$\lambda_1(H) \leq \mathcal{R}]\lambda_i(A) \leq \lambda_n(H) \quad ,$$

with equality guaranteed for symmetric matrices A (in which case we have $H = A$). Thus, we have that $\alpha_L \leq \alpha_S$ (as expected, given that a globally stable equilibrium must be locally stable as well).

In summary, we have shown that, provided that $r > \mathbb{0}$ and that we chose $\alpha > \alpha_S$ such that the symmetric part of A, H, is positive definite, dynamics will always converge to an (unspecified) saturated equilibrium. This is a *sufficient* condition for dynamics to converge to a saturated equilibrium, which can be made slightly more general. For example, whenever one can choose a positive vector $h > \mathbb{0}$ such that $D(h)A + A^T D(h)$ is positive definite, then the stability of dynamics is also ensured[143]. Because we are interested in an upper bound that is easy to calculate, we just analyze the case in which H is positive definite.

A.1.4 Assembly

This section discusses the assembly of systems for which $\alpha > \alpha_S$, i.e., whether the systems can be built from the bottom up through successive invasions. We can devise an "assembly graph" in which the nodes represent the subset of populations that can coexist, and the edges invasions moving the system from one state to another[54, 161]. Naturally, this graph representation is an especially good choice for systems in which the dynamics of any feasible sub-community settle at an equilibrium, invasions are rare, and spaced apart in time[54].

When $\alpha > \alpha_S$, then this relationship is maintained for any sub-system (because all the sub-matrices of H obtained by removing some rows and their corresponding columns are also positive definite). Hence, any feasible sub-community would also be (globally) stable, and might or might not be invasible by other populations. Take two sub-communities x_k, composed of k populations and x_{k+1} composed of the same populations, but with another population added. If both x_k and x_{k+1} are feasible, and both are stable because $\alpha > \alpha_S$, then the population that is added can attach itself to the resident community without causing extinctions.

Suppose that a GLV system has $\alpha > \alpha_S$ and a feasible equilibrium $x^\star > \mathbb{0}$. Then, determining whether there is a way to build the community from the ground up amounts to determining whether there is a path in the graph such that, at each step, a different population attaches itself to the community without causing extinctions.

A.2 General systems

We start our discussion on the effect of the strength of intraspecific competition α on coexistence by considering the case in which matrix B is a generic matrix. In the next section, we analyze the case in which B is a large random matrix instead.

A.2.1 Effect of average interaction strength

Here we show that the feasibility of the equilibrium $x^\star$ in Eq. (A.1) is related to that of the equilibrium of a simpler system, $y^\star$, thereby obtaining a canonical form for the study of feasibility in competitive GLV systems.

The system in Eq. (A.1) is feasible whenever $x^\star = A^{-1}\mathbb{1} = (\alpha I + B)^{-1}\mathbb{1} > \mathbb{0}$. We can write:

$$A = \alpha I + B = \alpha I + C + \mathbb{1}m^T \quad ,$$

where the columns of C sum to zero ($C^T\mathbb{1} = \mathbb{0}$), the vector $m \geq \mathbb{0}$ (because the system is competitive), I is the identity matrix of dimension n, and $\alpha \geq 0$. The rank-one matrix $\mathbb{1}m^T$ has constant columns with nonnegative coefficients, corresponding to the column means of B. Now consider the system:

$$(\alpha I + C)y^\star = \mathbb{1} \quad . \tag{A.3}$$

Note that the sum of all the $y_i^\star$ is positive:

$$\begin{aligned} \mathbb{1}^T(\alpha I + C)y^\star &= \mathbb{1}^T\mathbb{1} \\ \alpha\mathbb{1}^T y^\star + \mathbb{1}^T C y^\star &= n \\ \frac{1}{n}\mathbb{1}^T y^\star + 0 &= \frac{1}{\alpha} > 0 \quad . \end{aligned}$$

As such, the mean of the components of $y^\star$ is exactly $1/\alpha$, and is thus positive for any positive $\alpha > 0$. We can write $x^\star$, the solution of $Ax^\star = \mathbb{1}$, as a function of $y^\star$ using the Sherman-Morrison formula:

$$
\begin{aligned}
(\alpha I + B)x^\star &= \mathbb{1} \\
(\alpha I + C + \mathbb{1}m^T)x^\star &= \mathbb{1} \\
x^\star &= (\alpha I + C + \mathbb{1}m^T)^{-1}\mathbb{1} \\
x^\star &= \left((\alpha I + C)^{-1} - \frac{1}{1 + m^T(\alpha I + C)^{-1}\mathbb{1}}(\alpha I + C)^{-1}\mathbb{1}m^T(\alpha I + C)^{-1}\right)\mathbb{1} \\
x^\star &= y^\star - \frac{1}{1 + m^T y^\star} y^\star m^T y^\star \\
x^\star &= \left(1 - \frac{m^T y^\star}{1 + m^T y^\star}\right) y^\star \\
x^\star &= \frac{1}{1 + m^T y^\star} y^\star \quad .
\end{aligned}
$$

Thus, $x^\star$ simply related to $y^\star$, through multiplication by the scalar $1/(1 + m^T y^\star)$. As such, we have a feasible equilibrium $x^\star > \mathbb{0}$ whenever a) $y^\star > \mathbb{0}$ (i.e., $y^\star$ is feasible, and because $m^T y^\star = \sum_j m_j y_j^\star$ is the sum of products of nonnegative values, then the constant of proportionality is also positive), or, b) $y^\star < \mathbb{0}$ and $m^T y^\star < -1$ (i.e., all the components of $y^\star$ are negative, and sufficiently large to make the constant of proportionality negative as well). But we have just seen that the average of $y^\star$ is positive, thereby making case b) impossible. We conclude that $x^\star$ is feasible if and only if $y^\star$ is feasible.

Because infinitely many competitive systems in Eq. (A.1) map into the same Eq. (A.3), we say that the equation in C is the *canonical* form for studying the feasibility of the competitive systems that can be formed by adding positive columns to C.

A.2.2 A sufficiently large α ensures feasibility

Here we use the well-known Perron-Frobenius property for nonnegative matrices to show that for sufficiently large $\alpha = \alpha_\infty$ the feasibility of $y^\star$ (and thus of $x^\star$) is guaranteed, and is

maintained for any $\alpha > \alpha_\infty$. To this end, we divide both sides of Eq. (A.3) by $\alpha > 0$:

$$\left(I + \frac{1}{\alpha}C\right) y^\star = \frac{1}{\alpha}\mathbb{1} \quad .$$

We have shown above that $\mathbb{1}^T y^\star = n/\alpha$, but then $\frac{\alpha}{n}\,\mathbb{1}^T y^\star = 1$. Multiplying the right hand side by this value, we get:

$$\left(I + \frac{1}{\alpha}C\right) y^\star = \frac{1}{n}\mathbb{1}\mathbb{1}^T y^\star \quad .$$

Bringing the right-hand side to the left:

$$\left(I + \frac{1}{\alpha}C - \frac{1}{n}\mathbb{1}\mathbb{1}^T\right) y^\star = \mathbb{0}$$

and, finally,

$$\begin{aligned}\left(\frac{1}{\alpha}C - \frac{1}{n}\mathbb{1}\mathbb{1}^T\right) y^\star &= -y^\star \\ \left(\frac{1}{n}\mathbb{1}\mathbb{1}^T - \frac{1}{\alpha}C\right) y^\star &= y^\star \quad ,\end{aligned}$$

which shows that $y^\star$ is a right eigenvector of $\frac{1}{n}\mathbb{1}\mathbb{1}^T - \frac{1}{\alpha}C$, with associated eigenvalue $\lambda = 1$. Note that the matrix $\frac{1}{n}\mathbb{1}\mathbb{1}^T - \frac{1}{\alpha}C$ has left eigenvector $\mathbb{1}$, also associated with $\lambda = 1$. Now suppose we choose $\alpha = \alpha_\infty > n \max_{i,j} C_{ij}$; then, we have that a) the matrix $\frac{1}{n}\mathbb{1}\mathbb{1}^T - \frac{1}{\alpha_\infty}C$ has only positive entries; b) it is column stochastic (i.e., it is nonnegative with columns summing to 1), and therefore has spectral radius 1. But then $\frac{1}{n}\mathbb{1}\mathbb{1}^T - \frac{1}{\alpha_\infty}C$ has the Perron-Frobenius property, and thus $y^\star$ is positive, and the positivity of $y^\star$ is guaranteed for any $\alpha \geq \alpha_\infty$. Naturally, this choice of $\alpha = \alpha_\infty$ is overly conservative, but it is sufficient to show that there must exists some critical value $\alpha_F \leq \alpha_\infty$ such that: a) $y^\star$ is positive, and b) it remains positive for any $\alpha > \alpha_F$. Computing such a value is the main goal of the next two subsections.

A.2.3 Transitions to and from feasibility

We can track the value of $y_i^\star(\alpha)$, as we vary α, using Cramer's rule:

$$y_i^\star(\alpha) = \frac{\begin{vmatrix} \alpha + C_{1,1} & C_{1,2} & \cdots & 1 & \cdots & C_{1,n} \\ C_{2,1} & \alpha + C_{2,2} & \cdots & 1 & \cdots & C_{2,n} \\ \vdots & \vdots & & \vdots & & \vdots \\ C_{n,1} & C_{n,2} & \cdots & 1 & \cdots & \alpha + C_{n,n} \end{vmatrix}}{|\alpha I + C|} = \frac{|Q_i(\alpha)|}{|Q(\alpha)|} \quad ,$$

where $Q(\alpha) = \alpha I + C$, and $Q_i(\alpha)$ is obtained by substituting the ith column of $Q(\alpha)$ with the vector $\mathbb{1}$.

When $|Q(\alpha)| = 0$, the matrix is singular; this means that C has a real, negative eigenvalue λ_i such that by setting $\alpha = -\lambda_i$ we place an eigenvalue of $Q(\alpha)$ exactly at zero. We have two cases: if, as $\alpha \to -\lambda_i$, the determinant of the numerator $|Q_i(\alpha)|$ tends to a nonzero value, then $y_i^\star(\alpha)$ diverges as $\alpha \to -\lambda_i$; if instead $|Q_i(\alpha)| \to 0$ as $\alpha \to -\lambda_i$, then the solution $y_i^\star(\alpha)$ does not diverge around $\alpha = -\lambda_i$. Importantly, given that the mean of the solution is fixed and positive, whenever some solutions diverge, some components will tend to $+\infty$, while others to $-\infty$ around these singularities. Hence, the system cannot be feasible around any singularity that gives rise to divergences. We denote the largest value of α leading to a divergence as α_0. If no value of α leads to a divergence, then $\alpha_0 = 0$.

Now take α_L to be the minimum value of α such that $\min_j \mathcal{R}\rceil\, \lambda_j(\alpha_L I + C) = 0$ (as seen in Sec. A.1.1, this critical value is important for local stability); for any value $\alpha > \alpha_L$ the determinant $|Q(\alpha)|$ is positive, and thus the existence of a solution is guaranteed. This can be easily proven by considering that the determinant of a matrix is the product of its eigenvalues; then the eigenvalues of $Q(\alpha)$ for any $\alpha > \alpha_L$ are either real and positive, or complex and multiplied by their conjugate ($\lambda_j \lambda_j^* > 0$), yielding therefore a positive product, and thus determinant. Therefore, any divergence can only appear when $\alpha \leq \alpha_L$, and thus

$\alpha_0 \leq \alpha_L$.

Having considered the denominator, we turn to the numerator $|Q_i(\alpha)|$: whenever this determinant is zero, $y_i^\star(\alpha) = 0$, and thus this component of the solution transitions from negative to positive, or vice versa (because $|Q_i(\alpha)|$ is a polynomial in α and, as such, is a continuous function everywhere). We can characterize this determinant by performing some simplifications. The derivation is easier to write when the focal population $i = n$ is in last position—this can be accomplished for any i by reordering the rows and columns of the matrix. We have (for $i = n$):

$$|Q_i(\alpha)| = \begin{vmatrix} \alpha + C_{1,1} & C_{1,2} & \cdots & 1 \\ C_{2,1} & \alpha + C_{2,2} & \cdots & 1 \\ \vdots & \vdots & & \vdots \\ C_{n,1} & C_{n,2} & \cdots & 1 \end{vmatrix} = \begin{vmatrix} \alpha\widetilde{I} + \widetilde{C} & \mathbb{1} \\ c^T & 1 \end{vmatrix} \quad ,$$

where $\widetilde{I}$ and $\widetilde{C}$ are the corresponding matrices with the last row and column removed, and c^T is the last row of C with the last element removed. We can subtract the last row from all other rows without altering the determinant:

$$\begin{vmatrix} \alpha\widetilde{I} + \widetilde{C} & \mathbb{1} \\ c^T & 1 \end{vmatrix} = \begin{vmatrix} \alpha\widetilde{I} + \widetilde{C} - \mathbb{1}c^T & \mathbb{0} \\ c^T & 1 \end{vmatrix} \quad ,$$

which is a block-structured matrix, with determinant $|\alpha\widetilde{I} + \widetilde{C} - \mathbb{1}c^T|$. Finally, we note that $\tilde{C} - \mathbb{1}c^T = \tilde{B} - \mathbb{1}\tilde{m}^T - (\mathbb{1}b^T - \mathbb{1}\tilde{m}^T) = \tilde{B} - \mathbb{1}b^T$, and thus we can work either with matrix C or B (naturally, if $y_i^\star(\alpha) = 0$, necessarily $x_i^\star(\alpha) = 0$).

This means that $y_i^\star(\alpha) = 0$ whenever $\alpha \geq 0$ matches precisely a real, negative eigenvalue of $\tilde{B} - \mathbb{1}b^T$. Consider the eigenvalues of $\tilde{B} - \mathbb{1}b^T$, and call λ_i the most negative, real eigenvalue (if it exists); then, if $-\lambda_i > \alpha_0$, at $\alpha_i = -\lambda_i$ necessarily $y_i^\star(\alpha)$ crosses from negative to positive as α increases (because we have established that when $\alpha \geq \alpha_F$, $y_i^\star(\alpha)$

must be positive).

Now repeat the procedure for all i, and collect all the $\alpha_i > \alpha_0$ representing the last transition to positive values for each i (with $\alpha_i = 0$ if such a transition does not exist, or it appears before α_0); then necessarily for any $\alpha > \alpha_F = \max\{\alpha_0, \alpha_1, \ldots, \alpha_n\}$ the solution $y^\star(\alpha)$ is positive, and further increasing α maintains positivity.

To summarise these results, we analyze a simple example, showing the location of α_0 and α_i $(i = 1, \ldots, n)$. Take the matrix C:

$$C = \begin{pmatrix} -4 & 2 & 3 \\ -4 & -4 & 2 \\ 8 & 2 & -5 \end{pmatrix},$$

with eigenvalues $\lambda(C) = \{-9, -4, 0\}$. Then, $Q(\alpha)$ is singular when $\alpha \in \{4, 9\}$; at these points the three possible $Q_i(\alpha)$ are not singular, and therefore the solution $y^\star(\alpha)$ diverges around these points; we thus set $\alpha_0 = 9$.

The eigenvalues of $\widetilde{C}^{(1)} - \mathbb{1}(c^{(1)})^T$:

$$\widetilde{C}^{(1)} - \mathbb{1}(c^{(1)})^T = \begin{pmatrix} -4 & 2 \\ 2 & -5 \end{pmatrix} - \begin{pmatrix} 2 & 3 \\ 2 & 3 \end{pmatrix} = \begin{pmatrix} -6 & -1 \\ 0 & -8 \end{pmatrix}$$

are -6 and -8 and thus $y_1^\star(\alpha) = 0$ when we choose $\alpha = 6$ or $\alpha = 8$. Both transitions appear before the last divergence at $\alpha_0 = 9$, and hence the equilibrium of population 1 will be positive after the last divergence (and we set $\alpha_1 = 0$).

Repeating for population two, we have:

$$\widetilde{C}^{(2)} - \mathbb{1}(c^{(2)})^T = \begin{pmatrix} -4 & 3 \\ 8 & -5 \end{pmatrix} - \begin{pmatrix} -4 & 2 \\ -4 & 2 \end{pmatrix} = \begin{pmatrix} 0 & 1 \\ 12 & -7 \end{pmatrix} \quad ,$$

with eigenvalues $-\frac{1}{2}(7 \pm \sqrt{97})$; thus the equilibrium for population 2 will transition only at

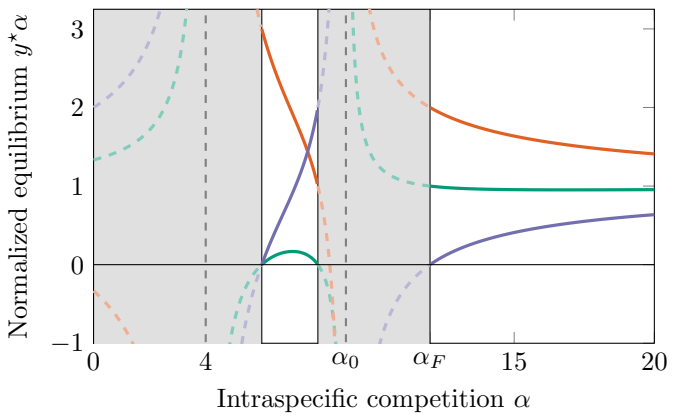

Figure A.2: **The components of $y^\star(\alpha)$ as a function of $\alpha \geq 0$.** Grey areas denote the values of α for which the equilibrium is not feasible, and the white regions correspond to values of α for which all components $y_i^\star(\alpha)$ (colors) are positive. As explained in the text, for two particular values of $\alpha = 4$ and $\alpha = 9$ (vertical dashed lines), the components of the solution diverge to $\pm\infty$, and thus feasibility is precluded around these points. We denote the largest value of α that leads to a divergence as α_0. After the last divergence, the component associated with population 3 (purple) is still negative, and transitions to a positive value at exactly $\alpha_3 = \alpha_F = 12$. The solution remains positive for any $\alpha > \alpha_F$.

$\alpha = \frac{1}{2}(7 + \sqrt{97})$, which is smaller than 9; hence the solution for the second population will be positive after the last divergence (and we set $\alpha_2 = 0$ as well).

Finally, considering population 3, we have:

$$\tilde{C}^{(3)} - \mathbb{1}(c^{(3)})^T = \begin{pmatrix} -4 & 2 \\ -4 & -4 \end{pmatrix} - \begin{pmatrix} 8 & 2 \\ 8 & 2 \end{pmatrix} = \begin{pmatrix} -12 & 0 \\ -12 & -6 \end{pmatrix} \quad ,$$

yielding a transition at $\alpha = 6$ and $\alpha = \alpha_3 = 12$.

Therefore, $\alpha_F = \max\{9, 0, 0, 12\} = 12$. Thus, for this system, all components of $y^\star$ will be positive for any $\alpha > 12$. This behavior is illustrated in Figure A.2.

A.2.4 Finding α_F via eigendecomposition

The results in the previous section are sufficient to devise an exact algorithm to determine α_F for a given system specified by the matrix C (or B). It consists of three steps:

1. Compute the eigenvalues of $-C$, and store the largest positive eigenvalue leading to a divergence in α_0; if none exist, $\alpha_0 = 0$.

2. For each i in $1, \ldots, n$:

   (a) Form the matrix $\widetilde{C}^{(i)}$ (by removing the ith row and column from C) and the corresponding $(c^{(i)})^T$ (i.e., the ith row of C with the ith coefficient removed);

   (b) Compute the eigenvalues of the matrix $\mathbb{1}(c^{(i)})^T - \widetilde{C}^{(i)}$;

   (c) Store the largest positive, real eigenvalue in α_i; if no eigenvalues are real and positive, or if all are smaller than α_0, then $\alpha_i = 0$.

3. $\alpha_F = \max\{\alpha_0, \alpha_1, \ldots, \alpha_n\}$.

From a computational standpoint, we note that the eigenvalue with the largest real part can be computed efficiently, for example via the Arnoldi iteration[177]. One could also utilize well-known bounds on eigenvalues to compute α_i only for the matrices that are more likely to produce a maximum.

For the example above, we find $\alpha_0 = 9$, $\alpha_1 = \alpha_2 = 0$, and $\alpha_3 = 12 = \alpha_F$.

A similar pattern can also be observed in the classic two-species Lotka-Volterra competition model with priority effects (Fig. A.3). Mirroring the example in the main text, Phase I is characterized by *locally* stable boundary equilibria – alternative stable states. Global stability of an unspecified boundary equilibrium (in this case, that where only species x_2 is present) is achieved first (Phase II), and as α keeps increasing, feasibility is achieved at last (Phase III), such that the two species coexist at a globally stable equilibrium.

A.3 Random systems

Having derived some general results in the previous section, we now turn to the case in which the matrix of interactions B is a large random matrix. This case has been studied for

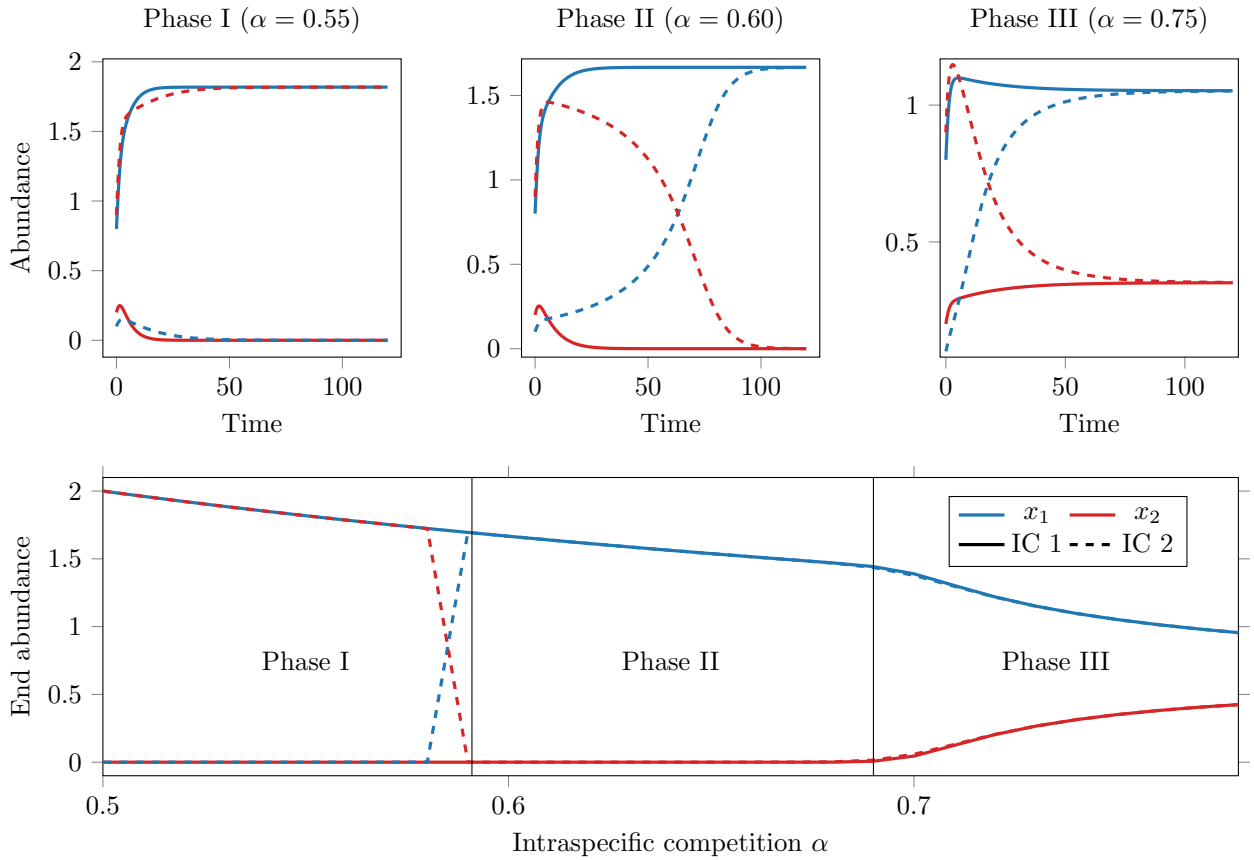

Figure A.3: **Three dynamical phases in the classic two–species Lotka–Volterra competition model.** Top row: time series for $\alpha \in \{\alpha_{\mathrm{I}}, \alpha_{\mathrm{II}}, \alpha_{\mathrm{III}}\}$ (here, $0.55, 0.60, 0.75$), with two initial conditions shown (linetypes; colors denote species). Bottom row: bifurcation diagram of equilibrium abundances versus the intraspecific competition strength α (x–axis), with line type indicating the initial condition (IC1 or IC2). As α increases (while a_{12}, a_{21} are fixed and $r_1 = r_2 = 1$), the system transitions through three regimes separated by the vertical guides: **Phase I (low α)**: interspecific effects dominate and priority effects appear—different initial conditions lead to alternative stable outcomes (each species can exclude the other). **Phase II (intermediate α)**: competitive exclusion is deterministic—the same species survives from any initial condition (unique attracting boundary equilibrium). **Phase III (high α)**: intraspecific competition dominates and a feasible interior coexistence equilibrium exists and attracts all initial conditions. All three panels use the same interspecific coefficients, varying only α across scenarios.

decades, producing a wealth of results. Here we show that previous results can be extended, generalized and refined in light of the derivations above. This section has two main goals: a) compute the probability that the equilibrium $x^\star$ of Eq. (A.1) is positive, given a value of α and the statistics of the random matrix B; b) show how these derivations have profound implications for the type of dynamics that can be observed for these systems.

A.3.1 Random systems with statistically equivalent populations

We start by defining what we mean by random systems. Naturally, dynamical systems in which some (all) of the parameters are sampled from random distributions are indeed random systems; here we focus on a subclass in which the model definition is closed under relabeling of the populations: by permuting the indices x_i of Eq. (A.1) we obtain the same random model. In practice, this simply means that there is no special "structure" making any of the populations behave differently from the others—the populations are *statistically equivalent*.

Among this subclass of models, the simplest to study is one in which the matrix of interactions is given by the sum of a random matrix B and a positive constant μ.

$$B' = B + \mu \mathbb{1}\mathbb{1}^T \quad ,$$

where we choose B such that: $B_{ii} = 0$ (this assumption can be relaxed, Sec. A.3.9), and $\mathbb{E}(B_{ij}) = 0$, $\mathbb{E}(B_{ij}^2) = 1$, $\mathbb{E}(B_{ij}B_{ji}) = \rho$ for every $i \neq j$. Thus the spectrum of B follows the elliptic law[178]: the eigenvalues of $B/\sqrt{n}$ are approximately uniformly distributed in an ellipse in the complex plane, with center $(0, 0i)$, horizontal semi-axis $1 + \rho$, and vertical semi-axis $1 - \rho$.

As we have shown in Section A.2.1, as long as the columns of B' sum to positive values (i.e., when the systems are competitive), the value of μ has no effect on feasibility. The value of μ also has no effect on the stability of the system[22]: the eigenvalues of B' will be

distributed in an ellipse, possibly with an outlier eigenvalue on the right of the bulk, and thus not influencing stability. Hence, α_F (the value at which the equilibrium is feasible, and feasibility is maintained when we increase α), α_L (the value at which all eigenvalues have positive real part), and α_S (the value at which the symmetric part of the matrix is positive definite) are the same for both B and B'.

Thus, without loss of generality, we can consider the case in which $\mu = 0$, and therefore the matrix of interactions follows the elliptic law. This also allows us to compare our results directly with other studies that have considered random matrices with coefficients sampled from distributions with mean zero[19, 20, 30].

A.3.2 Previous results

The oldest result in this area goes back to a response to May's article, by Alan Roberts[16]. Roberts used computer simulations to measure the probability that a feasible equilibrium would be locally stable for a GLV model, Eq. (A.1), in which populations were self–regulating ($A_{ii} = 1$), and interactions were randomly chosen to be $A_{ij} = \theta$ with probability 1/2 and $A_{ij} = -\theta$ otherwise. He found that the probability of stability conditional on feasibility was very large, and increasing with the size of the system.

The next main contribution was obtained by Lewi Stone as part of his PhD thesis[30], developed under the supervision of Roberts. Using techniques similar to those used here, Stone was able to approximate the probability of feasibility for matrices with random interactions sampled independently from an arbitrary distribution with mean zero. For example, a formula reported in Stone[31], and adapted to the notation employed in this work, reads:

$$p_F(\alpha) = \Phi\left(\frac{\alpha}{\sqrt{n-1}(1+\frac{n-1}{\alpha^2})^{\frac{1}{4}}}\right)^n \quad ,$$

where $p_F(\alpha) = P(x^\star > \mathbb{0}|\alpha)$, and $\Phi(\cdot)$ is the cumulative distribution function for the stan-

dard normal distribution. This formula was derived in[30] by approximating the solution of the linear system using the Neumann series (see Sec. A.3.7). Stone's thesis also reported larger computer simulations, in the spirit of Roberts, again confirming that feasible systems are almost invariably locally stable.

More recently, two articles[19, 20] used different techniques to show that there exist a critical value below which the probability of feasibility is negligible, and above which it is very high. In particular, using the notation adopted in this work, they found that the probability of feasibility is close to one for $\alpha \gg \sqrt{n}\sqrt{2\log n}$, and is close to zero for $\alpha \ll \sqrt{n}\sqrt{2\log n}$. Clenet *et al.*[20] considered matrices with correlated entries as well, finding that the threshold value for feasibility would not change substantially, and, importantly, noting that the transition would appear after that for global stability in these GLV systems. Also important for the work developed here, Liu *et al.*[50] showed, using yet a different technique, that correlation between the entries would have an effect on feasibility (increasing the probability of feasibility when the correlation is negative), but that the effect would be negligible for large systems.

Finally, Marcus *et al.*[51] considered stable, feasible GLV systems and increased the interaction strengths (equivalently, one could have decreased the strength of intraspecific interactions, as done here) until either the system becomes unfeasible, or unstable. They found that in general, the system loses feasibility before stability, consistently with the previous findings outlined above. Interestingly for our argument, they notice that in symmetric systems, feasibility would be often lost due to the components of the solution diverging to $\pm\infty$, a fact that will be key for the developments below. A similar argument was put forward by Stone[31].

Figure A.4 shows simulations measuring the probability of feasibility when varying both α (x-axis) and the correlation between entries (colors); the approximation by Stone[30] for $\rho = 0$, as well as the critical value by Bizeul & Najim[19] are also reported.

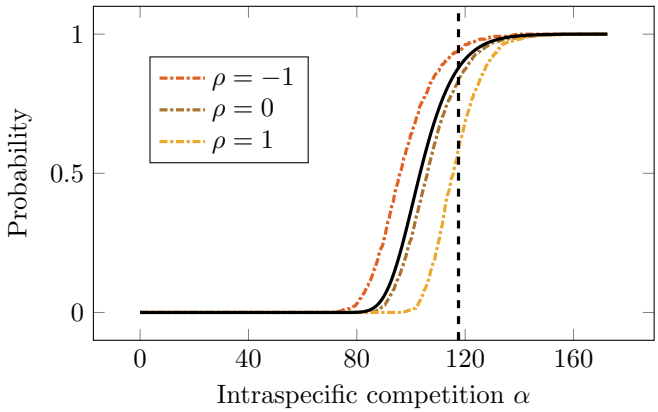

Figure A.4: **Probability of feasibility (i.e., $P(x^\star > \mathbb{0})$, y-axis) for a given level of intraspecific interaction α (x-axis).** The probability was computed by considering 1000 realizations of systems of size $n = 1000$ with interaction matrices B following the elliptic law (with the colors representing the off-diagonal correlation). The black line represents the approximation by Stone[31] for the case $\rho = 0$. The vertical dashed line is the critical value of Bizeul & Najim[19].

The goal of the next few sections is to generalize and improve these results in the light of what we have derived for general matrices. In particular, we will extend both the formula by Stone and the critical value of Bizeul & Najim for the case in which entries are correlated.

A.3.3 Feasibility when $\alpha = 0$

For large random systems, the probability of feasibility when $\alpha = 0$ is negligible. We can compute this probability exactly whenever the coefficients of B are sampled independently from a distribution that is symmetric about 0.

We want to compute the probability that $(\alpha I + C)y^\star = \mathbb{1}$ has a positive solution when $\alpha = 0$. Since the columns of C sum to 0 (see Section A.2.1), the right-hand side of the equation vanishes when we multiply the equations by the transpose of C:

$$Cy^\star = \mathbb{1}$$
$$C^T C y^\star = C^T \mathbb{1}$$
$$C^T C y^\star = \mathbb{0} \quad .$$

The matrix $C^T C$ is symmetric, positive semi-definite, and has an eigenvalue 0; all its eigenvectors are orthogonal. Then, whenever a feasible solution exists, solving the system of equations above is equivalent to solving $Cy^\star = \mathbb{0}$, i.e., $y^\star$ is a right eigenvector of C associated with the zero eigenvalue. Thus, $y^\star$ is defined up to a constant of proportionality, allowing us to set one of the components arbitrarily. Here we set $y^\star_n = 1$, and we partition C and $y^\star$ as:

$$C = \begin{pmatrix} \widetilde{C} & a \\ c^T & b \end{pmatrix} \quad y^\star = \begin{pmatrix} \widetilde{y} \\ 1 \end{pmatrix} \quad ,$$

where $b = -\sum_{j=1}^{n-1} a_j$. We can therefore write $n-1$ independent equations:

$$\widetilde{C}\widetilde{y} = -a$$
$$\widetilde{y} = -\widetilde{C}^{-1} a \quad .$$

For feasibility, we need all $\widetilde{y} > \mathbb{0}$ (because we have chosen a positive $y^\star_n$). To compute the probability that $\widetilde{y} > \mathbb{0}$ exactly, we exploit the assumptions that we have made: because of symmetry, the probability of observing a given C_{ij} (or the density of the distribution at C_{ij}, when the distribution is continuous), satisfies the equality $P(C_{ij}) = P(-C_{ij})$.

Then, we can follow the approach of Serván *et al.*[32], and define the diagonal matrices $K_i = D(s_i)$, where the s_i are the 2^n distinct vectors of length n containing either 1 or -1: $s_1 = (1, 1, 1, \ldots, 1)^T$, $s_2 = (1, -1, 1, \ldots, 1)^T$, $s_3 = (-1, -1, 1, \ldots, 1)^T$, $s_4 = (1, 1, -1, \ldots, 1)^T$, ..., $s_{2^n} = (-1, -1, -1, \ldots, -1)^T$. We partition these matrices as

well:

$$K_i = \begin{pmatrix} \widetilde{K_i} & \mathbb{0} \\ \mathbb{0}^T & \sigma_i \end{pmatrix} \quad .$$

Because of symmetry and independence, we have $P(C) = P(CK_i)$, given that multiplying C by $K_i = D(s_i)$ simply changes the signs of all the coefficients in the columns corresponding to negative signs in s_i. Finally, we write:

$$\widetilde{C}\widetilde{K_1}\widetilde{y} = -\sigma_1 a$$
$$\widetilde{y} = -\sigma_1 \widetilde{K_1}\widetilde{C}^{-1} a \quad ,$$

where we have used the fact $K_1 = I$. Now notice that by exchanging K_1 with K_i, we can change the signs of the components of $\widetilde{y}$; then, for each possible pattern of signs of $-\widetilde{C}^{-1}a$ there are exactly two choices of K_i that make the vector $\widetilde{y}$ all positive (one solution with $K_j = D(s_j)$, and the other with $K_l = D(-s_j)$). Given that $P(CK_i) = P(CK_j)$, and that there are 2^n matrices K_i, the probability of feasibility is exactly $2/2^n = 1/2^{n-1}$.

Thus, for a random system with B_{ij} sampled independently from a distribution that is symmetric about its mean, for two populations we have fifty percent probability of obtaining a feasible equilibrium, and the probability rapidly decreases, so that we have less than one in a thousand chance to find a feasible equilibrium for $n = 11$ and less than one in a million for $n = 21$.

A.3.4 Feasibility when $\alpha < \alpha_L$

We have shown above that the probability of feasibility is vanishingly small for $\alpha = 0$; here we show that the same holds true for any $\alpha < \alpha_L$. In this case, the support for the bulk of the spectrum of $\alpha I + B$ contains the point $(0, 0i)$, because the ellipse is not completely

contained in the right half of the complex plane. Because the matrix is large, and eigenvalues are approximately uniformly distributed inside the ellipse, we can always find an eigenvalue that is arbitrarily close to the origin, thereby causing some solutions to reach arbitrarily large absolute values—given that the determinant of matrix $Q(\alpha) = \alpha I + B$ (defined in Sec. A.2.3) must be arbitrarily close to zero. Because the mean of $y^\star$ is positive, components reaching large positive values must be balanced by some other components with negative values, and thus feasibility is precluded. Hence, the probability of feasibility at $\alpha < \alpha_L$ is close to zero. A similar argument is found (in the context of symmetric matrices), in Marcus *et al.*[51]. Therefore, we can assume that $\alpha_0 = \alpha_L$.

A.3.5 A single transition to feasibility when $\alpha > \alpha_L$

Having shown that, with high probability, the system is not feasible for $\alpha < \alpha_L$, we consider the dependence of each component of $y^\star(\alpha)$ on α, as it increases for $\alpha > \alpha_L$. We have seen in Section A.2.3 that $y_i^\star(\alpha)$ transitions (either from positive to negative, or vice versa) whenever $\alpha = \lambda_i$, and λ_i is a real, positive eigenvalue of the matrix

$$\widetilde{Q}_i = \mathbb{1}(b^{(i)})^T - \widetilde{B}^{(i)} \quad ,$$

where $\widetilde{B}^{(i)}$ is the matrix B with the row and column corresponding to i removed, and $(b^{(i)})^T$ is the ith row of B with coefficient i removed. If $\widetilde{B}^{(i)}$ is a large random matrix (i.e., if B is a large random matrix following the elliptic law), then perturbing it by adding a rank-one matrix has a simple effect on its spectrum: at most one eigenvalue moves outside of the bulk, while the remaining eigenvalues are fundamentally unchanged[179] (an example is provided in Fig. A.5). Thus, if the outlier eigenvalue is on the left of the bulk, then λ_i is negative and $y_i^\star(\alpha)$ cannot cross zero when choosing $\alpha > 0$. If, on the other hand, the outlier eigenvalue $\lambda_i > \alpha_L$ is positive, we can make $y_i^\star(\alpha) = 0$ by choosing $\alpha = \lambda_i$. Then, this transition must

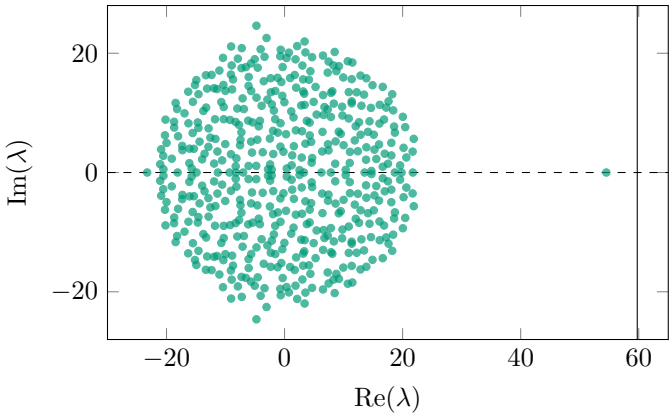

Figure A.5: **Spectrum of $\widetilde{Q}_i = \mathbb{1}(b^{(i)})^T - \widetilde{B}^{(i)}$ for a given i, when B is a large random matrix following the circular law.** When a large random matrix ($-\widetilde{B}^{(i)}$ in this case) is perturbed by summing a matrix with small rank (in this case, matrix $\mathbb{1}(b^{(i)})^T$ has rank 1), only a few of the original eigenvalues change substantially (one in the case of a rank-one matrix). Moreover, the eigenvalues are expected to be close to those of the small-rank matrix (vertical line).

bring $y_i^\star(\alpha)$ from negative to positive values: because we know that, for sufficiently large values of α, $y_i^\star(\alpha) > 0$, and that there are no divergences after α_L, then necessarily $y_i^\star(\alpha)$ becomes zero at this value, and remains positive when α is increased further (observe that $y_i^\star(\alpha)$ is a rational function —a quotient of two polynomials— in α, which is a continuous function above the largest point at which it diverge, i.e., for $\alpha > \alpha_0$; therefore, the change of sign follows by continuity of $y_i^\star(\alpha)$ for $\alpha > \alpha_L$). Hence, we can set $\alpha_i = \lambda_i$.

We have just shown that each matrix $Q_i(\alpha)$ has at most a single real eigenvalue to the right of the bulk, with value $\lambda_i = \alpha_i$. Moreover, when this positive outlier eigenvalue exists, component i transitions from negative to positive at $\alpha = \alpha_i$. But then we can order the α_i from smallest to largest, and at $\alpha_F = \max_i \alpha_i$, all components have crossed into positive values. Because for large random matrices feasibility is precluded (with very high probability) when $\alpha < \alpha_L$, we conclude that a) positivity is gained only at α_F, and b) it is never lost for larger values of α. Thus, large random matrices produce a much simpler picture of the dependence on α than small, or arbitrary matrices, in which, when we

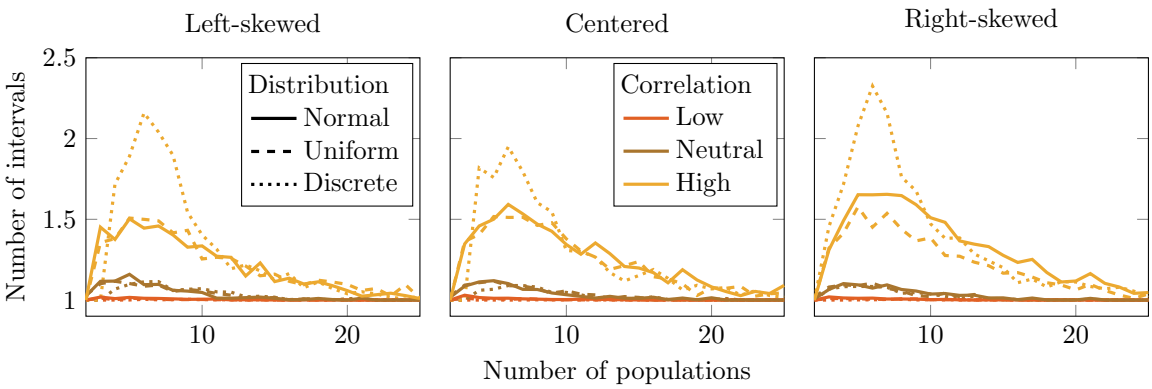

Figure A.6: **Transitions in and out of feasibility as system size grows.** For random systems of increasing size (n, x-axis), we count the number of disjoint intervals for α yielding a feasible equilibrium. As we increase n, the number of intervals converges to one, irrespective of correlation ρ or choice of distribution. Then, large random matrices will yield a single transition, occurring at α_F.

grow α, the equilibrium can transition from unfeasible to feasible several times (Sec. A.2.3). These findings are confirmed by simulations: when we count the number of disjoint intervals for α yielding a feasile equilibrium for random systems of increasing size, we see a rapid convergence to a single interval (Fig. A.6).

A.3.6 Approximating the probability of feasibility using the theory of small-rank perturbations of random matrices

We can use the argument above on the perturbation of random matrices with small-rank matrices to provide an estimate of the probability of feasibility. We write $P(x^\star > \mathbb{0}|\alpha) = p_F(\alpha)$. In light of the previous paragraph, this amounts to $P(\lambda_i < \alpha)$ for all n choices of i, where λ_i is either the largest real eigenvalue of $\mathbb{1}(b^{(i)})^T - \widetilde{B}^{(i)}$, when it exists, or $\lambda_i = 0$, when either the matrix has no positive eigenvalues, or all are smaller than α_L.

To approximate the location of λ_i, we follow O'Rourke and Renfrew[179], who have proven that, when A is a large random matrix following the elliptic law, uv^T is a rank-one matrix with real eigenvalue γ, and $|\gamma| > 1 + \rho$, then the spectrum of $A/\sqrt{n} + uv^T$ has an

outlier, real eigenvalue, λ_o, with:

$$\lambda_o = \gamma + \frac{\rho}{\gamma} + o(1) \quad .$$

Let λ_i be the outlier of matrix $\mathbb{1}(b^{(i)})^T - \widetilde{B}^{(i)}$. We want to find its location. Define $\gamma_i = \sum_j b_j^{(i)}$, i.e., the only nonzero eigenvalue of $\mathbb{1}(b^{(i)})^T$. Then, the outlier of $\frac{1}{\sqrt{n-1}}(\mathbb{1}(b^{(i)})^T - \widetilde{B}^{(i)})$ is located approximately at

$$\frac{\lambda_i}{\sqrt{n-1}} = \frac{\gamma_i}{\sqrt{n-1}} + \frac{\rho\sqrt{n-1}}{\gamma_i} \quad , \tag{A.4}$$

if $\left|\frac{\gamma_i}{\sqrt{n-1}}\right| > 1 + \rho$ holds. Otherwise, the outlier does not exists because it is contained in the bulk. For $\gamma_i > \sqrt{n-1}$, the right-hand side of Eq. (A.4) is maximized when γ_i is maximized, for any value of ρ; hence, the maximum $\lambda_i = \hat{\lambda}$ tends to be associated with the largest $\gamma_i = \hat{\gamma}$, which in turn is simply the maximum row sum of B.

Now we assume that the γ_is are independent and normally distributed, with mean zero and variance $n-1$; an assumption that is correct when $\rho = 0$ and n is sufficiently large, and is met only approximately for nonzero values of ρ (though the effect of the correlation on row sums must be negligible for large n). Thus, the variables $\tilde{\gamma}_i = \gamma_i/\sqrt{n-1}$ follow the standard normal distribution. The distribution of the maximum $\tilde{\gamma}$ therefore converges asymptotically (albeit quite slowly[180]) to the Gumbel distribution[19]. In particular, asymptotically we have:

$$P(\tilde{\gamma} < x) = \exp\left(-\exp\left(-((x - b_n)b_n)\right)\right) \quad ,$$

where b_n is a constant that can be chosen to guarantee a faster convergence to the Gumbel distribution. Here we follow Hall[180], and use $b_n = \sqrt{\mathcal{W}_0\left(\frac{n^2}{2\pi}\right)}$, where $\mathcal{W}_0(z)$ is the principal branch of the Lambert function. One can also Taylor-expand the function for large n,

obtaining:

$$\mathcal{W}_0\left(\frac{n^2}{2\pi}\right) \approx \log\frac{n^2}{2\pi} - \log\log\frac{n^2}{2\pi} + \frac{\log\log\frac{n^2}{2\pi}}{\log\frac{n^2}{2\pi}} + \cdots \quad .$$

We want to derive an approximate distribution for $\alpha_F = \sqrt{n-1}\,\tilde{\lambda}$, where, according to the small-rank perturbations, we have

$$\tilde{\lambda} \approx \tilde{\gamma} + \frac{\rho}{\tilde{\gamma}} \quad .$$

We now solve this equation for $\tilde{\gamma}$, obtaining:

$$\tilde{\gamma} \approx \frac{\tilde{\lambda} + \sqrt{\tilde{\lambda}^2 - 4\rho}}{2} \quad .$$

Substituting this value in the definition of the Gumbel distribution above, we have:

$$P(\tilde{\lambda} < x) = \exp\left(-\exp\left(-\left(\frac{x + \sqrt{x^2 - 4\rho}}{2} - b_n\right) b_n\right)\right) \quad .$$

Concluding, the probability that the system is feasible at α is the probability that $\alpha_F < \alpha$, and thus $\alpha_F/\sqrt{n-1} = \tilde{\lambda} < \alpha/\sqrt{n-1}$:

$$\begin{aligned} p_F(\alpha) &= P\left(\frac{\alpha_F}{\sqrt{n-1}} < \frac{\alpha}{\sqrt{n-1}}\right) = P(\tilde{\lambda} < \tilde{\alpha}) \\ &= \exp\left(-\exp\left(-\left(\frac{\tilde{\alpha} + \sqrt{\tilde{\alpha}^2 - 4\rho}}{2} - b_n\right) b_n\right)\right) \quad , \end{aligned} \tag{A.5}$$

where $\tilde{\alpha} = \alpha/\sqrt{n-1}$.

The Gumbel cumulative density function $\exp(-\exp(-x))$ describes a random variable with mode 0, median $-\log\log 2 \approx 0.366$ and mean ≈ 0.57721 (the Euler-Mascheroni constant). Thus, we expect the α_F for a given n and ρ to have the following statistics:

Mode of α_F. We solve:

$$\left(\frac{\tilde{\alpha}+\sqrt{\tilde{\alpha}^2-4\rho}}{2}-b_n\right)b_n=0$$

$$\tilde{\alpha}=b_n+\frac{\rho}{b_n}$$

$$\alpha=\sqrt{n-1}\left(b_n+\frac{\rho}{b_n}\right) \quad .$$

Choosing $b_n \approx \sqrt{2\log n}$ and $\rho = 0$, we recover the critical value of Bizeul & Najim[19].

Median and mean of α_F We now solve for $x = k$, obtaining:

$$\left(\frac{\tilde{\alpha}+\sqrt{\tilde{\alpha}^2-4\rho}}{2}-b_n\right)b_n=k$$

$$\tilde{\alpha}=b_n+\frac{k}{b_n}\frac{b_n\rho}{b_n^2+k}$$

$$\alpha=\sqrt{n-1}\left(b_n+\frac{k}{b_n}\frac{b_n\rho}{b_n^2+k}\right) \quad .$$

Choosing $k = -\log\log 2$ we obtain the approximate median, and using the Euler-Mascheroni constant, the mean.

While Eq. (A.5) is relatively simple and appealing, it tends to overestimate the probability of feasibility (i.e., underestimate the magnitude of the maximum λ_i) for low α, even when the matrices have considerable size. In fact, the equation is derived under the assumption that the maximum $\hat{\lambda} = \lambda_i$ is associated with the index i corresponding to the row with maximum row sum. While this is often the case, it is not universally true: the exact location of λ_i depends in fact on all of the eigenvalues and eigenvectors of both $\widetilde{B}^{(i)}$ and $\mathbb{1}(b^{(i)})^T$—accordingly, the theorem by O'Rourke and Renfrew[179] contains an unknown term of order one, describing the fluctuations in the outlier eigenvalue. Now, consider the index j associated with the row with the second largest row sum; for a large random matrix, γ_j will be extremely close to γ_i, and the corresponding λ_j might well be lager than λ_i, because of

the fluctuations captured in the term in $o(1)$. The same argument can be made for the third-largest γ_k, and so forth, at least up to a certain proportion of the γ_k. Overall, this means that the estimate of $\hat{\lambda}$ tends to be conservative (especially for low α), and that therefore the probability of feasibility is typically overestimated in this region. Fig. A.7 exemplifies this issue.

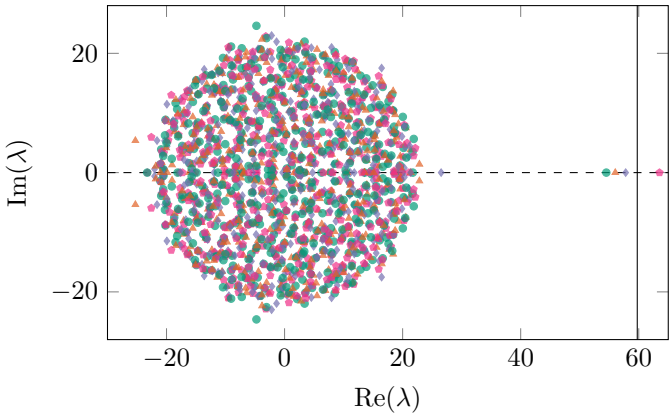

Figure A.7: **Spectra of several $Q_i = \mathbb{1}(b^{(i)})^T - \widetilde{B}^{(i)}$ matrices.** In green we have the spectrum of the matrix Q_i for the i associated with the largest row sum of B (i.e., $\gamma_i = \hat{\gamma}$), in orange that for the i associated with the second largest row sum, in purple that for the third largest row sum, and in pink that for the fourth largest row sum. Even though we would expect the outlier associated with the largest row sum to be the largest (and thus $\hat{\lambda} \approx \hat{\gamma}$, given that $\rho = 0$), we find that in this case the largest outlier is that associated with the fourth largest row sum. Because of this, we underestimate the value of α_F (vertical line).

Despite these limitations, Eq. (A.5) still captures qualitatively the results of simulations: the ordering and spacing of the curves when varying ρ is correct, and the formula, despite its simplicity, describes the shape of the transition to feasibility quite well. It also shows that these curves are *universal*—as long as the matrix B follows the elliptic law, the formula holds asymptotically, irrespective of the fine details of the distribution of B_{ij}. Figure A.8 shows the approximation along with the results of simulations for random systems with varying correlation parameter ρ.

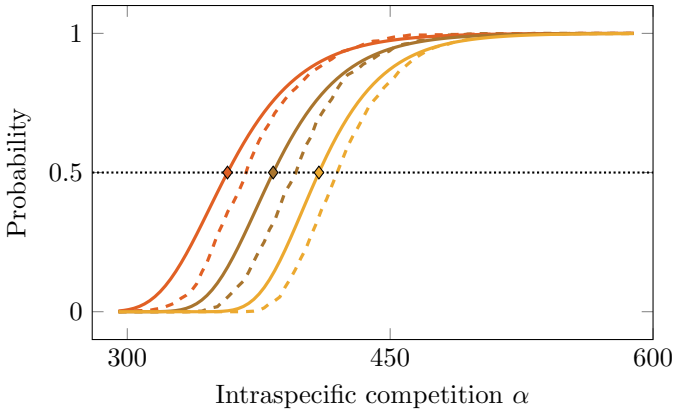

Figure A.8: **Small-rank approximation of the probability of feasibility.** Simulation results (dashed lines, colors representing the off-diagonal correlation, $n = 10000$), vs. the approximation in Eq. (A.5) for the probability of feasibility (y-axis) when α is varied (x-axis). The diamonds mark the median of the approximate distribution—i.e., the value of α for which the approximation returns $p_F = 1/2$. Note that the approximation captures the spacing caused by the correlation, but tends to overestimate the probability of feasibility, especially when α is low.

A.3.7 More accurate approximations of the probability of feasibility

In the section above, we have derived a coarse approximation for the probability of feasibility $p_F(\alpha)$, producing a simple and intuitive equation. The approximation is however inaccurate, and tends to overestimate the probability of feasibility for low values of α. To derive a more accurate approximation, we first state a general result: for any random model with statistically equivalent populations, the mean and correlation between the equilibrium values are fixed; the difference between the models is captured by the variance of the equilibrium values. Having established this result, we provide two methods to approximate the variance of the solution's components, one using the theory of iterative solutions of linear systems, and the other using the theory of resolvents.

When populations are statistically equivalent, then some measures of the distribution of the components of $y^\star$ are especially simple to derive. We have already seen that the expectation of $y_i^\star$, $\mathbb{E}(y_i^\star) = 1/\alpha$, and we denote the variance as $\mathbb{V}(y_i^\star) = \mathbb{E}((y_i^\star)^2) - \mathbb{E}(y_i^\star)^2$,

the covariance between $y_i^\star$ and $y_j^\star$, $\mathbb{Cov}(y_i^\star, y_j^\star) = \mathbb{E}(y_i^\star y_j^\star) - \mathbb{E}(y_i^\star)\mathbb{E}(y_j^\star)$, and their correlation $\mathbb{Cor}(y_i^\star, y_j^\star)$.

Given that the sum of $y_i^\star$ is exactly n/α, then, $(\sum_j y_j^\star)^2 = n^2/\alpha^2$. Expanding, we obtain:

$$\begin{aligned}
\left(\sum_j y_j^\star\right)^2 &= \frac{n^2}{\alpha^2} \\
\sum_j (y_j^\star)^2 + \sum_i \sum_{j \neq i} y_i^\star y_j^\star &= \frac{n^2}{\alpha^2} \\
n\mathbb{E}((y_i^\star)^2) + n(n-1)\mathbb{E}(y_i^\star y_j^\star) &= \frac{n^2}{\alpha^2} \\
\mathbb{V}(y_i^\star) + \mathbb{E}(y_i^\star)^2 + (n-1)\left(\mathbb{Cov}(y_i^\star, y_j^\star) + \mathbb{E}(y_i^\star)\mathbb{E}(y_j^\star)\right) &= n\mathbb{E}(y_i^\star)^2 \\
\mathbb{V}(y_i^\star) + \mathbb{E}(y_i^\star)^2 + (n-1)\left(\mathbb{Cov}(y_i^\star, y_j^\star) + \mathbb{E}(y_i^\star)^2\right) &= n\mathbb{E}(y_i^\star)^2 \\
\mathbb{V}(y_i^\star) + (n-1)\mathbb{Cov}(y_i^\star, y_j^\star) &= 0 \quad ,
\end{aligned}$$

where we have exploited the fact that, for a model with statistically equivalent populations, $\mathbb{E}(y_i^\star)\mathbb{E}(y_j^\star) = \mathbb{E}(y_i^\star)^2$, and that the covariance $\mathbb{Cov}(y_i^\star, y_j^\star)$ must be the same for all i, j. Thus, for *any* unstructured model, we have that the expected covariance is negative. Moreover, for a given variance $\mathbb{V}(y_i^\star) = \sigma^2_{y^\star}$, we have: $\sigma^2_{y^\star} + (n-1)\sigma^2_{y^\star}\mathbb{Cor}(y_i^\star, y_j^\star) = 0$ and thus $\mathbb{Cor}(y_i^\star, y_j^\star) = -1/(n-1)$ for all i and j. Note that this is the maximally negative correlation one can have for equicorrelated random variables. Thus, $y^\star$ has expectation $(1/\alpha)\mathbb{1}$, and covariance matrix $\sigma^2_{y^\star}\left(\frac{n}{n-1}I - \frac{1}{n-1}\mathbb{1}\mathbb{1}^T\right)$. Importantly, the only difference between different unstructured models with random parameters is the value of $\sigma^2_{y^\star}$, while the rest is unchanged. Analyzing increasingly complex models therefore reduces to the problem of determining the variance of $y^\star$.

The joint distribution of $y^\star$ is well-approximated by a multivariate normal[30] in the limit of large n, because of the central limit theorem. To show this, we expand the solution using the Neumann series (see Section A.3.7). Whenever $\alpha > \alpha_L$, the solution can be written as:

$$y^\star = \frac{1}{\alpha}\left(I + \frac{1}{\alpha}C\right)^{-1}\mathbb{1} = \frac{1}{\alpha}\sum_{k=0}^{\infty}\left(-\frac{1}{\alpha}\right)^k C^k\mathbb{1} \quad .$$

It is well known that any vector b follows a multivariate normal distribution if and only if, for an arbitrary vector w of the same dimension, the scalar product $w^T b$ is distributed according to a univariate normal distribution. Then, for an arbitrary vector w, we consider the scalar variable

$$\xi = w^T y^\star = \frac{1}{\alpha}\sum_{k=0}^{\infty}\left(-\frac{1}{\alpha}\right)^k w^T C^k\mathbb{1} \quad .$$

We want to show that ξ is normally distributed. Using the spectral decomposition $C = P\Lambda P^{-1}$, where Λ stands for the diagonal matrix of eigenvalues, and the columns of P contain eigenvectors, we can write

$$w^T C^k\mathbb{1} = \sum_{\ell=1}^{n}\lambda_\ell^k (P^T w)_\ell (P^{-1}\mathbb{1})_\ell \quad .$$

Then, $w^T C^k\mathbb{1}$ is a sum of n variables that are equally distributed. Thus, by the central limit theorem, in the limit $n \to \infty$, the distribution of $w^T C^k\mathbb{1}$ can be well-approximated by a univariate normal. The normality of ξ follows from the properties of linear combinations of normal random variables. Therefore, $y^\star$ is asymptotically distributed as

$$y^\star \sim \mathcal{N}\left(\frac{1}{\alpha}\mathbb{1}, \sigma_{y^\star}^2\left(\frac{n}{n-1}I - \frac{1}{n-1}\mathbb{1}\mathbb{1}^T\right)\right) \quad .$$

Because the joint distribution of $y^\star$ is well-approximated by a multivariate normal, we can calculate the probability of feasibility as a function of α, n, as well as $\sigma_{y^\star}^2$ by integrating the probability density function in the positive orthant of $\mathbb{R}^n$—what is called an "orthant probability":

$$p_F(n, \alpha, \sigma^2_{y^\star}) = \int_0^\infty \int_0^\infty \cdots \int_0^\infty \phi(y^\star) dy_1^\star dy_2^\star \cdots dy_n^\star \quad ,$$

where $\phi(y^\star)$ is the probability density function of the normal distribution above. For equicorrelated random variables, the multiple integral above can be reduced to a single integral (albeit involving complex variables when the correlation is negative, such as in this case[181]). Equivalently, one can use the theory of order statistics to write the density function of the first order statistics (i.e., the $\min_i(y_1^\star, y_2^\star, \ldots, y_n^\star)$) and integrate this density function for all positive values of the minimum.

When n is large, the fact that the components of $y^\star$ are slightly negatively correlated becomes less and less important, and we can treat them approximately as if they were independent. This simplification is common in high-dimensional probability: correlations of order $1/n$ vanish as $n \to \infty$.

Under this independence assumption, and given that the components of $y^\star$ are identically distributed, we can focus on the probability that $y_i^\star > 0$, and p_F is simply this value raised to the nth power.

Each random variable $y_i^\star$ has mean $\mathbb{E}(y_i^\star) = 1/\alpha$. To measure how much a given realization deviates from this mean, we define

$$\zeta_i = y_i^\star - \frac{1}{\alpha}.$$

Thus, ζ_i has mean zero, and feasibility requires

$$y_i^\star > 0 \iff \zeta_i > -\frac{1}{\alpha}.$$

To make the distribution dimensionless and comparable to the standard normal, we divide

by the standard deviation $\sigma_{y^\star}$:

$$\xi_i = \frac{\zeta_i}{\sigma_{y^\star}}.$$

Now each ξ_i is a random variable following the standard normal distribution (mean zero and unit variance). The feasibility condition becomes

$$\xi_i > -\frac{1}{\alpha\sigma_{y^\star}}.$$

For a standard normal variable ξ, the probability that it is larger than a threshold t is

$$\Pr(\xi > t) = 1 - \Phi(t),$$

where Φ is the cumulative distribution function (CDF) of the standard normal. If we plug $t = -1/(\alpha\sigma_{y^\star})$, we get

$$\Pr\left(\xi_i > -\tfrac{1}{\alpha\sigma_{y^\star}}\right) = 1 - \Phi\left(-\tfrac{1}{\alpha\sigma_{y^\star}}\right).$$

Because the standard normal distribution is symmetric about 0, we have

$$1 - \Phi(-z) = \Phi(z).$$

Therefore,

$$\Pr\left(\xi_i > -\tfrac{1}{\alpha\sigma_{y^\star}}\right) = \Phi\left(\tfrac{1}{\alpha\sigma_{y^\star}}\right). \tag{A.6}$$

Since we are treating the ξ_i as independent, the probability that *all* n inequalities hold is just the product of the probabilities for each one:

$$p_F(n, \alpha, \sigma^2_{y^\star}) \;\approx\; \left[\Pr\left(\xi_i > -\tfrac{1}{\alpha\sigma_{y^\star}}\right)\right]^n.$$

Substituting the expression A.6, we obtain

$$p_F(n, \alpha, \sigma_{y^\star}^2) \;\approx\; \Phi\left(\frac{1}{\alpha\sigma_{y^\star}}\right)^n . \tag{A.7}$$

A.3.8 Computing $\sigma_{y^\star}$ using resolvents

As described in the section above, one can approximate the probability of feasibility using Eq. (A.7) (cf., Eq. (1.3) of the main text). To this end, one just needs to compute the variance of a single component of the equilibrium solution $y^\star$. Here, we provide an approximation for the standard deviation $\sigma_{y^\star}$, obtained by computing the expectation of the resolvent of the linear system

$$(\alpha I + B)x^\star = \mathbb{1}\,.$$

As a result of this calculation, we obtain an approximated formula for the deviation $\sigma_{y^\star}$ which, together with Eq. (A.7), is able to capture accurately the behavior of the probability of feasibility as a function of α, even for small sizes. Importantly, this approximation is valid for arbitrary values of the correlation, $\rho \in [-1, 1]$. For example, Fig. A.9 shows the quality of the approximation for $n = 50$, and different correlation values.

Because B is a random matrix, the solution of the linear system (if it exists) is given by the random vector

$$x^\star = (\alpha I + B)^{-1}\mathbb{1}\,.$$

To calculate $\sigma_{y^\star}$: we first compute, in the limit of large system sizes ($n \to \infty$), the expectations of the equilibrium solution, $\mathbb{E}(x^\star)$, and the expectation of the scalar product $x^{\star T}x^\star$, $\mathbb{E}(x^{\star T}x^\star)$. With these two results, it is straightforward to evaluate asymptotically

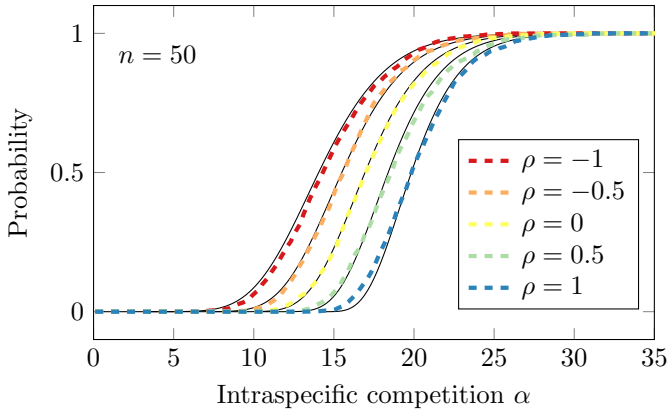

Figure A.9: **Resolvent approximation of the probability of feasibility.** Approximation using the resolvent method, cf. Eqs. (A.7) and (A.31), for matrices B of size $n = 50$, whose entries are sampled from normal distribution with off-diagonal correlation ρ (color). The approximations (solid lines) match the simulations (dashed lines) quite perfectly.

the variance $\sigma^2_{x^\star}$ of a single population as $\sigma^2_{x^\star} = \frac{1}{n}(\mathbb{E}(x^{\star T}x^\star) - \mathbb{E}(x^\star)^T\mathbb{E}(x^\star))$. Then, we use the proportionality relation between $x^\star$ and $y^\star$ to approximate the deviation $\sigma_{y^\star}$: because $y^\star = (\alpha I + C)^{-1}\mathbb{1}$ and $C = B - \mathbb{1}m^T$, one can use the Sherman-Morrison's formula to obtain

$$y^\star = \frac{1}{1 - m^T x^\star} x^\star.$$

Ignoring the correlation between $x^\star$ and $1 - m^T x^\star$, and approximating the expectation of the ratio by the ratio of expectations, we can write

$$y^\star = \frac{1}{1 - m^T x^\star} x^\star \approx \mathbb{E}\left(\frac{1}{1 - m^T x^\star}\right) x^\star \approx \frac{1}{\mathbb{E}\left(1 - m^T x^\star\right)} x^\star,$$

and therefore

$$\sigma_{y^\star} \approx \frac{\sigma_{x^\star}}{\mathbb{E}(1 - m^T x^\star)}, \tag{A.8}$$

where the standard deviations in this equation refer to the deviation of a single component of vectors $x^\star$ and $y^\star$ —all the components have the same expected deviation.

Because $\sigma^2_{x^\star} = \frac{1}{n}(\mathbb{E}(x^{\star T}x^\star) - \mathbb{E}(x^\star)^T\mathbb{E}(x^\star))$, approximating $\sigma_{y^\star}$ simply requires evaluating the expectations $\mathbb{E}(x^\star)$, $\mathbb{E}(x^{\star T}x^\star)$, and $\mathbb{E}(1 - m^T x^\star)$. We start with the cases $\rho = \pm 1$, which are easier to derive, and allow us to devise a route to obtain the general result for arbitrary ρ. In all the cases, it will be critical to employ a sort of "symmetrization" of matrix B (which is only ensured for $\rho = 1$, in which case the matrix is indeed symmetric).

Symmetric case, $\rho = 1$. First, we consider the case $\rho = 1$, i.e., the fully symmetric case ($B_{ij} = B_{ji}$). We have to compute the aforementioned expectations.

Computation of $\mathbb{E}(x^\star)$ using resolvents To begin with, we will focus on evaluating the expectation $\mathbb{E}(x^\star)$:

$$\mathbb{E}(x^\star) = \mathbb{E}((\alpha I + B)^{-1})\mathbb{1}.$$

Let $z \in \mathbb{C}$ be a complex number with non-zero imaginary part. Then the resolvent of matrix B is defined as the inverse $(zI + B)^{-1}$, and we want to evaluate its expectation

$$G(z) = \mathbb{E}((zI + B)^{-1}),$$

computed over the ensemble of random matrices to which B belongs. $G(z)$ can be expressed formally via the corresponding Neumann series expansion (which is always convergent if $\mathcal{I}⇳(z) > 0$). Our aim in this section is to obtain an asymptotic expression for $G(z)$, valid when $n \to \infty$, and then compute the expectations $\mathbb{E}(x^\star)$, $\mathbb{E}(x^{\star T}x^\star)$ and $\mathbb{E}(1 - m^T x^\star)$ in terms of $G(z)$. Once we have all the expressions, we will write $z = \alpha + i\epsilon$, and take the limit $\epsilon \to 0$ to obtain the final result.

In the limit $n \to \infty$, the expectation $G(z)$ of the resolvent satisfies the so-called matrix Dyson equation [182]:

$$G(z) = \frac{1}{z} I + \frac{1}{z} \mathbb{E}(BG(z)B)G(z). \tag{A.9}$$

This equation is exact for normally-distributed matrix entries B_{ij}, and is asymptotically true for arbitrary distributions (see Appendix A.5.2 for a derivation of this equation).

In order to solve this nonlinear equation, we make a guess for the expectation $\Sigma := \mathbb{E}(BG(z)B)$. Let G_{ij} be the elements of matrix $G(z)$. Since $\mathbb{E}(B_{ij}B_{kl}) = \delta_{ik}\delta_{jl} + \delta_{il}\delta_{jk}$ (where δ_{ij} stands for the Kronecker symbol) holds for $\rho = 1$, then

$$\Sigma_{il} = \mathbb{E}\left(\sum_{j,k} B_{ij}G_{jk}B_{kl}\right) = \sum_{j,k} \mathbb{E}(B_{ij}B_{kl})G_{jk},$$

because G_{jk} is an expectation itself. Hence

$$\Sigma_{il} = G_{li} + \delta_{il} \sum_{j} G_{jj}.$$

Therefore, in the limit $n \to \infty$, it is expected that the diagonal of matrix Σ dominates the off-diagonal entries. Thus, we adopt the guess $\Sigma = a(z)I$, and look for solutions for the function $a(z)$ —observe that, given that populations are statistically equivalent, we expect all the diagonal elements of the expectation $\mathbb{E}(BG(z)B)$ to be the same.

We substitute this assumption into Eq. (A.9) and solve for $G(z)$:

$$G(z) = \frac{1}{z} I + \frac{a(z)}{z} G(z); \qquad G(z) = (z - a(z))^{-1} I.$$

Now we can compute Σ in a different way:

$$\Sigma = \mathbb{E}(BG(z)B) = (z - a(z))^{-1}\mathbb{E}(B^2) = \frac{n-1}{z - a(z)} I = a(z)I,$$

where we have used that $\mathbb{E}((B^2)_{ii}) = \sum_j \mathbb{E}(B_{ij}B_{ji}) = \sum_j \mathbb{E}(B_{ij}^2) = n - 1$, and the last step

follows because the sum over j only contains $n-1$ terms (given that $B_{ii}=0$). In addition, if $i \neq k$, we have that $\mathbb{E}((B^2)_{ik}) = \sum_j \mathbb{E}(B_{ij}B_{jk}) = \sum_j(\delta_{ij}\delta_{jk}+\delta_{ik}\delta_{jj}) = \delta_{ik}+\delta_{ik}\sum_j \delta_{jj} = 0$. Thus, $\mathbb{E}(B^2) = (n-1)I$ and the last equation implies that the unknown function $a(z)$ satisfies the quadratic equation

$$a(z)(z-a(z)) = n-1.$$

Solving for $a(z)$, we obtain

$$a(z) = \frac{z \pm \sqrt{z^2-4(n-1)}}{2}.$$

According to the definition of the resolvent, $(zI+B)^{-1}$, it must behave as $z^{-1}I$ as $z \to \infty$. Therefore, Dyson equation (A.9) implies that $z^{-1}\Sigma \to 0$ as $z \to \infty$, which means that we have to choose the minus sign in $a(z)$. Consequently, the resolvent expectation is expressed as

$$G(z) = (z-a(z))^{-1}I = \frac{2}{z+\sqrt{z^2-4(n-1)}}I = \frac{z-\sqrt{z^2-4(n-1)}}{2(n-1)}I.$$

Having computed the resolvent expectation in the asymptotic limit $n \to \infty$, we immediately find an expression for the expected value of $x^\star$:

$$\mathbb{E}(x^\star) = \lim_{\epsilon \to 0} \mathbb{E}(((\alpha+i\epsilon)I+B)^{-1})\mathbb{1} = \lim_{\epsilon \to 0} G(\alpha+i\epsilon)\mathbb{1} = \frac{\alpha-\sqrt{\alpha^2-4(n-1)}}{2(n-1)}\mathbb{1}. \quad \text{(A.10)}$$

Computation of $\mathbb{E}(x^{\star T}x^\star)$ The second expectation to be computed can be written as

$$\mathbb{E}(x^{\star T}x^\star) = \mathbb{1}^T\mathbb{E}(((\alpha I+B)^{-1})^T(\alpha I+B)^{-1})\mathbb{1} = \mathbb{1}^T\mathbb{E}((\alpha I+B)^{-2})\mathbb{1},$$

because $((\alpha I + B)^{-1})^T = ((\alpha I + B)^T)^{-1} = (\alpha I + B)^{-1}$ (since $B^T = B$). Here we denote by $(\alpha I + B)^{-2}$ the square power of $(\alpha I + B)^{-1}$. Thus, we need to evaluate the expectation of $(\alpha I + B)^{-2}$. Let us define it as

$$K(z) = \mathbb{E}((\alpha I + B)^{-2}).$$

We show in the Appendix that $K(z)$ can be written in a simple way in terms of the derivative of $G(z)$, namely:

$$K(z) = -G'(z) = \frac{1}{2(n-1)} \left(\frac{z}{\sqrt{z^2 - 4(n-1)}} - 1 \right) I, \tag{A.11}$$

which implies that

$$\mathbb{E}(x^{\star T} x^\star) = \lim_{\epsilon \to 0} \mathbb{1}^T K(\alpha + i\epsilon)\mathbb{1} = \frac{n}{2(n-1)} \left(\frac{\alpha}{\sqrt{\alpha^2 - 4(n-1)}} - 1 \right). \tag{A.12}$$

Using the expression obtained above for $\mathbb{E}(x^\star)$, we find, after simplifications, the following asymptotic limit for the variance $\sigma^2_{x^\star}$:

$$\sigma^2_{x^\star} = \frac{1}{n}(\mathbb{E}(x^{\star T} x^\star) - \mathbb{E}(x^\star)^2) = \frac{1}{2(n-1)^2} \left(n - 1 - \alpha^2 + \frac{\alpha(\alpha^2 - 3(n-1))}{\sqrt{\alpha^2 - 4(n-1)}} \right). \tag{A.13}$$

Computation of $\mathbb{E}(1 - m^T x^\star)$ To evaluate the last expectation we need, we first observe that $(\alpha I + B)x^\star = \mathbb{1}$ implies, by left-multiplying by $\mathbb{1}^T$, that

$$\alpha \mathbb{1}^T x^\star + \mathbb{1}^T B x^\star = n.$$

Equivalently,

$$\frac{\alpha}{n}\mathbb{1}^T x^\star + m^T x^\star = 1,$$

because, by definition, $m = \frac{1}{n}B^T\mathbb{1}$. Therefore

$$1 - m^T x^\star = \frac{\alpha}{n}\mathbb{1}^T x^\star.$$

The expectation $\mathbb{E}(\mathbb{1}^T x^\star) = \mathbb{1}^T\mathbb{E}(x^\star)$ follows from $\mathbb{E}(x^\star)$: using Eq. (A.10), we finally obtain

$$\mathbb{E}(1 - m^T x^\star) = \frac{\alpha}{n}\mathbb{1}^T\mathbb{E}(x^\star) = \frac{\alpha^2 - \alpha\sqrt{\alpha^2 - 4(n-1)}}{2(n-1)}.$$

Substituting this result and Eq. (A.13) into Eq. (A.8), and after some simplifications, the approximation of $\sigma_{y^\star}$ finally reads

$$\sigma_{y^\star} \approx \frac{1}{\alpha}\sqrt{\frac{\alpha}{2\sqrt{\alpha^2 - 4(n-1)}} - \frac{1}{2}}. \tag{A.14}$$

This result is valid for $\rho = 1$, large n, and is well defined for $\alpha > 2\sqrt{n-1}$. In particular, this condition is satisfied for $\alpha \geq 2\sqrt{n} = \alpha_S$, i.e., above the global stability threshold for $\rho = 1$. The choice of the distribution for B_{ij} has no effect (asymptotically). This approximation compares very well with simulated data for the distributions considered here (Fig. A.9), even for small n.

Skew-symmetric case, $\rho = -1$. In order to proceed as in the symmetric case, we have to find a Dyson equation satisfied by the resolvent expectation $\mathbb{E}((\alpha I + B)^{-1})$. The formalism of the matrix Dyson equation can only be applied to Hermitian matrices [182]; however, for $\rho = -1$ matrix B is skew-symmetric ($B^T = -B$). In order for the Dyson equation to hold, we transform the original matrix in order to make it Hermitian: let $Q = iB$, where i is the

imaginary unit. Then $Q^\dagger = (iB)^\dagger = -iB^T = iB = Q$, and hence Q is Hermitian (here, † means complex conjugate transpose).

To solve $(\alpha I + B)x^\star = 1$ we focus on the transformed linear system

$$(i\zeta I + iB)x^\star = i\mathbb{1},$$

for $\zeta \in \mathbb{C}$. Then let $z = i\zeta$ (with positive imaginary part) and write the system to solve as $(zI + Q)x^\star = i\mathbb{1}$, with Q Hermitian. We just need to compute the expectation

$$G(z) = \mathbb{E}((zI + Q)^{-1})$$

The same matrix Dyson equation holds, see Eq. (A.9):

$$G(z) = \frac{1}{z}I + \frac{1}{z}\mathbb{E}(QG(z)Q)G(z). \tag{A.15}$$

Following the same arguments as before, we look for solutions such that $\mathbb{E}(BG(z)B) = a(z)I$. Therefore,

$$\mathbb{E}(QG(z)Q) = i^2\mathbb{E}(BG(z)B) = -a(z)I.$$

We introduce this expression into the Dyson equation and solve for $G(z)$:

$$G(z) = (z + a(z))^{-1}I.$$

Now, given that $G(z)$ is a multiple of the identity, we can evaluate $\mathbb{E}(QG(z)Q)$ in a different way:

$$\mathbb{E}(QG(z)Q) = -\mathbb{E}(BG(z)B) = -(z + a(z))^{-1}\mathbb{E}(B^2).$$

As for the symmetric case, one can check that $\mathbb{E}(B_{ij}^2) = 0$ for $i \neq j$. Only diagonal expectations remain: $\mathbb{E}(B_{ii}^2) = \sum_j \mathbb{E}(B_{ij}B_{ji}) = -\sum_j \mathbb{E}(B_{ij}^2) = -(n-1)$, because $B_{ii} = 0$ by definition. Therefore,

$$\mathbb{E}(QG(z)Q) = \frac{n-1}{z + a(z)} I.$$

As a consequence, $a(z)$ must satisfy the quadratic equation

$$a(z)(z + a(z)) + n - 1 = 0,$$

which yields

$$a(z) = \frac{-z \pm \sqrt{z^2 - 4(n-1)}}{2},$$

and

$$G(z) = \frac{2}{z \pm \sqrt{z^2 - 4(n-1)}} I.$$

In order for $G(z) \sim \frac{1}{z} I$ as $z \to \infty$, we have to choose the positive sign. Then, we can write

$$G(z) = \frac{z - \sqrt{z^2 - 4(n-1)}}{2(n-1)} I.$$

Now we go back to the original variable $z = i\zeta$ and matrix $Q = iB$:

$$G(i\zeta) = \mathbb{E}((i\zeta I + iB)^{-1}) = i^{-1}\mathbb{E}((\zeta I + B)^{-1}) = -i\mathbb{E}((\zeta I + B)^{-1}) = -iG(\zeta),$$

where $G(\zeta) = \mathbb{E}((\zeta I + B)^{-1})$ is the expectation we want to evaluate. On the other hand,

$$G(i\zeta) = -i\frac{\sqrt{\zeta^2 + 4(n-1)} - \zeta}{2(n-1)} I = -iG(\zeta).$$

Thus, by substituting $\zeta = \alpha + i\epsilon$, and taking the limit $\epsilon \to 0$, we find the following expression for the resolvent expectation in the skew-symmetric case:

$$G(\alpha) = \lim_{\epsilon \to 0} \mathbb{E}(((\alpha + i\epsilon)I + B)^{-1}) = \frac{\sqrt{\alpha^2 + 4(n-1)} - \alpha}{2(n-1)} I. \tag{A.16}$$

This result automatically implies that $\mathbb{E}(x^\star) = g(\alpha)\mathbb{1}$, where we have defined

$$g(\alpha) = \frac{\sqrt{\alpha^2 + 4(n-1)} - \alpha}{2(n-1)}. \tag{A.17}$$

Computation of $\mathbb{E}(x^{\star T} x^\star)$ Because $x^\star = (\alpha I + B)^{-1}\mathbb{1}$ and $x^{\star T} = \mathbb{1}^T(\alpha I - B)^{-1}$ (we have used, in the last calculation, that $B^T = -B$), we can write the expectation $\mathbb{E}(x^{\star T} x^\star)$ as

$$\mathbb{E}(x^{\star T} x^\star) = \mathbb{1}^T \mathbb{E}((\alpha I - B)^{-1}(\alpha I + B)^{-1})\mathbb{1}.$$

Now we resort to the identity

$$(\alpha I - B)^{-1}(\alpha I + B)^{-1} = \frac{1}{2\alpha}(\alpha I + B)^{-1} + \frac{1}{2\alpha}(\alpha I - B)^{-1},$$

which can be easily proven by left- and right-multiplying both sides by $\alpha I - B$ and $\alpha I + B$, respectively. By taking expectations, we obtain

$$\mathbb{E}((\alpha I - B)^{-1}(\alpha I + B)^{-1}) = \frac{1}{2\alpha}\mathbb{E}((\alpha I + B)^{-1}) + \frac{1}{2\alpha}\mathbb{E}((\alpha I - B)^{-1}).$$

It holds that $\mathbb{E}((\alpha I - B)^{-1}) = \mathbb{E}((\alpha I + B)^{-1})$ —this can be verified by solving Eq. (A.15)

for $Q = iB^T = -iB$. Therefore,

$$\mathbb{E}((\alpha I - B)^{-1}(\alpha I + B)^{-1}) = \frac{1}{\alpha}\mathbb{E}((\alpha I + B)^{-1}) = \frac{g(\alpha)}{\alpha} I, \tag{A.18}$$

and $\mathbb{E}(x^{\star T} x^\star) = n g(\alpha)/\alpha$. Notice that $\mathbb{E}(x^\star)^T \mathbb{E}(x^\star) = n g(\alpha)^2$, and thus

$$\sigma^2_{x^\star} = \frac{1}{n}(\mathbb{E}(x^{\star T} x^\star) - \mathbb{E}(x^\star)^T \mathbb{E}(x^\star)) = \frac{g(\alpha)}{\alpha} - g(\alpha)^2. \tag{A.19}$$

Final approximation for $\sigma_{y^\star}$ in the skew-symmetric case The calculation we did for the expectation $\mathbb{E}(1 - m^T x^\star)$ in the symmetric case is still valid in the skew-symmetric case,

$$\mathbb{E}(1 - m^T x^\star) = \frac{\alpha}{n} \mathbb{1}^T \mathbb{E}(x^\star) = \alpha g(\alpha).$$

Finally, substituting the last expression and Eq. (A.19) into Eq. (A.8), we find

$$\sigma_{y^\star} \approx \frac{\sqrt{g(\alpha)(\alpha^{-1} - g(\alpha))}}{\alpha g(\alpha)} = \frac{1}{\alpha}\sqrt{\frac{1}{\alpha g(\alpha)} - 1} = \frac{1}{\alpha}\sqrt{\frac{\sqrt{\alpha^2 + 4(n-1)}}{2\alpha} - \frac{1}{2}}, \tag{A.20}$$

where we have used that $1/g(\alpha) = (\sqrt{\alpha^2 + 4(n-1)} + \alpha)/2$ and performed some straightforward manipulations. Again, this expression is universal and does not depend (in the limit of large n) on the distribution chosen to draw matrix elements. It compares very well with simulations (Fig. A.9).

General case: arbitrary correlation. We take further advantage of the theory of resolvents to compute an approximation for $\sigma_{y^\star}$ for arbitrary values of the correlation coefficient ρ. We recover the two limits studied above ($\rho = 1$ and $\rho = -1$) as particular cases of this more general calculation. The rationale of the proof in the general case is based again on a

matrix Dyson equation. Having studied first the limiting cases $\rho = 1$ and $\rho = -1$, for which the derivation is simpler, one can intuit the general route to be followed to tackle the general case with arbitrary correlation.

One critical feature of the Dyson equation used in both cases is that it applies for Hermitian matrices. For $\rho = 1$, matrix B is symmetric by definition, and for $\rho = -1$ we applied the matrix Dyson equation used for $\rho = 1$ to matrix $Q = iB$, which is Hermitian (since satisfies $Q^\dagger = Q$). For arbitrary ρ we resort to the "Hermitization trick" due to Girko [21]: consider, for $z \in \mathbb{C}$, the $(2n) \times (2n)$ matrix

$$Q(z) = \begin{pmatrix} \mathbb{0} & zI + B \\ z^\star I + B^T & \mathbb{0} \end{pmatrix},$$

where $z^\star$ denotes the conjugate of complex number z, and $\mathbb{0}$ stands for the null matrix of dimension n. Matrix $Q(z)$ is called the Hermitization of matrix $zI + B$, for B real. One can see that Q is Hermitian, i.e., $Q^\dagger = Q$.

$Q(z)$ belongs to a general class of self-adjoint (Hermitian) random matrices with correlated entries, for which Alt and Krüger proved in [57] that the resolvent of matrix Q, defined as

$$S(z, w) := (iwI_2 + Q(z))^{-1},$$

satisfies, in the limit of large n, the following non-linear matrix Dyson equation:

$$-\begin{pmatrix} I & \mathbb{0} \\ \mathbb{0} & I \end{pmatrix} = \left(\begin{pmatrix} iwI & -zI \\ -z^\star I & iwI \end{pmatrix} + \Lambda(S(z, w)) \right) S(z, w), \tag{A.21}$$

where I is the identity matrix of dimension n, I_2 is the $(2n) \times (2n)$ identity matrix, and Λ is a matrix operator defined, for an arbitrary complex, square matrix A with dimension

$(2n) \times (2n)$, as

$$\Lambda(A) := \mathbb{E}((Q(z) - Z)A(Q(z) - Z)),$$

where $Z := \begin{pmatrix} \mathbb{0} & zI \\ z^\star I & \mathbb{0} \end{pmatrix}$. Observe that the expectation $\mathbb{E}((iwI_2 + Q(z))^{-1})$ also satisfies the same matrix Dyson equation, which is somewhat an extension of the Dyson equation used for $\rho = 1$ to "hermitized" matrices.

Can we extract the resolvent $(zI + B)^{-1}$ from the resolvent $S(z, w)$ of the Hermitized matrix? Let us partition S in two $n \times n$ square blocks as

$$S(z, w) = \begin{pmatrix} S_{11} & S_{12} \\ S_{21} & S_{22} \end{pmatrix}.$$

Then, matrix S satisfies

$$\begin{pmatrix} iwI & zI + B \\ z^\star I + B^T & iwI \end{pmatrix} \begin{pmatrix} S_{11} & S_{12} \\ S_{21} & S_{22} \end{pmatrix} = \begin{pmatrix} I & \mathbb{0} \\ \mathbb{0} & I \end{pmatrix},$$

which implies

$$iwS_{11} + (zI + B)S_{21} = I.$$

Therefore, the resolvent $(zI + B)^{-1}$ we want to calculate is the lower-left block of the augmented resolvent $S(z, w)$ evaluated at $w = 0$. Our goal is to compute an asymptotic approximation to $S(z, w)$ via the solution of the matrix Dyson equation (A.21).

As shown in [57], in the limit $n \to \infty$, the solution to Eq. (A.21) is of the form

$$S(z, w) = \begin{pmatrix} iv(z, w)I & b(z, w)^\star I \\ b(z, w)I & iv(z, w)I \end{pmatrix}, \tag{A.22}$$

where the imaginary part of v is positive, b takes values on the complex plane, and S satisfies $\mathcal{I}\Updownarrow(S) = \frac{1}{2i}(S - S^\dagger)$, which is positive definite. Since we are interested in the particular value $w = 0$, we can compute explicit expressions for functions v and b in terms of z. From now on, we omit the dependence on z and w in v and b.

In order to obtain explicit forms for v and b in terms of z, we first evaluate the expectation $\Lambda(S(z,w)) = \mathbb{E}((Q(z)-Z)S(z,w)(Q(z)-Z))$ at the solution given by Eq. (A.22). This yields

$$\Lambda(S(z,w)) = \begin{pmatrix} iv\mathbb{E}(BB^T) & b\mathbb{E}(B^2) \\ b^\star\mathbb{E}((B^T)^2) & iv\mathbb{E}(B^TB) \end{pmatrix} \tag{A.23}$$

Recall that $\mathbb{E}(B_{ij}^2) = 1$ and $\mathbb{E}(B_{ij}B_{ji}) = \rho$ for $j \neq i$, which implies that $\mathbb{E}(B^TB) = \mathbb{E}(BB^T) = (n-1)I$ and $\mathbb{E}(B^2) = \mathbb{E}((B^T)^2) = \rho(n-1)I$. Then $\Lambda(S(z,w))$ simplifies to

$$\Lambda(S(z,w)) = (n-1)\begin{pmatrix} ivI & b\rho I \\ b^\star\rho I & ivI \end{pmatrix}.$$

We obtain the non-linear system of equations satisfied by v and b by substituting Eqs. (A.22) and (A.23) into the matrix Dyson equation (A.21):

$$\begin{aligned} -1 &= -wv - zb + (n-1)(-v^2 + \rho b^2), \\ 0 &= wb^\star - zv + (n-1)(vb^\star + \rho vb). \end{aligned} \tag{A.24}$$

The two remaining equations are simply the complex conjugate of the two equations above. From the second equation we can solve for v:

$$v = -\frac{wb^\star}{(n-1)b^\star + (n-1)\rho b - z}, \tag{A.25}$$

and substitute into the first equation to get a fourth-order equation to be satisfied by b:

$$((n-1)\rho b^2 - zb + 1)((n-1)b^\star + (n-1)\rho b - z)^2 + w^2 b^\star((n-1)b^\star + (n-1)\rho b - z) - (n-1)w^2 b^{\star 2} = 0.$$

Since the solution of this polynomial equation will be a continuous function of w at $w = 0$, we can set $w = 0$ to get

$$((n-1)\rho b^2 - zb + 1)((n-1)b^\star + (n-1)\rho b - z)^2 = 0.$$

For v to be well defined, the only solution for b is the one that cancels the first factor:

$$b(z, 0) = \frac{z - \sqrt{z^2 - 4\rho(n-1)}}{2\rho(n-1)}, \tag{A.26}$$

where we have chosen the minus sign so that the resolvent $(zI + B)^{-1}$ behaves as $z^{-1}I$ in the limit $z \to \infty$ (recall that $(zI + B)^{-1} \approx S_{21}|_{w=0} = b(z, 0)I$ in the limit of large n). Therefore, we can obtain the expectation $\mathbb{E}(x^\star)$ by substituting $z = \alpha + i\epsilon$ in the expression for $b(z, 0)$ and letting $\epsilon \to 0$:

$$\mathbb{E}(x^\star) = \lim_{\epsilon \to 0} b(\alpha + i\epsilon, 0)\mathbb{1} = \frac{\alpha - \sqrt{\alpha^2 - 4\rho(n-1)}}{2\rho(n-1)}\mathbb{1}. \tag{A.27}$$

Note that this expectation is always a positive real number for $\alpha > 2\sqrt{\rho(n-1)}$, even for negative ρ. By taking the limit $\rho \to 0$ in the last equation we obtain $\mathbb{E}(x^\star) = \alpha^{-1}\mathbb{1}$ for $\rho = 0$. One can easily check that Eq. (A.27) reduces to Eq. (A.10) for $\rho = 1$ and Eq. (A.17) for $\rho = -1$.

Computation of $\mathbb{E}(x^{\star T} x^\star)$ As for the derivations above, we need to calculate the expectation $\mathbb{E}(x^{\star T} x^\star)$ in order to approximate σ_y according to Eq. (A.8). Here we follow an approach similar to the $\rho = -1$ case. Let us focus on the matrix product

$$W := (iwI_2 + Q(z))^{-1^\dagger}(iwI_2 + Q(z))^{-1} = (-iw^\star I_2 + Q(z))^{-1}(iwI_2 + Q(z))^{-1},$$

where in the last step we have used $Q^\dagger = Q$. This is in analogy with the product $(zI - B)^{-1}(zI + B)^{-1}$, which was used to compute the expectation $\mathbb{E}(x^{\star T}x^\star)$ in the skew-symmetric case ($\rho = -1$). For arbitrary correlation we use the resolvent of the Hermitization instead. By writing W as a block matrix, it satisfies

$$\begin{aligned}&(iwI_2 + Q(z))^\dagger W(iwI_2 + Q(z))\\ &\quad= \begin{pmatrix} -iw^\star I & zI + B \\ z^\star I + B^T & -iw^\star I \end{pmatrix}\begin{pmatrix} W_{11} & W_{12} \\ W_{21} & W_{22} \end{pmatrix}\begin{pmatrix} iwI & zI + B \\ z^\star I + B^T & iwI \end{pmatrix} = \begin{pmatrix} I & \mathbb{0} \\ \mathbb{0} & I \end{pmatrix}.\end{aligned}$$

Setting $w = 0$, the lower-right block of this equality implies

$$(z^\star I + B^T)W_{11}(zI + B) = I, \qquad W_{11} = (z^\star I + B^T)^{-1}(zI + B)^{-1}.$$

Therefore, the expectation of the upper-left block of matrix W is precisely related to the expectation we want to compute:

$$\mathbb{E}(x^{\star T}x^\star) = \mathbb{1}^T\mathbb{E}((\alpha I + B^T)^{-1}(\alpha I + B)^{-1})\mathbb{1}.$$

Thus, our next goal is to compute W. To this end, as we did in the skew-symmetric case, we write

$$W = c_1(-iw^\star I_2 + Q(z))^{-1} + c_2(iwI_2 + Q(z))^{-1}.$$

Substituting into $(iwI_2 + Q(z))^\dagger W(iwI_2 + Q(z)) = I_2$ we obtain the condition

$$c_1(iwI_2 + Q(z)) + c_2(-iw^\star I_2 + Q(z)) = I_2,$$

which implies that $c_1 = -c_2$ and $i(c_1 w - c_2 w^\star) = 1$. Therefore, $c_1 = \frac{i}{w+w^\star} = -c_2$ and we can write

$$W = -\frac{i}{w+w^\star}\left((iwI_2 + Q(z))^{-1} - (-iw^\star I_2 + Q(z))^{-1}\right) = -\frac{i}{w+w^\star}(S(z,w) - S(z,-w^\star)).$$

We now use the asymptotic limit of matrix S, given by Eq. (A.22), and Eq. (A.25) to obtain

$$W_{11} = \frac{v(z,w) - v(z,-w^\star)}{w+w^\star} I = -\frac{b^\star}{(n-1)b^\star + (n-1)\rho b - z} I,$$

which turns out to be independent of w (this is true in the limit $n \to \infty$). Therefore,

$$\mathbb{E}((\alpha I + B^T)^{-1}(\alpha I + B)^{-1}) = \lim_{\epsilon \to 0} \frac{-b^\star(\alpha + i\epsilon, 0)}{(n-1)b^\star(\alpha + i\epsilon, 0) + (n-1)\rho b(\alpha + i\epsilon, 0) - (\alpha + i\epsilon)} I. \tag{A.28}$$

Using Eq. (A.26), and after some simplifications, we finally get the asymptotic formula

$$\mathbb{E}((\alpha I + B^T)^{-1}(\alpha I + B)^{-1}) = \frac{2}{\alpha(\alpha + \sqrt{\alpha^2 - 4\rho(n-1)}) - 2(1+\rho)(n-1)} I. \tag{A.29}$$

One can use this expression to recover Eq. (A.12) for $\rho = 1$, and Eq. (A.18) for $\rho = -1$.

Final result for the deviation $\sigma_{y^\star}$ Let us define

$$g(\alpha) := \frac{\alpha - \sqrt{\alpha^2 - 4\rho(n-1)}}{2\rho(n-1)}, \qquad g_2(\alpha) := \frac{2}{\alpha^2 + \alpha\sqrt{\alpha^2 - 4\rho(n-1)}) - 2(1+\rho)(n-1)}.$$

Hence, $\mathbb{E}(x^\star) = g(\alpha)\mathbb{1}$ and $\mathbb{E}(x^{\star T}x^\star) = ng_2(\alpha)$. This allows to approximate the variance of $x^\star$ as

$$\sigma_{x^\star}^2 = \frac{1}{n}(\mathbb{E}(x^{\star T}x^\star) - \mathbb{E}(x^\star)^T\mathbb{E}(x^\star)) = g_2(\alpha) - g(\alpha)^2.$$

As in the particular cases $\rho = \pm 1$, the expectation $\mathbb{E}(1 - m^T x^\star)$ can be computed as

$$\mathbb{E}(1 - m^T x^\star) = \frac{\alpha}{n}\mathbb{1}^T\mathbb{E}(x^\star) = \alpha g(\alpha).$$

Finally, substituting into Eq. (A.8), we obtain:

$$\sigma_{y^\star} \approx \frac{\sqrt{g_2(\alpha) - g(\alpha)^2}}{\alpha g(\alpha)} = \frac{1}{\alpha}\sqrt{\frac{g_2(\alpha)}{g(\alpha)^2} - 1}. \tag{A.30}$$

After some simplifications, we deduce:

$$\frac{1}{\alpha\sigma_{y^\star}} \approx \sqrt{\frac{\alpha^2 + \alpha\sqrt{\alpha^2 - 4\rho(n-1)}}{2(n-1)} - (1+\rho)}, \tag{A.31}$$

which is Eq. (1.4) of the main text. For $\rho \leq 0$ this expression always yields a real number, and for $\rho > 0$ does so when $\alpha \geq 2\sqrt{\rho(n-1)}$; in both cases, the stability threshold $\alpha_S = \sqrt{2n(1+\rho)}$ is contained within the interval in which Eq. (A.31) is valid. The formula reduces to Eqs. (A.14) and (A.20) for $\rho = 1$ and $\rho = -1$, respectively. The agreement with the probability of feasibility obtained by sampling matrices is remarkable (Fig. A.9), even for moderate matrix sizes.

Observe that $(\alpha\sigma_{y^\star})^{-1}$, i.e., the argument of the standardized normal cumulative density

function in Eq. (A.7), can be written in terms of the re-scaled intraspecific competition $\tilde{\alpha} := \alpha/\sqrt{n-1}$, thereby being independent of n:

$$\frac{1}{\alpha\sigma_{y^\star}} \approx \sqrt{\frac{\tilde{\alpha}^2 + \tilde{\alpha}\sqrt{\tilde{\alpha}^2 - 4\rho}}{2} - (1+\rho)}.$$

However, this does not make all the probability of feasibility curves to collapse for different system sizes, because the probability of feasibility is precisely $\Phi((\alpha\sigma_{y^\star})^{-1})^n$, and rising the cumulative density function to the power of n introduces an intrinsic separation between the curves for finite n (see Fig. A.10, which provides a comparison between the resolvent approximation and the approximation via Richardson iteration presented below). This separation converges to zero as n increases. We show here that, as $n \to \infty$, the median of the PDF for feasibility as function of α, given by $\frac{d}{d\alpha}p_F(\alpha)$, grows unboundedly, whereas the width of the distribution tends to zero as n increases. The convergence to zero width is extremely slow, though. Mathematically, in the limit of infinitely many species, the transition from infeasibility to feasibility is sharp, although the transition point (which can be assimilated to the median of the PDF) occurs at $\tilde{\alpha}_{1/2} = \infty$. Given the slow rate of convergence to this limiting situation, even for very large values of n we will observe a smooth curve for the probability of feasibility (see Fig. A.10).

For finite n, we define the critical value of $\tilde{\alpha}$ as the intraspecific competition strength $\tilde{\alpha}_{1/2}$ such that $p_F(\tilde{\alpha}_{1/2}) = \frac{1}{2}$. Using the resolvent approximation, this condition is equivalent to

$$\sqrt{\frac{\tilde{\alpha}_{1/2}^2 + \tilde{\alpha}_{1/2}\sqrt{\tilde{\alpha}_{1/2}^2 - 4\rho}}{2} - (1+\rho)} = \sqrt{2}\mathrm{erf}^{-1}\left(2e^{-\frac{1}{n}\log 2} - 1\right),$$

where we used that the inverse CDF of the standard normal is expressed as $\Phi^{-1}(y) = \sqrt{2}\mathrm{erf}^{-1}(2y-1)$. Let $x_n := \sqrt{2}\mathrm{erf}^{-1}\left(2e^{-\frac{1}{n}\log 2} - 1\right)$. Then we can solve for $\tilde{\alpha}_{1/2}$ to obtain

$$\tilde{\alpha}_{1/2} = \frac{1+\rho+x_n^2}{\sqrt{1+x_n^2}}.$$

Because $\lim_{n\to\infty} x_n = \sqrt{2}\mathrm{erf}^{-1}(1) = \infty$, we obtain that $\lim_{n\to\infty} \tilde{\alpha}_{1/2} = \lim_{n\to\infty} |x_n| = +\infty$. Therefore, the "center" of the PDF, $\alpha_{1/2} = \sqrt{n-1}\tilde{\alpha}_{1/2}$, tends to infinity as well. This is consistent with previous estimations of this threshold[19, 20].

With regard to the width of the distribution, we use the quantiles $\tilde{\alpha}_\beta$ and $\tilde{\alpha}_{1-\beta}$ to define the width of the distribution: let $\tilde{\alpha}_\beta$ be such that $p_F(\tilde{\alpha}_\beta) = \beta$ (with $0 < \beta < 1$), i.e.,

$$\sqrt{\frac{\tilde{\alpha}_\beta^2 + \tilde{\alpha}_\beta\sqrt{\tilde{\alpha}_\beta^2 - 4\rho}}{2} - (1+\rho)} = \sqrt{2}\mathrm{erf}^{-1}\left(2e^{\frac{1}{n}\log\beta} - 1\right) =: x_\beta,$$

and the same definitions for $\tilde{\alpha}_{1-\beta}$ and $x_{1-\beta}$. Let β be small (for example, $\beta = 0.01$). The width of the PFD can be estimated as the difference $\tilde{\alpha}_{1-\beta} - \tilde{\alpha}_\beta$, which asymptotically tends to zero. Indeed,

$$\lim_{n\to\infty}(\tilde{\alpha}_{1-\beta} - \tilde{\alpha}_\beta) = \lim_{n\to\infty}\left(\frac{1+\rho+x_{1-\beta}^2}{\sqrt{1+x_{1-\beta}^2}} - \frac{1+\rho+x_\beta^2}{\sqrt{1+x_\beta^2}}\right) = \lim_{n\to\infty}(|x_{1-\beta}| - |x_\beta|).$$

The last limit can be evaluated as follows:

$$\lim_{n\to\infty}(|x_{1-\beta}| - |x_\beta|) = \sqrt{2}\lim_{n\to\infty}\left(\left|\mathrm{erf}^{-1}\left(2e^{\frac{1}{n}\log(1-\beta)} - 1\right)\right| - \left|\mathrm{erf}^{-1}\left(2e^{\frac{1}{n}\log\beta} - 1\right)\right|\right) =$$
$$\sqrt{2}\lim_{n\to\infty}\left(\mathrm{erf}^{-1}(1) - \mathrm{erf}^{-1}(1)\right) = 0,$$

because both $e^{\frac{1}{n}\log(1-\beta)}$ and $e^{\frac{1}{n}\log\beta}$ tend to one as $n \to \infty$. Therefore, in the limit $n \to \infty$, the width of the distribution tends to zero, thus the transition becomes sharper and sharper, and displaces to the right without reaching a finite transition value in the limit, because the

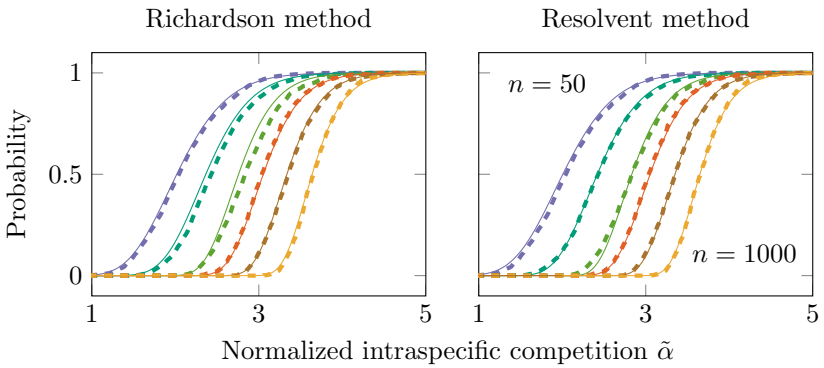

Figure A.10: **Approximate probability of feasibility for the two approximations presented in the text.** Left panel: approximation based on Richardson's iteration; Right panel: approximation based on resolvents. Intraspecific competition is normalized ($\tilde{\alpha} = \alpha/\sqrt{n-1}$) so that the argument of $\Phi(\cdot)$, i.e., the CDF of the standard normal distribution that appears in Eq. (1.3) of the main text, does not depend on n. We observe a very good agreement with simulations for both methods, even for small sizes: colder colors illustrate the case of $n = 50$ (with purple for $\rho = -1$, teal for $\rho = 0$ and green for $\rho = 1$) and warmer colors the case of $n = 1000$ (with orange, brown and yellow marking $\rho = -1, 0, 1$, respectively). Dashed lines report simulated data. While Richardson's method tends to overestimate p_F for small sizes, the resolvent method overestimates (underestimates) it for negative (positive) correlations and small sizes. Finally, note the very slow convergence to a sharp transition with n, and the displacement to the transition to the right.

transition occurs at $\tilde{\alpha}_{1/2} \to \infty$ (the median grows unboundedly). It is important to remark that the convergence of $p_F(\tilde{\alpha})$ to a step function centered at $\tilde{\alpha} = \infty$ is very slow, as Fig. A.10 shows.

Finally, we use this approximation to estimate the probability of feasibility at the stability threshold, $\alpha_S \approx \sqrt{2n(1+\rho)}$, obtaining:

$$p_F(\alpha_S) \approx \Phi\left(\sqrt{\frac{1+\rho+\sqrt{n(1+\rho)(n-(n-2)\rho)}}{n-1}}\right)^n.$$

The probability of feasibility at the stability threshold tends to zero as n increases. For example, for $n = 50$, we find $p_F(\alpha_S) \approx 2.4 \times 10^{-4}$ for $\rho = 0$, $p_F(\alpha_S) \approx 6 \times 10^{-8}$ for $\rho = 1$ and $p_F(\alpha_S) \approx 8.9 \times 10^{-16}$ for $\rho = -1$.

A.3.9 Resolvent-based approximation for arbitrary correlation and low variability in self-regulation.

Here, we consider the case in which the interaction matrix is defined as

$$A = \alpha I + D(a) + B,$$

where again B_{ij} $(i \neq j)$ are i.i.d. random variables with zero mean and variance 1, $D(x)$ stands for a diagonal matrix with vector x in the diagonal, and $a = (a_k)$ is a vector of i.i.d. random variables with the same distribution as B_{ij} but zero mean and variance σ_α^2. As usual, we assume that a_k and B_{ij} are independent variables. Because $B_{ii} = 0$, this new definition of interaction coefficients introduces variability in self-regulation. Intra-specific interactions now have mean α and variance σ_α^2.

The matrix Dyson equation formalism applied to the hermitization of matrix $W = D(a) + B$ does not apply in this case because the entries of that matrix are not i.i.d. variables, given the different variance of the diagonal. However, if $\sigma_\alpha = 1$ all the entries are i.i.d., then the procedure applied above for $\sigma_\alpha = 0$ remains valid and we expect (by continuity of the solution) that it will be valid in a neighborhood of $\sigma_\alpha = 1$. So we will extend that methodology for $\sigma_\alpha \approx 1$ and will check the validity of the approximation as the variance of the self-regulation terms increases.

The hermitization procedure applied in the previous subsection requires to insert, in Eq. (A.23), the modifications $\mathbb{E}(W^T W) = \mathbb{E}(W W^T) = \mathbb{E}((D(a) + B)^T (D(a) + B)) = \mathbb{E}(D(a)^2) + \mathbb{E}(B^T B) = (\sigma_\alpha^2 + n - 1)I$ and $\mathbb{E}(W^2) = \mathbb{E}((W^T)^2) = \mathbb{E}((D(a) + B)^2) = \mathbb{E}(D(a)^2) + \mathbb{E}(B^2) = (\sigma_\alpha^2 + \rho(n-1))I$, which hold true because $\mathbb{E}(B) = \mathbb{E}(D(a)) = \mathbb{0}$. Observe that these expectations reduce to the former ones for $\sigma_\alpha = 0$. In order to compute the expectations $\mathbb{E}(x^\star)$ and $\mathbb{E}(x^{\star T} x^\star)$, we have to solve the matrix Dyson equation (A.21)

with a modified definition of the function $\Lambda(\cdot)$, which now reads as

$$\Lambda(S(w,z)) = \begin{pmatrix} iv\mathbb{E}(WW^T) & b\mathbb{E}(W^2) \\ b^\star\mathbb{E}((W^T)^2) & iv\mathbb{E}(W^TW) \end{pmatrix} = \begin{pmatrix} (\sigma_\alpha^2+n-1)I & (\sigma_\alpha^2+\rho(n-1))I \\ (\sigma_\alpha^2+\rho(n-1))I & (\sigma_\alpha^2+n-1)I \end{pmatrix}$$

when $S(w,z)$ is substituted by the asymptotic solution given by Eq. (A.22). Now we solve Eq. (A.21) looking for solutions of the same form as above (Eq. (A.22)). In this case, we have to solve the following quadratic system in (v,b):

$$\begin{aligned} -1 &= -wv - zb + (n-1)(-v^2+\rho b^2) + \sigma_\alpha^2(-v^2+b^2), \\ 0 &= wb^\star - zv + (n-1)(vb^\star + \rho vb) + \sigma_\alpha^2(b^\star+b)v, \end{aligned} \tag{A.32}$$

where, again, the symbol * denotes complex conjugate. In fact, we are only interested in obtaining $b(z, w=0)$. Solving for v in the second equation yields

$$v = -\frac{wb^\star}{(\sigma_\alpha^2+n-1)b^\star + (\sigma_\alpha^2+\rho(n-1))b - z}.$$

Substituting into the first equation and setting $w=0$ we find that $b(z,0)$ satisfies the quadratic equation $(\sigma_\alpha^2+\rho(n-1))b^2 - zb + 1 = 0$, which can be solved to obtain

$$b(z,0) = \frac{z - \sqrt{z^2 - 4(\sigma_\alpha^2+\rho(n-1))}}{2(\sigma_\alpha^2+\rho(n-1))}, \tag{A.33}$$

where we have chosen the minus sign so that the resolvent $(zI+B)^{-1}$ behaves as $z^{-1}I$ in the limit $z\to\infty$. Changing $z = \alpha + i\epsilon$ and taking the limit $\epsilon \to 0$ we finally obtain $\mathbb{E}(x^\star) = h(\alpha)\mathbb{1}$, where we have defined

$$h(\alpha) := \frac{\alpha - \sqrt{\alpha^2 - 4(\sigma_\alpha^2 + \rho(n-1))}}{2(\sigma_\alpha^2 + \rho(n-1))} = \frac{2}{\alpha + \sqrt{\alpha^2 - 4(\sigma_\alpha^2 + \rho(n-1))}}. \tag{A.34}$$

In order to evaluate, in the case of non-zero variance in self-regulation, the expectation $\mathbb{E}(x^{\star T} x^\star)$, we resort to the same argument as before, and use Eq. (A.28) with b now given by Eq. (A.33). This gives $\mathbb{E}((\alpha I + D(a) + B^T)^{-1}(\alpha I + D(a) + B)^{-1}) = h_2(\alpha) I$ with

$$h_2(\alpha) := \frac{2}{\alpha^2 + \alpha\sqrt{\alpha^2 - 4(\sigma_\alpha^2 + \rho(n-1))} - 2(1+\rho)(n-1) - 4\sigma_\alpha^2} I. \tag{A.35}$$

Finally, as in Eq. (A.30), we can approximate

$$\alpha^2 \sigma_{y^\star}^2 \approx \frac{h_2(\alpha)}{h(\alpha)^2} - 1.$$

This leads to the following approximation for the variance $\sigma_{y^\star}^2$:

$$\frac{1}{(\alpha\sigma_{y^\star})^2} \approx \frac{\alpha^2 + \alpha\sqrt{\alpha^2 - 4(\sigma_\alpha^2 + \rho(n-1))} - 2\sigma_\alpha^2(1-\rho)}{2(\sigma_\alpha^2 + n - 1)} - (1+\rho). \tag{A.36}$$

We can use this formula to evaluate the probability of feasibility as $p_F(\alpha, \sigma_\alpha^2) = \Phi((\alpha\sigma_{y^\star})^{-1})^n$ when small variability is introduced in self-regulation coefficients ($\sigma_\alpha^2 > 0$). Consistently, this formula reduces to Eq. (A.31) for $\sigma_a^2 = 0$. Moreover, we expect this formula to hold in a neighborhood of $\sigma_\alpha = 1$, so by continuity this approximation should be accurate for small deviations $\sigma_\alpha \in [0, 1+\delta]$, for $\delta > 0$ small. The overall effect of the variability in self-regulation is to increase the values of average self-regulation (α) that allow for feasibility. Does the result $\alpha_F > \alpha_S$ hold (almost surely) in this case?

Universality results in random matrix theory [183] state that for the case studied here ($\sigma_\alpha \approx 1$), the stability threshold also follows the Wigner law (See Methods). As such,

since the effect of adding σ_α on feasibility, is to move the curve to the right, we expect our results to remain the same (that is, $\alpha_S < \alpha_F$ almost surely). Finally, we take advantage of Eq. (A.36) to approximate the probability of feasibility as $p_F(\alpha_S, \sigma_\alpha) = \Phi((\alpha_S \sigma_{y^\star})^{-1})^n$ at the threshold of global stability, α_S. For instance, we can obtain, for $\sigma_\alpha = 1$ and $n = 50$, such value for $\rho = 0$, $p_F(\alpha_S, \sigma_\alpha) = 1.3 \times 10^{-4}$. Therefore, we find again that $\alpha_F > \alpha_S$ holds almost surely for small variances.

A.3.10 Computing $\sigma_{y^\star}$ by iteration

In this section, we approximate $\sigma_{y^\star}$ by approximating $y^\star$ for a given α. To this end, we use two well-known results.

Neumann series. Whenever the spectral radius of A, $\xi(A) < 1$, the inverse of $(I - A)$ can be written as:

$$(I - A)^{-1} = \sum_{k=0}^{\infty} A^k \quad ,$$

where $A^0 = I$.

Take the system in $y^\star$, and divide both sides by $\alpha > 0$:

$$\left(I + \frac{1}{\alpha} C\right) y^\star = \frac{1}{\alpha} \mathbb{1} \quad .$$

Whenever the spectral radius of C, $\xi(C) < \alpha$, we can write:

$$
\begin{aligned}
y^\star &= \frac{1}{\alpha}\left(I + \frac{1}{\alpha}C\right)^{-1}\mathbb{1} \\
&= \frac{1}{\alpha}\sum_{k=0}^{\infty}\left(-\frac{1}{\alpha}C\right)^{k}\mathbb{1} \\
&= \frac{1}{\alpha}\left(I - \frac{1}{\alpha}C + \frac{1}{\alpha^2}C^2 - \cdots\right)\mathbb{1} \\
&= \frac{1}{\alpha}\mathbb{1} - \frac{1}{\alpha^2}C\mathbb{1} + \frac{1}{\alpha^3}C^2\mathbb{1} - \cdots \quad .
\end{aligned}
$$

We note that whenever $\alpha > \alpha_L$, the Neumann series converges.

Richardson iteration. The system $Ax = b$ can be solved iteratively, starting from an initial guess $x(0)$ as:

$$
x(k+1) = (I - \omega A)x(k) + \omega b \quad ,
$$

where ω is an iteration parameter that can always be chosen such that the iteration converges to the solution of $Ax = b$. When $A = A^T$ and is positive definite, the optimal iteration parameter is simply:

$$
\omega = \frac{2}{\lambda_1(A) + \lambda_n(A)} \quad ,
$$

i.e., the reciprocal of the average between the smallest and the largest eigenvalue of A.

If we multiply the equations we want to solve by $(I + \frac{\kappa}{\alpha}C^T)$, the right-hand side of the equations is unchanged, because $C^T\mathbb{1} = \mathbb{0}$:

$$
\left(I + \frac{\kappa}{\alpha}C^T\right)\left(I + \frac{1}{\alpha}C\right)y^\star = \frac{1}{\alpha}\mathbb{1} \quad .
$$

However, the left-hand side changes, and thus the speed at which an iterative method would converge to its solution depends on κ.

Based on numerical simulations, to speed up convergence we choose three different values of κ, depending on the correlation between the entries of B; in particular, we choose $\kappa = 1$ when the correlation is $\rho = -1$ and B is skew-symmetric; $\kappa = 0$ when $\rho = 0$, and $\kappa = -1$ when $\rho = 1$ and B is symmetric.

We start with $\rho = -1$, and multiply both sides of the system of equations by $\left(I + \frac{1}{\alpha}C^T\right)$:

$$\begin{aligned}
\left(I + \frac{1}{\alpha}C^T\right)\left(I + \frac{1}{\alpha}C\right)y^\star &= \frac{1}{\alpha}\left(I + \frac{1}{\alpha}C^T\right)\mathbb{1} \\
\left(I + \frac{1}{\alpha}(C + C^T) + \frac{1}{\alpha^2}C^TC\right)y^\star &= \frac{1}{\alpha}\mathbb{1} \\
\left(I + \frac{1}{\alpha}(B - \mathbb{1}m^T + B^T - m\mathbb{1}^T) + \frac{1}{\alpha^2}(B^T - m\mathbb{1}^T)(B - \mathbb{1}m^T)\right)y^\star &= \frac{1}{\alpha}\mathbb{1} \\
\left(I + \frac{1}{\alpha}(B - \mathbb{1}m^T - B - m\mathbb{1}^T) + \frac{1}{\alpha^2}(-B - m\mathbb{1}^T)(B - \mathbb{1}m^T)\right)y^\star &= \frac{1}{\alpha}\mathbb{1} \\
\left(I + \frac{1}{\alpha}(-\mathbb{1}m^T - m\mathbb{1}^T) + \frac{1}{\alpha^2}(-B^2 - n\,mm^T)\right)y^\star &= \frac{1}{\alpha}\mathbb{1} \\
Sy^\star &= \frac{1}{\alpha}\mathbb{1} \quad .
\end{aligned}$$

Note that, a) the multiplication does not alter the right-hand side of the equations; b) S is positive semi-definite, because it is of the form G^TG; c) when $\rho = -1$, B is skew-symmetric, and thus $B^T = -B$; d) when $\rho = -1$, necessarily $m^T\mathbb{1} = 0$ (hence the two matrices $\mathbb{1}m^T$ and $m\mathbb{1}^T$ are nilpotent—have all eigenvalues zero).

Next, we choose the iteration parameter, by approximating $S \approx (I - \frac{1}{\alpha^2}B^2)$. Given that the eigenvalues of B^2 are the squared eigenvalues of B, we have $\lambda_1(B^2) \approx -4n$ and $\lambda_n(B^2) \approx 0$. Hence:

$$\omega = \frac{2}{(1 - \frac{1}{\alpha^2}0) + (1 + \frac{1}{\alpha^2}4n)} = \frac{\alpha^2}{\alpha^2 + 2n} \quad .$$

Finally, we take $y(0) = \frac{1}{\alpha}\mathbb{1} - \frac{1}{\alpha^2}C\mathbb{1}$ (as given by the first two terms of the Neumann series), $y(1) = (I - \omega S)y(0) + \frac{1}{\alpha}\omega\mathbb{1}$, and compute the approximate variance as:

$$\mathbb{V}(y_i^\star) = \mathbb{E}((y_i^\star)^2) - \mathbb{E}(y_i^\star)^2 \approx \frac{1}{n}\mathbb{E}(y(1)^T y(1)) - \frac{1}{\alpha^2} \quad .$$

Note that this approximation will depend on the first few moments of the distribution of B_{ij} (and not only on their mean and variance, as in the approximation using small-rank perturbations, or that using resolvents). The expectation of $y(1)^T y(1)$ is presented in Appendix A.5.

For $\rho = 1$, we multiply both sides of the system of equations by $\left(I - \frac{1}{\alpha}C^T\right)$, instead:

$$\begin{aligned}
\left(I - \frac{1}{\alpha}C^T\right)\left(I + \frac{1}{\alpha}C\right) y^\star &= \frac{1}{\alpha}\left(I - \frac{1}{\alpha}C^T\right)\mathbb{1} \\
\left(I + \frac{1}{\alpha}(C - C^T) - \frac{1}{\alpha^2}C^T C\right) y^\star &= \frac{1}{\alpha}\mathbb{1} \\
\left(I + \frac{1}{\alpha}(B - \mathbb{1}m^T - B^T + m\mathbb{1}^T) - \frac{1}{\alpha^2}(B^T - m\mathbb{1}^T)(B - \mathbb{1}m^T)\right) y^\star &= \frac{1}{\alpha}\mathbb{1} \\
\left(I + \frac{1}{\alpha}(B - \mathbb{1}m^T - B + m\mathbb{1}^T) - \frac{1}{\alpha^2}(B - m\mathbb{1}^T)(B - \mathbb{1}m^T)\right) y^\star &= \frac{1}{\alpha}\mathbb{1} \\
\left(I + \frac{1}{\alpha}(m\mathbb{1}^T - \mathbb{1}m^T) - \frac{1}{\alpha^2}(B^2 - n\, mm^T)\right) y^\star &= \frac{1}{\alpha}\mathbb{1} \\
H y^\star &= \frac{1}{\alpha}\mathbb{1} \quad .
\end{aligned}$$

Note that, a) the multiplication again does not alter the right-hand side of the equations; b) H is positive semi-definite as long as $\alpha > \alpha_L$; c) when $\rho = 1$, B is symmetric, and thus $B^T = B$.

Next, we choose the iteration parameter, by approximating $H \approx (I - \frac{1}{\alpha^2}B^2)$. Given that the eigenvalues of B^2 are the squared eigenvalues of B, we have $\lambda_n(B^2) \approx 4n$ and $\lambda_1(B^2) \approx 0$. Hence:

$$\omega = \frac{2}{(1 - \frac{1}{\alpha^2}0) + (1 - \frac{1}{\alpha^2}4n)} = \frac{\alpha^2}{\alpha^2 - 2n} \quad .$$

Finally, we take $y(0) = \frac{1}{\alpha}\mathbb{1} - \frac{1}{\alpha^2}C\mathbb{1}$, $y(1) = (I - \omega H)y(0) + \frac{1}{\alpha}\omega\mathbb{1}$, and compute the approximate variance as before. Also for this case, the details of the calculation are presented in Appendix A.5.

For $\rho = 0$ we choose $\kappa = 0$, leaving the system unchanged. Given that we can safely assume that $\alpha > \alpha_L$, we have that $I - \omega(I + \frac{1}{\alpha}C) = (1 - \omega)I - \frac{\omega}{\alpha}C$ has spectral radius less than one (and thus the iteration converges) when we choose $\omega = 1$, such that the Richardson iteration matches what one would obtain by truncating the Neumann series. Finally, we set $y(0) = \frac{1}{\alpha}\mathbb{1} - \frac{1}{\alpha^2}C\mathbb{1}$ and compute the variance as done for the other cases. The details of the calculation are also presented in Appendix A.5.

We conclude by stressing that we a) have started with a guess given by the truncation of the Neumann series that includes only the first two terms, and b) have performed only one step of the Richardson iteration. While the calculations are already quite elaborate for these choices, including either more terms of the Neumann series, or performing more than one step for the Richardson iteration (possibly, updating the parameter ω) would almost certainly result in an even more accurate approximation—allowing one to model smaller systems, or systems in which the distribution of coefficients has extreme skewness/kurtosis, etc. Appendix A.5 shows that the approximation above is however quite precise for moderate n and the distributions we have been analyzing in this work.

A.3.11 Consequences for dynamics

In Sections A.3.6 and A.3.8, we have shown that, for large n, a random competitive system that is feasible is also stable. The competitive GLV system can give rise to all types of dynamics, including limit cycles (for $n \geq 3$) and chaos (for $n \geq 4$) [52, 53]. Non-equilibrium coexistence via limit cycles or chaos requires a *feasible* equilibrium[14], but we have seen in Sec. A.1.3 that whenever $\alpha > \alpha_F$, then $\alpha > \alpha_S \geq \alpha_L$, and thus the stability of the

equilibrium is ensured for any choice of $r > \mathbb{0}$. Hence, we conclude that limit cycles or chaos are going to be almost impossible to observe for large random competitive systems.

If the relationship $\alpha_F > \alpha_S$ is maintained for moderate sizes n as well (as suggested by the calculations in Sec. A.3.8), then the dynamical consequences are even more far-reaching. In a competitive GLV system, lack of feasibility guarantees that one or more populations will go extinct[14]. Suppose that we initialize a random competitive system with n populations at arbitrary initial conditions; this system will have a certain α. If $\alpha > \alpha_F$, the system is feasible and stable; trajectories will converge to the equilibrium, and if the equilibrium is perturbed, dynamics will return to it. If, on the other hand, $\alpha < \alpha_F$, then the system is not feasible, and therefore some populations will go extinct. There are two distinct cases:

Case i): $\alpha_S < \alpha$: the system will converge to a saturated equilibrium (as shown by the Lyapunov function in Section A.1.3); the same populations will go extinct irrespective of the (positive) initial conditions; the populations that go extinct cannot re-invade the system; the populations that coexist do so stably, and when their densities are perturbed, the system will asymptotically return to the saturated equilibrium.

Case ii): $\alpha < \alpha_S$: this is the most interesting case. Some populations will go extinct, because there is no feasible equilibrium. However, which populations will go extinct *depends on the initial conditions*. The system can therefore display priority effects and alternative stable states. Every time a population goes extinct, the system size shrinks to $n-1$, $n-2$, etc. Accordingly, the threshold values α_S and α_F are also decreased, while the value of α is unchanged. As such, provided that the α_S for the reduced system is still smaller than the corresponding α_F, the system will keep losing populations until $\alpha > \alpha_S$, thus eventually attaining Case i).

Therefore, for large n (and provided that $\alpha_S < \alpha_F$ when populations are lost), the ultimate result is always the same: the surviving populations coexist robustly at a globally-attractive equilibrium. Moreover, while the populations that went extinct at the onset of

the dynamics could potentially re-invade the system (only when we start in Case ii), the last few populations (i.e., those that went extinct once $\alpha > \alpha_S$) cannot.

These results, obtained for isolated systems in which populations that are lost cannot reinvade the system are in contrast to those obtained when instead a small but constant influx of each population enters the system at all times; in this case, Bunin[162] showed that for some critical value of α dynamics transition from equilibria to complex, chaotic oscillations. Further analysis shows that the constant influx of immigrants is key to achieve non-equilibrium coexistence, such that when turning off the immigration chaos typically *fades away*[184].

A.3.12 Consequences for assembly

We can go a step further, and consider whether these systems, obtained by collapsing a larger system, can instead be built from the ground up. As discussed above, we consider the case in which invasions are spaced apart, rather than having a constant influx as in the study by Bunin[162] .

Take a system with n populations coexisting at a feasible equilibrium $x^\star$ (i.e., we have $\alpha > \alpha_F$), possibly obtained by collapsing a larger system, as detailed in the previous section. If we have $\alpha > \alpha_F > \alpha_S$, which is almost invariably the case for a large system, then any feasible sub-community is automatically stable, and might or might not be invaded by the remaining populations.

In such a case, determining whether the equilibrium $x^\star$ can be built by sequential introduction of population can be accomplished by considering an assembly graph where the nodes are the feasible sub-communities that can be formed by selecting some of the n population (out of 2^n possibilities, including the “empty" state in which all populations are absent), and an edge connects two nodes if an invasion can move the system from one state to the

other[54]. If the system can be built from the ground up, then there exists a path in the graph connecting the empty state all the way up to the state with n populations (Fig. A.11).

We performed simulations in which a) we built a feasible system of n populations, b) built the corresponding assembly graph, and c) tallied the probability of finding such a path in the graph as we increased n. Figure A.12 shows that, even for moderate n, the probability is very high, and rapidly converges to one.

Taken collectively, our results show that *robust, stable coexistence* (of a sub-community) *is the norm* for large random competitive communities. For large system with random parameters, dynamics will not display cycles or chaos. Moreover, the final community (i.e., that obtained once the dynamics have elapsed, and extinctions have occurred) is such that priority effects are excluded. The final community can be assembled from the ground-up by introducing one population at a time.

A.4 Distribution of the coefficients B_{ij}

Here we detail the distributions we have used to sample interaction coefficients, including their probability distribution/mass functions, and the first six moments (needed for the Richardson approximation). All the distributions are shifted and re-scaled in order to have mean zero and unit variance. We chose a distribution that is discrete and has finite support; a distribution that is continuous and has finite support, and one that is continuous and has infinite support. For each distribution, we include a parameter β that can be varied to regulate the skewness of the distributions. The three distributions are drawn in Fig. A.13.

A.4.1 Skew normal distribution

The PDF is given by

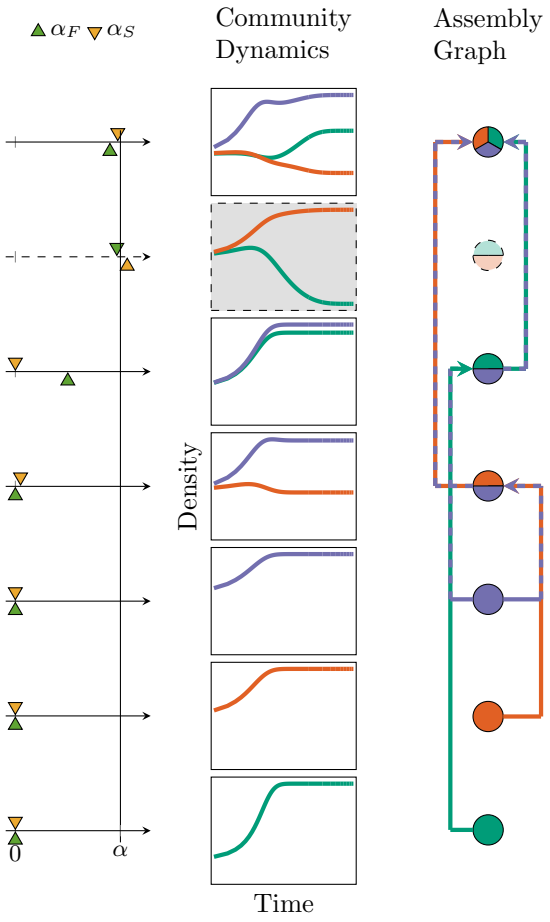

Figure A.11: **Assembly graph for a simple competitive community.** We show how the interplay between the values of α, α_S and α_F (left) determine dynamics (center), and therefore the existence and connectivity of nodes (right) in the assembly graph associated with the system. Starting from the top, we consider a three-species community with $\alpha > \alpha_F > \alpha_S$; thus, the three populations coexist stably (center, showing typical dynamics) and this community is a node in the assembly graph (right). For the three two-species communities that we can form, we have that $\alpha > \alpha_F$ for two of them, while for one community $\alpha_F > \alpha$, and therefore dynamics will lead to extinctions; consequently, the corresponding node is not present in the assembly graph. Finally, by definition, all single-species communities are feasible and stable. We connect two nodes in the assembly graph if an invasion can transition the system from a sub-community (node in the graph) to another. We say that the full community can be built from the ground up via sequential invasions if there is a path starting at a node encoding a single-species community and ending with the full community.

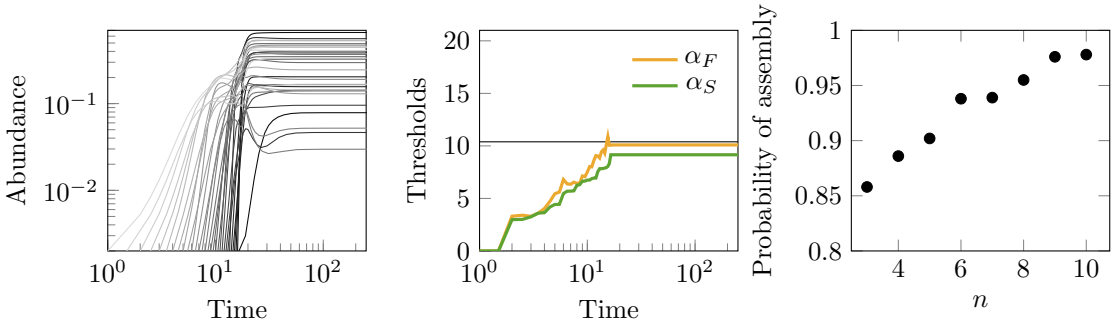

Figure A.12: **Bottom-up assembly of the main-text community.** The first two panels show the assembly of the community in the main text example (Fig. 1.4), by sequentially invading the system, one population at a time ("bottom-up" assembly). The simulation shows a case in which at each invasion (bottom-right, color corresponding to the time of invasion) the system grows in size, virtually without extinctions, since α_F (almost always) remains below α. Additionally, we have $\alpha_S < \alpha_F$ throughout assembly, such the system remains in phase III throughout. As populations are added to the community, both α_F and α_S grow, eventually reaching the values found for top-down assembly. As we vary n (x-axis), we calculate the probability that a random, feasible system can be built from the ground up via successive invasions (y-axis). We performed 1000 simulations for each n, constructed the corresponding assembly graph, and, for each graph, we determined whether a path starting from the empty state reaches the node corresponding to the full community. The probability that such a path exists, and therefore the system can be built from the ground up, rapidly converges to one as n increases.

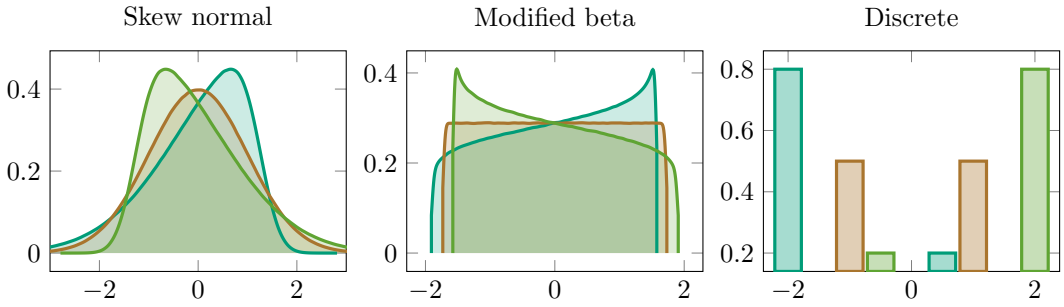

Figure A.13: **Distributions used to sample the interaction coefficients.** For our simulations, we sampled the coefficients B_{ij} from distributions with mean zero and unit variance. We choose a continuous distribution with infinite support (Skew normal), a continuous distribution with finite support (Modified beta) and a discrete distribution with finite support (Discrete) to probe the generality of our results. For each distribution, we include a parameter (β) that controls the skewness (colors).

$$\Phi(x) = \frac{2}{\sigma\sqrt{2\pi}} \exp\left(-\frac{x-\mu}{2\sigma^2}\right) \int_{-\infty}^{\beta\left(\frac{x-\mu}{\sigma}\right)} \frac{1}{\sqrt{2\pi}} \exp\left(-\frac{t^2}{2}\right)$$

with expectation

$$\mathbb{E}(x) = \mu + \frac{\sqrt{\frac{2}{\pi}}\beta\sigma}{\sqrt{1+\beta^2}}$$

and variance

$$\mathbb{V}(x) = \sigma^2\left(1 - \frac{2\beta^2}{\pi(1+\beta^2)}\right)$$

We then solve the system of equations $\mathbb{E}(x) = 0$ and $\mathbb{V}(x) = 1$ for μ and σ, obtaining

$$\mu^\star = -\frac{\sqrt{2}\beta}{\sqrt{\pi + \beta^2(\pi-2)}} \qquad \sigma^\star = \frac{\sqrt{\pi(1+\beta^2)}}{\sqrt{\pi + \beta^2(\pi-2)}}$$

Finally, we sample interactions from the skew normal distribution with $\mu = \mu^\star$ and $\sigma = \sigma^\star$. The moments of the resulting distribution are given in the table below. Note that for $\beta = 0$ we recover the standard normal distribution.

$$\begin{aligned}
\mu_1 &= 0 \\
\mu_2 &= 1 \\
\mu_3 &= -\frac{\sqrt{2}(\pi-4)\beta^3}{(\pi + (\pi-2)\beta^2)^{3/2}} \\
\mu_4 &= \frac{-12\beta^4 + 3\pi^2(1+\beta^2)^2 - 4\pi\beta^2(3+\beta^2)}{(\pi + (\pi-2)\beta^2)^2} \\
\mu_5 &= \frac{\sqrt{2}\beta^3(-10(\pi-4)\pi + (16 + (20-7\pi)\pi)\beta^2)}{(\pi + (\pi-2)\beta^2)^{5/2}} \\
\mu_6 &= \frac{-40\beta^6 + 15\pi^3(1+\beta^2) - 20\pi\beta^4(9+5\beta^2) - 6\pi^2\beta^2(155 + 10\beta^2 + \beta^4)}{(\pi + (\pi-2)\beta^2)^3}
\end{aligned}$$

A.4.2 Discrete distribution

The PMF is given by

$$\Phi(x) = \begin{cases} \xi_1 & \text{with probability } p \\ \xi_2 & \text{with probability } 1-p \end{cases}$$

The expectation is

$$\mathbb{E}(x) = \xi_1 p + \xi_2(1-p)$$

and the variance is

$$\mathbb{V}(x) = \xi_1^2 p + \xi_2^2(1-p) - E(x)^2$$

We solve the system of equations imposing that $\mathbb{E}(x) = 0$ and $\mathbb{V}(x) = 1$ for ξ_2 and p, obtaining

$$p = \frac{1}{1+\xi_1^2} \qquad \beta = -\frac{1}{\xi_1}$$

We call $\beta = \xi_1$; this parameter controls the skewness of the distribution. For $\beta = 1$ we obtain the Bernoulli distribution with outcomes ± 1 and skewness 0. The first six moments for this distribution are

$$\begin{aligned}
\mu_1 &= 0 \\
\mu_2 &= 1 \\
\mu_3 &= \beta - \frac{1}{\beta} \\
\mu_4 &= \beta^2 - 1 + \frac{1}{\beta^2} \\
\mu_5 &= \frac{1}{\beta^3}(\beta^2 - 1)(\beta^4 + 1) \\
\mu_6 &= \beta^4 - \beta^2 + 1 - \frac{1}{\beta^2} + \frac{1}{\beta^4}
\end{aligned}$$

A.4.3 Beta distribution

The PDF is given by

$$\Phi(x) = \frac{x^{\xi_1 - 1}(1-x)^{\xi_2 - 1}}{\mathtt{B}(\xi_1, \xi_2)}$$

where $\mathtt{B}(\xi_1, \xi_2) = \frac{\Gamma(\xi_1)\Gamma(\xi_2)}{\Gamma(\xi_1+\xi_2)}$, and Γ is the Gamma function. The expectation is

$$\mathbb{E}(x) = \frac{\xi_1}{\xi_1 + \xi_2}$$

and the variance

$$\mathbb{V}(x) = \frac{\xi_1 \xi_2}{(\xi_1 + \xi_2)^2(\xi_1 + \xi_2 + 1)}$$

The beta distribution has support between 0 and 1, and therefore it cannot have mean zero and unit variance. For this reason, we perform a change of variables to shift it and re-scale it. That is, we sample x from a beta distribution and then construct another random variable z by subtracting the mean (shift) and dividing by the square root of the variance (re-scale). The result is a random variable following the beta distribution with mean 0 and variance 1. We take $\xi_1 = 1/\beta$, $\xi_2 = \beta$, and define:

$$z = \sqrt{\frac{1 + \beta + \beta^2}{\beta^3}}(-1 + x + x\beta^2)$$

The first six moments of the distribution defined by the random variable z are

$$\mu_1 = 0$$

$$\mu_2 = 1$$

$$\mu_3 = \frac{2(\beta-1)\sqrt{1+\frac{1}{\beta}+\beta}}{1+\beta}$$

$$\mu_4 = -21 + \frac{6}{\beta} + \beta\left(6 + \frac{54}{1+\beta(3+\beta)}\right)$$

$$\mu_5 = \frac{4(\beta-1)(1+\frac{1}{\beta}+\beta)^{3/2}(6+5\beta+5\beta^3+6\beta^4)}{(1+\beta)(1+\beta(3+\beta))(1+\beta(4+\beta))}$$

$$\mu_6 = \frac{5(1+\beta+\beta^2)^2(24+\beta(-22+\beta(16+\beta(-1-22\beta+24\beta^2))))}{\beta^2(1+\beta(3+\beta))(1+\beta(4+\beta))(1+\beta(5+\beta))}$$

When $\beta = 1$, we recover the uniform distribution $\mathcal{U}[-\sqrt{3}, \sqrt{3}]$, which has mean zero, unit variance, and zero skewness.

A.5 Calculation of $\sigma_{y^\star}$

Here we present the details of the calculations for the approximation of $\sigma_{y^\star}$.

A.5.1 Through iterative solutions of linear systems

We have discussed the approach to approximating the variance $\sigma^2_{y^\star}$ as $\sigma^2_{y^\star} \approx \frac{1}{n} y(1)^T y(1) - \frac{1}{\alpha^2}$, where $y(1)$ is given by the first step of the Richardson iteration:

$$y(1) = y(0) - \omega M y(0) + \omega b$$

We have chosen: a) $y(0)$ as given by the first two terms of the Neumann series, $y(0) = \frac{1}{\alpha}\mathbb{1} - \frac{1}{\alpha^2} C\mathbb{1}$; b) the right-hand side $b = \frac{1}{\alpha}\mathbb{1}$; c) the choice of ω and M depend on the correlation, as follows:

$\rho = -1$	$\rho = 0$	$\rho = 1$
$\omega = \dfrac{\alpha^2}{\alpha^2 + 2n}$	$\omega = 1$	$\omega = \dfrac{\alpha^2}{\alpha^2 - 2n}$
$M = \left(I + \dfrac{1}{\alpha}C^T\right)\left(I + \dfrac{1}{\alpha}C\right)$	$M = \left(I + \dfrac{1}{\alpha}C\right)$	$M = \left(I - \dfrac{1}{\alpha}C^T\right)\left(I + \dfrac{1}{\alpha}C\right)$

To compute the approximate variance, we take a generic matrix $B = (B_{ij})$ of size n, compute the Richardson iteration, and then the approximate variance:

$$\begin{aligned}
\sigma^2_{y^\star} &\approx \frac{1}{n} y(1)^T y(1) - \frac{1}{\alpha^2} \\
&= \frac{1}{n}\left((y(0) - \omega M y(0) + \omega b)^T (y(0) - \omega M y(0) + \omega b)\right) - \frac{1}{\alpha^2} \\
&= \frac{1}{n}\big(y(0)^T y(0) + \omega^2 y(0)^T M^T M y(0) + \omega^2 b^T b - 2\omega y(0)^T M y(0) \\
&\qquad + 2\omega b^T y(0) - 2\omega^2 b^T M y(0)\big) - \frac{1}{\alpha^2}
\end{aligned} \tag{A.37}$$

Each term of the expansion ($y(0)^T y(0)$, $\omega^2 y(0)^T M^T M y(0)$, etc.) is a polynomial that depends on some of the coefficients B_{ij}, as well as n, α and ω. To compute the expected variance, we then take the expectation of each of the terms; in particular, we need to determine the expectation of polynomials in B_{ij}, such as $B_{ij}^p B_{kl}^q$. When the coefficients are independent (e.g., $\rho = 0$), only the terms in which all the coefficients are raised to a power greater than one will yield a non-zero expectation. In particular, we write:

$$\begin{aligned}
\mathbb{E}(B_{ij}) &= 0 \\
\mathbb{E}(B_{ij}^2) &= \mu_2 \\
\mathbb{E}(B_{ij}^3) &= \mu_3 \\
\mathbb{E}(B_{ij}^4) &= \mu_4 \\
&\cdots
\end{aligned}$$

Such that for example $\mathbb{E}(B_{ij}^2 B_{kl}^3) = \mu_2\mu_3$. Note that two distributions might have both $\mathbb{E}(B_{ij}) = 0$ and $\mathbb{E}(B_{ij}^2) = 1$, but different higher moments (for example, the standard normal distribution yields $(\mu_2, \mu_3, \mu_4, \mu_5, \mu_6) = (1, 0, 3, 0, 15)$, while when we assign $B_{ij} = 1$ or $B_{ij} = -1$ with equal probability, we obtain $(\mu_2, \mu_3, \mu_4, \mu_5, \mu_6) = (1, 0, 1, 0, 1)$); hence, the approximations will take the first few moments (up to μ_6, for the choice of starting conditions and Richardson iteration) of the distribution of coefficients into account.

When entries are correlated, we have a more difficult task at hand, because for example $\mathbb{E}(B_{ij}B_{ji}) = \rho$, and this relationship needs to be accounted for when taking higher powers (such that $\mathbb{E}(B_{ij}^2 B_{ji}^2) \neq 0$). However, the problem is simplified when we consider either $\rho = 1$ or $\rho = -1$, in which cases $\mathbb{E}(B_{ij}B_{ji}) = \mathbb{E}(B_{ij}^2) = \mu_2$ (when $\rho = 1$) or $\mathbb{E}(B_{ij}B_{ji}) = \mathbb{E}(-B_{ij}^2) = -\mu_2$ (when $\rho = -1$), and thus we just need to take the powers of B_{ij} into account. For simplicity, we thus consider only the cases of $\rho = 0$, $\rho = -1$, and $\rho = 1$. The calculations can be extended to the case of a general ρ, the cost being to have to keep track of many more combinations of coefficients.

Computing these expectations becomes increasingly complex. We start from the terms that do not depend on the choice of M (and therefore are the same irrespective of the correlation).

The simplest terms in Eq. (A.37) are $b^T b$:

$$b^T b = \frac{1}{\alpha^2}\mathbb{1}^T\mathbb{1} = \frac{n}{\alpha^2}$$

and

$$b^T y(0) = \frac{n}{\alpha^2}$$

A term that is slightly more complicated to compute is $y(0)^T y(0)$, which will depend on the correlation, but not on the choice of M. We report the detailed calculation, because this

is the approach we followed to compute all the remaining terms. We can write $y(0)^T y(0)$ as:

$$\begin{aligned}
y(0)^T y(0) &= \left(\left(\frac{1}{\alpha}\mathbb{1}^T - \frac{1}{\alpha^2}\mathbb{1}^T C^T\right)\left(\frac{1}{\alpha}\mathbb{1} - \frac{1}{\alpha^2}C\mathbb{1}\right)\right) \\
&= \mathbb{1}^T\left(\frac{1}{\alpha^2}I + \frac{1}{\alpha^4}C^T C\right)\mathbb{1} \\
&= \frac{n}{\alpha^2} + \frac{1}{\alpha^4}\mathbb{1}^T\left((B^T - m\mathbb{1}^T)(B - \mathbb{1}m^T)\right)\mathbb{1} \\
&= \frac{n}{\alpha^2} + \frac{1}{\alpha^4}\mathbb{1}^T\left(B^T B - n\, mm^T\right)\mathbb{1} \\
&= \frac{n}{\alpha^2} + \frac{1}{\alpha^4}\left(\mathbb{1}^T B^T B\mathbb{1} - n\,\mathbb{1}^T mm^T\mathbb{1}\right) \\
&= \frac{n}{\alpha^2} + \frac{1}{\alpha^4}\left(\mathbb{1}^T B^T B\mathbb{1} - n\,(m^T\mathbb{1})^2\right) \\
&= \frac{n}{\alpha^2} + \frac{1}{\alpha^4}\left(\sum_i\sum_j\sum_k B_{ik}B_{jk} - n\left(\frac{1}{n}\sum_i\sum_j B_{ij}\right)^2\right) \\
&= \frac{n}{\alpha^2} + \frac{1}{\alpha^4}\left(\sum_i\sum_j\sum_k B_{ik}B_{jk} - \frac{1}{n}\left(\sum_i\sum_j B_{ij}\right)^2\right)
\end{aligned}$$

Next, we need to take the expectations for these sums:

$$\mathbb{E}(y(0)^T y(0)) = \frac{n}{\alpha^2} + \frac{1}{\alpha^4}\left(\mathbb{E}\left(\sum_i\sum_j\sum_k B_{ik}B_{jk}\right) - \frac{1}{n}\mathbb{E}\left(\left(\sum_i\sum_j B_{ij}\right)^2\right)\right)$$

These expectations depend on the second moment $\mu_2 = 1$ as well as the correlation ρ; in particular, we have:

$$\mathbb{E}\left(\sum_i\sum_j\sum_k B_{ik}B_{jk}\right) = \mathbb{E}\left(\sum_i\sum_k B_{ik}B_{ik}\right) + \mathbb{E}\left(\sum_i\sum_{j\neq i}\sum_k B_{ik}B_{jk}\right) = n(n-1)\mu_2 + 0$$

and, using that $\mu_2 = 1$:

$$E\left(\left(\sum_i \sum_j B_{ij}\right)^2\right) = E\left(\sum_i \sum_j B_{ij}^2\right) + E\left(\sum_i \sum_j \sum_{k\neq i} \sum_{l\neq j} B_{ij}B_{kl}\right)$$
$$= n(n-1)\mu_2 + n(n-1)\rho = n(n-1)(1+\rho)\mu_2$$

Thus yielding:

$$\mathbb{E}(y(0)^T y(0)) = \frac{n}{\alpha^2} + \frac{1}{\alpha^4}\mu_2(n-1)(n-1-\rho).$$

Independent entries, $\rho = 0$ For the remaining four terms in Eq. (A.37), we need to perform calculations that differ for $\rho = 0$, $\rho = -1$ and $\rho = 0$, because in each case we have a different matrix M. We start with the simplest case, which is obtained when the coefficients of B are sampled independently, and $\rho = 0$. We have:

$$M = I + \frac{1}{\alpha}C$$
$$\mathbb{E}(b^T b) = \frac{n}{\alpha^2}$$
$$\mathbb{E}(b^T y(0)) = \frac{n}{\alpha^2}$$
$$\mathbb{E}(y(0)^T y(0)) = \frac{n}{\alpha^2} + \frac{1}{\alpha^4}(n-1)^2\mu_2$$

We need to compute the remaining terms. $b^T My(0)$ is very easy to compute:

$$b^T My(0) = b^T y(0) = \frac{n}{\alpha^2}$$

Computing $y(0)^T My(0)$ is more involved, but can be accomplished using the same approach used for $y(0)^T y(0)$, and noting that only the symmetric part of M matters. We obtain:

$$\mathbb{E}(y(0)^T My(0)) = \frac{n}{\alpha^2} - \frac{(n-1)^2}{n\alpha^5}\mu_3$$

Finally, the most complicated term, $y(0)^T M^T y(0)$, for which we obtain:

$$\mathbb{E}(y(0)^T M^T M y(0)) = \frac{n}{\alpha^2} + \frac{(n-1)(n^4 - 3n^3 + 4n^2 - 6n + 3)}{n^2\alpha^6}\mu_2^2 + \frac{(n-1)^2}{n^2\alpha^6}\mu_4$$

Combining the terms according to Eq. (A.37), we find that the expected variance for $\rho = 0$ is:

$$\mathbb{E}(\sigma_{y^\star}^2) \approx \frac{\mu_2(n-1)^2}{\alpha^4 n} + \frac{2\mu_3(n-1)^2}{\alpha^5 n^2} + \frac{\mu_4(n-1)^2}{\alpha^6 n^3} + \frac{\mu_2^2\left(n^4 - 3n^3 + 4n^2 - 6n + 3\right)(n-1)}{\alpha^6 n^3}$$

A few notable features of this equation are: a) the approximation depends on the first few moments of the distribution, and not only on the mean and variance of B_{ij}; b) the moment μ_3, summarizing the skewness of the distribution, is multiplied by a positive coefficient, hence a positive skew will increase the variance (and hence decrease the probability of feasibility, compared to a negative skew); c) however, the terms associated with the higher moments vanish when n is large and $\alpha > \sqrt{n}$, again confirming that for sufficiently large n the behavior will be universal.

Symmetric entries, $\rho = 1$ We repeat the calculation for the case of symmetric matrices B, for which we choose a different matrix M and a different parameter ω, in order to speed up the convergence. We have:

$$M = \left(I - \frac{1}{\alpha}C^T\right)\left(I + \frac{1}{\alpha}C\right)$$
$$\mathbb{E}(b^T b) = \frac{n}{\alpha^2}$$
$$\mathbb{E}(b^T y(0)) = \frac{n}{\alpha^2}$$
$$\mathbb{E}(y(0)^T y(0)) = \frac{n}{\alpha^2} + \frac{1}{\alpha^4}(n-1)(n-2)\mu_2$$

We need to compute the remaining terms:

$$b^T M y(0) = \frac{n}{\alpha^2} + \mu_3 \frac{(n-1)(n-2)^2}{n\alpha^5}$$

$$\begin{aligned}\mathbb{E}(y(0)^T M y(0)) = \frac{n}{\alpha^2} &- \frac{(n-1)(n-2)(n^3-5n^2+18n-12)}{n^2\alpha^6}\mu_2^2 \\ &+ \frac{2(n-1)(n-2)^2}{n\alpha^5}\mu_3 - \frac{(n-1)(n-2)^3}{n^2\alpha^6}\mu_4\end{aligned}$$

$$\begin{aligned}\mathbb{E}(y(0)^T M^T M y(0)) = \frac{n}{\alpha^2} &+ \frac{(n-1)(n-2)(n^3-5n^2+18n-12)}{n^2\alpha^6}\mu_2^2 \\ &+ \frac{(n-1)(n-2)(n^5-17n^4+105n^3-392n^2+724n-432)}{n^3\alpha^8}\mu_2^3 \\ &- \frac{4(n-1)(n-2)(n^4-12n^3+49n^2-88n+40)}{n^3\alpha^7}\mu_3\mu_2 \\ &+ \frac{2(n-1)(n-2)(n^4-14n^3+56n^2-92n+64)}{n^3\alpha^8}\mu_3^2 \\ &+ \frac{2(n-1)(n-2)(2n^4-17n^3+76n^2-140n+92)}{n^3\alpha^8}\mu_4\mu_2 \\ &+ \frac{2(n-1)(n-2)^2}{n\alpha^5}\mu_3 - \frac{2(n-1)(n-2)^4}{n^3\alpha^7}\mu_5 + \frac{(n-1)(n-2)^4}{n^3\alpha^7}\mu_6\end{aligned}$$

Combining all terms, we find that the expected variance for $\rho = 1$ is:

$$
\begin{aligned}
\mathbb{E}(\sigma^2_{y^\star}) \approx & \frac{\mu_2(n-1)(n-2)}{\alpha^4 n} - \frac{4\mu_3(n-1)(n-2)^2\omega}{\alpha^5 n^2} \\
& - \frac{4\mu_2\mu_3(n-1)\left(n^4-12n^3+49n^2-88n+40\right)(n-2)\omega^2}{\alpha^7 n^4} \\
& + \frac{\mu_6(n-1)(n-2)^4\omega^2}{\alpha^8 n^4} - \frac{2\mu_5(n-1)(n-2)^4\omega^2}{\alpha^7 n^4} \\
& + \frac{\mu_2^2(n-2)(n-1)\left(n^3-5n^2+18n-12\right)\omega^2}{\alpha^6 n^3} \\
& + \frac{2\mu_2^2(n-2)(n-1)\left(n^3-5n^2+18n-12\right)\omega}{\alpha^6 n^3} \\
& + \frac{2\mu_3^2(n-1)\left(n^4-14n^3+56n^2-92n+64\right)(n-2)\omega^2}{\alpha^8 n^4} \\
& + \mu_4\left(\frac{(n-1)(n-2)^3\omega^2}{\alpha^6 n^3} + \frac{2(n-1)(n-2)^3\omega}{\alpha^6 n^3}\right) \\
& + \frac{2\mu_2\mu_4(n-1)\left(2n^4-17n^3+76n^2-140n+92\right)(n-2)\omega^2}{\alpha^8 n^4} \\
& + \frac{\mu_2^3(n-1)\left(2n^5-17n^4+105n^3-392n^2+724n-432\right)(n-2)\omega^2}{\alpha^8 n^4}
\end{aligned}
$$

Skew-symmetric entries, $\rho = -1$ Finally, we compute the expectation for all the terms when the matrix B is skew-symmetric, again choosing a different matrix M and a different parameter ω, in order to speed up the convergence. We have:

$$
\begin{aligned}
M &= \left(I + \frac{1}{\alpha}C^T\right)\left(I + \frac{1}{\alpha}C\right) \\
\mathbb{E}(b^T b) &= \frac{n}{\alpha^2} \\
\mathbb{E}(b^T y(0)) &= \frac{n}{\alpha^2} \\
\mathbb{E}(y(0)^T y(0)) &= \frac{n}{\alpha^2} + \frac{1}{\alpha^4}(n-1)n\mu 2
\end{aligned}
$$

We find:

$$b^T M y(0) = \frac{n}{\alpha^2}$$

$$\mathbb{E}(y(0)^T M y(0)) = \frac{n}{\alpha^2} + \frac{(n-1)(n-2)(n-3)}{\alpha^6}\mu_2^2 - \frac{(n-1)(n-2)}{\alpha^6}\mu_4$$

$$\begin{aligned}
\mathbb{E}(y(0)^T M^T M y(0)) = &\frac{n}{\alpha^2}\frac{(n-1)(n-2)(n-3)}{\alpha^6}\mu_2^2 \\
&+ \frac{(n-1)(n-2)(n^3-15n^2+45n-60)}{n\alpha^8}\mu_2^3 \\
&+ \frac{2(n-1)(n-2)(n^2-8n+14)}{3n\alpha^8}\mu_3^2 \\
&+ \frac{(n-1)(n-2)}{\alpha^6}\mu_4 \\
&+ \frac{2(n-1)(n-2)(2n^2-10n+15)}{n\alpha^8}\mu_4\mu_2 \\
&+ \frac{(n-1)(n-2)^2}{n\alpha^8}\mu_6
\end{aligned}$$

Putting all these terms together, we find that the expected variance for $\rho = -1$ is:

$$\begin{aligned}
\mathbb{E}(\sigma_{y^\star}^2) \approx &\frac{2\mu_3^2(n-2)(n-1)((n-8)n+14)\omega^2}{3\alpha^8 n^2} \\
&+ \frac{\mu_6(n-2)^2(n-1)\omega^2}{\alpha^8 n^2} + \frac{\mu_4(n-2)(n-1)\omega\left(30\mu_2\omega + 4\mu_2 n^2\omega + \alpha^2 n(\omega-2)\right)}{\alpha^8 n^2} \\
&+ \frac{\mu_2(n-1)\left(\alpha^4 n^2 + \mu_2(n-2)\omega^2\left(\alpha^2(n-3)n + \mu_2(n(n(2n-15)+45)-60)\right)\right)}{\alpha^8 n^2} \\
&- \frac{2\mu_2^2\alpha^2(n-3)(n-2)(n-1)\omega}{\alpha^8 n} - \frac{20\mu_2\mu_4(n-2)(n-1)\omega^2}{\alpha^8 n}
\end{aligned}$$

where $\omega = \frac{\alpha^2}{\alpha^2+2n}$.

A.5.2 Using resolvents

Dyson equation derivation. In this section we present the derivation of the Dyson equation (A.9) for symmetric random matrices. We start from the resolvent of matrix B,

$$H(z) = (zI + B)^{-1},$$

i.e., the inverse of matrix $zI + B$. The Neumann series expansion for $H(z)$ is convergent for any $z \in \mathbb{C}$ such that $\mathcal{I}\Updownarrow(z) > 0$. Recall that the expectation of the resolvent is denoted as $G(z) = \mathbb{E}(H(z))$. The equation above can be rewritten as

$$zH(z) - I = -BH(z).$$

We subtract, from both sides, the matrix product $\Sigma H(z)$, with $\Sigma = \mathbb{E}(B\mathbb{E}(H(z))B) = \mathbb{E}(BG(z)B)$. Thus, we get

$$-I + (zI - \Sigma)H(z) = -BH(z) - \Sigma H(z).$$

Taking expectations on both sides of this equation, we obtain

$$\mathbb{E}(-I + (zI - \Sigma)H(z)) = -\mathbb{E}(BH(z) + \Sigma H(z)).$$

Because Σ is an expectation, this expression reduces to

$$-I + (zI - \Sigma)G(z) = -\mathbb{E}(BH(z) + \Sigma H(z)).$$

It can be shown in general that the right-hand side of this equation is negligible up to leading order, as $n \to \infty$, for arbitrary distributions [182]. Hence the resolvent satisfies the matrix equation

$$(zI - \mathbb{E}(BG(z)B))G(z) = I.$$

After elementary manipulations, this equation can be rewritten in the usual form, see Eq. (A.9).

Proof of Eq. (A.11)**.** Let $K(z) = \mathbb{E}((zI + B)^{-2})$. Here we show that $K(z) = -G'(z)$, where $G(z)$ is the expectation of the resolvent, $G(z) = \mathbb{E}((zI + B)^{-1})$, and the prime stands for the derivative with respect to z.

To compute the derivative, let us introduce a real parameter $q \neq 0$ that we can use to take derivatives with respect to it. We define $H_q(z) = (zI+qB)^{-1}$ and $L_q(z) = (zI+qB)^{-2}$, so $H_1(z) = H(z)$, with $H(z) = (zI + B)^{-1}$, and $L_1(z) = L(z)$, with $L(z) = (zI + B)^{-2}$. Observe that $\mathbb{E}(H(z)) = G(z)$ and $\mathbb{E}(L(z)) = K(z)$. It holds that

$$H_q(z) = \left(q\left(\frac{z}{q}I + B\right)\right)^{-1} = \frac{H(z/q)}{q}.$$

On the other hand, because $\mathcal{I}\Updownarrow(z) > 0$, the Neumann series for $L_q(z)$ converges. We compute it using the Neumann series for $H_q(z)$:

$$H_q(z) = \left(z\left(I + \frac{q}{z}B\right)\right)^{-1} = \frac{1}{z}\sum_{k=0}^{\infty}\left(-\frac{q}{z}\right)^k B^k.$$

Hence

$$L_q(z) = \frac{1}{z^2}\sum_{k=0}^{\infty}\left(-\frac{q}{z}\right)^k B^k \sum_{l=0}^{\infty}\left(-\frac{q}{z}\right)^l B^l.$$

We write the product of the two series using the Cauchy product, i.e.,

$$L_q(z) = \frac{1}{z^2}\sum_{s=0}^{\infty} c_s(z, q),$$

with $c_s(z,q)$ defined as

$$c_s(z,q) = \sum_{j=0}^{s} \left(-\frac{q}{z}\right)^j B^j \left(-\frac{q}{z}\right)^{s-j} B^{s-j} = (s+1)\left(-\frac{q}{z}\right)^s B^s.$$

Therefore

$$L_q(z) = \frac{1}{z^2}\sum_{s=0}^{\infty}(s+1)\left(-\frac{q}{z}\right)^s B^s = \frac{1}{z}H_q(z) + \frac{1}{z^2}\sum_{s=1}^{\infty} s\left(-\frac{q}{z}\right)^s B^s.$$

The second term in the last equation can be written in terms of a derivative of $H_q(z)$ with respect to q:

$$\begin{aligned}\frac{\partial}{\partial q}H_q(z) &= \frac{1}{z}\frac{\partial}{\partial q}\sum_{k=0}^{\infty}\left(-\frac{q}{z}\right)^k B^k = -\frac{1}{z^2}\sum_{k=1}^{\infty} k\left(-\frac{q}{z}\right)^{k-1} B^k \\ &= -\frac{1}{z^2}\left(-\frac{z}{q}\right)\sum_{k=1}^{\infty} k\left(-\frac{q}{z}\right)^k B^k = \frac{1}{qz}\sum_{k=1}^{\infty} k\left(-\frac{q}{z}\right)^k B^k\end{aligned}$$

Therefore,

$$\sum_{s=1}^{\infty} s\left(-\frac{q}{z}\right)^s B^s = qz\frac{\partial}{\partial q}H_q(z),$$

and it holds that

$$L_q(z) = \frac{1}{z}H_q(z) + \frac{q}{z}\frac{\partial}{\partial q}H_q(z).$$

Now we use that $H_q(z) = H(z/q)/q$ to compute the partial derivative:

$$\frac{\partial}{\partial q}H_q(z) = -\frac{1}{q^2}H(z/q) - \frac{z}{q^3}H'(z/q).$$

Upon substitution of this result into the equation for $L_q(z)$, and using the expression of $H_q(z)$ in terms of $H(z)$, we find

$$L_q(z) = \frac{1}{qz}H(z/q) + \frac{q}{z}\left(-\frac{1}{q^2}H(z/q) - \frac{z}{q^3}H'(z/q)\right) = -\frac{1}{q^2}H'(z/q).$$

Making the substitution $q = 1$ we get $L(z) = -H'(z)$.

To conclude the proof, we take expectations on both sides of the equation,

$$K(z) = \mathbb{E}(L(z)) = -\mathbb{E}(H'(z)).$$

By differentiating the Neumann series, we obtain

$$H'(z) = -\frac{1}{z^2}\sum_{k=0}^{\infty}(k+1)\left(-\frac{1}{z}\right)^k B^k,$$

and taking expectations

$$\mathbb{E}(H'(z)) = -\frac{1}{z^2}\sum_{k=0}^{\infty}(k+1)\left(-\frac{1}{z}\right)^k \mathbb{E}(B^k).$$

On the other hand, by definition

$$G(z) = \mathbb{E}((zI+B)^{-1}) = \frac{1}{z}\sum_{k=0}^{\infty}\left(-\frac{1}{z}\right)^k \mathbb{E}(B^k).$$

By taking the derivative of $G(z)$ with respect to z we finally obtain

$$G'(z) = -\frac{1}{z^2}\sum_{k=0}^{\infty}(k+1)\left(-\frac{1}{z}\right)^k \mathbb{E}(B^k) = \mathbb{E}(H'(z))$$

and the result $K(z) = -G'(z)$ is proved.

APPENDIX B

SUPPLEMENTARY MATERIAL: EMERGENT FEASIBILITY IN RANDOM ECOLOGICAL SYSTEMS WITH HIGHER-ORDER INTERACTIONS

Reading guide. This supplement is arranged so that a reader after one specific result can go straight to it. Section B.1 fixes notation and recalls the projective-geometry background for counting equilibria. Sections B.2–B.4 build the random GLV model with higher-order interactions in three increasingly explicit forms—compact tensor (Sec. B.2), traditional (Sec. B.3), and polynomial (Sec. B.4). Section B.5 introduces the Kostlan–Shub–Smale (KSS) random polynomial system and its known root counts, and Sec. B.6 shows that the random GLV model is exactly such a system. Sections B.7–B.8 treat the ecologically central quantity, the probability of feasibility P_f: first a numerical and analytical estimate (Sec. B.7), then an exact, assumption-free upper bound from linear programming (Sec. B.8). Sections B.9–B.11 recast everything in the language of integral geometry (Sec. B.9), extend the counts to general orthogonally invariant ensembles (Sec. B.10), and record what is known for ensembles that are not orthogonally invariant (Sec. B.11). Section B.12 shows that the Jacobian of a KSS ensemble is a Gaussian matrix, and an Appendix reports numerical relaxations of the modeling assumptions. A reader interested only in feasibility can skip directly to Sections B.7–B.8; one interested in the underlying mathematics will find it concentrated in Sections B.9–B.11.

B.1 Definitions and notation

Here we fix the notation used throughout and review the geometric setting—projective space—needed to count the equilibria of polynomial systems. Readers comfortable with

these conventions can move on without loss.

In this section, we introduce preliminary definitions and notation conventions with the goal of making the text self-contained, and easily accessible to an interdisciplinary audience, ranging from ecologists, evolutionary biologists, to physicists, and mathematicians.

Throughout this material we will be dealing with scalars, matrices, and tensors of arbitrary order. Scalars are denoted by non-capitalized letters with subscripts. For example, the abundance of population i is a scalar, denoted by x_i. Vectors are obtained by dropping the index. For example, the abundance vector for the populations in a community is x. Matrices are denoted by capital letters. For example, the matrix with pairwise interactions of a community is denoted by A. Tensors of order greater than 2 are also denoted by capital letters. To avoid confusion, their dimension is stated when they are introduced. Slices of tensors are denoted by capital letters with subscripts. For example, if B is a tensor of order 3 (a 3 dimensional array $3 \times 3 \times 3$), then B_i is a slice of such tensor, that is, a 3×3 matrix, and B_{ij} is a 3×1 column vector.

Multi-index notation will also be used throughout. As such, we will mark multi-indices in bold font, and indices in regular font. For example, the multi-index $\boldsymbol{j}$ containing n different indices is denoted $\boldsymbol{j} = (j_1, \dots j_n)$.

Derivatives with respect to time are represented with dots, i.e. $\frac{dx}{dt} = \dot{x}$

B.1.1 Projective Space

In algebraic geometry, projective space is the preferred space when studying zero sets of systems of polynomial equations. It is obtained by adding the *hyperplane at infinity* (B.1) to *affine space* $\mathbb{C}^n$ (or $\mathbb{R}^n$). The reason why projective space is preferred over affine space is that it is compact: zeros of polynomial systems can't "escape" to infinity.

The formal definition of (complex) projective space $\mathbb{P}^n$ is as the set of lines through the

origin in $\mathbb{C}^{n+1}$:

$$\mathbb{P}^n := (\mathbb{C}^{n+1} \setminus \{0\})/\sim,$$
$$\text{where } x \sim y \ :\Leftrightarrow\ \exists \lambda \in \mathbb{C} \setminus \{0\} : x = \lambda y \quad .$$

A line in $\mathbb{C}^{n+1}$/a point in $\mathbb{P}^n$ can be described by coordinates $[x_1 : \cdots : x_{n+1}]$ of one point on the line. The colon notation underlines $[x_1 : \cdots : x_{n+1}] = [\lambda x_1 : \cdots : \lambda x_{n+1}]$ for every $\lambda \in \mathbb{C}$, $\lambda \neq 0$.

We have an embedding $\mathbb{C}^n \hookrightarrow \mathbb{P}^n$ given by $(x_1, \ldots, x_n) \mapsto [x_1 : \cdots : x_n : 1]$. This shows we have a disjoint union

$$\mathbb{P}^n = \mathbb{C}^n \cup H \quad , \tag{B.1}$$

where $H = \{[x_1 : \cdots : x_{n+1}] \in \mathbb{P}^n \mid x_{n+1} = 0\}$ is the hyperplane at infinity.

Similarly, we define real projective space $\mathbb{RP}^n$ as the set of lines through the origin in $\mathbb{R}^{n+1}$. In the same way, $\mathbb{RP}^n$ is the disjoint union of $\mathbb{R}^n$ and the real hyperplane at infinity. To get some intuition about projective space, think about the cases $n = 1$ and $n = 2$. The real projective line $\mathbb{RP}^1$ is obtained by taking the real line $\mathbb{R}$ and adding a point at infinity; i.e., we connect the loose ends of $\mathbb{R}$ at infinity thus obtaining a circle. For the real projective plane $\mathbb{RP}^2$ we add a line at infinity to the plane $\mathbb{R}^2$. This line is obtained by adding a point at infinity for every direction in $\mathbb{R}^2$ (but opposite directions are identified).

Finally, we define a notion of volume on real projective space. We have a $2:1$ map $p : S^n \to \mathbb{RP}^n$ of the n-dimensional sphere S^n in $\mathbb{R}^{n+1}$ onto $\mathbb{RP}^n$ defined by $p(x_1, \ldots, x_{n+1}) = [x_1 : \cdots : x_{n+1}]$. As a subset of $\mathbb{R}^{n+1}$ the sphere carries the usual Lebesgue measure, which means we can measure volumes of (measurable) subsets of the sphere. If we have subset $U \subset \mathbb{RP}^n$ such that $p^{-1}(U)$ is k-dimensional and measurable, we define the k-dimensional

projective volume to be

$$\mathrm{vol}_k(U) := \frac{\mathrm{vol}_k(p^{-1}(U))}{2} \quad .$$

For instance,

$$\mathrm{vol}_n(\mathbb{RP}^n) := \frac{1}{2}\mathrm{vol}_n(S^n) = \frac{\pi^{(n+1)/2}}{\Gamma(\frac{n+1}{2})} \quad .$$

We can now place our system in this setting. Written homogeneously, its equilibria are points in $\mathbb{P}^n$, and Bézout's theorem guarantees that a generic degree-d system of n such polynomials has exactly d^n complex roots in $\mathbb{P}^n$, with probability one over the random coefficients. The ecologically relevant roots are those on the affine chart $\tilde{x}_{n+1} = 1$, i.e. in $\mathbb{R}^n$; by the disjoint union (B.1) any remaining roots would lie on the hyperplane at infinity $\tilde{x}_{n+1} = 0$. Setting $\tilde{x}_{n+1} = 0$ reduces the system to n homogeneous polynomials in only n variables, an overdetermined system that generically has no solution in $\mathbb{P}^{n-1}$; hence, with probability one, none of the d^n roots escapes to infinity. The complex count, and with it the expected real count $\mathbb{E}[N_{\mathbb{R}}] = d^{n/2}$ obtained below, therefore holds over $\mathbb{R}^n$.

With notation and the projective picture in hand, we now introduce the ecological model.

B.2 GLV with HOIs

Consider a GLV model representing the abundance dynamics of n populations, which we write as

$$\dot{x_i} = x_i \sum_{j=1}^{n+1} T_{ij}\tilde{x}_i \quad , \tag{B.2}$$

where T is a $n \times (n+1)$ matrix of coefficients, and $\tilde{x}$ is an $(n+1) \times 1$ vector where the first n components are population abundances, and the last component is the constant 1

$$T = \begin{pmatrix} A_{11} & \dots & A_{1n} & r_1 \\ \vdots & \ddots & \vdots & \vdots \\ A_{n1} & \dots & A_{nn} & r_n \end{pmatrix} \quad \tilde{x} = \begin{pmatrix} x_1 \\ \vdots \\ x_n \\ 1 \end{pmatrix}$$

Consider now the extension of model B.2 to account for higher-order interactions. In the case of three-way HOIs, the model can be written as

$$\dot{x_i} = x_i \sum_{jk}^{n+1} T_{ijk} \tilde{x}_i \tilde{x}_k \quad . \tag{B.3}$$

For generalized HOIs of order d, this model reads

$$\dot{x_i} = x_i \sum_{j_1 \dots j_d}^{n+1} T_{i j_1 \dots j_d} \tilde{x}_{j_1} \dots \tilde{x}_{j_d} \quad . \tag{B.4}$$

We assume the simplest random parametrization of the tensor T. Each entry of T is sampled independently from a standard Gaussian distribution, i.e., $T_{i j_1 \dots j_d} \sim N(0, 1)$

Next we unpack this tensor to recover the familiar GLV equations and to see how the interaction order sets the variance of each coefficient.

B.3 Traditional representation of GLV with HOIs

Expanding the compact model term by term, we recover the traditional GLV equations and show that a coefficient of order p is the sum of $\binom{d}{p}$ independent entries of T, so that its variance is $\binom{d}{p}$.

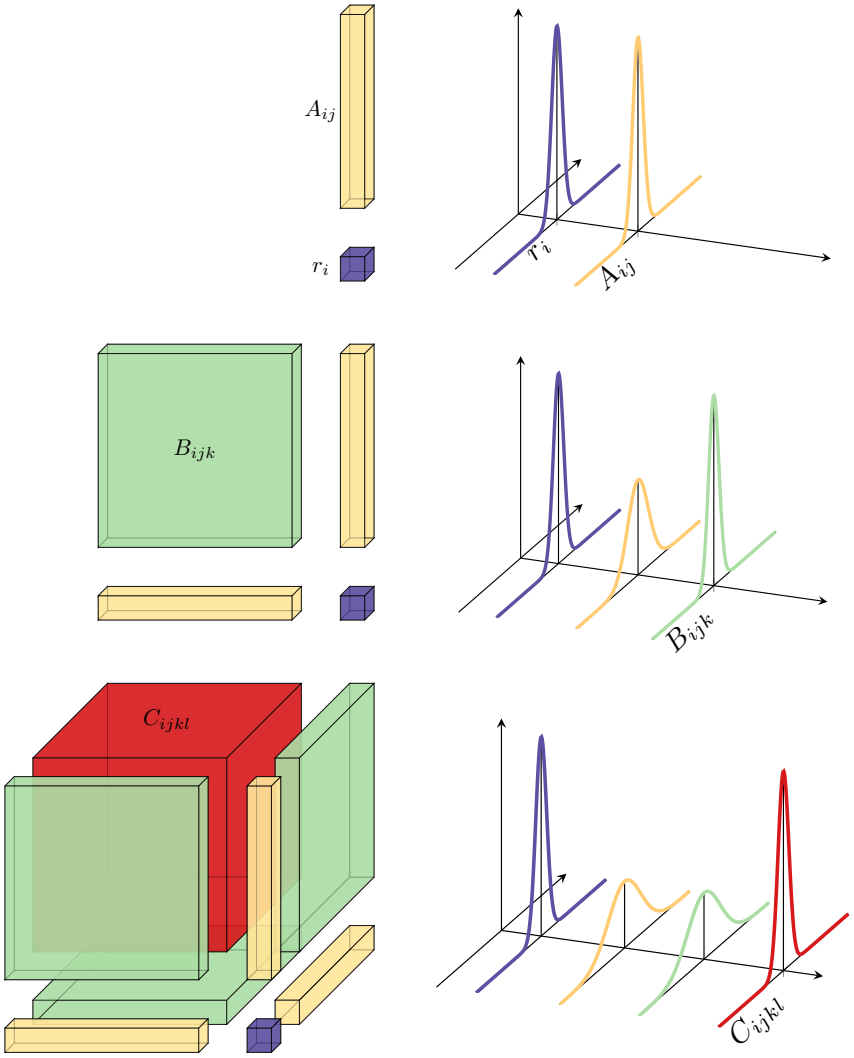

Figure B.1: **The ith slice of T: T_i, of the tensor T for $d = 1$ (top), $d = 2$ (middle), and $d = 3$ (bottom).** For three-way interactions ($d = 2$), the matrix T_i is composed of one sub-matrix, B_i, two vectors, A_{ij}, and one scalar r_i. When we perform the summation in Eq. B.4 green matrix B_i will give rise to quadratic terms of the form $B_{ijk}x_jx_k$. The yellow vectors A_i are on the nth row and column of the matrix T_i. As such, they will give rise linear terms of the form $A_{ij}x_jx_n$ and $A_{ij}x_nx_j$, which are linear because $x_n = 1$. Finally, the purple scalar r_i will give rise to 0th order terms of the form $r_ix_nx_n$. In the case of $d = 3$, T_i is now a tensor, but the same reasoning as above applies. The only difference arises in the variance structure, due to the different geometries of dimensions 2, and 3. For $d = 2$, the variances of B_{ijk} and r_i will be 1, but those of A_{ij} will be 2. For $d = 3$, the variances of C_{ijkl} and r_i will be 1, while those of A_{ij} and B_{ijk} will be 3.

Note that if we expand the matrix multiplication of model B.2, we can re-write the GLV in its traditional form, that is:

$$\begin{aligned}\dot{x_i} &= x_i \left(\sum_{j=1}^{n} T_{ij}\tilde{x}_j + T_{i,n+1}\tilde{x}_{n+1} \right) \\ &= x_i \left(\sum_{j=1}^{n} A_{ij}x_j + r_i \right) \quad , \end{aligned} \tag{B.5}$$

with $A_{ij} = T_{ij}$ and $r_i = T_{i,n+1}$. This tensor, partitioned in its inner and outer layers, is represented in the top row of Fig. B.1. The variances of the coefficients A_{ij} and r_i are also plotted next to it.

Similarly, if we expand Eq. B.3, separating the terms in which an index takes the value $n+1$ (where $\tilde{x}_{n+1} = 1$), we get

$$\begin{aligned}\dot{x}_i &= x_i \Bigg(\sum_{j,k=1}^{n} T_{ijk}\tilde{x}_j\tilde{x}_k + \sum_{k=1}^{n} T_{i,n+1,k}\tilde{x}_{n+1}\tilde{x}_k \\ &\qquad + \sum_{j=1}^{n} T_{i,j,n+1}\tilde{x}_j\tilde{x}_{n+1} + T_{i,n+1,n+1}\tilde{x}_{n+1}\tilde{x}_{n+1} \Bigg) \\ &= x_i \left(\sum_{j,k=1}^{n} T_{ijk}\, x_j x_k + \sum_{j=1}^{n} \left(T_{i,n+1,j} + T_{i,j,n+1} \right) x_j + T_{i,n+1,n+1} \right) \\ &= x_i \left(\sum_{j,k=1}^{n} B_{ijk}\, x_j x_k + \sum_{j=1}^{n} A_{ij}\, x_j + r_i \right) \quad , \end{aligned}$$

with

$$B_{ijk} = T_{ijk}, \qquad A_{ij} = T_{i,n+1,j} + T_{i,j,n+1}, \qquad r_i = T_{i,n+1,n+1} \quad .$$

The pairwise coefficient now collects two entries of T, one from each of the two edges of the slice T_i (the yellow columns in the second row of Fig. B.1). The two entries are independent standard Gaussians, so A_{ij} is Gaussian with variance 2, while B_{ijk} and r_i, each a single entry, keep variance 1 (right panel).

For the 4-way interaction model ($d = 3$), separating in the same way the terms in which one, two or three indices take the value $n + 1$ gives

$$\begin{aligned}\frac{\dot{x_i}}{x_i} &= \sum_{j,k,l=1}^{n} T_{ijkl}\, x_j x_k x_l + \sum_{j,k=1}^{n} \left(T_{i,j,k,n+1} + T_{i,j,n+1,k} + T_{i,n+1,j,k}\right) x_j x_k \\ &\quad + \sum_{j=1}^{n} \left(T_{i,j,n+1,n+1} + T_{i,n+1,j,n+1} + T_{i,n+1,n+1,j}\right) x_j + T_{i,n+1,n+1,n+1} \\ &= \sum_{j,k,l=1}^{n} C_{ijkl}\, x_j x_k x_l + \sum_{j,k=1}^{n} B_{ijk}\, x_j x_k + \sum_{j=1}^{n} A_{ij}\, x_j + r_i \quad ,\end{aligned}$$

where C_{ijkl} and r_i are single entries of T, while B_{ijk} and A_{ij} are each the sum of three: the three faces and the three edges of the cube T_i (third row of Fig. B.1). Their variances are therefore 1, 3, 3 and 1.

These examples follow one rule. In the expansion of Eq. B.4, the coefficient of order $p \leq d$, $\Gamma^{(d)}_{ij_1\ldots j_p}$, multiplies $x_{j_1} \cdots x_{j_p}$ and collects every entry of T_i whose indices are $j_1, \ldots, j_p$ in this order, with $n + 1$ in the remaining $d - p$ positions. There are $\binom{d}{p}$ ways to choose the positions of the abundance indices; the entries are distinct, hence independent, and no entry of T enters two different coefficients. As such, we can write the per-capita growth rate of the GLV with generalized HOIs as

$$\begin{aligned}\frac{\dot{x}_i}{x_i} = F(x_1, \ldots, x_n) = \Gamma^{(d)}_i + \sum_{j_1} \Gamma^{(d)}_{ij_1} x_{j_1} + \cdots + \sum_{j_1 \ldots j_p} \Gamma^{(d)}_{ij_1\ldots j_p} x_{j_1} \cdots x_{j_p} \\ + \cdots + \sum_{j_1 \ldots j_d} \Gamma^{(d)}_{ij_1\ldots j_d} x_{j_1} \cdots x_{j_d} \quad ,\end{aligned} \tag{B.6}$$

where the coefficients $\Gamma^{(d)}_{ij_1\ldots j_p}$ are independent Gaussians with mean 0 and variance

$$\mathrm{Var}[\Gamma^{(d)}_{ij_1\ldots j_p}] = \binom{d}{p} \quad .$$

Having tracked how the interaction order sets the variance of each coefficient, we now group terms by monomial to reach the polynomial form, where a finer variance structure appears.

B.4 Polynomial representation of GLV with HOIs

As seen in the previous section, the coefficients of the GLV model when expressed in its traditional form have a special variance structure. Here we perform one more step by grouping together coefficients associated with the same monomials. This last step expresses the GLV model in its polynomial form, that is, an expression where coefficients have been group according to monomials of the same order/configuration. In the case of interactions of order 0 and 1, given by Eq. B.5, the polynomial form of the model is the same as the traditional form, since r_i is the only coefficient of order 0 in equation i, and A_{ij} is the only coefficient of order 1 for equation i and population j per population j. For three-way coefficients however, the correspondence is not unique. For example, monomials of the form $x_j x_k$, with $j \neq k$ will appear twice; once multiplying the coefficient B_{ijk} and once multiplying the coefficient B_{ikj}. As such, we can group them as

$$B_{ijk}x_j x_k + B_{ikj}x_k x_j = (B_{ijk} + B_{ikj})x_j x_k = a_{11}^{(i)} x_j x_k \quad .$$

On the contrary, the monomial x_j^2 will only appear once, associated with the coefficient B_{ijj}. As such, the variance of the polynomial coefficients associated with monomials of degree 2 of the example above are

$$\mathrm{Var}[a_{|\boldsymbol{l}|=2}^{(i)}] = \begin{cases} \mathrm{Var}[a_{11}^{(i)}] = 2 \\ \mathrm{Var}[a_{20}^{(i)}] = 1 \end{cases} \quad ,$$

where $\boldsymbol{l}$ is a set of n natural numbers indicating the exponent of each variable in the monomial associated with the coefficient in the ith equation $a^{(i)}_{\boldsymbol{l}}$. $|\boldsymbol{l}|$ is the sum of the elements in the set, which is always 2 for three-way interactions. In the case of four-way interactions, we would have that monomials of the form $x_j x_k x_l$, where $j \neq k \neq l$, would appear three times

$$C_{ijkl}x_jx_kx_l + C_{iljk}x_lx_jx_k + C_{iklj}x_kx_lx_j + C_{ijlk}x_jx_lx_k + C_{ikjl}x_kx_jx_l + C_{ilkj}x_lx_kx_j = (C_{ijkl} + C_{iljk} + C_{iklj} + C_{ijlk} + C_{ikjl} + C_{ilkj})x_jx_kx_l = a^{(i)}_{111}x_jx_kx_l$$

On the contrary, when the three indices take the same value, the corresponding monomial x_j^3 would only appear once

$$C_{ijjj}x_j^3 = a^{(i)}_{300}x_j^3 \quad .$$

Alternatively, if two coefficients take the same value but one is different, we get

$$(C_{ijjk} + C_{ijkj} + C_{ikjj}) = a^{(i)}_{210}x_j^2x_k \quad .$$

As such, the variance of the polynomial coefficients associated with monomials of degree 3 we considered in this example are

$$\mathrm{Var}[a^{(i)}_{|\boldsymbol{l}|=3}] = \begin{cases} \mathrm{Var}[a^{(i)}_{111}] = 6 \\ \mathrm{Var}[a^{(i)}_{210}] = 3 \\ \mathrm{Var}[a^{(i)}_{300}] = 1 \quad . \end{cases}$$

The examples above show that the variance of the polynomial coefficient depends not only on the degree of its corresponding monomial (as the in the previous section describing the variance structure of the GLV coefficients), but also on its configuration. That is, on how

the total degree is distributed among the variables. In general, given monomial of degree $p \leq d$ with configuration $\boldsymbol{l}$, to compute its variance we need to count the number of ways of arranging p distinct objects into n distinct bins, with l_1 objects in the first bin, l_2 objects in the second bin, and so on. This is precisely the combinatorial interpretation of the multinomial coefficient. Thus, expression for the variance of the polynomial coefficients of the GLV model has the form

$$\mathrm{Var}(a_{\boldsymbol{l}}^{(i)}) = \binom{d}{\boldsymbol{l}} = \frac{d!}{l_1! \dots l_n!(d - |\boldsymbol{l}|)!} \quad . \tag{B.7}$$

This polynomial structure is precisely that of the Kostlan–Shub–Smale ensemble, which we define next.

B.5 KSS system of random polynomials

We introduce the Kostlan–Shub–Smale (KSS) ensemble of random polynomials and recall its known root counts: the expected number of real roots, the vanishing of the normalized variance, and the resulting count of positive roots.

Consider a system $\boldsymbol{P}$ of n polynomials with common degree $d > 1$, on n variables. The ith equation of such system can be written as

$$P_i(x_1, \dots, x_n) = \sum_{|\boldsymbol{l}| \leq d} a_{\boldsymbol{l}}^{(i)} \boldsymbol{x}^{\boldsymbol{l}} \quad , \tag{B.8}$$

where

1. $\boldsymbol{l} = \{l_1, \dots, l_n\} \in \mathbb{N}^{[0,n]}$, and $|\boldsymbol{l}| = \sum_{k=1}^{n} l_k$,
2. $a_{\boldsymbol{l}}^{(i)} = a_{l_1,\dots,l_n}^{(i)} \in \mathbb{R}$, $|\boldsymbol{l}| \leq d$,
3. $\boldsymbol{x} = (x_1, \dots, x_n)$ and $\boldsymbol{x}^{\boldsymbol{l}} = \prod_{k=1}^{n} x_k^{l_k}$.

We say that the system $\boldsymbol{P}$ has the Kostlan-Shub-Smale (KSS) distribution [10, 185] if the coefficients $a_{\boldsymbol{l}}^{(i)}$ are i.i.d. random variables with mean 0 and variance

$$\mathrm{Var}(a_{\boldsymbol{l}}^{(i)}) = \binom{d}{\boldsymbol{l}} = \frac{d!}{l_1! \dots l_n!(d - |\boldsymbol{l}|)!} \quad . \tag{B.9}$$

Importantly, for this class of systems of polynomials, it has been shown [186] that the expected number of real roots is

$$\mathbb{E}[N_{\mathbb{R}}] = \sqrt{d^n} \tag{B.10}$$

Additionally, [187] showed that the variance of the normalized number of real roots vanishes in the for $d \geq 3$ in the limit of $n \to \infty$, that is

$$\lim_{n\to\infty} \mathrm{Var}\left[\frac{N_{\mathbb{R}}}{\sqrt{d^n}}\right] = 0 \quad . \tag{B.11}$$

These two results can be easily cast into statements about the number of positive roots. To do so we rely on the fact that the coefficients of P_i are sampled from a distribution centered at zero. As such, the sign of each component of the roots are not biased in any direction. Thus, the asymptotic behavior of the variance of the positive roots will remain, and, by symmetry, the expected number of positive roots is just [117, 188]

$$\mathbb{E}[N_+] = \frac{1}{2^n}\mathbb{E}[N_{\mathbb{R}}] = \left(\frac{\sqrt{d}}{2}\right)^n \tag{B.12}$$

Numerical simulations of the system in Eq. B.8 (Fig. B.2, dots) using homotopy continuation [83, 125] (Chapter 3), track well both of the theoretical curves (Eqs. B.10 and B.12). Importantly, one can see from Eq. B.12 that the expected number of positive roots becomes 1 for $d = 4$, and grows with n for $d > 4$. In the next section, we establish the connection between this system and the GLV model. Thereafter, we make use of such connection to

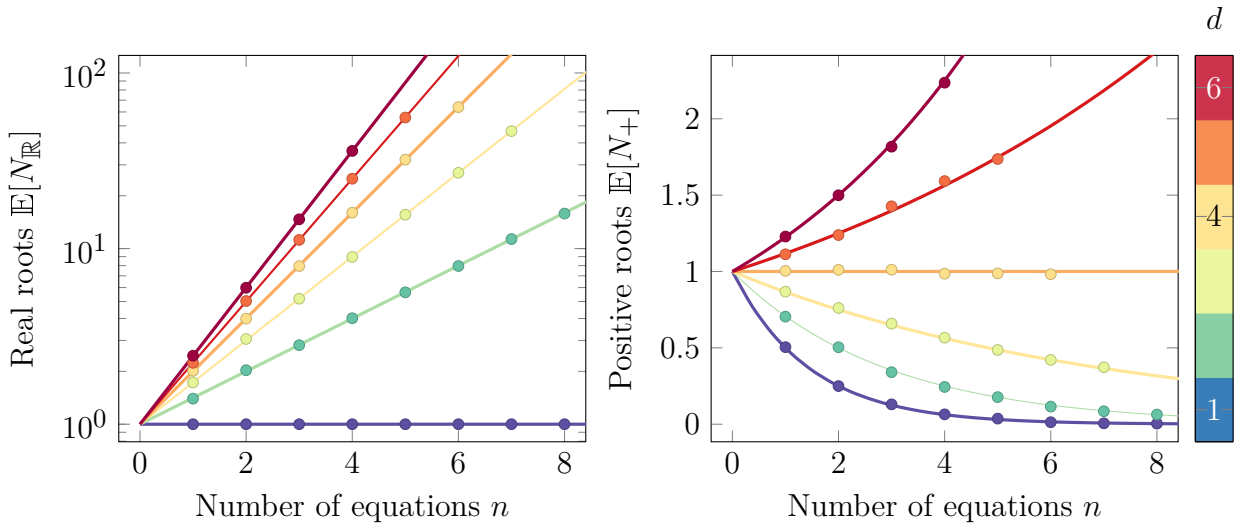

Figure B.2: **Expected number of real roots and positive roots.** On the left panel we plot (semilog scale) the expected number of real roots (Eq. B.10) for different values of d, and overlay the average value of real roots obtained from simulations of the KSS polynomial system. On the right panel we plot the expected number of positive solutions. Importantly, this number grows with n for $d > 4$. Each point averages 10^3 independent realizations of the system.

study the ecological consequences of the divergence of the number of positive roots.

These statements hold for any KSS system; we now show that the random GLV model is one, so all of them transfer to it.

B.6 From KSS to GLV

Here we show that the system of polynomials arising when solving for feasible equilibria of Eq. B.2 is precisely the KSS system of random polynomials when the coefficients in $r, A, B, \ldots$ are sampled with mean 0, and appropriate variances. Recently, this equivalence has been shown for the replicator equation with higher order interactions [117].

First, we expand Eq. B.8 as

$$\begin{aligned} P_i(x_1, \dots x_n) &= \sum_{|\boldsymbol{l}| \leq d} a_{\boldsymbol{l}}^{(i)} \prod_{k=1}^{n} x_k^{l_k} \\ &= \sum_{|\boldsymbol{l}|=0} a_{0\dots0}^{(i)} + \sum_{|\boldsymbol{l}|=1} a_{l_1\dots l_n}^{(i)} \prod_{k=1}^{n} x_k^{l_k} + \cdots + \sum_{|\boldsymbol{l}|=d} a_{l_1\dots l_n}^{(i)} \prod_{k=1}^{n} x_k^{l_k} \quad . \end{aligned} \tag{B.13}$$

The first commonality between systems in Eqns. B.13 and B.6 is that they have the same total degree; that is $h = d$. We can now identify coefficients of Eq. B.6 with the corresponding coefficients of Eq. B.13 that multiply monomials of equal degree. For the first term in the sum of Eq. B.13, that with $|\boldsymbol{l}| = 0$, there is only one monomial of degree 0; (that is, the scalar 1). As such, the corresponding coefficient in the GLV model (Eq. B.6) is simply

$$r_i = a_{0\dots0}^{(i)}$$

For r_i to be a coefficient of the KSS system, its variance should be that of Eq. B.9

$$\mathrm{Var}[r_i] = \binom{d}{\boldsymbol{l}} = \frac{d!}{0!d!} = 1 \quad .$$

For the coefficients of the second term of the sum in Eq. B.13 (those paired with monomials of degree $|\boldsymbol{l}| = 1$), the corresponding coefficients in the GLV model would be

$$\begin{aligned} \sum_{j_1} A_{ij_1} x_{j_1} &= \sum_{|\boldsymbol{l}|=1} a_{l_1\dots l_n}^{(i)} \prod_{k=1}^{n} x_k^{l_k} \\ A_{i1}x_1 + A_{i2}x_2 + \cdots + A_{in}x_n &= a_{10\dots0}^{(i)} x_1 + a_{01\dots0}^{(i)} x_2 + \dots a_{00\dots1}^{(i)} x_n \\ A_{ij} &= a_{\boldsymbol{l}_j}^{(i)} \quad , \end{aligned}$$

where $\boldsymbol{l}_j$ denotes the multiindex of all zeros and a 1 in position j. As before, the variance of

the A_{ij} coefficients should be

$$\mathrm{Var}[A_{ij}] = \binom{d}{d-1} = d \quad ,$$

Next, we identify with the GLV coefficients associated with interactions of order 3, B_{ijk}, with the coefficients of monomials of degree $|\boldsymbol{l}| = 2$ in Eq. B.13

$$\sum_{|\boldsymbol{l}|=2} a^{(i)}_{l_1 \ldots l_n} \prod_{k=1}^{n} x_k^{l_k} = \sum_{j_1 j_2} B_{i j_1 j_2} x_{j_1} x_{j_2}$$

$$\begin{aligned} B_{i11}x_1^2 + (B_{i12} + B_{i21})x_1x_2 + \cdots + & \\ (B_{i1n} + B_{in1})x_1x_n + & \\ (B_{i2n} + B_{in2})x_2x_n + \cdots + B_{inn}x_n^2 = & \; a^{(i)}_{20\ldots0}x_1^2 + a^{(i)}_{11\ldots0}x_1x_2 + a^{(i)}_{10\ldots1}x_1x_n + \ldots \\ & \; a^{(i)}_{10\ldots1}x_1x_n + a^{(i)}_{01\ldots1}x_2x_n + \cdots + a^{(i)}_{00\ldots2}x_n^2 \end{aligned}$$

The first thing to note from the above expression is that for $|\boldsymbol{l}| = 2$, we sometimes find more than one GLV parameter per KSS coefficient. In particular, when $j = k$ the correspondence is 1 to 1, but when $j \neq k$ it is 1 to 2. This is due to the commutative property of multiplication. Therefore, the variance of the B_{ijk} coefficients appears to be index dependent. Let us apply Eq. B.9 to each case, we have that

$$\mathrm{Var}[B_{ijj}] = \mathrm{Var}[a^{(i)}_{0\ldots2\ldots0}] = \frac{1}{2}d(d-1)$$

and

$$\mathrm{Var}[B_{ijk}] + \mathrm{Var}[B_{ikj}] = \mathrm{Var}[a^{(i)}_{0\ldots1\ldots1\ldots0}]$$

Without loss of generality we assume the variances of coefficients with indices $\{j, k\}$ that are

permutations of each other to be the same. Plugging in Eq. B.9, we get

$$\mathrm{Var}[B_{i\sigma(jk)}] = \frac{1}{2}d(d-1) \quad ,$$

where $\sigma(jk)$ denotes permutations of the set $\{j, k\}$. Conveniently, the variance of the element B_{ijk} turns out to not depend on its position on the tensor. As we will see next, this is not an artifact specific to order 2, but a general feature.

Lastly, we consider the general case of monomials of order $|\boldsymbol{l}| = p$

$$\sum_{|\boldsymbol{l}|=p} a^{(i)}_{l_1 \dots l_n} \prod_{k=1}^{n} x_k^{l_k} = \sum_{j_1 j_2} T_{i j_1 \dots j_p} x_{j_1} \dots x_{j_p} \quad .$$

Due to the commutative property, identifying coefficients on the same monomials leads to the following equality for any given monomial of degree p

$$a^{(i)}_{l_1 \dots l_n} = \sum_{\sigma(j_1 \dots j_p)} T_{i j_1 \dots j_p} \quad , \tag{B.14}$$

where the sum is taken over all the permutations of the multiset $\mathcal{S} = \{j_1 \dots j_p\}$. Taking the variance on both sides leads to

$$\mathrm{Var}[a^{(i)}_{l_1 \dots l_n}] = \mathrm{Var}\left[\sum_{\sigma(\mathcal{S})} T_{i j_1 \dots j_p}\right] = r\mathrm{Var}[T_{i j_1 \dots j_p}] \quad , \tag{B.15}$$

where the sum is not performed over different values of indices; that is, given a multiset of indices, $\mathcal{S}$, we sum over all the distinguishable permutations of such set $\sigma(\mathcal{S})$. There are a total of r number of permutations of $\mathcal{S}$, and we have used that the variance of the sum of sum of variances since $T_{i\sigma(\mathcal{S})}$ are i.i.d.

Given a multiset of p objects such that there are p_1 identical objects of type 1, p_2 identical

objects of type 2... and p_k identical objects of type k, the number of permutations of such multiset is

$$r = \frac{p!}{p_1! \cdots p_k!}$$

Note that since we are identifying coefficients, the numbers $p_1, \ldots, p_k$ are indeed $l_1, \ldots, l_k$. Making these substitutions and plugging in Eq. B.9 into Eq. B.15, we can solve for the variance of any coefficient of $T_{ij_1 \ldots j_p}$ arriving to

$$\mathrm{Var}[T_{ij_1 \ldots j_p}] = \frac{l_1! \cdots l_n!}{d!} \frac{d!}{l_1! \ldots l_n! (d-p)!} = \frac{d!}{p!(d-p)!} = \binom{d}{p} \quad . \tag{B.16}$$

Surprisingly, this variance only depends on the coefficient order, p, and the overall order of HOIs in the ecosystem, d (see Fig. B.3). Note that the largest variance occurs when the maximum size of the group of simultaneously interacting populations (the order of the interaction, $d+1$) is largest (top row of Fig. B.3). Specifically, the maximum is reached when the size of the interacting group of populations (coefficient order, p) is half of the maximum allowed size, $p = \frac{1}{2}(d+1)$.

We have shown that, as long as the coefficients of the GLV model are sampled from a Gaussian distribution with mean 0 and variance given by Eq. B.16, then it holds that

$$F_i(x_1, \ldots, x_n) \equiv P_i(x_1, \ldots x_n) \quad .$$

As such, all the results derived for the KSS system of random polynomials can be applied to the random GLV with higher-order interactions.

With the equivalence in place, every KSS result applies to the model. We turn to the quantity of ecological interest, the probability of feasibility.

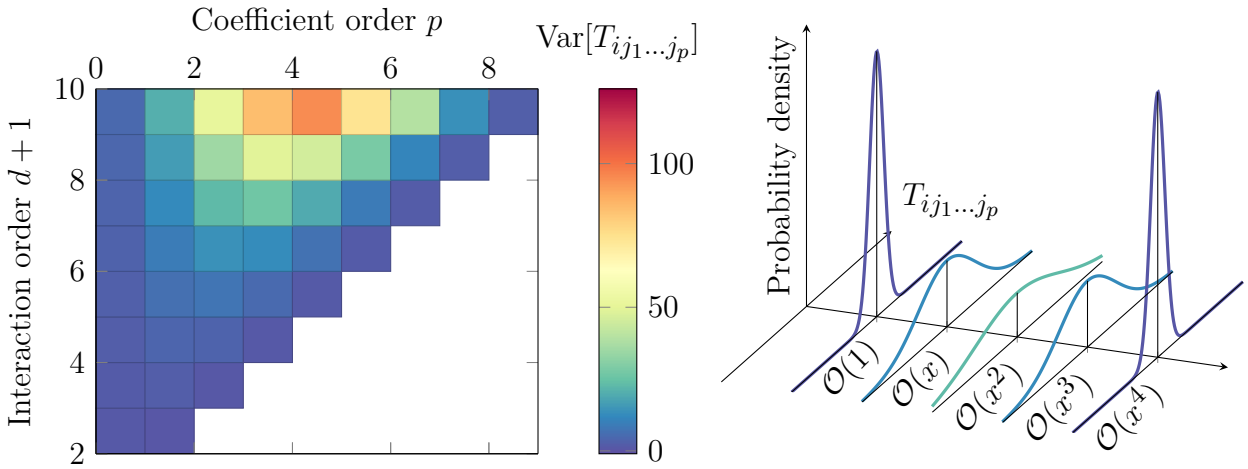

Figure B.3: **Variance of the GLV coefficients**. (left) We plot the variance obtained in Eq. B.16 as a function of coefficient order p (x-axis) and overall interaction order of the system d (y-axis). For a given coefficient order p (vertical stripes), its variance increases as the interaction order of the system increases. On the other hand, for a given interaction order d (horizontal stripes), the variance of the coefficient reaches a maximum for intermediate values of its order. (right) For interaction order $d = 4$ we plot the probability distributions from which we sample the coefficients associated to each monomial. The extreme monomials, with powers 0 and 4 have coefficients sampled from normal distributions with the smallest variance. The the middle monomials, those with degree 2 (we label them generically as x^2) are sampled from a distribution with the largest variance.

B.7 Probability of feasibility

Real ecosystems exhibit only one equilibrium at a time. Thus, the ecologically relevant quantity is the probability of feasibility; P_f. This is the probability of having at least one solution with all positive components, which we compute as

$$P_f = \sum_{i=1}^{d^n} P(N_+ = i) = 1 - P(N_+ = 0) \quad , \tag{B.17}$$

that is, we sum over the probabilities of having any number of feasible solutions greater than 0 ($i \in [1, d^n]$). The probability distribution $P(N_+)$ has discrete support in the integers $\mathbb{Z} \in [0, d^n]$, and expected value given by Eq. B.12 but is otherwise unknown for arbitrary d. As such, we can only approximate $P(N_+)$ given a sufficiently large ensemble of equilibria of

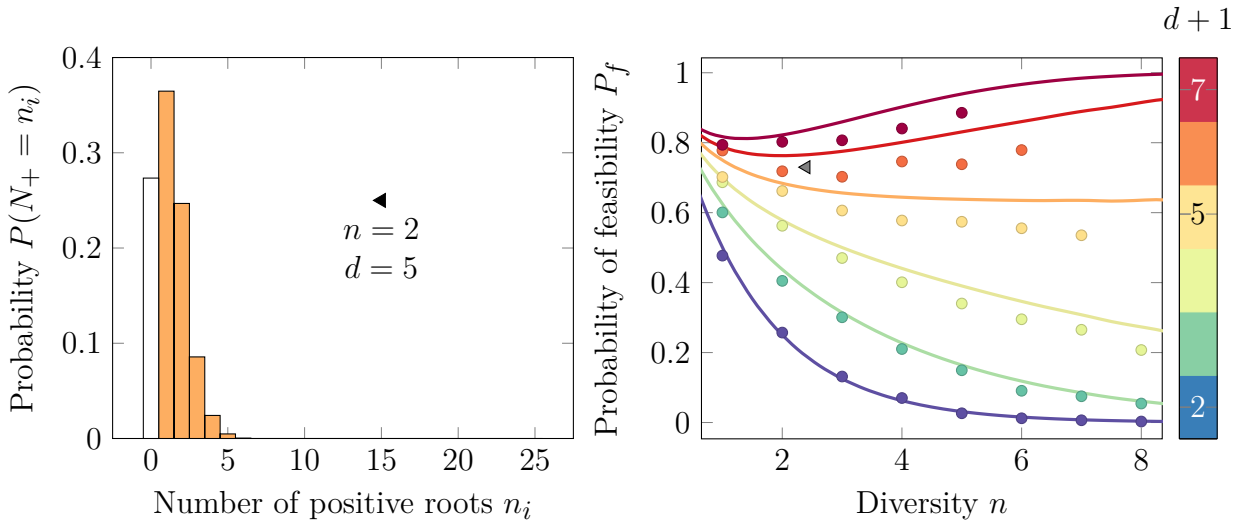

Figure B.4: **Distribution of the number of positive roots, and the probability of feasibility.** Left: Numerical approximation of the probability distribution $P(N_+)$ for $d = 5$, and $n = 2$. The height of the ith bar is obtained by dividing the number of times that we observe i positive solutions by the total number of carried simulations (in this case, 1000). Right: probability of feasibility (P_f, y-axis) as a function of diversity (n, x-axis) and interaction order (d, colors) for computationally tractable values of n, and d. P_f decreases with n for $d \leq 5$, but approaches 1 for $d > 5$. Points and lines are numerical and theoretical approximations, respectively. Black triangular marker connects the two plots: that is, adding the heights of the orange bars in the left yields the numerical approximation of P_f (y-axis) plotted on the right. Each point on the right is likewise computed from 10^3 realizations per (n, d).

random GLV systems obtained numerically. An example of this numerical approximation for $d = 5$ and $n = 2$ is shown in the histogram of Fig. B.4. We then can compute P_f for different values of n and d using Eq. B.17. This would be equivalent to adding the colored bars of the histogram in Fig. B.4. In the right panel of Fig. B.4, we show numerical estimations (points) of P_f for computationally tractable values of n and d. Furthermore, we can try to approximate P_f analytically by subtracting the probability to have 0 positive roots from

one, obtaining:

$$\begin{aligned} P_f &\approx 1 - (p_1 p_- + p_2 p_- p_- + \cdots + p_{d^n} p_-^{d^n}) \\ &= 1 - \sum_{n_i=0}^{d^n} p_i \left(1 - \frac{1}{2^n}\right)^{n_i} \\ &= 1 - \mathbb{E}[f(n_i)] \quad . \end{aligned} \tag{B.18}$$

Here, p_i is the probability that system B.6 has n_i real roots. The function $f(n_i) = (1-2^{-n})^{n_i}$, is the probability that none of the n_i roots are feasible. We sum over all possible number of real roots; from 0 (found when all roots are complex) to d^n (when all roots are real). In Eq. B.18 we have assumed independence in the probability of having no positive roots; that is, the probability that one root has does not have all positive components does not depend on the sign of the components of other roots. This assumption only works for $d = 1$, because the number of roots is 1. In fact, the case where $d = 1$ has been well characterized by [32] (blue line in Fig. B.4). In this case, $d^n = 1$, and Eq. B.18 reduces to

$$P_f = \frac{1}{2^n} \quad .$$

Note however, that this approximation is not exact for arbitrary d.

Since we know the first moment of the random variable n_i (Eq. B.10), we can use it to approximate $\mathbb{E}[f(i)]$ through a Taylor expansion around the mean

$$\begin{aligned} P_f &\approx 1 - \left(f(\bar{X}) + \frac{df}{dn_i}\Big|_{n_i=\bar{X}} \mathbb{E}[n_i - \bar{X}] + \mathcal{O}\left(E[(n_i - \bar{X})^2]\right)\right) \\ &\approx 1 - \left(f(\bar{X})\right) \\ &\approx 1 - \left(1 - \frac{1}{2^n}\right)^{d^{n/2}} \quad . \end{aligned} \tag{B.19}$$

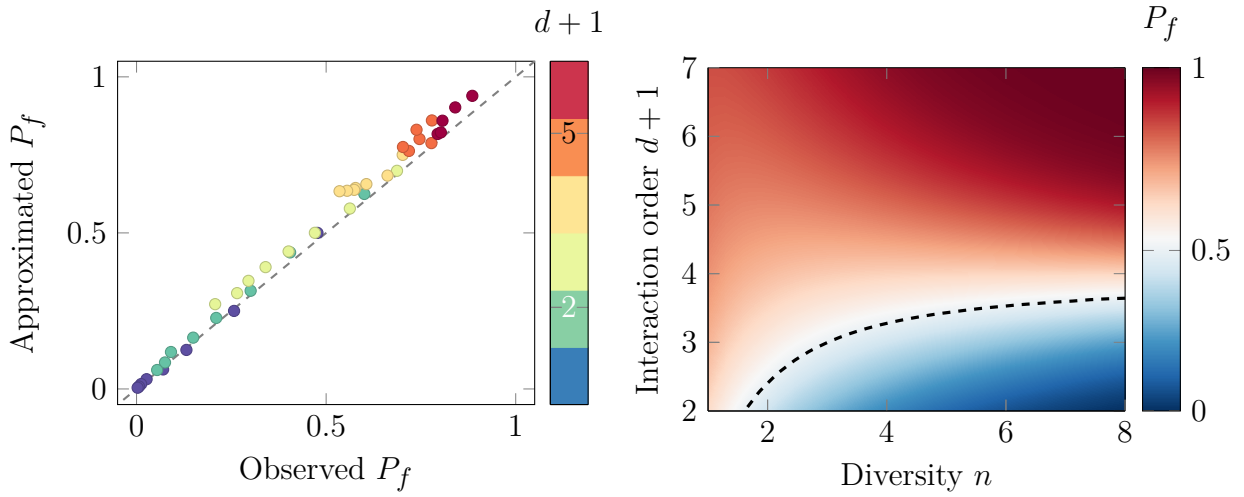

Figure B.5: **Accuracy of the approximation, and an upper bound on P_f.** (left) Approximated probability of feasibility versus the observed probability of feasibility in simulations. Different colors correspond to different values of interaction order d, and points within one color represent different values of n. The one to one line (dashed grey) is plotted for reference. Each point is a Monte Carlo estimate from 10^3 independent realizations. (right) Heat map of the upper bound of P_f (computed from Eq. B.19) as a function of both n and d. Level set where $P_f = 0.5$ is plotted as dashed line for reference.

Here we have truncated the expansion to the first order. This truncation becomes more accurate as n increases, since the variance vanishes in the limit of high diversity (Eq. B.11, [187]). As such, the expected value of the number of positive roots is the first-order statistical approximation of the random variable N_+. In Fig B.4, we plot this approximation in solid lines. In Fig B.5 (left panel) we show that the approximation is very good even for moderately high n, and thus we plot the heat map (right panel) of P_f as a function of d and n obtain from Eq. B.19. In this limit, the scenario that we would see is that the approximated P_f converges to 0 if $d < 4$, or 1 if $d > 4$. Importantly, the first order approximation is an upper bound for P_f. We can see this using Jensen's inequality, which has the form

$$\psi\left(\sum_i p_i x_i\right) \leq \sum_i p_i \psi(x_i) \quad , \tag{B.20}$$

where $p_i \geq 0$, $\sum_i p_i = 1$, and ψ is convex. In our case, $\psi(x_i) = f(n_i)$. This function is convex on n_i, since its second derivative

$$\frac{d^2 f}{dn^2} = f(n_i) \log^2 \left(1 - 2^{-n}\right) > 0$$

is always positive. We apply this inequality to Eq. B.18 by multiplying Eq. B.20 by -1, and adding 1, arriving to

$$1 - \sum_i p_i f(n_i) \leq 1 - f\left(\sum_i p_i n_i\right)$$
$$P_f \leq 1 - f(\bar{X}) \quad . \tag{B.21}$$

This estimate rests on an independence assumption that is uncontrolled at finite diversity; we next replace it with an exact bound.

B.8 An exact upper bound to P_f

The analytical expression in Eq. B.19 is an approximation based on the assumption that the signs of polynomial root are independent from each other.

Here we show that the error introduced by the independence assumption is small for large n. As such, the approximation is valid in the thermodynamic limit ($n \to \infty$). To do so, compute an exact upper bound to P_f using linear programming. P_f is the probability to have at least one (but possibly more than one) positive equilibrium. To calculate this probability we have to add the probabilities to have i positive roots, p_i where $i \neq 0$ (see Fig B.4, left panel). That is, we maximize P_f over the probability density vector p, subject to the constraints that (i), the elements of p sum to 1, (ii), the expected value of the resulting probability distribution matches that in Eq. B.12. To warm up, before considering the

complete problem, we consider a simpler (only loosely constrained) version of it. That is, we attempt to minimize the probability of feasibility over the variables p_i (probability densities), only subjected to the constraint that the elements of the vector p are nonnegative and add to 1.

$$\begin{aligned} \max_{p} \quad & 1 - p_0 \\ \text{s.t.} \quad & \sum_{i=0}^{d^n} p_i = 1 \quad . \end{aligned}$$

This problem has infinite solutions of the form

$$p^\star = (0, p_1, \ldots, p_{d^n}) \quad . \tag{B.22}$$

That is, put the weight anywhere but on p_0, such that $P_f = 1$ (see Eq. B.17). In Fig. B.6**A**, this would correspond to solutions laying on the right edge of the triangular plane. Note that the maximizer of $1 - p_0$ is also the minimizer of p_0, which is the problem we solve.

Next, we introduce the constraint on the expected value of the distribution $P(N_+)$, which we know is given by Eq. B.12. The optimization problem can now be stated (now as a minimization problem) as

$$\begin{aligned} \min_{p} \quad & p_0 \\ \text{s.t.} \quad & (i) \sum_{i=0}^{d^n} p_i = 1 \\ & (ii) \sum_{i=0}^{d^n} i p_i = \frac{\sqrt{d^n}}{2^n} \quad , \end{aligned} \tag{B.23}$$

where $\mathbb{E}[N_+]$ is given by Eq. B.12.

The geometric representation of Eq. B.23 is plotted in Fig. B.6, left panel. We perform this minimization in general, for a range of n and d values, and plot the results in Fig. B.6. We observe that P_f^U is decreasing when $d < 4$, and equal to 1 when $d \geq 4$. This implies that P_f has to be strictly decreasing in n when the interaction order is less than 4, but could

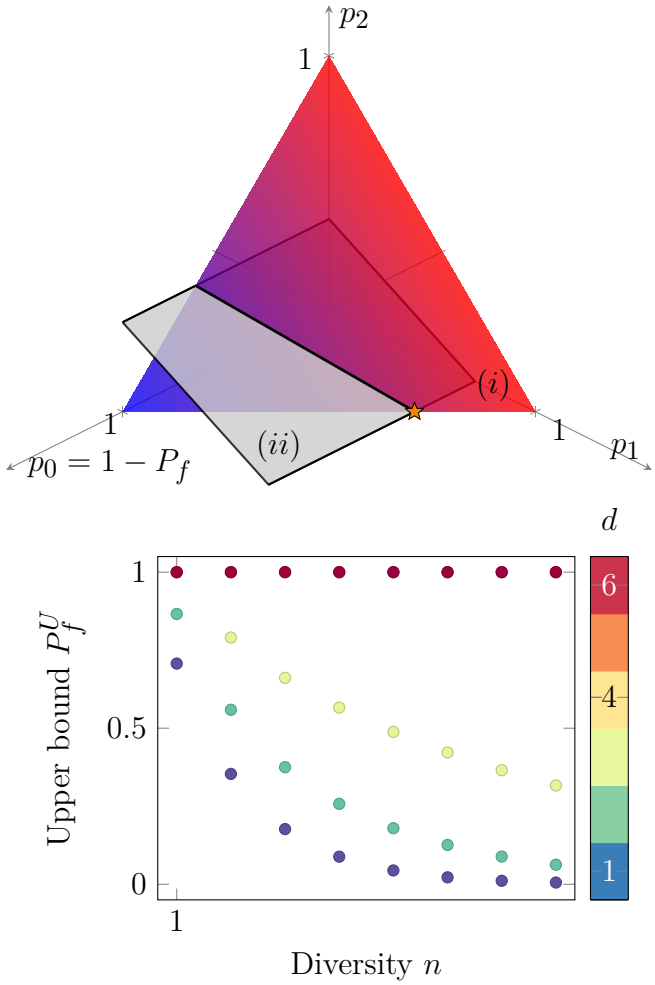

Figure B.6: **Using linear programming to obtain an exact upper bound of P_f.** (left) Geometric representation of the optimization problem for $d = 2$, $n = 1$. Triangular plane corresponds to constraint (i) in Eq. B.23. This plane is colored according to the function we want to maximize, more red colors corresponding to higher values. The black plane parallel to the axis of p_0 corresponds to constraint (ii) in Eq. B.23. The solution must lie in the intersection between the two planes, since only there both constraints are satisfied. Specifically, the optimal value is reached at the point marked with an orange star, since it is there where P_f is maximum (most red part). (right) Exact upper bound of P_f obtained through linear programming. Importantly P_f cannot increase with n when $d < 4$, because its upper bound decreases with n. On the contrary, for $d \geq 4$, the upper bound is always one, meaning that P_f could increase with n.

potentially increase otherwise.

The bound confirms that feasibility must fall with diversity when $d < 4$ and may rise otherwise. We close by placing these counts in a broader mathematical framework.

B.9 Integral Geometry

We recast the root counts in the language of integral geometry, where Howard's formula expresses the expected number of equilibria as a product of expected degrees.

The Kostlan-Shub-Smale-Edelman identity (B.10) is part of a more general mathematical framework, called *integral geometry*. We refer to the seminal paper by Kostlan and Edelman [13] that explains how integral geometry is used in the context of random polynomials.

Each random polynomial f defines a *random projective hypersurface*

$$X(f) := \{x \in \mathbb{RP}^n \mid f(x) = 0\}.$$

We denote its *expected degree* by

$$\operatorname{edeg}(f) := \mathbb{E}\left[\#(X(f) \cap L)\right] \quad ,$$

where L is a random line, that is independent of f, and defined by choosing $n-1$ independent linear equations with independent standard Gaussian coefficients.

Let us consider n independent random real homogeneous polynomials $f_1, \ldots, f_n$ in $n+1$ variables. We assume that the distribution of each f_i is *orthogonally invariant* meaning that satisfies $f_i(x) \sim f_i(Ox)$ for every orthogonal matrix $O \in O(n+1)$. For instance, the KSS ensemble satisfies this property.

Howard's integral geometry formula [189], generalized by Bürgisser and Lerario [190, Theorem 3.19], states that under this assumption $X(f_1) \cap \cdots \cap X(f_n)$ consists of finitely

many points almost surely, and that

$$\begin{aligned} E[N_{\mathbb{R}}] &= \mathbb{E}\left[\#\left(X(f_1) \cap \cdots \cap X(f_n)\right)\right] \\ &= \operatorname{edeg}(f_1) \cdots \operatorname{edeg}(f_n) \quad . \end{aligned} \tag{B.24}$$

Using the same argument as for (B.12) we get for the expected number of feasible equilibria:

$$\mathbb{E}[N_+] = \frac{\operatorname{edeg}(f_1) \cdots \operatorname{edeg}(f_n)}{2^n} \quad . \tag{B.25}$$

More generally, we consider $k < n$ homogeneous polynomials in $n+1$ variables. This is the case when we are interested in states of the Lotka-Volterra models (Eq. (2.1)) where only a subset of variables is stable. [190, Theorem 7.2] yields that $X(f_1) \cap \cdots \cap X(f_k)$ almost surely is $(n-k)$-dimensional and that

$$\mathbb{E}\left[\operatorname{vol}_{n-k}(X(f_1) \cap \cdots \cap X(f_k))\right] = \operatorname{vol}_{n-k}(\mathbb{RP}^{n-k}) \cdot \operatorname{edeg}(f_1) \cdots \operatorname{edeg}(f_k) \quad .$$

This viewpoint applies to any orthogonally invariant ensemble, a generality we exploit in the final section.

B.10 Expected number of zeros of orthogonally invariant ensembles

We compute the expected degree for general orthogonally invariant ensembles, recovering the KSS count, allowing unequal degrees, and contrasting it with the real Fubini–Study ensemble.

Recall that we call a random ensemble of polynomials f in $n+1$ variables orthogonally invariant, if $f(x) \sim f(Ox)$ for every orthogonal matrix $O \in O(n+1)$. The KSS ensemble is

orthogonally invariant.

A KSS system f of degree d has

$$\text{edeg}(f) = \sqrt{d} \quad .$$

We therefore recover (B.10) from (B.24):

$$E[N_{\mathbb{R}}] = \mathbb{E}\left[\#\left(X(f_1) \cap \cdots \cap X(f_n)\right)\right] = d^{n/2} \quad ,$$

where $f_1, \ldots, f_n \overset{\text{iid}}{\sim}$ KSS of degree d.

Interestingly, the formula also works when the KSS polynomials have differing degrees. Suppose that we have $f_i \sim$ KSS of degree d_i. Then,

$$E[N_{\mathbb{R}}] = (d_1 \cdots d_n)^{\frac{1}{2}} \quad .$$

This is the case of Lotka-Volterra models (Eq. (2.1)) when the dynamics of population i has interaction order d_i with the other populations. Here, we have for the number of positive solutions (B.25)

$$\mathbb{E}[N_+] = \frac{(d_1 \cdots d_n)^{\frac{1}{2}}}{2^n} \quad . \tag{B.26}$$

As a function of n, when $d_1 \cdots d_n$ grows faster/slower than 4^n, this function is increasing/decreasing. For instance, taking $d_1 = 2d$ and $d_2 = \cdots = d_n = d$, we have that $\mathbb{E}[N_+]$ increases precisely when $d > 2$.

More generally, for $f_i \sim$ KSS of degree d_i, we have

$$\mathbb{E}\left[\text{vol}_{n-k}(X(f_1) \cap \cdots \cap X(f_k))\right] = \text{vol}_{n-k}(\mathbb{RP}^{n-k}) \cdot (d_1 \cdots d_k)^{\frac{1}{2}} \quad .$$

Again, the volume of positive solutions inside this is given by dividing the right-hand side by 2^n.

What about expected volumes of other ensembles? Fyodorov, Lerario and Lundberg [191] give a detailed answer. All orthogonally invariant random polynomials can be parameterized as follows (see [13]). Let $g_{j,\ell}$, where $j \in J_\ell$, be the standard basis of spherical harmonics of degree ℓ on the sphere S^n. The nonnegative weights $p_d(d), p_d(d-2), \ldots,$ parameterize all invariant random homogeneous polynomial in $x = (x_1, \ldots, x_{n+1})$ of degree d via

$$f(x) = \sum_{d-\ell \text{ is even}} p_d(\ell) \sum_{j \in J_\ell} T_{j,\ell} \, \|x\|^{d-\ell} \, g_{j,\ell}(x/\|x\|) \quad ,$$

where $\|x\|^2 = x_1^2 + \cdots + x_{n+1}^2$ and the $T_{j,\ell}$ are i.i.d. standard Gaussian random variables.

In [191, Theorem 1 & Section 8, Example 3] it is shown that for every $0 < h \leq 1$ and any integrable function $\psi : \mathbb{R}_{>0} \to \mathbb{R}$ with subgaussian tails, if we define the random ensemble f via

$$p_d(\ell) = \frac{1}{d^h} \, \psi\left(\frac{\ell}{d^h}\right) \quad , \tag{B.27}$$

then we have

$$c_1 \, d^h \leq \operatorname{edeg}(f) \leq c_2 \, d^h \quad ,$$

where $c_1, c_2 > 0$ are constants (independent of d, but not of n).

For instance, the KSS ensemble has $h = \frac{1}{2}$. Another interesting example is the *real Fubini-Study ensemble* (see [191, Section 8, Example 2]), which is defined by taking a random polynomial uniformly from the unit sphere in the L^2-norm in the space of all homogeneous polynomials in $n+1$ variables of degree d. This ensemble has $h = 1$. Therefore, by the formula above, if $f_1, \ldots, f_n$ are i.i.d. real Fubini-Study of degree d, we have

$$c_1' d^n \leq E[N_{\mathbb{R}}] \leq c_2' d^n \quad ,$$

where $c_1', c_2' > 0$ are independent of d. In this case,

$$c_1' \left(\frac{d}{2}\right)^n \leq E[N_+] \leq c_2' \left(\frac{d}{2}\right)^n \quad .$$

Compared to our analysis in Section B.2, where we considered asymptotics in n, we can't immediately use the last formula to study how $E[N_+]$ grows as a function of n, because we don't know how the constants c_1', c_2' depend on n. Nevertheless, we still get the asymptotic behavior in d: while the number of real/positive zeros of the KSS ensemble grows as $d^{n/2}$, the number of real/positive zeros of the real Fubini-Study ensemble grows as d^n. In general, if we have a system of polynomials from an ensemble defined by (B.27), then the number grows as $d^{h \cdot n}$. This is a qualitative difference in how these numbers grow.

These results tie the growth of feasible equilibria to a single ensemble-dependent exponent. Further numerical relaxations of the KSS assumptions are collected in the Appendix.

B.11 Other random ensembles

Integral geometry exploits orthogonal invariance. There are other random polynomial ensembles, that are not orthogonally invariant, but we still know their expected value of real roots.

Most notably, Mathis [192] presents a formula for the following ensemble. Suppose the degree d can be written as $d = \delta \cdot n$. Then, consider the following (non-homogeneous) ensemble:

$$f(x) = \sum_{0 \leq a_1, \ldots, a_n \leq \delta} \sqrt{\binom{\delta}{a_1} \cdots \binom{\delta}{a_n}}\, T_a\, x_1^{a_1} \cdots x_n^{a_n},$$

where the $T_a = T_{a_1,\ldots,a_n}$ are i.i.d. standard Gaussian random variables. This ensemble is not orthogonally invariant (since it doesn't use all monomials of degree at most d), but it's invariant under reflection of the variables; which is needed for our argument that $E[N_+] =$

$\frac{1}{2^n}E[N_{\mathbb{R}}]$. Mathis proves in [192, Proposition 4.36] that if we take independent $f_1, \ldots, f_n$ with $\deg(f_i) = d_i$ from this ensemble one has

$$E[N_{\mathbb{R}}] = \frac{n!\, b_n}{(2m)^m} \sqrt{d_1 \cdots d_n},$$

where $b_n = \frac{\pi^{n/2}}{\Gamma(n/2+1)}$ is the volume of the standard Euclidean unit ball in $\mathbb{R}^n$.

B.12 Distribution of the Jacobian of a Kostlan system

Feasibility is necessary for coexistence but not sufficient; whether a feasible equilibrium is stable is decided by the spectrum of the community matrix, which at a root x of the dynamics equals $\mathrm{diag}(x)\, Jf(x)$. Since the equilibria are themselves the random roots of f, the relevant object is the Jacobian at a fixed point x. Here we show this conditioned Jacobian is again Gaussian and compute its covariance, providing the starting point for a stability analysis of feasible high-d equilibria.

Fix a point $x = (x_1, \ldots, x_n) \in \mathbb{R}^n$. Consider a system $f = (f_1, \ldots, f_n)$ of i.i.d. Kostlan polynomials. What is the distribution of

$$Jf(x) \mid \Big(f(x) = 0\Big),$$

i.e., what is the distribution of the Jacobian

$$Jf(x) = \left(\frac{\partial f_i}{\partial x_j}\right)_{1 \le i,j \le n}$$

conditioned on the event that x is a zero of f. Since this event has probability zero, we need to make sense of it: $\{f \mid f(x) = 0\}$ is a linear space in the space of polynomial systems. A Gaussian random variable restricted to a linear space is still Gaussian. We are interested in

the distribution of $Jf(x)$ with respect to the Gaussian distribution on $\{f \mid f(x) = 0\}$.

To compute this we first view x as a point

$$[x_1 : \cdots : x_n : 1] \in \mathbb{RP}^n,$$

and the f_i as homogeneous polynomials in $n+1$ variables. Let also

$$x' = \frac{(x_1, \ldots, x_n, 1)^T}{\sqrt{x_1^2 + \cdots x_n^2 + 1}}$$

be the corresponding point on the sphere. Writing

$$\tilde{J}f(x) = \left(\frac{\partial f_i}{\partial x_j}\right)_{1 \le i \le n, 1 \le j \le n+1}$$

for the projective Jacobian we have

$$Jf(x) = \tilde{J}f(x)\, P, \tag{B.28}$$

where

$$P = \begin{pmatrix} I_n \\ 0 \end{pmatrix} \in \mathbb{R}^{(n+1)\times n}$$

is the projection matrix that projects onto the first n columns.

There is an orthogonal matrix $O \in O(n+1)$ with

$$Ox' = (0, \ldots, 0, 1) =: e.$$

Write $g(x) = f(O^T x)$. Since f is Kostlan, also g ist Kostlan. We have

$$\tilde{J}g(e) = \tilde{J}f(O^T e)\, O^T = \tilde{J}f(x')\, O^T. \tag{B.29}$$

Furthermore,

$$g(x) = x_{n+1}^d\, a + x_{n+1}^d\, \sqrt{d}\, A(x_1, \ldots, x_n)^T + \cdots,$$

where the dots on the right mean lower-order terms. Since $f(x) = 0$, we have $g(e) = 0$, which is equivalent to $a = 0$. The matrix $A \in \mathbb{R}^{n \times n}$ has i.i.d. standard normal entries, because g is Kostlan. We obtain:

$$\tilde{J}g(e) = \begin{pmatrix} \sqrt{d}A & 0 \end{pmatrix} = \sqrt{d}A\, P^T.$$

By (B.29):

$$\tilde{J}f(x') = \tilde{J}g(e)\, O = \sqrt{d}A\, P^T\, O.$$

The law of linearly transforming Gaussians yields

$$Jf(x') \sim N(0, d\,\Sigma'),$$

where

$$\Sigma' = I_n \otimes (O^T P P^T O)$$

Since the entries of $\tilde{J}f(x')$ are homogeneous polynomials of degree $d-1$, setting $\lambda = \sqrt{x_1^2 + \cdots + x_n^2 + 1}$ we have

$$\tilde{J}f(x) = \tilde{J}f(\lambda\, x') = \lambda^{d-1} \tilde{J}f(x') \sim N(0, \lambda^{2(d-1)}\, d\,\Sigma').$$

Finally, by (B.28)

$$JF(x) = \tilde{J}F(x)\, P \sim N(0, \lambda^{2(d-1)}\, d\,\Sigma),$$

where

$$\begin{aligned}\Sigma &= (I_n \otimes P^T)\Sigma'(I_n \otimes P) \\ &= I_n \otimes (P^T O^T P P^T O P) \\ &= I_n \otimes (U^T U), \qquad U = P^T O P.\end{aligned}$$

Note that $\Sigma = \Sigma(x)$ depends on x, because O depends on x. We have proved the following result.

Theorem: $Jf(x) \mid (f(x) = 0)$ is a random matrix that has centered Gaussian entries with covariance matrix given by $d\,\lambda^{2(d-1)}\,\Sigma(x)$.

B.13 Supporting numerical experiments

This appendix collects supporting numerical experiments that probe how robust the feasibility results are to relaxing the KSS assumptions, one that asks whether the feasible equilibria they produce are dynamically stable, and one that enumerates every real root of the sampled systems to test the two statements on which Eq. B.18 rests: that the signs of the components of a root show no bias in any direction, and that the signs of distinct roots are independent. Throughout we call the one-sided ensemble *sign-restricted*: each coefficient is folded onto a half-line, $a \sim \pm|\mathcal{N}(0, \sigma^2)|$, which preserves the second moment and breaks the reflection symmetry that the symmetry argument of the Methods uses. We avoid *truncated*, which in the random-polynomial literature denotes conditioning on the norm of the coefficient vector – a rotationally invariant operation, and one that leaves the root counts unchanged.

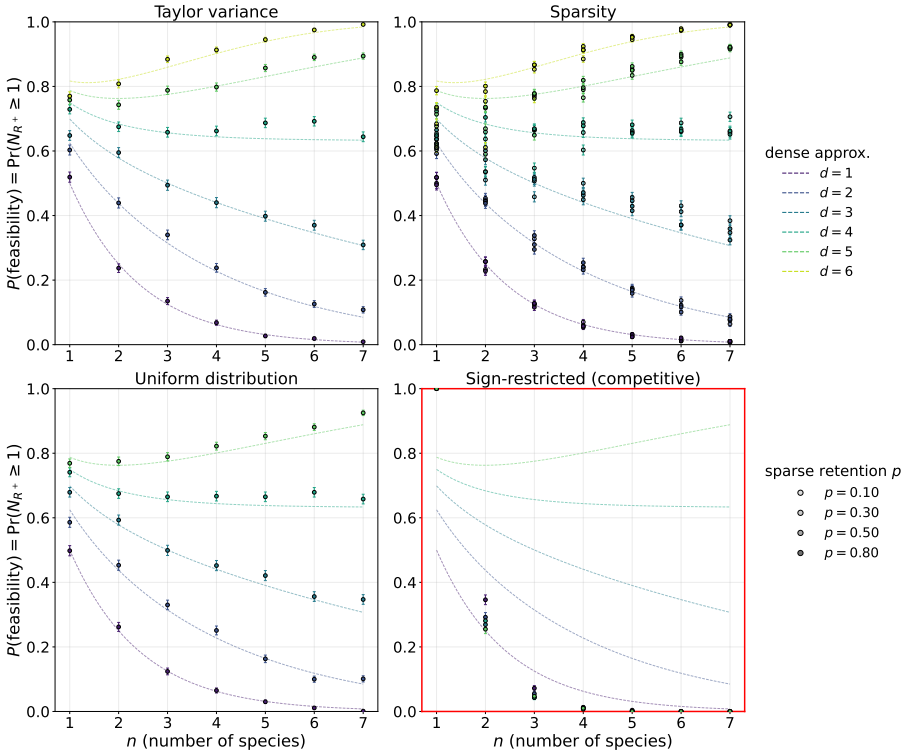

Figure B.7: **Probability of feasibility $P_f = \Pr(N_+ \geq 1)$ as a function of population number n for the four relaxations of the KSS ensemble: Taylor variance schedule (top-left), per-coefficient Bernoulli sparsity (top-right), Uniform coefficient distribution (bottom-left), and sign-restricted draws (bottom-right, framed in red).** In each panel, color encodes the polynomial degree $d \in \{1, \ldots, 6\}$ and dashed lines overlay the KSS dense independent-root approximation $P_f \approx 1 - (1 - 2^{-n})^{d^n/2}$. The Taylor and Uniform panels track the KSS curve closely, confirming that swapping the variance schedule or the coefficient family (at fixed second moment) preserves the KSS feasibility scaling. The sparse panel encodes retention probability $p \in \{0.10, 0.30, 0.50, 0.80\}$ via marker opacity; deviations from the dense reference grow as p decreases. The sign-restricted panel is framed in red because sign restriction breaks the KSS pattern: feasibility collapses to near zero for all but the smallest (n, d). Markers are Monte Carlo estimates over $K = 1000$ trials per cell (error bars: ± 1 SE).

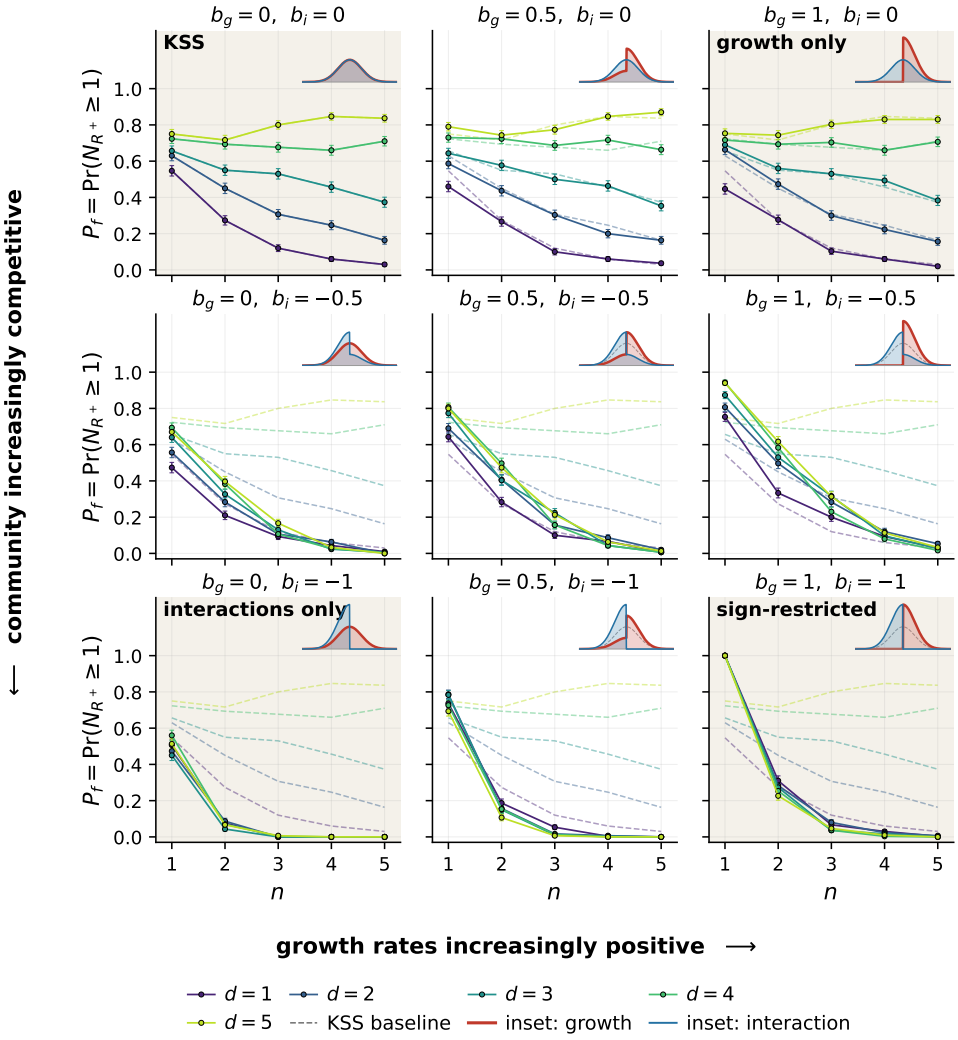

Figure B.8: **Probability of feasibility P_f as a function of population number n across the 3×3 grid of sign restrictions.** Each coefficient is folded onto one half-line with probability $|b|$: the growth-rate bias increases from left to right ($b_g = 0, 1/2, 1$) and the interactions become increasingly competitive from top to bottom ($b_i = 0, -1/2, -1$), so the top-left panel is the KSS ensemble and the bottom-right one the sign-restricted (purely competitive) ensemble of Fig. 2.2**b**. The fold preserves the second moment of every coefficient, so the panels differ in sign structure alone. Insets show the resulting distribution of growth rates (red) and interactions (blue) against the symmetric case (grey dashed), on a scale shared across the grid. Color encodes the polynomial degree $d \in \{1, \ldots, 5\}$, and dashed curves repeat the KSS panel in every cell for comparison. P_f is unchanged along a row but collapses down a column: restricting the growth rates leaves the transition intact, whereas restricting the interactions removes it, already at $b_i = -1/2$. Markers are Monte Carlo estimates over $K = 300$ trials per cell (error bars: ± 1 SE).

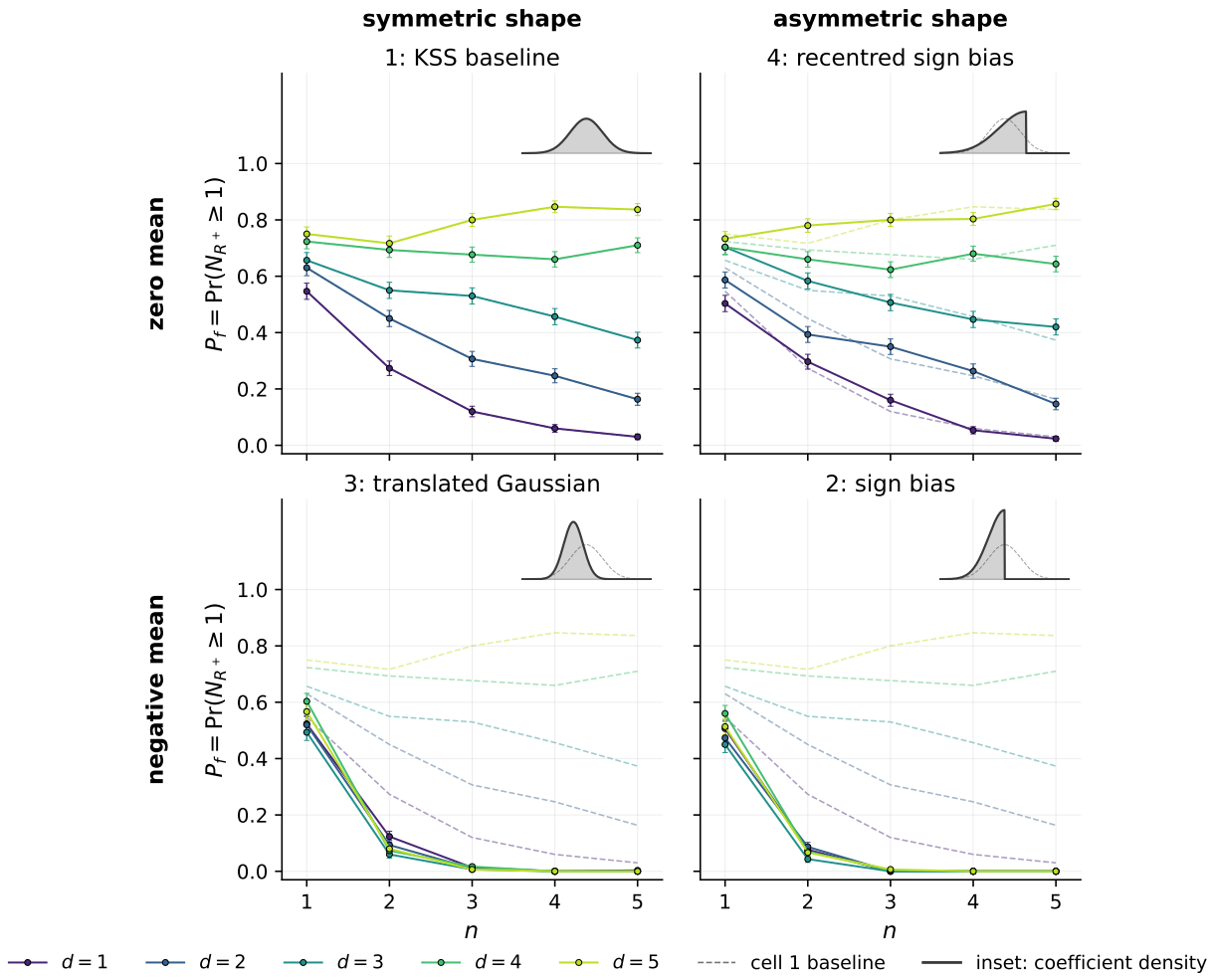

Figure B.9: **Probability of feasibility P_f as a function of population number n for the four coefficient distributions that separate a nonzero mean from a skew.** Rows fix the mean of the interaction coefficients (zero above, negative below) and columns their shape (symmetric on the left, folded onto one sign on the right): cell 1 is the KSS ensemble, cell 2 the fully competitive fold ($b_i = -1$) of Fig. B.8, cell 3 a symmetric Gaussian translated to carry the mean that the fold induces, and cell 4 that same fold recentred at zero and rescaled back to the common variance. All four hold $\mathbb{E}[a^2] = \sigma^2$, so the panels differ in the mean and the shape alone. Insets show the resulting distribution of the interaction coefficients against the symmetric case (grey dashed), on a scale shared across the grid. Color encodes the polynomial degree $d \in \{1, \ldots, 5\}$, and dashed curves repeat cell 1 in every panel for comparison. P_f follows the rows and not the columns: skewing the distribution while holding its mean at zero leaves the transition intact, whereas a nonzero mean removes it whether or not the distribution is skewed. Markers are Monte Carlo estimates over $K = 300$ trials per cell (error bars: ± 1 SE).

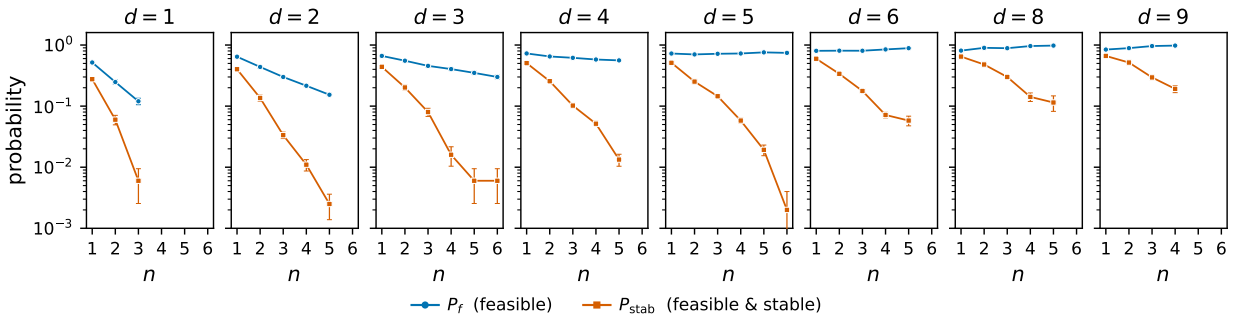

Figure B.10: **Feasibility is not the binding constraint above the transition.** Probability of feasibility $P_f = \Pr(N_+ \geq 1)$ (blue circles) and probability of *stable* feasibility P_{stab}, that at least one feasible equilibrium has every eigenvalue of the community matrix $M = \text{diag}(x^*)\, J(x^*)$ in the left half-plane (orange squares), as a function of population number n; one panel per polynomial degree d. Both are measured on the same communities, so the vertical gap between the curves is the fraction of feasible communities in which every feasible equilibrium is unstable. Every feasible equilibrium of every community is enumerated, and M is evaluated from the symbolic Jacobian. P_f stops decaying with n and turns up for $d > 4$, whereas P_{stab} falls with n at every d: the constraint on coexistence moves from feasibility to stability. Downward triangles are rule-of-three upper bounds $3/K$ for cells in which no stable feasible equilibrium was observed. Note the logarithmic vertical axis. Markers are Monte Carlo estimates over $K = 96$–2500 trials per cell (error bars: ± 1 SE).

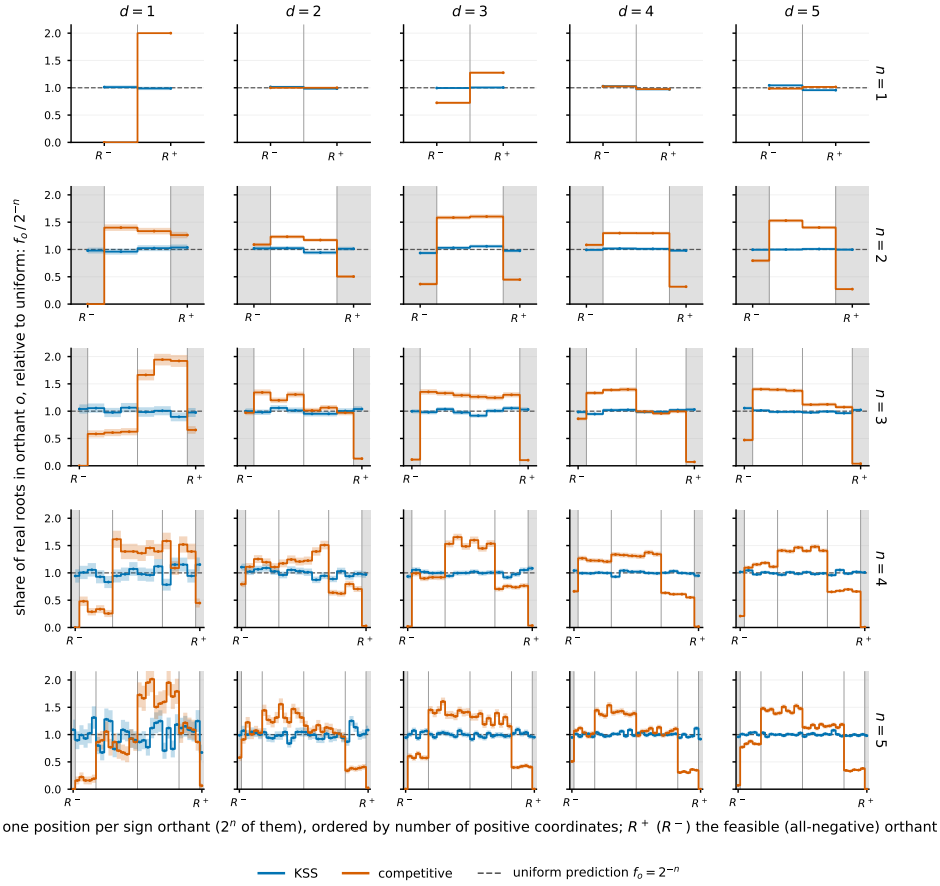

Figure B.11: **The signs of the components of a root show no bias in any direction, and sign restriction removes that property.** Share f_o of the real roots falling in sign orthant o, relative to the uniform value 2^{-n}, for the KSS ensemble (blue) and for a competitive ensemble that folds the growth rates onto the positive half-line and the interactions onto the negative one at the same variance schedule (orange); one panel per (n, d), every real root of every sampled system enumerated. The 2^n orthants run along the horizontal axis ordered by their number of positive coordinates $k = 0, \ldots, n$, the all-negative orthant $\mathbb{R}^-$ at the left and the all-positive, feasible orthant $\mathbb{R}^+$ at the right, both shaded, since sign restriction depletes the two extremes rather than a scattered set of orthants. Under KSS the histogram is flat, f_o departing from 2^{-n} by at most 0.022 anywhere on the grid, and the measured expectations reproduce Eq. B.10 and Eq. B.12 to within 3% and 9% for $d \geq 2$. Under sign restriction it is not: at $n = 5$ the share reaching $\mathbb{R}^+$ falls to 10^{-4} or below against a uniform $1/32$. Bands are ± 1 bootstrap SE over $K = 1000$ trials per cell.

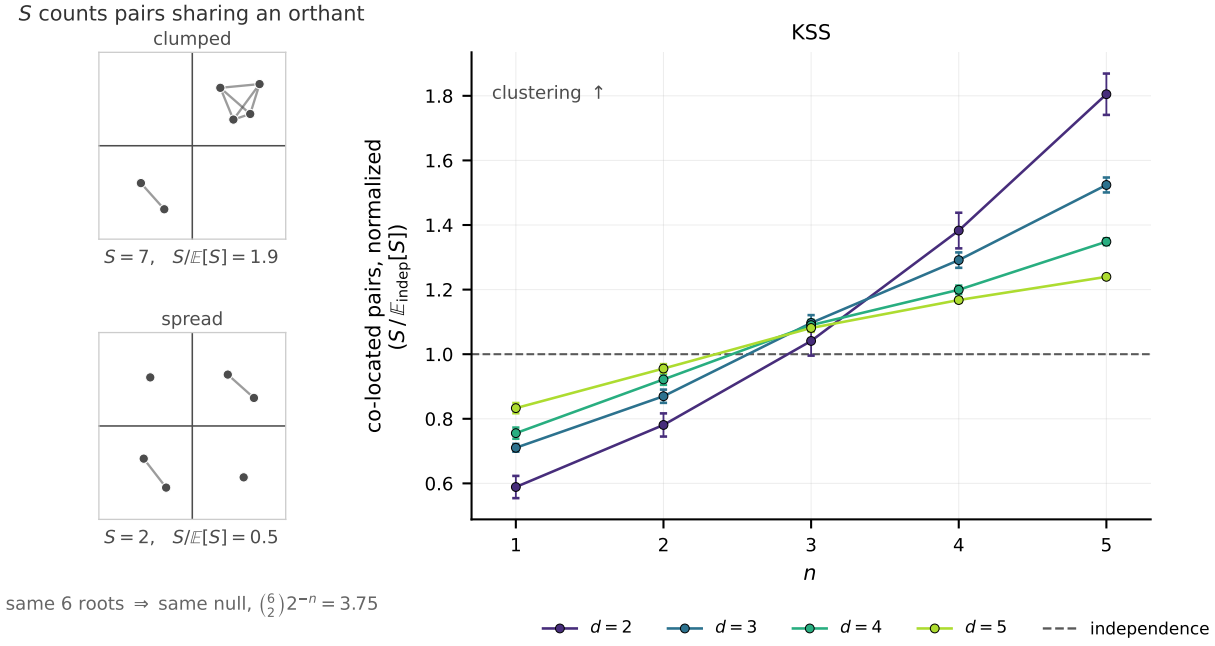

Figure B.12: **The signs of distinct roots are not independent, and the departure grows with population number.** Number of pairs of real roots sharing an orthant, $S = \sum_o \binom{N_o}{2}$, measured per trial and divided by the value $\binom{N}{2}2^{-n}$ it would take if the orthant of each root were drawn independently; the ratio is formed from sums over trials, never from a mean of per-trial ratios. KSS ensemble only, the independence step being what Eq. B.18 assumes and the sign-restricted ensemble already failing the uniformity it rests on (Fig. B.11). Color encodes the polynomial degree d; $d = 1$ is omitted, a linear system having exactly one real root per trial, which leaves S undefined. The left column is a schematic rather than data: the same six roots dealt into the four orthants of $n = 2$ two ways, clumped above and spread below, with one chord per co-located pair. Both arrangements share the same number of roots and therefore the same reference value, which is the point, since S measures the arrangement and not the count. Roots repel at $n = 1, 2$ (S between 0.59 and 0.96) and cluster from $n = 3$ (S between 1.04 and 1.80), so independence holds only where the two regimes cross between $n = 2$ and $n = 3$, and the error it introduces grows with n and shrinks with d. Error bars are ± 1 bootstrap SE over $K = 1000$ trials per cell.

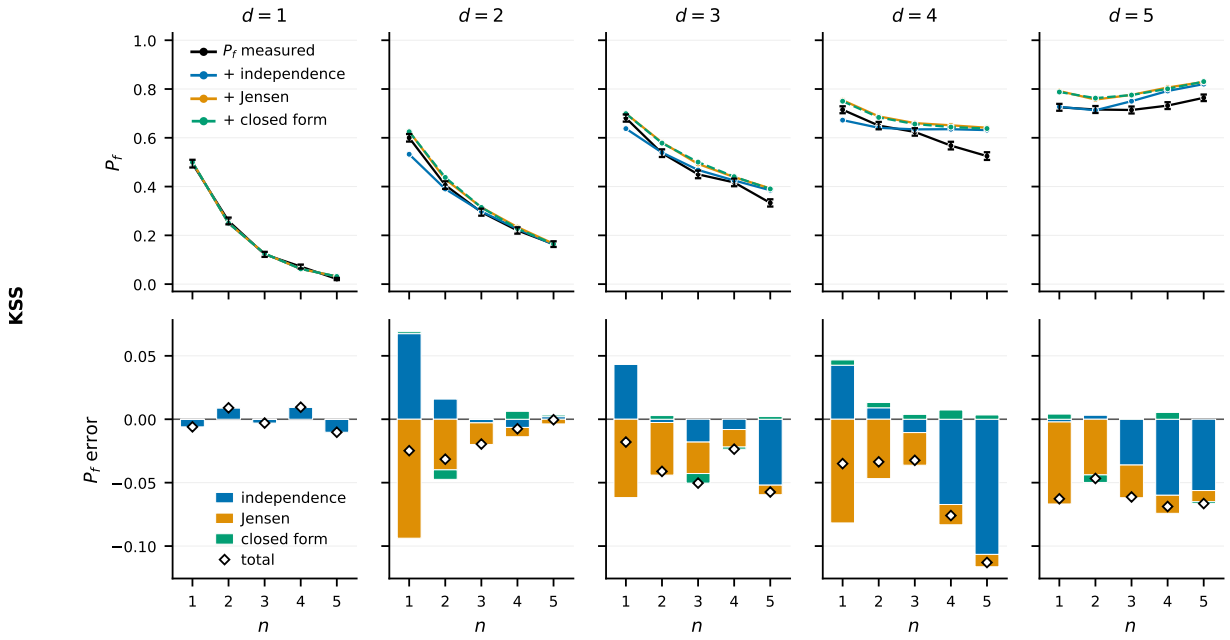

Figure B.13: **The closed form for P_f separates into three errors that partly cancel.** Top row: four estimates of the probability of feasibility, all computed from the same trials, as a function of population number n, one panel per polynomial degree d. The first is the fraction of trials carrying at least one feasible equilibrium; the second replaces it by Eq. B.18 evaluated on the empirical law of the real-root count, so the gap to it is the cost of assuming independence; the third moves the expectation inside, as in Eq. B.19, so the gap is the Jensen term, negative because $(1 - 2^{-n})^t$ is convex in t; the fourth substitutes the closed form of Eq. B.10, so the gap is the residual of that identity. Bottom row: the same three gaps as signed stacked bars, colored to match the level each descends to, with their total as a diamond. The independence and Jensen terms carry the discrepancy and have opposite signs over most of the grid, so they partly cancel, whereas the closed-form residual stays within ± 0.008, which doubles as a check on Eq. B.10. The three sum to the measured P_f minus its closed form, at most 0.113 in absolute value for $d \geq 2$. Error bars are ± 1 SE over $K = 1000$ trials per cell.

APPENDIX C

SUPPLEMENTARY INFORMATION: TIPPING POINTS ARE TYPICAL IN ECOSYSTEMS WITH HIGHER-ORDER INTERACTIONS

C.1 Model

We consider generalized Lotka–Volterra (GLV) dynamics with higher-order interactions (HOIs):

$$\dot{x}_i = x_i \left[r_i + (1-\alpha) \sum_{j=1}^{n} A_{ij}\, x_j + \alpha \sum_{j,k=1}^{n} B_{ijk}\, x_j x_k \right], \quad i = 1, \ldots, n, \tag{C.1}$$

where x_i is the abundance of species i, r_i its intrinsic growth rate, A_{ij} the pairwise interaction coefficient, and B_{ijk} the three-way higher-order interaction coefficient. The parameter $\alpha \in [0, 1]$ controls the relative weight of higher-order versus pairwise terms, recovering the classical GLV model when $\alpha = 0$.

We decompose the growth-rate vector as

$$\mathbf{r} = \mathbf{r}^0 + \delta\, \mathbf{u}, \tag{C.2}$$

where $\mathbf{r}^0$ is a baseline growth-rate vector that supports a feasible, locally stable coexistence equilibrium, $\mathbf{u}$ is a unit vector specifying the direction of environmental change, and $\delta \geq 0$ its magnitude. By varying $\mathbf{r}$ along fixed directions $\mathbf{u}$, we probe the robustness of coexistence to environmental forcing.

C.1.1 Feasibility and equilibrium tracking

A coexistence equilibrium $\mathbf{x}^\star \in \mathbb{R}^n_{>0}$ satisfies, for each species,

$$r_i + (1-\alpha)\sum_j A_{ij}\, x_j^\star + \alpha \sum_{j,k} B_{ijk}\, x_j^\star x_k^\star = 0. \tag{C.3}$$

For $\alpha > 0$ this is a system of n coupled quadratic equations in $\mathbf{x}^\star$, and the inverse problem—determining the set of growth-rate vectors $\mathbf{r}$ for which a positive solution exists—is not analytically tractable in general. We therefore assume a known feasible equilibrium at the baseline $\mathbf{r}^0$ and track the solution branch numerically as δ varies. This assumption is also computationally enabling: systems of quadratic polynomials have in general 2^n solutions, so tracking all of them simultaneously would be computationally intractable for the larger communities we study in the main text.

Concretely, when we perturb the growth rate as $\mathbf{r}^0 + \delta\,\mathbf{u}$ (see Eq. (3.2)), Eq. (C.3) becomes

$$H_i(\mathbf{x}, \delta) \;=\; (r_i + \delta\, u_i) + (1-\alpha)\sum_j A_{ij}\, x_j + \alpha \sum_{j,k} B_{ijk}\, x_j x_k \;=\; 0, \tag{C.4}$$

with $H = (H_1, \ldots, H_n)$. Wherever the Jacobian $\frac{\mathrm{d}H}{\mathrm{d}\mathbf{x}}$ is invertible, the implicit function theorem guarantees that $\mathbf{x}^\star(\delta)$ is locally a differentiable function of δ. Implicit differentiation yields the ODE

$$\frac{\mathrm{d}H}{\mathrm{d}\mathbf{x}}\,\dot{\mathbf{x}} \;+\; \frac{\mathrm{d}H}{\mathrm{d}\delta} \;=\; 0. \tag{C.5}$$

Together with the initial condition $\mathbf{x}^\star = \mathbf{1}$ at $\delta = 0$, this defines an initial-value problem that we solve using the polynomial homotopy continuation software `HomotopyContinuation.jl` [11, 125].

C.1.2 Local stability

The local stability of a coexistence equilibrium $\mathbf{x}^\star$ is determined by the Jacobian

$$J_{ij}(\mathbf{x}^\star) = x_i^\star \left[(1-\alpha)\, A_{ij} + \alpha \sum_{k=1}^{n} \Big(B_{ijk} + B_{ikj} \Big)\, x_k^\star \right] + \underbrace{\delta_{ij}\, f_i(\mathbf{x}^\star)}_{=0}, \tag{C.6}$$

where $f_i(\mathbf{x}^\star)$ is the per-capita growth rate of species i (the bracketed term in Eq. C.1), which vanishes at equilibrium, and δ_{ij} is the Kronecker delta. The equilibrium is locally stable when all eigenvalues of J have negative real part. Crucially, J depends on $\mathbf{x}^\star$, which itself depends on $\mathbf{r}$ through Eq. (C.3), establishing the chain of dependence $J\Big(\mathbf{x}^\star(\mathbf{r})\Big)$. Changes in environmental conditions therefore alter stability, through both changes in abundances, and the state-dependent higher-order terms in the Jacobian.

Equation (C.6) shows that the community Jacobian factors as

$$J = D(\mathbf{x}^\star)\, J_F, \tag{C.7}$$

where $D(\mathbf{x}^\star) = \mathrm{diag}(x_1^\star, \ldots, x_n^\star)$ and

$$(J_F)_{ij} \;=\; (1-\alpha)\, A_{ij} \;+\; \alpha \sum_{k=1}^{n} \Big(B_{ijk} + B_{ikj} \Big)\, x_k^\star \tag{C.8}$$

is the Jacobian of the per-capita growth rates. Because the determinant of a product is the product of the determinants,

$$\det J \;=\; \det D(\mathbf{x}^\star)\;\det J_F \;=\; \left(\prod_{i=1}^{n} x_i^\star \right) \det J_F. \tag{C.9}$$

This factorization reveals that $\det J$ can vanish via two distinct mechanisms:

1. **Transcritical bifurcation.** One (or more) equilibrium abundances $x_i^\star \to 0$, so

$\prod_i x_i^\star = 0$. A species is smoothly driven to extinction.

2. **Fold (saddle–node) bifurcation.** All abundances remain positive, but $\det J_F = 0$. The per-capita Jacobian J_F becomes singular while every species is still present.

Note that J_F coincides with the Jacobian $\frac{\mathrm{d}H}{\mathrm{d}\mathbf{x}}$ of the homotopy system (C.4). At a fold, therefore, the implicit function theorem fails: $\frac{\mathrm{d}H}{\mathrm{d}\mathbf{x}}$ is no longer invertible, so the equilibrium branch $\mathbf{x}^\star(\delta)$ ceases to be a smooth, real-valued function of δ. The continuation path cannot be extended further as a real solution, and the equilibrium disappears abruptly. The next section describes how we detect and distinguish these two boundary types in practice.

C.2 Boundary detection with homotopy continuation

For each perturbation direction $\mathbf{u}$, we track the coexistence equilibrium from $\delta = 0$ to a pre-set upper limit $\delta_{\max} = 10^3$ using coefficient-parameter homotopy continuation (see Algorithm C.3). The tracker advances a homotopy parameter $t \in [1, 0]$, where $t = 1$ corresponds to $\delta = 0$ and $t = 0$ to $\delta = \delta_{\max}$, smoothly deforming the model parameters along the ray $\mathbf{r}_0 + \delta\,\mathbf{u}$ and carrying the equilibrium branch $\mathbf{x}(t)$ along with it (see Fig. C.1). At each continuation step we monitor the tracked solution for three types of boundary events: *gradual boundary*, where a species abundance x_i crosses zero; *stability loss*, where the real part of the leading eigenvalue $\lambda_{\max}$ of the Jacobian crosses zero (indicating a Hopf bifurcation); and *abrupt boundaries*, detected when the tracker itself fails to converge, indicating that the equilibrium branch has ceased to exist via a saddle-node bifurcation (see Fig. C.1). When a feasibility or stability event is detected between two consecutive continuation steps, a bisection procedure refines the critical parameter value to within tolerance (red band in Fig. C.1). The three boundary types (and the no-boundary case) are defined precisely as follows.

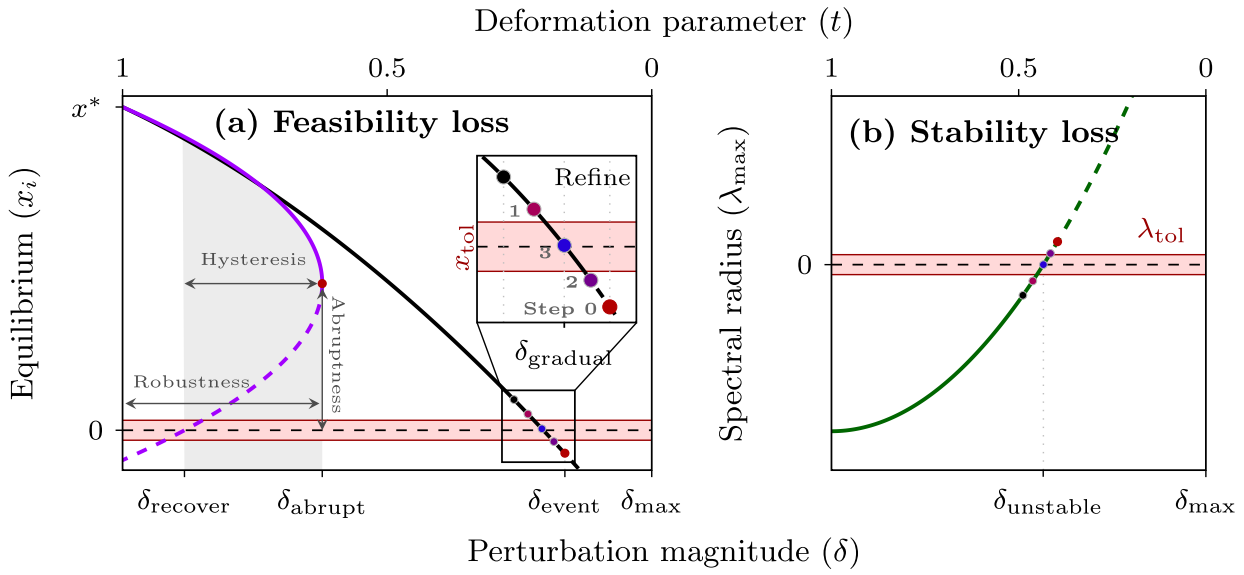

Figure C.1: **Schematic of the three boundary types detected by the homotopy continuation algorithm.** Quantities are shown as a function of perturbation magnitude δ (bottom x-axis, equivalently, deformation parameter $t = 1 - \delta/\delta_{\text{max}}$, top x-axis). (a) Feasibility loss. Two mechanisms are shown: a gradual boundary (black), where a species equilibrium x_i smoothly declines and crosses the feasibility threshold x_{tol} at δ_{gradual}; and an abrupt boundary (violet), where a saddle-node bifurcation annihilates the stable equilibrium at δ_{abrupt}, causing a discontinuous drop in abundance. The vertical distance from the fold point to zero quantifies the abruptness of the transition. The shaded region between δ_{recover} and δ_{abrupt} marks the hysteresis zone, where the system cannot recover by simply reversing the perturbation. The distance from 0 to δ_{abrupt} is a measure of ecosystem robustness. These three quantities are plotted in the Fig. 3.3. (b) Stability loss. The leading eigenvalue λ_{max} increases with δ and crosses the stability threshold $-\lambda_{\text{tol}}$ at δ_{unstable}, signalling loss of dynamical stability before any species becomes infeasible (Hopf bifurcation).

1. **Gradual boundary** (`transcritical`): The minimum component of the real part of the tracked equilibrium drops below $x_{tol} = 10^{-9}$. This signals that at least one species has been driven to zero abundance, corresponding to a transcritical bifurcation.

2. **Unstable boundary** (`hopf`): The equilibrium remains feasible but loses local stability. Stability is monitored by computing the maximum real part λ_{max} of the eigenvalues of the community Jacobian $J = D(\mathbf{x}^\star)J_F$, where $D(\mathbf{x})$ is a diagonal matrix with the vector $\mathbf{x}$ in the diagonal, and J_F is the Jacobian of the per-capita growth rates

(Eq. C.8). The equilibrium is declared unstable when $\lambda_{\max} > 10^{-9}$.

3. **Abrupt boundary** (`fold`): The tracker fails because the Jacobian J_F of the per-capita growth rates (Eq. C.8) becomes singular as the fold is approached: at a fold bifurcation, two real solution branches (one stable, one unstable) collide and annihilate, so the matrix $\frac{\mathrm{d}H}{\mathrm{d}\mathbf{x}}$ in Eq. C.5 ceases to be invertible. Since the implicit function theorem requires invertibility of this Jacobian to guarantee that $\mathbf{x}(\delta)$ remains a smooth, real-valued function of δ, the theorem's hypotheses fail at the fold. Consequently, the continuation path cannot be extended further as a real solution branch.

4. **No boundary** (`success`): The equilibrium remains feasible and stable up to $\delta_{\max}$.

When a gradual or unstable boundary event is detected between consecutive homotopy-continuation steps at path parameters t_{prev} (last safe state, black marker in Fig. C.1(a), inset) and t_{cur} (first event state, red, Step 0, marker in the inset), the event location is refined by re-tracking on progressively smaller t-intervals; a bisection algorithm that finds solution via homotopy continuation.

Concretely, the tracker is re-initialised at the state $(\mathbf{x}_{\text{cur}}, t_{\text{cur}})$ with the goal of stepping back toward t_{prev}. The adaptive step-size control is tightened: the maximum step size is set to $\Delta t/2$ where $\Delta t = |t_{\text{prev}} - t_{\text{cur}}|$, and the maximum number of steps is set to $\lceil 1/\Delta t \rceil$.

At each refinement step, the tracker advances and the relevant event indicator is re-evaluated:

- **Negative event** (`find_zero`): the indicator is the abundance x_i of the species that crossed zero. If $|x_i| \leq x_{tol}$, the current t is accepted. If x_i overshoots (changes sign relative to the initial direction), the function recurses on the sub-interval $[t'_{\text{prev}}, t'_{\text{cur}}]$ bracketed by the last two tracker states.

- **Unstable event** (`find_stability`): the indicator is $\lambda_{\max}$. If $|\lambda_{\max}| \leq \lambda_{\text{tol}}$, t is accepted. If $\lambda_{\max}$ crosses back below the threshold, the function recurses on the new sub-interval.

Because a transcritical bifurcation simultaneously drives $x_i \to 0$ and generically pushes $\lambda_{\max}$ through zero (the zero-abundance eigenvector enters the community matrix), the two events can coincide along a perturbation ray. Concretely, if at homotopy parameter t^* both $x_i(t^*) \leq x_{tol}$ and $\lambda_{\max}(t^*) \geq \lambda_{\text{tol}}$, the event is classified as `negative` (feasibility loss via transcritical bifurcation), not `unstable`.

Refinement terminates when either (i) the indicator is within tolerance, (ii) the tracker step size Δt collapses to zero, or (iii) the tracker can no longer reduce the interval (recursive base case). The final homotopy parameter t_{end} determines the critical perturbation via $\Delta\mathbf{r}_c = (1-, t_{\text{end}})\,\mathbf{p}_{\text{target}}$ and $\delta_c = \|\Delta\mathbf{r}_c\|$.

C.2.1 Post-boundary dynamics and reversibility

Once a boundary has been localised along a perturbation ray, two further routines—whose pseudocode is given in Appendix C.11—characterise what lies beyond it. The first, PostBoundaryDynamics (Algorithm C.4), asks where the system actually settles after the collapse. We push the perturbation slightly past the critical value, integrate the GLV+HOI ODE forward, and remove species whose abundance falls below an extinction threshold. Integration is stopped once every surviving species has settled.

The second routine, BacktrackPerturbation (Algorithm C.5, also in Appendix C.11), tests whether reducing the driver returns the community to its original coexistence state, or whether the collapse leaves a persistent imprint. We restrict the dynamics to the surviving species and continue this collapsed equilibrium back toward the pristine state, monitorig feasibility, loss of stability, and invasibility of the absent species.

Once a candidate recovery point is found, to determine what the community does we step a small distance past that point, reseed the state by combining the pre-boundary equilibrium on the surviving species with a small invasion amplitude on each extinct species, and integrate the full n-dimensional ODE under an extinction callback. The endpoint is classified into three cases. First, every species—including the previously extinct ones—is alive at the end, and the trajectory has reattached to an n-species coexistence branch; this constitutes recovery. Any other outcome does not. For instance, if (1) the reseeded invaders all die out again and the system relaxes back onto the same collapsed attractor; or (2) if the trajectory settles on a different surviving subset.

C.3 Computing the feasibility boundaries analytically for $n = 2$

We discuss how to compute the gradual and abrupt boundaries analytically. For this we substitute in (C.3) $A'_{ij} = (1-\alpha)A_{ij}$ and $B'_{jki} = \alpha B_{jki}$, and obtain polynomials

$$f_i(\mathbf{x}, \mathbf{r}, \mathbf{A'}, \mathbf{B'}) = r_i + \sum_{j=1}^{n} A'_{ij} x_j \; + \; \sum_{j,k=1}^{n} B'_{jki}\, x_j x_k.$$

The gradual boundary consist of those parameters $\mathbf{r}, \mathbf{A'}, \mathbf{B'}$, such that there exists an $\mathbf{x}^\star$ with

$$\begin{aligned} &x_1^\star \cdot x_2^\star \cdots x_n^\star = 0 \quad \text{and} \\ &f_1(\mathbf{x}^\star, \mathbf{r}, \mathbf{A'}, \mathbf{B'}) = \cdots = f_n(\mathbf{x}^\star, \mathbf{r}, \mathbf{A'}, \mathbf{B'}) = 0 \end{aligned}$$

The first condition means that at least one entry of $\mathbf{x}^\star$ is zero, while the second line implies that $\mathbf{x}^\star$ is a solution of (C.3). These polynomials generate a *polynomial ideal* [25]

$$I_{\text{gradual}} = \langle x_1 \cdot x_2 \cdots x_n, f_1, \cdots, f_n \rangle.$$

Using the theory of elimination (see [25, Chapter 3]), we can eliminate $\mathbf{x}$ from this ideal. Then, we substitute back $A'_{ij} = (1-\alpha)A_{ij}$ and $B'_{jki} = \alpha B_{jki}$, and obtain an ideal J_{gradual} generated by polynomials in $\mathbf{r}, \alpha, \mathbf{A}, \mathbf{B}$, that define the Zariski-closure of the gradual boundary. Elimination can be done on a computer, for instance, using the computer algebra system `Macaulay2` [158]. We find that the gradual boundary is the zero set of a single polynomial; i.e., J_{gradual} is a principal ideal generated by

$$\Delta_{\text{gradual}} = \alpha^2 \cdot P \cdot Q,$$

where

$$\begin{aligned}
Q &= r_1^2\alpha B_{222}^2 - 2r_1r_2\alpha B_{122}B_{222} - r_1\alpha^2 A_{12}A_{22}B_{222} \\
&\quad + r_1\alpha^2 A_{22}^2 B_{122} + 2r_1\alpha A_{12}A_{22}B_{222} - 2r_1\alpha A_{22}^2 B_{122} \\
&\quad - r_1 A_{12}A_{22}B_{222} + r_1 A_{22}^2 B_{122} + r_2^2\alpha B_{122}^2 + r_2\alpha^2 A_{12}^2 B_{222} \\
&\quad - r_2\alpha^2 A_{12}A_{22}B_{122} - 2r_2\alpha A_{12}^2 B_{222} + 2r_2\alpha A_{12}A_{22}B_{122} \\
&\quad + r_2 A_{12}^2 B_{222} - r_2 A_{12}A_{22}B_{122}; \\
P &= r_1^2\alpha B_{211}^2 - 2r_1r_2\alpha B_{111}B_{211} - r_1\alpha^2 A_{11}A_{21}B_{211} \\
&\quad + r_1\alpha^2 A_{21}^2 B_{111} + 2r_1\alpha A_{11}A_{21}B_{211} - 2r_1\alpha A_{21}^2 B_{111} \\
&\quad - r_1 A_{11}A_{21}B_{211} + r_1 A_{21}^2 B_{111} + r_2^2\alpha B_{111}^2 + r_2\alpha^2 A_{11}^2 B_{211} \\
&\quad - r_2\alpha^2 A_{11}A_{21}B_{111} - 2r_2\alpha A_{11}^2 B_{211} + 2r_2\alpha A_{11}A_{21}B_{111} \\
&\quad + r_2 A_{11}^2 B_{211} - r_2 A_{11}A_{21}B_{111}.
\end{aligned}$$

Similarly, for the abrupt boundary we can eliminate $\mathbf{x}$ from the ideal

$$I_{\text{abrupt}} = \langle \det J_F, f_1, \cdots, f_n \rangle,$$

where J_F denotes the Jacobian matrix of the per-capita growth rates (see Eq. C.8).

The eliminant is called a *tact invariant* in algebraic geometry. It defines the locus of pairs of quadrics in the plane that meet tangentially [142]. Eventually, we obtain the ideal I_{abrupt} generated by polynomials in $\mathbf{r}, \alpha, \mathbf{A}, \mathbf{B}$, that define the Zariski-closure of the abrupt boundary. Again, J_{abrupt} is generated by the polynomial

$$
\begin{aligned}
\Delta_{\text{abrupt}} = \alpha^4 \cdot (&256 r_1^4 \alpha^4 B_{111}^2 B_{211}^2 B_{222}^4 \\
&- 128 r_1^4 \alpha^4 B_{111}^2 B_{211} B_{212}^2 B_{222}^3 \\
&+ 16 r_1^4 \alpha^4 B_{111}^2 B_{212}^4 B_{222}^2 \\
&- 256 r_1^4 \alpha^4 B_{111} B_{112} B_{211}^2 B_{212} B_{222}^3 \\
&+ 128 r_1^4 \alpha^4 B_{111} B_{112} B_{211} B_{212}^3 B_{222}^2 \\
&- 16 r_1^4 \alpha^4 B_{111} B_{112} B_{212}^5 B_{222} - \cdots \\
&\quad \cdots \\
&- 8 A_{12}^2 A_{21}^4 A_{22}^2 B_{111}^2 B_{122}^2 - 2 A_{12}^2 A_{21}^4 A_{22}^2 B_{111} B_{112}^2 B_{122} \\
&+ A_{12}^2 A_{21}^4 A_{22}^2 B_{112}^4 + 8 A_{12}^2 A_{21}^3 A_{22}^3 B_{111}^2 B_{112} B_{122} \\
&- 2 A_{12}^2 A_{21}^3 A_{22}^3 B_{111} B_{112}^3 - 4 A_{12}^2 A_{21}^2 A_{22}^4 B_{111}^3 B_{122} \\
&+ A_{12}^2 A_{21}^2 A_{22}^4 B_{111}^2 B_{112}^2).
\end{aligned}
$$

This polynomial has 17.586 terms, which underscores the complexity of elimination. For bigger n computing elimination ideals quickly becomes infeasible. Recently, methods from numerical algebraic geometry have emerged to tackle elimination ideals [159] which are infeasible to compute using exact computer algebra.

C.4 Parameter sampling protocol: construction, scaling, and constraints

Our simulations pursue two goals that pull in opposite directions. On one hand, we want communities drawn from a broad random ensemble so that results reflect the generic, typical behavior of ecosystems with higher-order interactions rather than the idiosyncrasies of any particular parameter choice. On the other hand, we want a controlled design in which the quantity of interest – HOI strength α – is the an unconfounded variable, so that differences in boundary composition can be attributed causally to nonlinearity. We reconcile these goals by imposing structure only where causal attribution demands it, and leaving everything else to random variation.

Concretely, we draw interaction coefficients independently from broad distributions, ensuring ensemble diversity, but we then apply two targeted constraints: (i) a planted equilibrium, so that all communities share the same baseline coexistence state $\mathbf{x}^\star = \mathbf{1}$ at $\mathbf{r}^0 = \mathbf{1}$ regardless of α, μ_A, and μ_B; and (ii) a spectral normalisation that guarantees local stability at the baseline for all α. We describe these steps in turn.

Off-diagonal entries are drawn independently:

$$\tilde{A}_{ij} \sim \mathcal{N}(\mu_A,\ \tfrac{1}{n}), \qquad \tilde{B}_{ijk} \sim \mathcal{N}(\mu_B,\ \tfrac{1}{n^2}), \tag{C.10}$$

where μ_A and μ_B control the mean of pairwise and higher-order interactions, respectively. In our sign convention, $\mu_A > 0$ and $\mu_B > 0$ correspond to net facilitation, while $\mu_A < 0$ and $\mu_B < 0$ correspond to net competition. The variance scalings ensure that both the pairwise and aggregated HOI contributions to the per-capita growth rate remain $O(1)$ as community size n grows: the row sum $\sum_j A_{ij}x_j$ involves n terms each of variance $1/n$, and the slice sum $\sum_{j,k} B_{ijk}x_jx_k$ involves n^2 terms each of variance $1/n^2$. The construction below applies

uniformly for any choice of (μ_A, μ_B); the main text studies three regimes varying μ_B at $\mu_A = 0$, and here we include variable μ_A (see Fig. C.3).

Next, we aim to construct A and B from the random draws $\tilde{A}$, $\tilde{B}$ so that $\mathbf{x}^\star = \mathbf{1}$ is a locally stable equilibrium for all α. The Jacobian (C.6) evaluated at $\mathbf{x}^\star = \mathbf{1}$ takes the form

$$J(\alpha) = (1-\alpha)\, A + \alpha\, \hat{B}, \tag{C.11}$$

where $\hat{B}_{ij} = \sum_k (B_{ijk} + B_{ikj})$. Define the symmetric parts of the pairwise and aggregated HOI matrices as

$$S_A = \tfrac{1}{2}(A + A^\top), \qquad (S_B)_{ij} = \hat{B} + \hat{B}^\top = \tfrac{1}{4} \sum_k \Big(B_{ijk} + B_{ikj} + B_{jik} + B_{jki} \Big). \tag{C.12}$$

A sufficient condition for Hurwitz stability is that the symmetrised combination is negative definite: $(1-\alpha)\, S_A + \alpha\, S_B \prec 0$. Since this is a convex combination with non-negative weights, it suffices that both sectors be separately negative definite:

$$S_A \prec 0 \qquad \text{and} \qquad S_B \prec 0. \tag{C.13}$$

Step 1: zero-sum diagonals. We set the diagonal entries of $\tilde{A}$ and $\tilde{B}$ to enforce zero row and slice sums:

$$\tilde{A}_{ii} = -\sum_{j \neq i} \tilde{A}_{ij}, \qquad \tilde{B}_{iii} = -\sum_{(j,k) \neq (i,i)} \tilde{B}_{ijk}, \tag{C.14}$$

so that $\sum_j \tilde{A}_{ij} = 0$ and $\sum_{j,k} \tilde{B}_{ijk} = 0$ for every species i. Off-diagonal entries are unchanged.

Step 2: rescaling and self-regulation. The matrices $\tilde{A}$ and $\tilde{B}$ will not generally satisfy (C.13). A natural approach is to subtract a diagonal shift, giving interaction matrices $\tilde{A}_{ij} - \delta_A\, \delta_{ij}$ and $\tilde{B}_{ijk} - \delta_B\, \delta_{ijk}$ for sufficiently large $\delta_A, \delta_B > 0$. However, this changes the

row and slice sums from zero to $-\delta_A$ and $-\delta_B$ respectively, so the equilibrium condition at $\mathbf{x} = \mathbf{1}$ would not be achieved. We resolve this by observing that, for any $\delta_A > 0$,

$$\tilde{A}_{ij} - \delta_A \, \delta_{ij} \;=\; \delta_A \left(\frac{\tilde{A}_{ij}}{\delta_A} - \delta_{ij} \right). \tag{C.15}$$

Since multiplying a matrix by a positive scalar preserves the sign of every eigenvalue, the symmetric part of the matrix $\tilde{A} - \delta_A \, I$ is negative definite if and only if that of $\tilde{A}/\delta_A - I$ is. The same factorisation applies slice-wise to the HOI tensor. The final interaction matrices are therefore

$$A_{ij} = \frac{\tilde{A}_{ij}}{\delta_A} - \delta_{ij}, \qquad B_{ijk} = \frac{\tilde{B}_{ijk}}{\delta_B} - \delta_{ijk}, \tag{C.16}$$

where δ_{ij} is the Kronecker delta, $\delta_{ijk} = 1$ iff $i = j = k$, and the spectral thresholds $\delta_A, \delta_B > 0$ are determined below.

This construction simultaneously achieves the two constraints mentioned at the beginning of the section. The zero-sum properties are preserved under uniform rescaling ($\sum_j A_{ij} = 0/\delta_A - 1 = -1$ and $\sum_{j,k} B_{ijk} = 0/\delta_B - 1 = -1$), so the equilibrium condition at $\mathbf{x}^\star = \mathbf{1}$ with $r_i = 1$ reads

$$1 + (1 - \alpha)(-1) + \alpha(-1) = 0,$$

which holds identically for all $\alpha \in [0, 1]$, independent of δ_A, δ_B, μ_A, and μ_B. At the same time, the stability conditions (C.13) reduce to constraints on the spectral thresholds, which we now determine.

Choosing the spectral thresholds. The spectral thresholds δ_A and δ_B must each absorb two contributions: the bulk fluctuations of the random matrix and any mean-field spike induced by a nonzero interaction mean. We handle both sectors in parallel, decomposing each

symmetric matrix into its deterministic mean part and a centred (zero-mean) fluctuation:

$$S_A = \mathbb{E}[S_A] + \tilde{S}_A, \qquad S_B = \mathbb{E}[S_B] + \tilde{S}_B, \tag{C.17}$$

where $\tilde{S}_A$ and $\tilde{S}_B$ denote the centred parts. In Appendix C.7 we show that both mean matrices share the same centring-matrix structure:

$$\mathbb{E}[S_A] = -n\mu_A\left(I - \frac{\mathbf{1}\mathbf{1}^\top}{n}\right), \qquad \mathbb{E}[S_B] = -n^2\mu_B\left(I - \frac{\mathbf{1}\mathbf{1}^\top}{n}\right), \tag{C.18}$$

with spectra $n\mu_A$ (mult. $n-1$), 0 (eigenvector $\mathbf{1}$) and $n^2\mu_B$ (mult. $n-1$), 0 (eigenvector $\mathbf{1}$) respectively. The $O(n)$ versus $O(n^2)$ prefactors reflect the number of terms aggregated in each sector: n pairwise terms per row versus n^2 HOI terms per slice.

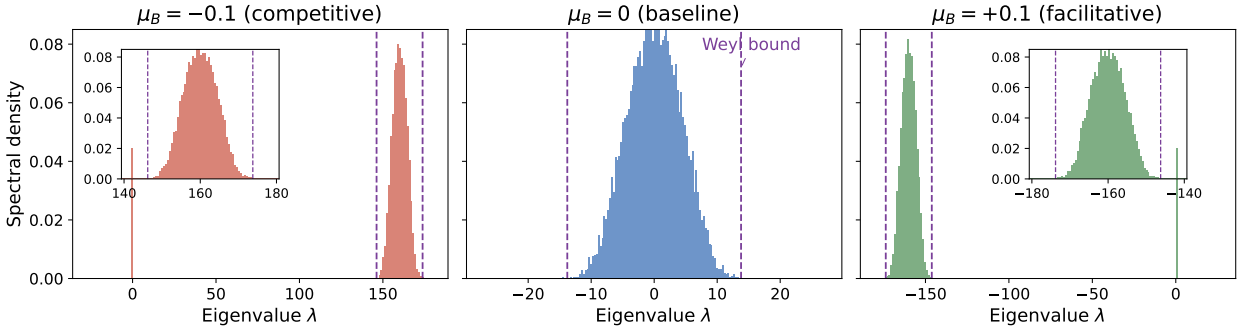

Figure C.2: **Spectral density of S_B across the three μ_B regimes.** For $n = 32$, panels show how the spectrum shifts with the mean HOI sign. In the baseline ($\mu_B = 0$), the spectrum is centred at zero. In the facilitative ($\mu_B > 0$) and competitive ($\mu_B < 0$) regimes, the mean-field eigenvalues of $\mathbb{E}[S_B]$ shift the bulk away from the origin (to the left under facilitation, to the right under competition), while the top eigenvalue (near the $\mathbf{1}$ direction) remains near the fluctuation edge. The pairwise matrix S_A exhibits analogous behaviour across μ_A regimes, with the spike scaled by $n\mu_A$ rather than $n^2\mu_B$.

Because the three regimes are structurally identical across sectors, we describe them once and apply the prescription to both δ_A and δ_B. Let S denote either S_A or S_B, let $\tilde{S}$ denote its centred part, and let $\mu \in \{\mu_A, \mu_B\}$ denote the corresponding interaction mean. From

the factorisation (C.15), stability requires $\delta > \lambda_{\max}(S)$; the regime-dependent prescription (illustrated in Figure C.2 for the HOI sector) is detailed next

Baseline ($\mu = 0$). The mean matrix vanishes: $\mathbb{E}[S] = 0$, so $\tilde{S} = S$ and the prescription above reduces to $\delta_A = \lambda_{\max}(S_A)$ and $\delta_B = \lambda_{\max}(S_B)$, which inherit an $O(\sqrt{\log n})$ scaling (Appendix C.8).

Facilitative regime ($\mu > 0$). The $(n-1)$-fold eigenvalue of $\mathbb{E}[S]$ is negative, pushing the bulk of the spectrum of S into the negative half-line, while $\lambda_{\max}(\mathbb{E}[S]) = 0$ along the $\mathbf{1}$ direction. Any threshold $\delta > \lambda_{\max}(\tilde{S})$ suffices for negative definiteness. To maintain a consistent (comparable) construction with the baseline regime, we set the threshold using the fluctuation matrix:

$$\delta_A = \lambda_{\max}(\tilde{S}_A), \qquad \delta_B = \lambda_{\max}(\tilde{S}_B),$$

with the same $O(\sqrt{\log n})$ asymptotics.

Competitive regime ($\mu < 0$). The $(n-1)$-fold eigenvalue of $\mathbb{E}[S]$ flips positive, producing a spectral spike that dominates the top eigenvalue of the full matrix: $\lambda_{\max}(S_A) \sim n|\mu_A|$ and $\lambda_{\max}(S_B) \sim n^2|\mu_B|$. The threshold must absorb the spike directly:

$$\delta_A = \lambda_{\max}(S_A) = O(n), \qquad \delta_B = \lambda_{\max}(S_B) = O(n^2).$$

Ecologically, this reflects a basic constraint: predominantly competitive communities require commensurately strong self-regulation to prevent species from suppressing one another to extinction [18, 77] (Chapter 1), with the required self-regulation strength scaling with community size. A side-effect of this $O(n^2)$ inflation is that the rescaled HOI entries become small, $|B_{ijk}| \sim 1/(|\mu_B|\, n^3)$ — two orders of magnitude smaller in n than in the other two regimes, where $|B_{ijk}| \sim 1/(n\sqrt{\log n})$. The cubic term therefore contributes weakly to the

per-capita Jacobian until α approaches one, so α indexes nonlinearity on a different scale in the competitive regime than in the neutral and facilitative ones (see Section C.6.1 for a coordinate-free comparison, and Appendix C.8 for the full scaling argument).

Results across (μ_A, μ_B) combinations. We repeated the full boundary-detection protocol across a 3×3 grid of interaction means $(\mu_A, \mu_B) \in \{-0.1, 0, 0.1\}$, keeping all other aspects of the sampling protocol unchanged (Fig. C.3; the analogous 3×3 grids for the remaining boundary classes—gradual, unstable, and successful directions—are reported in Figs. C.13, C.14, and C.15). The qualitative signatures identified in the main text survive across all nine combinations: fold boundaries become increasingly prevalent as α grows; facilitative HOIs ($\mu_B > 0$) produce the steepest and most complete transition to the fold-dominated regime; and the effect of community size reverses sign across μ_B (folds become rarer with n under competitive or mixed HOIs, but more common under facilitative HOIs). Shifting μ_A modulates slightly the α-location at which folds start to dominate but does not alter these qualitative trends.

C.4.1 Purely competitive systems

Fold bifurcations have traditionally been associated with positive-feedback architectures in which a subset of interactions must be net-facilitative for a saddle–node to arise [35]. In our sampling protocol, by contrast, off-diagonal entries of A and B are drawn from symmetric distributions and therefore contain both positive and negative coefficients even in the $\mu_A, \mu_B > 0$ regime. A natural objection is that the folds we observe might simply reflect the presence of this positive minority: remove the positive entries and the folds would disappear. This section tests that hypothesis directly.

We examine a parameterization in which every interaction coefficient is strictly non-positive by construction. Off-diagonal and diagonal entries alike are drawn from a half-

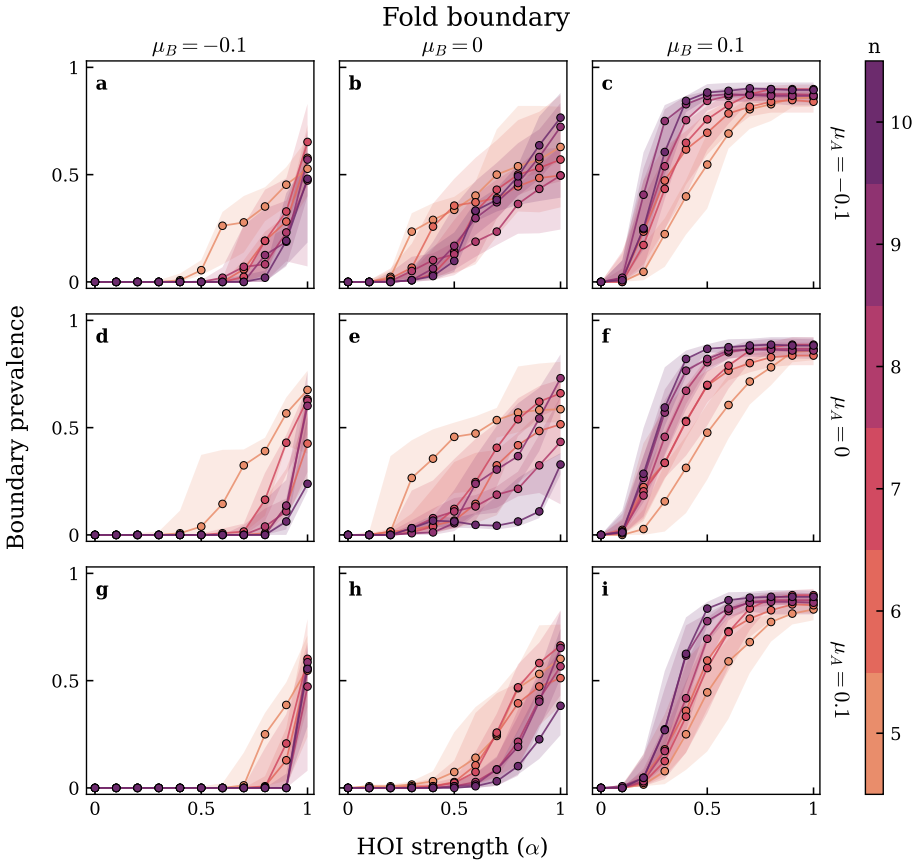

Figure C.3: **Fold-boundary prevalence across the (μ_A, μ_B) plane.** Each panel shows the fraction of perturbation directions terminating at a fold (abrupt) boundary as a function of HOI strength α, for community sizes $n = 5$–10 (colours). Columns vary the mean higher-order interaction $\mu_B \in \{-0.1, 0, 0.1\}$; rows vary the mean pairwise interaction $\mu_A \in \{-0.1, 0, 0.1\}$. Points are medians across 50 community replicates at each (n, α) condition; shaded bands span the interquartile range. The central row ($\mu_A = 0$, all three values of μ_B) reproduces Fig. 3.3. The six surrounding panels confirm that the three qualitative patterns established in the main text—(i) fold prevalence rises monotonically with α, (ii) facilitative HOIs ($\mu_B > 0$) produce the earliest and most complete transition to the fold-dominated regime, and (iii) the effect of community size on fold prevalence reverses sign across μ_B (diversity suppresses folds when $\mu_B \leq 0$ but amplifies them when $\mu_B > 0$)—are robust to the mean sign of pairwise interactions.

normal distribution and negated:

$$A_{ij} \;=\; -\big|\tilde{A}_{ij}\big|, \quad \tilde{A}_{ij} \sim \mathcal{N}\big(0,\, \sigma_A^2/n\big); \qquad B_{ijk} \;=\; -\big|\tilde{B}_{ijk}\big|, \quad \tilde{B}_{ijk} \sim \mathcal{N}\big(0,\, \sigma_B^2/n^2\big), \tag{C.19}$$

with $\sigma_A = \sigma_B = 1$ so that per-capita contributions remain $O(1)$ in n. The community is therefore purely competitive: every pairwise and higher-order interaction has its sign fixed a priori, and the resulting A and B bear no spectral-rescaling structure. We instead set the growth rates to the equilibrium condition at $\mathbf{x}^\star = \mathbf{1}$:

$$r_i(\alpha) \;=\; -\Big[\,(1-\alpha)\sum_j A_{ij} \;+\; \alpha \sum_{j,k} B_{jki}\,\Big], \tag{C.20}$$

Crucially, nothing guarantees that this equilibrium is locally stable: the Jacobian spectrum at $\mathbf{x}^\star$ is determined entirely by the random draw. This protocol therefore strips away both the zero-sum construction and the α-uniform stability guarantee, leaving only the bare planted equilibrium and the competitive-sign constraint.

Because stability is no longer enforced by construction, we partition the resulting bank into two subsets (Fig. C.16). The *full* bank retains every replicate, including those that lose stability as α grows or were unstable to begin with. The *stable-throughout* subset retains only those replicates whose coexistence equilibrium is locally stable across the entire α grid, matching the stability condition that the main-text construction imposes by design. Retaining replicates that happen to be stable by chance, rather than by imposed self-regulation, isolates the effect of the competitive-sign constraint on fold-boundary prevalence while still tracking the stable coexistence branch studied in the main text.

In both subsets, fold-boundary prevalence rises with α while the prevalence of gradual (negative-transcritical) boundaries declines (Fig. C.16)—the same qualitative signature established in the main text and reinforced across the (μ_A, μ_B) grid of Fig. C.3. Only a small

fraction of replicates remain stable across the entire α grid, and this fraction shrinks rapidly with n, as expected when stability is left to chance under random draws.

C.5 Global stability rules out fold bifurcations

The results of the previous section show that the statistical properties of the interaction tensors—their means, variances, and the relative weight of higher-order terms—exert a decisive influence on the prevalence of fold bifurcations at feasibility boundaries. In some regimes folds are virtually guaranteed; in others they are rare. This raises a natural question: under what conditions on the interaction tensors A and B can fold bifurcations be ruled out entirely?

A fold (saddle–node) bifurcation is, by definition, the collision and annihilation of two equilibrium branches as a parameter is varied [15]. At the fold point, two real equilibria merge. Consequently, a necessary condition for the existence of a fold bifurcation in parameter space is that the system admit more than one non-negative equilibrium for some values of the parameters. Here we derive a sufficient condition directly on A and B that guarantees global asymptotic stability of the coexistence equilibrium on the positive orthant, thereby precluding fold bifurcations.

A standard condition that implies uniqueness of the coexistence equilibrium is global asymptotic stability on the positive orthant $\mathbb{R}^n_{>0}$. If every trajectory initiated in $\mathbb{R}^n_{>0}$ converges to a single equilibrium $\mathbf{x}^\star$, then $\mathbf{x}^\star$ is necessarily the only equilibrium in $\mathbb{R}^n_{>0}$: any other interior equilibrium would itself be a fixed point of the dynamics and hence could not converge to $\mathbf{x}^\star$, contradicting global convergence. Combined with the observation above, global asymptotic stability of the coexistence equilibrium on $\mathbb{R}^n_{>0}$ directly rules out fold bifurcations.

We therefore seek conditions on A and B under which the coexistence equilibrium of

Eq. (C.1) is globally asymptotically stable on $\mathbb{R}^n_{>0}$.

To derive such conditions, we employ the classical Goh Lyapunov function [14, 120, 143], which is non-negative on $\mathbb{R}^n_{>0}$ and vanishes only at $\mathbf{x}^\star$:

$$V(\mathbf{x}) \;=\; \sum_{i=1}^{n} \left(x_i - x_i^\star - x_i^\star \ln \frac{x_i}{x_i^\star} \right). \tag{C.21}$$

Along trajectories of Eq. (C.1), and using $\dot{x}_i = x_i f_i(\mathbf{x})$ together with $f_i(\mathbf{x}^\star) = 0$, the time derivative of V takes the form

$$\dot{V} \;=\; \sum_{i=1}^{n} \frac{x_i - x_i^\star}{x_i}\, \dot{x}_i \;=\; (\mathbf{x} - \mathbf{x}^\star)^\top f(\mathbf{x}) \;=\; (\mathbf{x} - \mathbf{x}^\star)^\top \Big(f(\mathbf{x}) - f(\mathbf{x}^\star) \Big). \tag{C.22}$$

Global asymptotic stability on $\mathbb{R}^n_{>0}$ follows if $\dot{V} < 0$ for all $\mathbf{x} \in \mathbb{R}^n_{>0} \setminus \{\mathbf{x}^\star\}$.

To express $\dot{V}$ as a quadratic form in $(\mathbf{x} - \mathbf{x}^\star)$, we parametrise the straight path from $\mathbf{x}^\star$ to $\mathbf{x}$ as $\mathbf{z}(t) = \mathbf{x}^\star + t(\mathbf{x} - \mathbf{x}^\star)$, so that $\mathbf{z}(0) = \mathbf{x}^\star$, $\mathbf{z}(1) = \mathbf{x}$, and $d\mathbf{z}/dt = \mathbf{x} - \mathbf{x}^\star$. By the fundamental theorem of calculus,

$$f(\mathbf{x}) - f(\mathbf{x}^\star) \;=\; \int_0^1 \frac{d}{dt} f\Big(\mathbf{z}(t)\Big)\, dt \;=\; \left[\int_0^1 \nabla f\Big(\mathbf{x}^\star + t(\mathbf{x} - \mathbf{x}^\star)\Big)\, dt \right] (\mathbf{x} - \mathbf{x}^\star). \tag{C.23}$$

Substituting into Eq. (C.22) yields the quadratic form

$$\dot{V} \;=\; (\mathbf{x} - \mathbf{x}^\star)^\top \left[\int_0^1 \nabla f\Big(\mathbf{x}^\star + t(\mathbf{x} - \mathbf{x}^\star)\Big)\, dt \right] (\mathbf{x} - \mathbf{x}^\star). \tag{C.24}$$

For the GLV+HOI dynamics, and assuming without loss of generality the symmetrisation $B_{ijk} = B_{ikj}$, the per-capita growth rates are $f_i(\mathbf{x}) = r_i + (1-\alpha)\sum_j A_{ij} x_j + \alpha \sum_{j,k} B_{ijk} x_j x_k$, with Jacobian entries

$$\frac{\partial f_i}{\partial x_\ell} \;=\; (1-\alpha) A_{i\ell} + 2\alpha \sum_k B_{i\ell k}\, x_k. \tag{C.25}$$

Introducing the slice matrices $B_k := (B_{ijk})_{ij}$, this reads in matrix form

$$\nabla f(\mathbf{x}) \;=\; (1-\alpha)\,A \;+\; 2\alpha \sum_{k=1}^{n} x_k\, B_k. \tag{C.26}$$

Evaluating along the path $\mathbf{z}(t) = \mathbf{x}^\star + t(\mathbf{x}-\mathbf{x}^\star)$ and integrating,

$$\int_0^1 \nabla f\Big(\mathbf{z}(t)\Big)\, dt \;=\; (1-\alpha)\,A \;+\; \alpha \sum_{k=1}^{n} (x_k + x_k^\star)\, B_k, \tag{C.27}$$

where we used $\int_0^1 \Big(x_k^\star + t(x_k - x_k^\star)\Big)\, dt = (x_k + x_k^\star)/2$. Substituting back into Eq. (C.24),

$$\dot V(\mathbf{x}) \;=\; (\mathbf{x}-\mathbf{x}^\star)^\top \left[(1-\alpha)\,A \;+\; \alpha \sum_{k=1}^{n} \frac{x_k + x_k^\star}{2}\, B_k\right] (\mathbf{x}-\mathbf{x}^\star). \tag{C.28}$$

Sufficient conditions. A quadratic form $\mathbf{v}^\top M \mathbf{v}$ is negative for all $\mathbf{v} \neq 0$ iff the symmetric part $S_M := (M + M^\top)/2$ is negative definite. Applying this to the bracketed matrix in Eq. (C.28), and defining $S_A := (A + A^\top)/2$ and $(S_k)_{ij} := (B_{ijk} + B_{jik})/2$, the map $\mathbf{x} \mapsto \dot V(\mathbf{x})$ is strictly negative on $\mathbb{R}^n_{>0} \setminus \{\mathbf{x}^\star\}$ whenever the matrix

$$M(\mathbf{x}) \;=\; (1-\alpha)\, S_A \;+\; \alpha \sum_{k=1}^{n} \frac{x_k + x_k^\star}{2}\, S_k \tag{C.29}$$

is negative definite for every $\mathbf{x} \in \mathbb{R}^n_{>0}$. Because $(x_k + x_k^\star)/2 > 0$ on the positive orthant, $M(\mathbf{x})$ is a non-negative combination of S_A and the symmetrised slice matrices $\{S_k\}_{k=1}^n$. A sufficient condition is therefore that each of these matrices be separately negative definite:

$$S_A \;\prec\; 0 \qquad \text{and} \qquad S_k \;\prec\; 0 \quad \text{for every } k = 1, \dots, n. \tag{C.30}$$

When condition (C.30) holds, $\dot V < 0$ on $\mathbb{R}^n_{>0} \setminus \{\mathbf{x}^\star\}$ and the coexistence equilibrium $\mathbf{x}^\star$ is globally asymptotically stable on the positive orthant and fold bifurcations are precluded.

The slice-wise condition (C.30) is strictly stronger than local stability of the coexistence equilibrium (see Eq. C.13). Local stability only constrains the symmetrised community Jacobian evaluated at the single point $\mathbf{x} = \mathbf{x}^\star$, where the slice contributions are weighted by the specific equilibrium abundances $x_k^\star$. In contrast, condition (C.30) requires the combination in Eq. (C.29) to be negative definite for *all* $\mathbf{x} \in \mathbb{R}^n_{>0}$. The gap between these two conditions delineates the regime in which multiple equilibria—and hence fold bifurcations—can arise.

The same slice-wise condition (C.30) can be derived in the related context of nonlinear complementarity problems (NCP) [160], where it guarantees uniqueness of the NCP solution via strict monotonicity of the associated mapping $F = -f$ on $\mathbb{R}^n_{>0}$. Since the non-negative equilibria of Eq. (C.1) are exactly the solutions of the NCP with mapping $F = -f$, the NCP perspective provides an independent route to the same conclusion on uniqueness. The Lyapunov argument given here has the additional advantage of yielding global asymptotic stability (a dynamical statement) rather than uniqueness alone.

C.6 Robustness and generality of fold-mediated collapse

The main-text results rely on a tightly controlled ensemble: the baseline equilibrium is planted at $\mathbf{x}^\star = \mathbf{1}$ for every realization, pairwise and higher-order terms are mixed through a single convex knob $\alpha \in [0, 1]$, the spectral rescaling of Sec. C.4 enforces Hurwitz stability at the baseline for all α.

C.6.1 Quantifying nonlinearity without α

Before we can ask whether the main-text pattern survives in other parameterizations or other models, we need a replacement for α that can be evaluated in any system. To this end, this section introduces two model-agnostic measures of nonlinearity—a local one built from derivatives at the coexistence equilibrium, and a nonlocal one built from the geometry

of the boundary scan. Equipped with these, we then relax the assumptions of the main text in sequence: first the parameterization, keeping the GLV+HOI functional form (Sec. C.6.2); then the functional form (Sec. C.6.3). The same pattern persists once all controls are lifted, illustrating the breadth of our findings.

A local metric.

We define the first metric from a local Taylor expansion of the per-capita growth rate f around the baseline coexistence equilibrium $\mathbf{x}^\star$.

Given any smooth dynamical system $\dot{x}_i = x_i\, f_i(\mathbf{x})$ and a coexistence equilibrium $\mathbf{x}^\star \in \mathbb{R}^n_{>0}$, let

$$J_{ij} \;:=\; \left.\frac{\partial f_i}{\partial x_j}\right|_{\mathbf{x}^\star}, \qquad H_{ijk} \;:=\; \left.\frac{\partial^2 f_i}{\partial x_j\,\partial x_k}\right|_{\mathbf{x}^\star} \tag{C.31}$$

denote the Jacobian and Hessian of the per-capita rates at $\mathbf{x}^\star$. Expanding f about $\mathbf{x}^\star$ and collecting, for each species i, the first- and second-order contributions evaluated at the equilibrium abundance scale,

$$T_1[i] \;:=\; \sum_j J_{ij}\, x_j^\star, \qquad T_2[i] \;:=\; \tfrac{1}{2}\sum_{j,k} H_{ijk}\, x_j^\star\, x_k^\star, \tag{C.32}$$

we average their magnitudes across species,

$$P \;:=\; \tfrac{1}{n}\sum_{i=1}^{n} |T_1[i]| \quad \text{(linear magnitude)}, \qquad Q \;:=\; \tfrac{1}{n}\sum_{i=1}^{n} |T_2[i]| \quad \text{(quadratic magnitude)}, \tag{C.33}$$

and define the Taylor effective nonlinearity as the quadratic share

$$\alpha_{\text{eff}}^{\text{Taylor}} \;:=\; \frac{Q}{P+Q} \;\in\; [0,1]. \tag{C.34}$$

By construction $\alpha_{\text{eff}}^{\text{Taylor}} = 0$ when f is exactly linear at $\mathbf{x}^\star$ and it grows as the quadratic

response dominates. The metric is a functional of f alone: it is invariant under multiplicative rescalings of f (such as the time rescaling used in Section C.6.3 to polynomialise rational systems), independent of how interactions are parameterized, and well-defined for any smooth model.

Closed form for the main-text parameterization. For the main-text construction of Section C.4 we imposed constrains so that $\mathbf{x}^\star = \mathbf{1}$ is a coexistence equilibrium at $\mathbf{r} = \mathbf{1}$ for every $\alpha \in [0, 1]$ and for every realization of the random tensors. Under this construction, $\alpha_{\text{eff}}^{\text{Taylor}}$ reduces to (See Appendix)

$$\alpha_{\text{eff}}^{\text{Taylor}} = \frac{\alpha}{1 + 2\alpha}, \qquad \alpha \in [0, 1], \tag{C.35}$$

Note that this nonlinearity proxy is a monotonically increasing function of alpha, confirming that it is indeed a valid measure of HOI strength.

A nonlocal metric

The Taylor-based nonlinearity of is a purely local quantity: P and Q are built from the Jacobian and Hessian evaluated at the coexistence equilibrium $\mathbf{x}^\star$ (Eqs. (C.32)–(C.34)). For systems whose nonlinearity is near the equilibrium the previous metric would capture the nonlinearity well. However, a fold bifurcation can happen far from $\mathbf{x}^\star$ somewhere in the nonnegative orthant. A system whose per-capita rates look nearly affine at $\mathbf{x}^\star$ can therefore still harbour a fold a finite distance away, and will be assigned a small $\alpha_{\text{eff}}^{\text{Taylor}}$ even when its tipping structure at the coexistence boundary is strongly nonlinear.

We therefore introduce a second, nonlocal metric that measures how much of the per-capita rate f over the tipping-relevant region of state space cannot be captured by *any* affine model. Intuitively: if f happens to be affine throughout the region the boundary-

scan traverses, the system cannot fold within that region. Conversely, residual variance of f against its best affine approximation provides a direct, coordinate-free measure of the nonlinearity present in the coexistence region.

The boundary-scan of Section C.2 sweeps a family of rays outward from $\mathbf{x}^\star$ in environmental space and records, for each ray, the last stable coexistence state $\mathbf{x}_k^{\mathrm{pre}}$ reached before coexistence is lost. We therefore measure non-linearity in this region $\mathcal{H}$.

Let $f : \mathbb{R}^n_{\geq 0} \to \mathbb{R}^n$ denote the per-capita rate at the unperturbed baseline $\mathbf{r} = \mathbf{r}^0$ (no perturbation applied). We draw M samples $\{\mathbf{x}^{(m)}\}_{m=1}^M$ from $\mathcal{H}$ by assigning Dirichlet$(\alpha_{\mathrm{dir}}, \ldots, \alpha_{\mathrm{dir}})$ weights to the hull vertices; the concentration $\alpha_{\mathrm{dir}} = 0.1 < 1$ biases each draw toward a few vertices at a time, so that the sample set as a whole spreads throughout $\mathcal{H}$ rather than clustering near its centroid as a uniform Dirichlet would. The vertices themselves are appended to the sample set so that the extreme preboundary states are always present in the fit; we use 2000 samples.

Stacking the samples into $X \in \mathbb{R}^{n\times(M+|\mathcal{V}|)}$ (where $\mathcal{V}$ is the vertex set) and evaluating the per-capita rates column-wise gives a response matrix $Y \in \mathbb{R}^{n\times(M+|\mathcal{V}|)}$ with $Y_{:,m} = f(\mathbf{x}^{(m)})$. We then fit the best affine model,

$$Y \;\approx\; \mathbf{a} + B\,X, \qquad (\hat{\mathbf{a}}, \hat{B}) \;=\; \underset{\mathbf{a},B}{\arg\min} \left\| Y - \mathbf{a} - B\,X \right\|_{\mathrm{F}}^2, \tag{C.36}$$

We define the hull nonlinearity metric as the minimized residual,

$$\alpha_{\mathrm{eff}}^{\mathrm{hull}} \;:=\; \frac{\sum_{i,m}\left(Y_{im} - \hat{Y}_{im}\right)^2}{\sum_{i,m}\left(Y_{im} - \bar{Y}_i\right)^2} \;\in\; [0,1]. \tag{C.37}$$

By construction $\alpha_{\mathrm{eff}}^{\mathrm{hull}} = 0$ if and only if f is affine on $\mathcal{H}$ (the best linear model captures *all* of its variation), and it grows as the residual dominates.

Validation on the main-text ensemble. We now compare our hull-based nonlinearity diagnostic against the main-text ensemble. To this end, we compute $\alpha_{\text{eff}}^{\text{hull}}$ for all the models in the main-text systems, and plot it against α of those systems. The parallel between the two datasets is striking. Across all three μ_B regimes, the shape of $\alpha_{\text{eff}}^{\text{hull}}(\alpha)$ (Fig. C.4a–c) closely mirrors the shape of fold prevalence as a function of α reported in Fig. 3.3. In the competitive ($\mu_B = -0.1$) and mixed ($\mu_B = 0$) banks, both quantities rise gradually from near zero as α increases, with smaller communities climbing faster than larger ones. Moreover, in both diagnostics the rise with α is steeper in the mixed bank than in the competitive bank, matching the relative ordering of fold prevalence between these two regimes in the main text. In the facilitative bank ($\mu_B = 0.1$), both quantities instead jump almost immediately to a plateau at moderate α and remain there, independent of n. That $\alpha_{\text{eff}}^{\text{hull}}$—a purely geometric diagnostic—reproduces the regime-specific qualitative behavior of fold prevalence suggests it captures the geometric feature underlying fold-mediated collapse.

For the competitive and mixed banks, the relationship between $\alpha_{\text{eff}}^{\text{hull}}$ and fold prevalence is indeed monotonically increasing. In the facilitative bank, the same plot is uninformative: $\alpha_{\text{eff}}^{\text{hull}}$ saturates at ≈ 0.25–0.30 almost as soon as HOIs are turned on, while fold prevalence continues to rise with α, so any plot of folds against $\alpha_{\text{eff}}^{\text{hull}}$ would reduce to a nearly vertical band with no resolving power. We therefore replaced the inset in panel c with fold prevalence against $\alpha_{\text{eff}}^{\text{Taylor}}$, which retains variation across the range of α we explore and makes the continued growth of fold prevalence visible.

The need to switch diagnostics between panels reveals that the two are capturing different regions of nonlinearity and are best read as complementary. The Taylor measure is a *local* quantity: it weighs the pairwise and higher-order contributions to the per-capita growth rate at a single reference equilibrium, and so grows smoothly with α as HOI terms are dialed up in magnitude. The hull measure, by contrast, examines nonlinearity at the further regions of the coexistence domain.

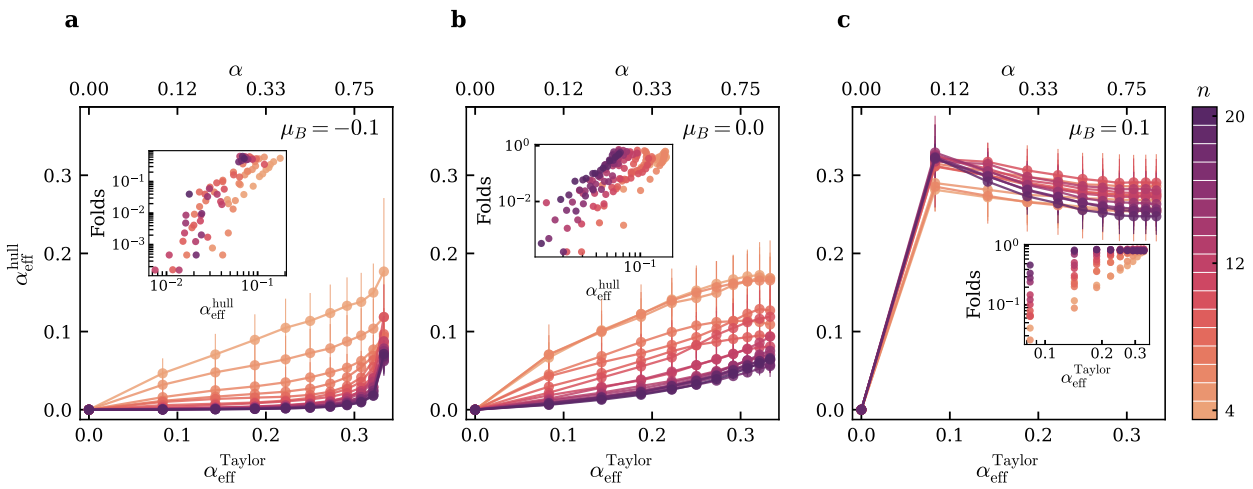

Figure C.4: **Hull nonlinearity vs. Taylor nonlinearity for the three main-text banks.** Mean hull-based effective nonlinearity $\alpha_{\text{eff}}^{\text{hull}}$ (Section C.6.1, Eq. (C.37)) plotted against the local Taylor metric $\alpha_{\text{eff}}^{\text{Taylor}}$ (Section C.6.1, Eq. (C.34)) for each of the three main-text parameterizations: **(a)** $\mu_B = -0.1$, **(b)** $\mu_B = 0.0$, **(c)** $\mu_B = 0.1$. Each curve corresponds to a fixed diversity n (colors). The top axis (secondary) shows the original mixing parameter α via the closed-form inversion implied by Eq. (C.35); both x-axes therefore index the same grid. Markers and lines show the mean across ~ 50 replicates per cell; vertical error bars show ± 1 standard deviation of $\alpha_{\text{eff}}^{\text{hull}}$ across replicates.

C.6.2 Robustness to alternative parameterizations

Equipped with these two measures of nonlinearity, we can now test whether fold prevalence is an artifact of the main-text controls rather than of HOIs themselves. To do so, we keep the GLV+HOI functional form but replace the main-text parameterization with the independent constrained-HOI framework of Gibbs et al. [145], which imposes none of our controls.

The Gibbs et al. framework

The Gibbs et al. framework starts from the same GLV+HOI dynamics as in the main text, but with sign conventions matching the ecological interpretation directly:

$$\dot{x}_i = x_i\Big(R_i - \sum_j A_{ij}\, x_j - \sum_{j,k} B_{ijk}\, x_j\, x_k\Big), \tag{C.38}$$

where $R_i > 0$ are intrinsic growth rates, A_{ij} encodes pairwise interactions (with $A_{ij} > 0$ representing competition and the diagonal $A_{ii} > 0$ representing self-regulation), and B_{ijk} represents higher-order interactions. We have intentionally matched the notation to the original contribution [145] to emphasize that we are using the exact same systems. Given a target equilibrium $\mathbf{x}^\star > 0$ and a sampled pairwise matrix A, the higher-order tensor B is constrained so that $\mathbf{x}^\star$ satisfies the equilibrium condition:

$$R_i = \sum_j A_{ij}\, x_j^\star + \sum_{j,k} B_{ijk}\, x_j^\star\, x_k^\star, \qquad i = 1, \ldots, n. \tag{C.39}$$

Crucially, A and B jointly balance R at the target equilibrium—neither component alone need support feasibility. This is fundamentally different from our main-text construction, where A and B are each independently designed so that $\mathbf{x}^\star = \mathbf{1}$ is an equilibrium for all α. In addition, this framework has no interpolation parameter α; the relative importance of HOIs varies across systems and must be quantified post hoc, using the metrics of Sec. C.6.1.

Within this framework, Gibbs et al. identify three qualitatively distinct regimes (Q1, Q2, Q3) in which HOIs commonly produce stable coexistence; each regime involves different pairwise statistics, target abundances, and stabilization mechanisms. We generated systems in all three, providing natural variation in interaction structure while staying within parameter regions where stability is common. Full regime specifications are given in the Appendix C.10.

System generation and acceptance

For each parameter combination we generated candidate systems at community size $S = 20$ by sampling pairwise interactions A and computing the constrained HOI tensor B as described above, using growth rates $R_i = 1$ and target abundances $\mathbf{x}^\star$ determined by the regime. We restricted generation to parameter combinations where the probability of sta-

bility (estimated from 100 replicates per combination) exceeds 0.9. This threshold ensures a high acceptance rate during rejection sampling: because each candidate system is drawn from the prescribed distributions over A and B and then accepted or discarded based on a Jacobian eigenvalue check, a low acceptance rate would mean that surviving systems are a heavily filtered subset, distorting the statistical structure of the interactions. By operating in the high-acceptance region of parameter space, we ensure that accepted systems are typical draws from the Gibbs constrained distributions rather than rare outliers that happen to be stable.

Figure C.5 shows the probability of stability across the three regimes, replicating the parameter sweeps of Gibbs et al. Filled dots indicate the parameterizations meeting the $P(\text{stability}) > 0.9$ threshold used to populate the system bank used here.

Boundary detection and results

Given the bank of stable systems produced by the procedure above, we tested each one for fold-mediated coexistence loss. For each system we set up the polynomial equilibrium system

$$(r_i^0 + \delta\ u_{ik}) - \sum_j A_{ij}\, x_j - \sum_{j,k} B_{ijk}\, x_j\, x_k = 0, \qquad i = 1, \ldots, n, \tag{C.40}$$

where k index the perturbation direction, and applied the boundary-detection algorithm described in Sec. C.2. Figure C.6 shows the results. Because we have dropped all controls—working with an orthogonal parameterization, exploring parameter combinations with different interaction statistics than in the main text, and computing nonlinearity post hoc—the results are expectedly noisier than our controlled simulations. Nevertheless, the central pattern is clear: folds become more common for higher α_{eff}.

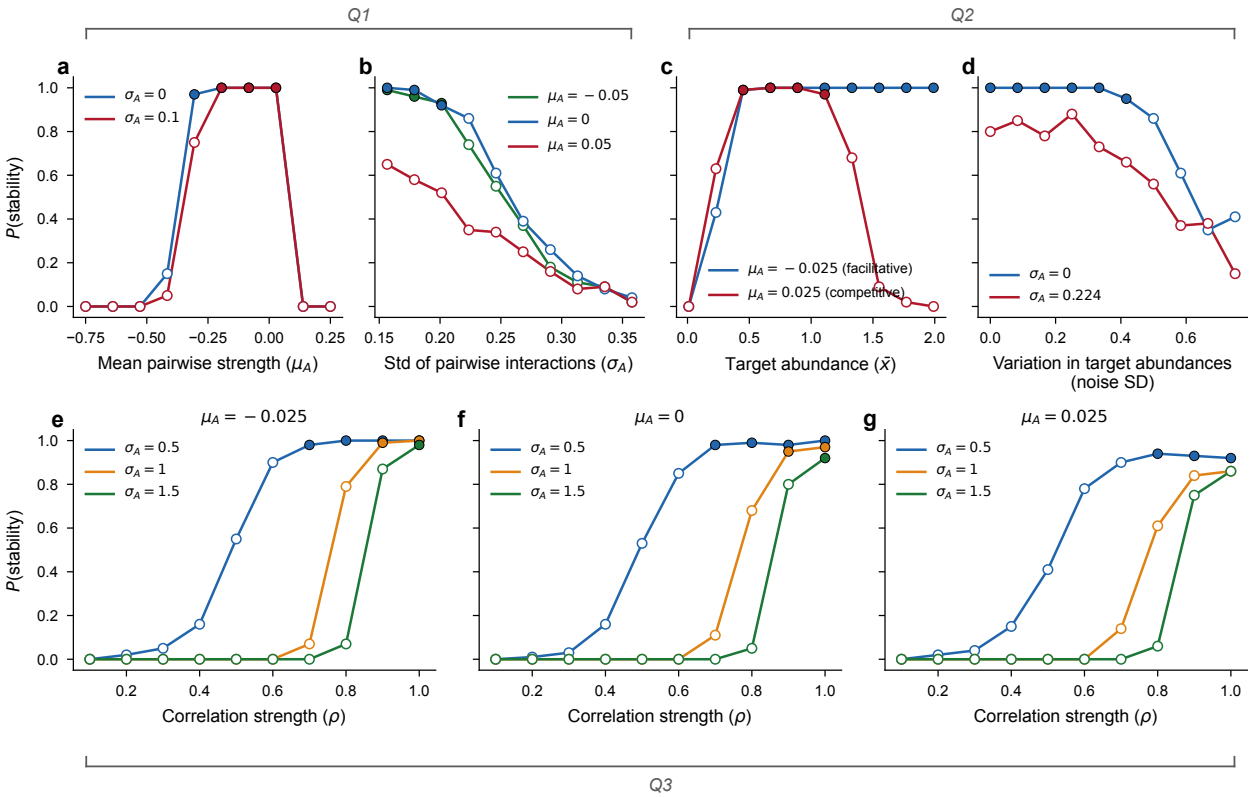

Figure C.5: **Probability of stability across the three Gibbs regimes, replicating the parameter sweeps of Gibbs et al. with $S = 20$ species. (a, b)** Regime Q1: P(stability) as a function of mean pairwise interaction strength μ_A **(a)** and standard deviation σ_A **(b)**, with HOI coefficients constrained via Dirichlet sampling. **(c, d)** Regime Q2: P(stability) as a function of target abundance $\bar{x}$ **(c)** and noise in target abundances **(d)**. **(e–g)** Regime Q3: P(stability) as a function of anti-correlation strength p for three values of μ_A, with curves colored by $\sigma_A \in \{0.5, 1.0, 1.5\}$. Filled circles indicate parameterizations with $P(\text{stability}) > 0.9$ used in this work; open circles denote those below the threshold.

C.6.3 Robustness to alternative functional forms

This step requires a preliminary observation. The higher-order tensor B_{ijk} of the main text is a phenomenological object: it captures the net effect of one species on the interaction between two others, but does not specify the mechanism producing that effect. What experiments and ecological models routinely document instead are nonlinear functional responses that make per-capita interaction effects depend on community state [5, 193]. As such, in this section we now loosen the functional form itself and ask whether fold-mediated collapse

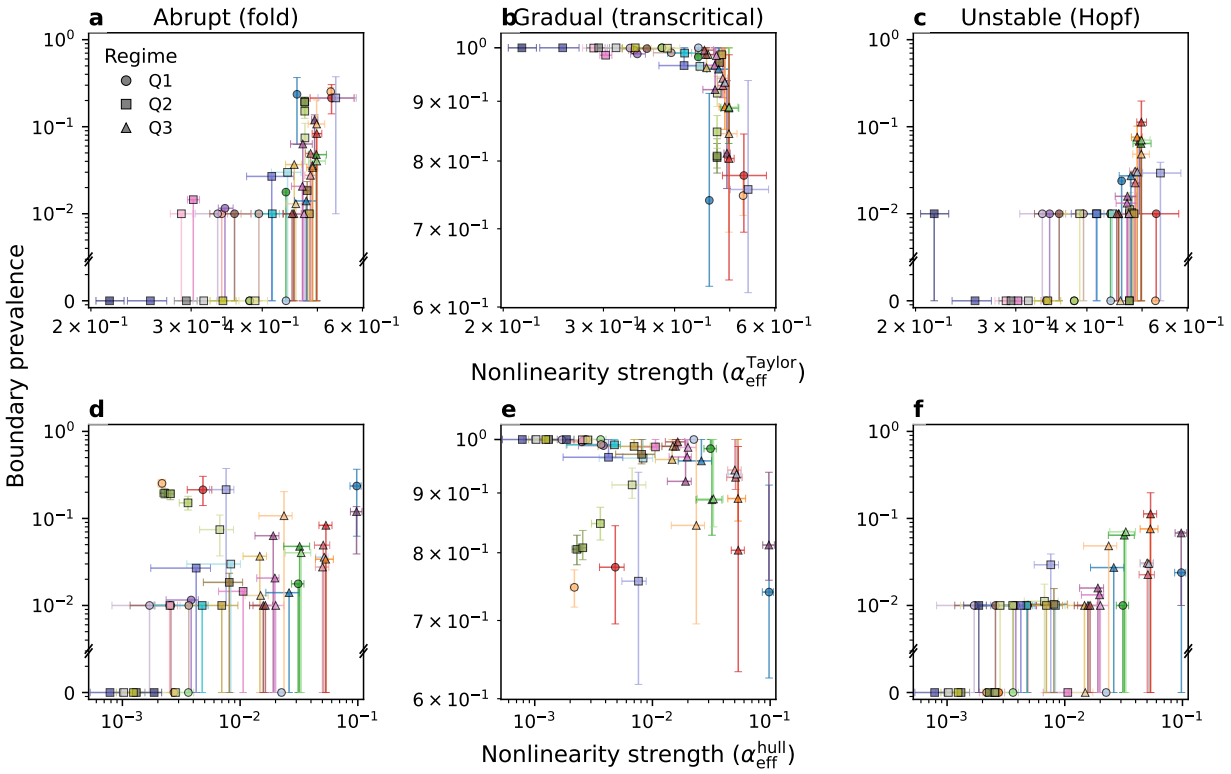

Figure C.6: **Boundary-type prevalence vs. effective nonlinearity strength in the Gibbs bank ($n = 20$).** Each point aggregates one parameterization across its replicates (47 parameterizations, 4612 stable systems, 128 random parameter rays per system). Marker position gives the means of the effective nonlinearity α_{eff} on the x-axis and the fraction of rays terminating in the indicated boundary type on the y-axis; error bars span the 25th–75th percentile across replicates. Marker shape encodes the parameter regime, color encodes the parameterization id (filled circles in Fig. C.5. **a, d:** fraction of rays ending at a fold (abrupt loss of coexistence). **b, e:** fraction ending at a negative-crossing boundary (gradual loss). **c, f:** fraction ending at a loss-of-stability boundary. **Top row (a–c):** x-axis is the Taylor-expansion estimate $\alpha_{\text{eff}}^{\text{Taylor}}$ (Eq. C.34). **Bottom row (d–f):** x-axis is the convex-hull estimate $\alpha_{\text{eff}}^{\text{hull}}$ (Eq. C.37).

remains common in published multispecies models that were not built around a three-way interaction tensor—models with saturating mutualistic responses, allometric trophic networks, ecosystem-engineering feedbacks, Allee effects, and Holling-type predation.

We start by showing that the two descriptions are formally equivalent: any pairwise model whose per-capita growth rates are rational or smooth functions of abundances can be

recast, exactly or locally, as a GLV model with effective higher-order interactions. Consider a general ecological model:

$$\dot{x}_i = x_i\, g_i(\mathbf{x}), \tag{C.41}$$

where each per-capita growth rate g_i is a rational function of the abundances and can therefore be written as a ratio of polynomials,

$$g_i(\mathbf{x}) \;=\; \frac{P_i(\mathbf{x})}{Q_i(\mathbf{x})}, \tag{C.42}$$

with numerator $P_i(\mathbf{x})$ and denominator $Q_i(\mathbf{x})$ polynomials in $\mathbf{x}$, and $Q_i(\mathbf{x}) > 0$ for $\mathbf{x} > 0$ (the standard form taken by saturating, handling-time, and Holling-type responses). Define

$$S(\mathbf{x}) \;\equiv\; \prod_{j=1}^{n} Q_j(\mathbf{x}), \tag{C.43}$$

the product of all denominators, which is strictly positive on the positive orthant. Rescaling time globally by $d\tau = S(\mathbf{x})\, dt$ and applying the chain rule gives

$$\frac{dx_i}{d\tau} \;=\; x_i\, S(\mathbf{x})\, g_i(\mathbf{x}) \;=\; x_i\, P_i(\mathbf{x}) \prod_{j\neq i} Q_j(\mathbf{x}), \tag{C.44}$$

which is now a polynomial in $\mathbf{x}$ for every i, since the only denominator Q_i has been cancelled by S. The right-hand side has a transparent algebraic structure: it is a *product* of polynomials in the species abundances, one factor P_i from the focal numerator and one factor Q_j from each of the remaining denominators. Expanding this product generates monomials of total degree well above two whose coefficients are precisely the effective higher-order interaction tensors of the polynomial reformulation. In other words, the saturation hidden inside each Q_j, once cleared, manifests as explicit polynomial coupling of three or more species at a time: HOIs are not added by hand but emerge mechanically from the algebra of multiplying

rational responses through. Because the two systems are the same up to a change of units of time, the bifurcation structure—including the existence and location of fold bifurcations at the feasibility boundary—is identical in both formulations.

This transformation shows that any model with saturating nonlinearities is, from the standpoint of equilibrium analysis, a GLV model with higher-order interactions—potentially of very high order.

An alternative route to effective higher-order interactions does not require the per-capita growth rates to be rational. For any smooth nonlinear model of the form (C.41), we can Taylor-expand each per-capita growth rate $g_i(\mathbf{x})$ around a reference equilibrium $\mathbf{x}^\star$:

$$g_i(\mathbf{x}) = g_i(\mathbf{x}^\star) + \sum_j \left.\frac{\partial g_i}{\partial x_j}\right|_{\mathbf{x}^\star} (x_j - x_j^\star) + \frac{1}{2}\sum_{j,k} \left.\frac{\partial^2 g_i}{\partial x_j \partial x_k}\right|_{\mathbf{x}^\star} (x_j - x_j^\star)(x_k - x_k^\star) + \cdots \quad \text{(C.45)}$$

The zeroth-order term gives the intrinsic growth rate at equilibrium, the first-order derivatives yield the standard pairwise interaction coefficients, and the second-order derivatives define effective three-way higher-order interactions $B^{\text{eff}}_{ijk} = \frac{1}{2}\,\partial^2 g_i/\partial x_j \partial x_k|_{\mathbf{x}^\star}$. Higher-order terms in the expansion correspond to interactions of progressively higher order. Truncating at second order recovers the GLV+HOI model in Eq. (C.1), with effective interaction tensors A and B determined by the local curvature of the nonlinear functional responses. This approach is more general than the time-rescaling method above—it applies to any sufficiently smooth model, not only those with rational nonlinearities—but it is inherently local: the effective HOI coefficients depend on the reference equilibrium, and the approximation degrades far from it. The two approaches are thus complementary: the time-rescaling provides an exact, global polynomial reformulation when the nonlinearities are rational, while the Taylor expansion provides a local HOI approximation for arbitrary smooth nonlinearities.

C.6.4 Published model specifications and parameterizations

Based on the connection between nonlinearities and effective HOIs established above, we apply our boundary-scan algorithm to several published pairwise models with nonlinear functional responses (see refs. [36, 138, 146–148]). For each model the procedure is the same:

1. **Sample a feasible, stable equilibrium.** We draw parameters from the distributions specified by the original study and numerically locate a coexistence equilibrium $\mathbf{x}^\star > 0$ that is locally stable through numerical integration, discarding replicates that fail to converge.

2. **Polynomialise.** Because our homotopy-continuation (HC) scanner requires a polynomial system, we clear denominators in every per-capita growth equation to obtain an equivalent polynomial system $\mathbf{G}(\mathbf{x}; \boldsymbol{\delta r}) = \mathbf{0}$, where $\boldsymbol{\delta r} = \delta\, \mathbf{u}$ is the parameter perturbation and $\mathbf{u}$ is a unit direction drawn from the appropriate subspace. Clearing denominators can in principle introduce spurious solutions that are absent in the original system; however, because we always track an equilibrium branch seeded at a feasible equilibrium of the original dynamics, those extra solutions remain outside our computational scope.

3. **Perturb and track.** Starting from $\mathbf{x}^\star$, we use coefficient-parameter homotopy continuation to track the coexistence branch as δ increases, classifying the first boundary encountered as gradual, abrupt, or unstable using the algorithm described in Sec. C.2.

Unlike the canonical GLV-HOI models studied in the main text, where a mixing parameter α interpolates between pairwise and higher-order regimes, these published models possess emergent nonlinearity that cannot be tuned up or down. We therefore treat each model as a single data point at a fixed value of the two measures of effective higher-order strength α_{eff}

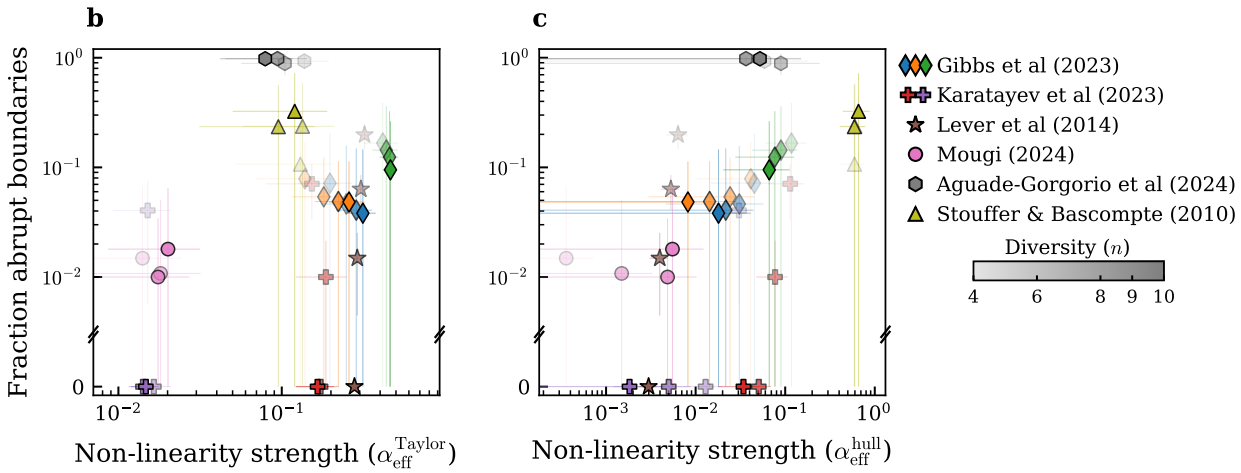

Figure C.7: **Fraction of abrupt boundaries versus two alternative non-linearity metrics.** Each marker is a bank of models grouped by family and diversity n; vertical and horizontal bars show the standard deviation of the fold fraction and of the non-linearity metric within the group, respectively. (**a**) Non-linearity strength measured by the Taylor-expansion unified metric $\alpha_{\text{eff}}^{\text{Taylor}}$. (**b**) Non-linearity strength measured by $\alpha_{\text{eff}}^{\text{hull}}$. Marker shape and colour identify the model family (legend, right); marker opacity encodes species richness n (colourbar, right). Both panels share the same y-axis.

(defined above) rather than scanning over an α-grid. The figure with results is presented in Fig. C.7

Both panels of Fig. C.7 show an overall positive association between effective nonlinearity strength and the prevalence of abrupt (fold) boundaries, consistent with the link between higher-order interactions and fold-mediated collapse established in the main text. The correlation is, however, visibly tighter under the hull metric $\alpha_{\text{eff}}^{\text{hull}}$ than under the local Taylor metric $\alpha_{\text{eff}}^{\text{Taylor}}$, suggesting that for the models and diversities considered here the global notion of nonlinearity—which probes f across the convex hull spanning the equilibrium and the pre-boundary states—is the more faithful descriptor, and that the nonlinearity driving collapse lives far enough from the equilibrium that the local Taylor expansion at $\mathbf{x}^\star$ underrepresents it.

The remainder of the section provides the full dynamical equations, parameterizations, and perturbation protocols used for each of the five published models analysed in this study.

Plant-pollinator network (Lever et al, 2014)

Original model. The community comprises S_P plant species and S_A pollinator (animal) species [36], indexed $i = 1, \ldots, S_P$ and $k = 1, \ldots, S_A$, respectively. Species ordering in the state vector is $\mathbf{x} = (P_1, \ldots, P_{S_P}, A_1, \ldots, A_{S_A})^\top$, with $n = S_P + S_A$.

Plant dynamics:

$$\frac{dP_i}{dt} = P_i \left[r_i^P + \frac{\sum_{k=1}^{S_A} \gamma_{ik}^P \, A_k}{1 + h_i^P \sum_{k=1}^{S_A} \gamma_{ik}^P \, A_k} - \sum_{j=1}^{S_P} c_{ij}^P \, P_j \right] + \mu_P \,, \tag{C.46}$$

Pollinator dynamics:

$$\frac{dA_k}{dt} = A_k \left[r_k^A - d_A + \frac{\sum_{i=1}^{S_P} \gamma_{ki}^A \, P_i}{1 + h_k^A \sum_{i=1}^{S_P} \gamma_{ki}^A \, P_i} - \sum_{l=1}^{S_A} c_{kl}^A \, A_l \right] + \mu_A \,. \tag{C.47}$$

The bipartite interaction topology is fully connected ($\gamma_{ik}^P, \gamma_{ki}^A > 0$ for all plant–pollinator pairs). Mutualistic benefit coefficients are normalised by partner degree via the trade-off parameter θ:

$$\gamma_{ik}^P = \frac{\gamma_{ik}^{P,0}}{d_i^\theta} \,, \qquad \gamma_{ki}^A = \frac{\gamma_{ki}^{A,0}}{d_k^\theta} \,, \tag{C.48}$$

where $d_i = \sum_k \mathbf{1}[\gamma_{ik}^P > 0]$ is the degree of plant i (and analogously for pollinators), and $\gamma_{ik}^{P,0}, \gamma_{ki}^{A,0}$ are baseline strengths. For this model, we resolved the bifurcation structure explicitly.

Bifurcation diagram construction (Fig. 3.4A). To resolve the full bifurcation structure of the Lever et al. model explicitly, we construct the diagram in Fig.4A as follows. We set up a parameter homotopy in `HomotopyContinuation.jl` that varies pollinator mortality d_A from 0 (the baseline) to a target value, holding all other parameters fixed. Starting from the numerically obtained coexistence equilibrium at $d_A = 0$, we track the stable coexistence

with homotopy continuation using d_A as perturbation parameter. The tracker terminates when the Jacobian $\frac{\mathrm{d}H}{\mathrm{d}\mathbf{x}}$ becomes singular, indicating a fold bifurcation at a critical mortality d_A^c. To locate the unstable branch that meets the stable branch at this fold, we evaluate the system at a parameter value slightly before the fold ($d_A \lesssim d_A^c$), compute the near-singular direction of the Jacobian via SVD, and use it to seed a Newton search for a second, distinct equilibrium. Once found, this unstable equilibrium is continued backward (toward $d_A = 0$) using the same parameter homotopy, yielding the unstable branch. To confirm that the stable algebraic branch correspond to realized dynamics, we overlay numerical integration of the original ODE system (C.46)–(C.47). A forward sweep integrates the system to steady state at each of a sequence of d_A values (using the previous endpoint as the initial condition), tracing the stable branch until the fold, after which the system collapses to a zero-abundance attractor. A backward sweep then integrates from the collapsed state as d_A is reduced, revealing hysteresis: recovery occurs at a d_A value corresponding to the terminus of the unstable branch, well below d_A^c. The combined algebraic branches (stable and unstable, shown as solid and dashed lines) together with the forward and backward integration endpoints (shown as triangles) constitute the bifurcation diagram in Fig. 3.4A.

Parameterization. All parameters are drawn independently for each replicate from the distributions listed in Table C.1. Only replicates converging to a strictly positive equilibrium ($x_i^* > 10^{-2}$ for all i) are retained.

Perturbation protocol. Perturbation directions $\mathbf{u} \in \mathbb{R}^n$ are constructed with *zero entries for plant species* and unit-normalised random Gaussian entries in the pollinator subspace: $\mathbf{u} = (0, \ldots, 0, u_{S_P+1}, \ldots, u_n)^\top$ with $(u_{S_P+1}, \ldots, u_n) \sim \mathcal{N}(0, I_{S_A})$ normalised to unit length. This reflects the ecological scenario in which pollinator mortality is the driver of community collapse, consistent with the original study.

Table C.1: **Parameters of the plant–pollinator model (Lever et al., 2014).**

Parameter	Description	Distribution	Value / Range
r_i^P, r_k^A	Intrinsic growth rates	Uniform	[0.05, 0.35]
h_i^P, h_k^A	Handling times (saturating response)	Uniform	[0.15, 0.30]
c_{ij}^P $(i \neq j)$	Interspecific competition (plants)	Uniform	[0.01, 0.05]
c_{ii}^P	Intraspecific competition (plants)	Uniform	[0.80, 1.10]
c_{kl}^A $(k \neq l)$	Interspecific competition (pollinators)	Uniform	[0.01, 0.05]
c_{kk}^A	Intraspecific competition (pollinators)	Uniform	[0.80, 1.10]
$\gamma_{ik}^{P,0}$	Baseline mutualistic benefit (plant ← pollinator)	Uniform	[0.80, 1.20]
$\gamma_{ki}^{A,0}$	Baseline mutualistic benefit (pollinator ← plant)	Uniform	[0.80, 1.20]
θ	Degree trade-off exponent	Fixed	0.5
μ_P, μ_A	Immigration	Fixed	0
d_A	Additional pollinator mortality	Fixed	0

Replicates. 50 parameter replicates per species richness, 128 perturbation directions per replicate. Community sizes: $n \in \{4, 6, 8, 10\}$ (with $S_P = S_A = n/2$).

Resource-consumer food web with density-mediated feedbacks (Karatayev et al, 2023).

Original model. The community consists of n_R resource species N_i $(i = 1, \ldots, n_R)$ and n_C consumer species C_k $(k = 1, \ldots, n_C)$ [138], with $n = n_R + n_C$ and state vector $\mathbf{x} = (N_1, \ldots, N_{n_R}, C_1, \ldots, C_{n_C})^\top$.

Two feedback modes are considered:

FMI (Feeding-Mediating Interactions). Resource species become less edible at high density, creating a density-dependent feeding interaction.

Resource dynamics:

$$\frac{dN_i}{dt} = N_i \left[r_i \left(1 - \frac{(1-a)\, N_i + a \sum_j N_j}{K_i} \right) - \sum_k \sigma_{ik} \left(1 - \frac{f_i\, N_i}{K_i} \right) \delta_k\, C_k \right], \tag{C.49}$$

Consumer dynamics:

$$\frac{dC_k}{dt} = C_k \left[\delta_k\, b_k \sum_i \sigma_{ik} \left(1 - \frac{f_i\, N_i}{K_i} \right) N_i - m \right] - \beta_k\, C_k^2 . \tag{C.50}$$

RMI (Recruitment-Mediating Interactions). Resource density modulates consumer recruitment efficiency rather than edibility.

Resource dynamics:

$$\frac{dN_i}{dt} = N_i \left[r_i \left(1 - \frac{(1-a)\, N_i + a \sum_j N_j}{K_i} \right) - \sum_k \sigma_{ik}\, \delta_k\, C_k \right], \tag{C.51}$$

Consumer dynamics:

$$\frac{dC_k}{dt} = C_k \left[\delta_k\, b_k \left(\sum_i \sigma_{ik}\, N_i \right) \left(1 - \sum_i \omega_{ik}\, \frac{f_i\, N_i}{K_i} \right) - m \right] - \beta_k\, C_k^2 . \tag{C.52}$$

Parameterization. Parameters are sampled following the defaults of [138] (Table C.2). All ξ draws are independent Uniform$(-1, 1)$. The consumer preference matrix σ_{ik} is drawn column-wise from a log-normal distribution with $\sigma_{\log} = 0.5$ and then column-normalised. The recruitment weight matrix ω_{ik} (RMI mode) is drawn row-wise from a Gamma(1) distribution and row-normalised. Resources and consumers are split evenly: $n_R = \lfloor n/2 \rfloor$, $n_C = n - n_R$.

Perturbation protocol. Perturbation directions have zero entries for resource species and unit-normalised Gaussian entries in the consumer subspace: $\mathbf{u} = (0, \ldots, 0,\, u_{n_R+1}, \ldots, u_n)^\top$,

Table C.2: **Parameters of the resource–consumer food web (Karatayev et al., 2023).**

Parameter	Description	Baseline	Sampling
K_i	Resource carrying capacity	$\bar{K} = 1.35$	$\bar{K}\,(1 + 0.15\,\xi_i)$
r_i	Resource intrinsic growth rate	$\bar{r} = 1.0$	$\bar{r}\,(1 + 0.15\,\xi_i)$
δ_k	Consumer grazing rate	$\bar{\delta} = 1.1$	$\bar{\delta}\,(1 + 0.15\,\xi_k)$
b_k	Consumer conversion efficiency	$\bar{b} = 1.0$	$\bar{b}\,(1 + 0.15\,\xi_k)$
β_k	Consumer density dependence	$\bar{\beta} = 0.15$	$\bar{\beta}\,(1 + 0.15\,\xi_k)$
f_i	Edibility/recruitment feedback	$\bar{f} = 0.8$	$\bar{f}\,(1 + 0.125\,\xi_i)$
m	Baseline consumer mortality	0.025	Fixed
a	Interspecific resource competition	0.025	Fixed
σ_{ik}	Diet specialisation matrix	—	LogNormal, column-normalised
ω_{ik}	Recruitment weight matrix (RMI)	—	Gamma(1), row-normalised

reflecting consumer mortality as the perturbation parameter.

Replicates. 50 replicates per species richness, 128 directions per replicate, for each of FMI and RMI feedback modes. Community sizes: $n \in \{4, 6, 8, 10\}$ (i.e. $n_R = n_C \in \{2, 3, 4, 5\}$).

Ecosystem-engineering food web (Mougi, 2024)

Original model. The model [146] describes an n-species food web with directed trophic links, where a subset of "engineer" species modify the environment and thereby alter the growth rates and interaction strengths experienced by "receiver" species. These engineering effects create effective higher-order interactions.

Species dynamics:

$$\frac{dx_i}{dt} = x_i \left[r_i\,\mathcal{B}_i(\mathbf{x}) - s_i\,x_i + \mathcal{G}_i(\mathbf{x})\,\frac{\sum_j e_{ij}\,a_{ij}\,x_j}{1 + \sum_j h_{ij}\,a_{ij}\,x_j} - \sum_{\text{pred}\,p} \frac{\mathcal{G}_p(\mathbf{x})\,a_{pi}\,x_p}{1 + \sum_j h_{pj}\,a_{pj}\,x_j} \right], \qquad \text{(C.53)}$$

where $\mathcal{B}_i$ and $\mathcal{G}_i$ are engineering modifications of the growth rate and trophic interaction

strength, respectively. The engineering factors take the form

$$\mathcal{B}_i(\mathbf{x}) = 1 + \sum_{\text{eng}\, e} (\beta_{ei} - 1)\, \frac{x_e}{x_e + E_e^0}\,, \qquad \mathcal{G}_i(\mathbf{x}) = 1 + \sum_{\text{eng}\, e} (\gamma_{ei} - 1)\, \frac{x_e}{x_e + E_e^0}\,, \tag{C.54}$$

where the sums run over engineer species e, and β_{ei}, γ_{ei} are the engineering coefficients (> 1: facilitation, < 1: inhibition), and $E_e^0 > 0$ is a half-saturation constant for the engineering effect. Non-receiver species have $\mathcal{B}_i = \mathcal{G}_i = 1$.

Parameterization. Parameters are sampled as listed in Table C.3. The trophic network is a random directed graph with connectance 1.0 (fully connected): for each unordered pair (i, j) with $i < j$, a directed trophic link is created with random orientation. The numbers of engineer and receiver species are chosen so that the "engineering dominance" $(n_{\text{eng}}/n)\times(n_{\text{rec}}/n)$ lies in $[0.08, 0.20]$. Engineering coefficients for each engineer–receiver pair: with probability $q_r \in [0.1, 0.3]$, $\beta_{ei} \sim \text{Uniform}(0, 1)$ (inhibition), otherwise $\text{Uniform}(1, 2)$ (facilitation); with probability $q_a \in [0.7, 0.9]$, $\gamma_{ei} \sim \text{Uniform}(0, 1)$, otherwise $\text{Uniform}(1, 2)$.

Table C.3: **Parameters of the ecosystem-engineering food web (Mougi, 2024).**

Parameter	Description	Distribution	Value / Range
r_i	Baseline intrinsic growth rate	Uniform	[0.2, 1.0]
s_i	Self-regulation coefficient	Fixed	1.0
a_{ij}	Attack rate (if trophic link exists)	Uniform	[0.0, 0.01]
e_{ij}	Assimilation efficiency	Uniform	[0.1, 0.25]
h_{ij}	Handling time (Type II response)	Uniform	[1.0, 10.0]
E_e^0	Engineering half-saturation	Uniform	[0.0, 0.1]
β_{ei}	Engineering effect on growth rate	See text	$[0, 2]$
γ_{ei}	Engineering effect on trophic strength	See text	$[0, 2]$

Perturbation protocol. Perturbation directions are full-dimensional: $\mathbf{u} \sim \mathcal{N}(\mathbf{0}, I_n)$, normalised to unit length. The perturbation $\boldsymbol{\delta r} = \delta\,\mathbf{u}$ is added to the baseline growth rates r_i.

Replicates. 50 replicates per species richness, 128 directions per replicate. Community sizes: $n \in \{4, 6, 8, 9\}$.

Facilitation-competition community with Allee effects (Aguadé-Gorgorió et al. 2024)

Original model. The model [147] describes n species with saturating facilitation (generating Allee-like effects) and linear competition:

$$\frac{dx_i}{dt} = x_i \left[\sum_{j=1}^{n} \frac{A_{ij}\, x_j}{\gamma_j + x_j} - d_i - \sum_{j=1}^{n} B_{ij}\, x_j \right], \tag{C.55}$$

where $A_{ij} \geq 0$ is a facilitation matrix (diagonal: Allee-type self-facilitation; off-diagonal: mutualism), $B_{ij} \geq 0$ is a competition matrix (diagonal: self-regulation; off-diagonal: interspecific competition), $\gamma_j > 0$ are half-saturation constants, and $d_i > 0$ are per-species death rates (perturbation parameters in the HC scan). The saturating facilitation generates effective higher-order interactions when expanded around equilibrium.

Parameterization. Parameters follow the protocol of [147], using log-normal distributions (Table C.4). All matrices are dense (no sparsity masking). The interspecific means $\bar{A}$ and $\bar{B}$, as well as the heterogeneity σ_{inter}, are drawn once per replicate; individual A_{ij}, B_{ij} are then drawn from the corresponding log-normal.

Table C.4: **Parameters of the facilitation–competition community (Aguadé-Gorgorió et al., 2024).**

Parameter	Description	Distribution	Mean / Range
Intraspecific (sampled independently per species)			
γ_i	Half-saturation constant	LogNormal$(\ln(\bar{\gamma}),\ \ln(1.1))$	$\bar{\gamma} = 1.0$
d_i	Death rate	LogNormal$(\ln(\bar{d}),\ \ln(1.1))$	$\bar{d} = 0.1$
A_{ii}	Self-facilitation (Allee)	LogNormal$(\ln(\bar{A}_{\text{diag}}),\ \ln(1.1))$	$\bar{A}_{\text{diag}} = 0.5$
B_{ii}	Self-regulation	LogNormal$(\ln(\bar{B}_{\text{diag}}),\ \ln(1.1))$	$\bar{B}_{\text{diag}} = 0.1$
Interspecific (means drawn once per replicate)			
A_{ij} $(i \neq j)$	Mutualistic facilitation	LogNormal$(\ln(\bar{A}),\ \ln(\sigma_{\text{inter}}))$	$\bar{A} \sim \text{Uniform}(0^+, 0.5)$
B_{ij} $(i \neq j)$	Interspecific competition	LogNormal$(\ln(\bar{B}),\ \ln(\sigma_{\text{inter}}))$	$\bar{B} \sim \text{Uniform}(0^+, 0.14)$
σ_{inter}	Interaction heterogeneity	Uniform(1.00001, 3.0001)	—

Perturbation protocol. Perturbation directions are full-dimensional: $\mathbf{u} \sim \mathcal{N}(\mathbf{0}, I_n)$, normalised to unit length. The perturbation is added to the death rates: $d_i \to d_i + \delta\, u_i$.

Replicates. 50 replicates per species richness, 128 directions per replicate. Community sizes: $n \in \{4, 6, 8, 10\}$.

Allometric trophic network (Stouffer & Bascompte, 2010)

Original model. The model [148] uses a niche-model food web [194] with allometrically scaled metabolic rates and Holling Type II functional responses. The state variable B_i denotes the biomass of species i.

Basal (producer) species:

$$\frac{dB_i}{dt} = B_i\left[1 - \frac{\sum_{\text{basal}\, j} B_j}{K}\right] - \sum_{\text{pred}\, p} \frac{x_p\, y_p\, w_{pi}\, B_p\, B_i}{e_{pi}\left(B_0 + \sum_{\text{prey}\, j'} w_{pj'}\, B_{j'}\right)}\,, \tag{C.56}$$

Consumer species:

$$\frac{dB_i}{dt} = B_i\left[-x_i + \frac{x_i\, y_i \sum_{\text{prey } j} w_{ij}\, B_j}{B_0 + \sum_{\text{prey } j} w_{ij}\, B_j}\right] - \sum_{\text{pred } p} \frac{x_p\, y_p\, w_{pi}\, B_p\, B_i}{e_{pi}\Big(B_0 + \sum_{\text{prey } j'} w_{pj'}\, B_{j'}\Big)}\,, \tag{C.57}$$

where $x_i = (a_x/a_r)\,(M_i/M_b)^{-0.25}$ is the mass-specific metabolic rate of consumer i (allometrically scaled), $y_i = a_y/a_x$ is the maximum ingestion rate relative to metabolic rate, w_{ij} is the attack rate of consumer i on prey j, e_{ij} is the assimilation efficiency, M_i is the body mass of species i, K is the shared basal carrying capacity, and B_0 is the half-saturation constant of the functional response.

Parameterization. Parameter values are listed in Table C.5. The food web topology is generated using the niche model [194]

Table C.5: **Parameters of the allometric trophic network (Stouffer & Bascompte, 2010).**

Parameter	Description	Distribution	Value
K	Basal carrying capacity	Fixed	1.0
B_0	Functional-response half-saturation	Fixed	0.5
M_b	Basal body mass	Fixed	1.0
a_r	Basal mass-specific metabolic rate	Fixed	1.0
a_x	Consumer mass-specific metabolic rate	Fixed	0.314
a_y	Maximum ingestion rate constant	Fixed	$8\,a_x = 2.512$
e_{ij}	Assimilation efficiency	Fixed	0.85
w_{ij}	Attack rate per trophic link	LogNormal$(-3.0,\ 1.5)$	—
M_i	Consumer body mass	MCMC (see text)	—

Perturbation protocol. Perturbation directions are full-dimensional: $\mathbf{u} \sim \mathcal{N}(\mathbf{0}, I_n)$, normalised to unit length. For basal species, the perturbation shifts the intrinsic growth rate: $1 + \delta r_i$ replaces 1 in Eq. (C.56). For consumers, the perturbation shifts the metabolic rate:

$-x_i + \delta r_i$ replaces $-x_i$ in Eq. (C.57).

Replicates. 50 replicates per species richness, 128 directions per replicate. Community sizes: $n \in \{4, 6, 8, 10\}$.

C.7 Mean matrices of S_A and S_B

We compute the mean matrices for both the pairwise symmetric matrix $S_A = \frac{1}{2}(A + A^\top)$ and the symmetric HOI aggregation matrix $(S_B)_{ij} = \frac{1}{4}\sum_k (B_{ijk} + B_{ikj} + B_{jik} + B_{jki})$, working before the diagonal rescaling in Eq. (C.16). In both cases, the zero-row-sum (resp. zero-slice-sum) constraint creates a deterministic coupling between off-diagonal and diagonal entries that shifts the spectrum away from the origin whenever the interaction mean is nonzero (See Fig. C.2).

Pairwise sector: $\mathbb{E}[S_A]$

Recall that $\tilde{A}_{ij} \sim \mathcal{N}(\mu_A, n^{-1})$ for $i \neq j$, with the zero-row-sum constraint $\tilde{A}_{ii} = -\sum_{j \neq i} \tilde{A}_{ij}$ (See Eq. C.14).

Off-diagonal ($i \neq j$). The entries $\tilde{A}_{ij}$ and $\tilde{A}_{ji}$ are independent unconstrained draws, so

$$\mathbb{E}[(S_A)_{ij}] = \tfrac{1}{2}\,\mathbb{E}[\tilde{A}_{ij} + \tilde{A}_{ji}] = \mu_A.$$

Diagonal ($i = j$). By the zero-sum constraint,

$$\mathbb{E}[(S_A)_{ii}] = \mathbb{E}[\tilde{A}_{ii}] = -(n-1)\mu_A.$$

Combining:

$$\mathbb{E}[S_A] = \mu_A \, \mathbf{1}\mathbf{1}^\top - n\mu_A \, I,$$

which factors as

$$\mathbb{E}[S_A] = -n\mu_A \left(I - \frac{\mathbf{1}\mathbf{1}^\top}{n} \right). \tag{C.58}$$

The matrix inside parentheses is the *centring matrix* (projecting onto the complement of $\mathbf{1}$), with eigenvalues 1 (multiplicity $n-1$) and 0 (eigenvector $\mathbf{1}$). The spectrum of $\mathbb{E}[S_A]$ is therefore $\{-n\mu_A$ (mult. $n-1$), 0 (eigenvector $\mathbf{1})\}$.

HOI sector: $\mathbb{E}[S_B]$

Recall that $\tilde{B}_{ijk} \sim \mathcal{N}(\mu_B, n^{-2})$, with the zero-slice-sum constraint $\tilde{B}_{iii} = -\sum_{(j,k)\neq(i,i)} \tilde{B}_{ijk}$.

Off-diagonal ($i \neq j$). When $i \neq j$, none of the four summands in $(S_B)_{ij}$ hits a triple-diagonal entry. All entries are therefore unconstrained draws of $\tilde{B}$, each of mean μ_B; with $4n$ terms in total and a $\frac{1}{4}$ prefactor,

$$\mathbb{E}[(S_B)_{ij}] = \tfrac{1}{4}(4n\mu_B) = n\mu_B.$$

Diagonal ($i = j$). Collecting identical pairs: $(S_B)_{ii} = \frac{1}{2}\sum_k (\tilde{B}_{iik} + \tilde{B}_{iki})$. Consider $\sum_k \tilde{B}_{iik}$; splitting at $k = i$:

$$\sum_k \tilde{B}_{iik} = \tilde{B}_{iii} + \sum_{k\neq i} \tilde{B}_{iik}.$$

The first term is the negative of $n^2 - 1$ draws of mean μ_B (See Eq. C.14); the second is $n-1$ draws. Their expectations sum to $-(n^2-1)\mu_B + (n-1)\mu_B = -n(n-1)\mu_B$. By an identical argument with indices two and three swapped, $\mathbb{E}[\sum_k \tilde{B}_{iki}] = -n(n-1)\mu_B$. Therefore

$$\mathbb{E}[(S_B)_{ii}] = \tfrac{1}{2}\Big(-n(n-1)\mu_B - n(n-1)\mu_B\Big) = -n(n-1)\mu_B.$$

Combining:

$$\mathbb{E}[S_B] = n\mu_B \mathbf{1}\mathbf{1}^\top - n^2\mu_B I,$$

which factors as

$$\mathbb{E}[S_B] = -n^2\mu_B\left(I - \frac{\mathbf{1}\mathbf{1}^\top}{n}\right). \tag{C.59}$$

The spectrum of $\mathbb{E}[S_B]$ is $\{-n^2\mu_B$ (mult. $n-1$), 0 (eigenvector $\mathbf{1}$)$\}$.

Equations (C.58) and (C.59) share the same centring-matrix form. The two sectors differ only in the scalar prefactor ($-n\mu_A$ versus $-n^2\mu_B$), reflecting the different combinatorial footprint of pairwise versus three-way interactions: a pairwise row aggregates $O(n)$ entries whereas an HOI slice aggregates $O(n^2)$. In both cases, facilitative means ($\mu_A, \mu_B > 0$) produce a negative spike in the $(n-1)$-dimensional subspace orthogonal to $\mathbf{1}$, while competitive means ($\mu_A, \mu_B < 0$) produce a positive spike. This is the structural basis for the regime-dependent choice of spectral thresholds in Sec. C.4.

C.8 Scaling of the spectral thresholds

Both δ_A and δ_B are determined by top eigenvalues of random symmetric matrices with zero-sum diagonal structure; the only differences are the entry variance and, when $\mu_A \neq 0$ or $\mu_B \neq 0$, the deterministic mean-field spike derived in Appendix C.7. We derive the common scaling via Weyl's inequality, the semicircle law, and the asymptotics of Gaussian maxima, treating both sectors in parallel.

General strategy. For $S \in \{S_A, S_B\}$, we decompose $S = \mathbb{E}[S] + \tilde{S}$, where $\tilde{S}$ is the centred (zero-mean) fluctuation. In the baseline and facilitative regimes the threshold is set by $\lambda_{\max}(\tilde{S})$; in the competitive regime it is set by $\lambda_{\max}(S)$ itself, which is dominated by the mean-field spike. For the centred part we further decompose $\tilde{S} = W + D$ into a hollow (zero-diagonal) Wigner matrix W and a diagonal D inherited from the zero-sum shift. Weyl's

inequality gives the upper bound $\lambda_{\max}(\tilde{S}) \le \lambda_{\max}(W) + \lambda_{\max}(D)$, and we bound each term separately using the semicircle law and the Gaussian-maximum asymptotic [195]:

$$\max_{1\le i\le n} |Z_i| = \sigma_D \sqrt{2\log n}\,(1 + o(1)) \qquad \text{a.s. as } n \to \infty, \tag{C.60}$$

for i.i.d. $Z_i \sim \mathcal{N}(0, \sigma_D^2)$.

Pairwise threshold δ_A

Baseline and facilitative regimes ($\mu_A \ge 0$). We compute $\lambda_{\max}(\tilde{S}_A)$.

Off-diagonal (Wigner) contribution. For $i \ne j$, $(\tilde{S}_A)_{ij} = \frac{1}{2}(\tilde{A}_{ij} + \tilde{A}_{ji}) - \mu_A$. Since $\tilde{A}_{ij}$ and $\tilde{A}_{ji}$ are independent draws of variance $1/n$, $\mathrm{Var}((\tilde{S}_A)_{ij}) = 1/(2n)$. The hollow part W_A is therefore a Wigner matrix with upper-triangular variance $1/(2n)$, and the semicircle law gives $\lambda_{\max}(W_A) \xrightarrow{a.s.} \sqrt{2}$.

Diagonal contribution. The diagonal of $\tilde{S}_A$ is $\tilde{A}_{ii} + (n-1)\mu_A$. Since $\tilde{A}_{ii} = -\sum_{j\ne i} \tilde{A}_{ij}$ is a sum of $n-1$ independent $\mathcal{N}(\mu_A, n^{-1})$ draws, the centred diagonal has variance $(n-1)/n \to 1$. Applying (C.60) with $\sigma_D = 1$ gives $\lambda_{\max}(D_A) = \sqrt{2\log n}\,(1 + o(1))$.

Combining via Weyl's inequality:

$$\delta_A = \lambda_{\max}(\tilde{S}_A) \le \sqrt{2} + \sqrt{2\log n}\,(1 + o(1)) = O(\sqrt{\log n}). \tag{C.61}$$

Competitive regime ($\mu_A < 0$). The $(n-1)$-fold eigenvalue of $\mathbb{E}[S_A]$ is $+n|\mu_A| > 0$, producing a spike that dominates $\lambda_{\max}(S_A)$. In this regime we set

$$\delta_A = \lambda_{\max}(S_A) \sim n|\mu_A| = O(n), \tag{C.62}$$

so that the threshold absorbs the mean-field spike.

HOI threshold δ_B

Baseline and facilitative regimes ($\mu_B \geq 0$). We compute $\lambda_{\max}(\tilde{S}_B)$.

Off-diagonal (Wigner) contribution. For $i \neq j$, $(\tilde{S}_B)_{ij} = (S_B)_{ij} - n\mu_B$ is $\frac{1}{4}$ times a sum of $4n$ independent centred draws each of variance n^{-2}, so $\mathrm{Var}((\tilde{S}_B)_{ij}) = \frac{1}{16} \cdot 4n \cdot n^{-2} = 1/(4n)$. The hollow part W_B is a Wigner matrix with upper-triangular variance $1/(4n)$, and the semicircle law gives $\lambda_{\max}(W_B) \xrightarrow{a.s.} 1$.

Diagonal contribution. From Appendix C.7, $(S_B)_{ii}$ involves $2n(n-1)$ independent $\mathcal{N}(\mu_B, n^{-2})$ draws with a $\frac{1}{2}$ prefactor, so the centred diagonal has variance $\frac{1}{4} \cdot 2n(n-1) \cdot n^{-2} = (n-1)/(2n) \to 1/2$. Applying (C.60) with $\sigma_D = 1/\sqrt{2}$ gives $\lambda_{\max}(D_B) = \sqrt{\log n}\,(1 + o(1))$.

Combining via Weyl's inequality:

$$\delta_B = \lambda_{\max}(\tilde{S}_B) \leq 1 + \sqrt{\log n}\,(1 + o(1)) = O(\sqrt{\log n}). \tag{C.63}$$

Competitive regime ($\mu_B < 0$). The $(n-1)$-fold eigenvalue of $\mathbb{E}[S_B]$ is $+n^2|\mu_B| > 0$, dominating $\lambda_{\max}(S_B)$. We set

$$\delta_B = \lambda_{\max}(S_B) \sim n^2|\mu_B| = O(n^2). \tag{C.64}$$

Numerical verification

Figure C.8 verifies the bounds numerically. In the baseline regime both thresholds exhibit the predicted $O(\sqrt{\log n})$ scaling and stay well under the Weyl bounds for every replicate; in the competitive regime, the mean-field spike produces the expected $O(n)$ scaling for δ_A and $O(n^2)$ scaling for δ_B, with the empirical means tracking the analytic bounds tightly.

The baseline and facilitative regimes are statistically more similar to each other than either is to the competitive regime, and this gap is a direct consequence of the very differ-

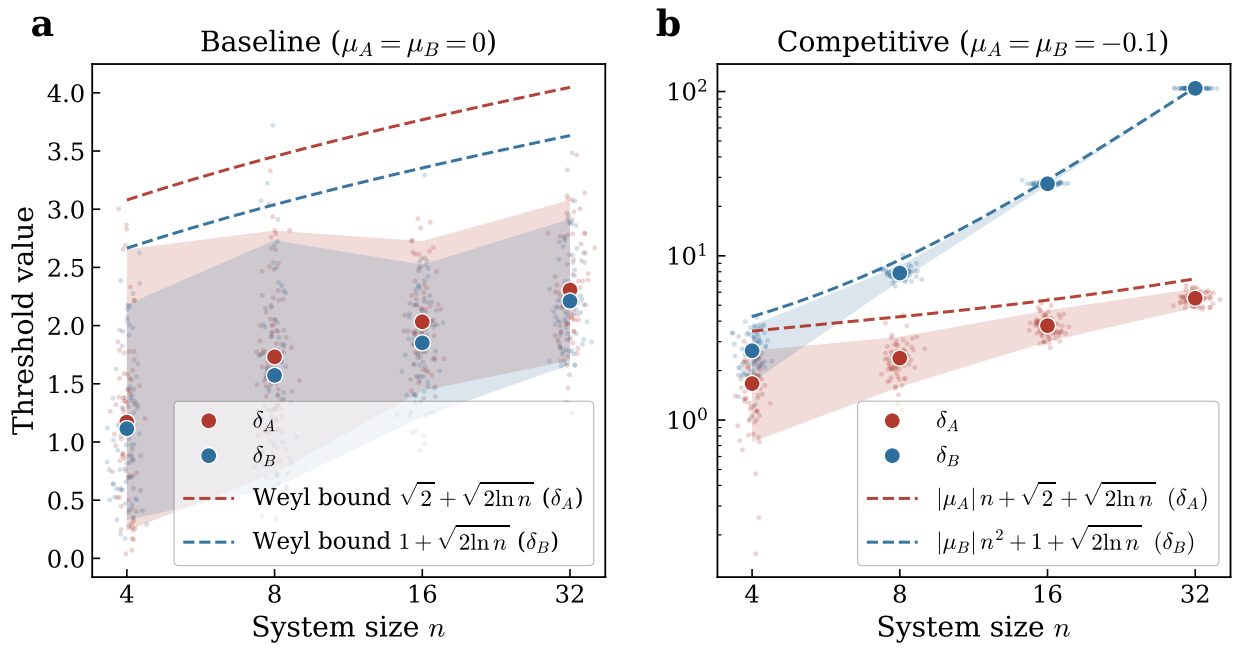

Figure C.8: **Numerical verification of the upper bounds on the spectral thresholds δ_A and δ_B.** Each panel overlays δ_A (red) and δ_B (blue) for system sizes $n \in \{4, 8, 16, 32\}$, with 80 replicate draws per n: semi-transparent dots are individual replicates, filled circles are sample means, and shaded bands are [5, 95]% percentile envelopes. Dashed lines (matching colour) are the analytic upper bounds. **(a)** Baseline regime ($\mu_A = \mu_B = 0$), linear scale. The fluctuations are bounded by the Weyl-type bounds $\sqrt{2} + \sqrt{2\ln n}$ for δ_A and $1 + \sqrt{2\ln n}$ for δ_B (Eqs. (C.61)–(C.63)). **(b)** Competitive regime ($\mu_A = \mu_B = -0.1$), log scale. The deterministic mean-field spike from Appendix C.7 dominates the spectrum, yielding $\delta_A \sim |\mu_A|\, n$ and $\delta_B \sim |\mu_B|\, n^2$; the plotted bounds add the centred-fluctuation Weyl correction to this mean-field contribution. The facilitative regime ($\mu_A, \mu_B > 0$) is omitted: after the bank's mean-field centring, its δ_A and δ_B distributions coincide with the baseline.

ent scaling of δ_A and δ_B. After the mean-field centring applied in Sec. C.4, the baseline and facilitative regimes share the same centred-Wigner spectrum and the same $O(\sqrt{\log n})$ thresholds; in the competitive regime, no analogous centring is available because the rank-$(n-1)$ spike is positive and must be absorbed into the threshold itself. This is the price we pay for guaranteeing linear stability of the unperturbed coexistence equilibrium uniformly in α: imposing global stability under purely competitive interactions is known to require strong self-regulation [77] (Chapter 1), and here that requirement is enforced by inflating δ_A

and δ_B to $O(n)$ and $O(n^2)$ respectively. The downstream consequence for the dynamics is that, after rescaling, the HOI-tensor entries satisfy $|B_{ijk}| \sim |\mu_B|^{-1} n^{-3}$ in the competitive case, against $|B_{ijk}| \sim 1/(n\sqrt{\log n})$ in the other two regimes — two orders of magnitude smaller in n for moderate system sizes. The cubic term therefore contributes negligibly to the per-capita Jacobian until α approaches one, which is also why fold bifurcations — whose existence requires the HOI contribution to be commensurate with the pairwise contribution — are scarce in the competitive simulations and only emerge at large α.

C.9 Derivation of α_{eff}^{Taylor}

To derive the closed form equivalence between the model-agnostic local nonlinearity measure α_{eff}^{Taylor} proposed in Section C.6.1, start by differentiating f_i (bracketed terms in Eq. C.1) once, which yields

$$J_{ij} \;=\; (1-\alpha)\, A_{ij} \;+\; \alpha \sum_{l=1}^{n} \Big(B_{ijl} + B_{ilj} \Big). \tag{C.65}$$

Summing over j with $x_j^\star = 1$ and applying Eq. C.14,

$$\begin{aligned} T_1[i] \;=\; \sum_j J_{ij} \;&=\; (1-\alpha) \sum_j A_{ij} \;+\; \alpha \sum_{j,l} \Big(B_{ijl} + B_{ilj} \Big) \\ &=\; (1-\alpha)(-1) \;+\; 2\alpha\,(-1) \;=\; -(1+\alpha). \end{aligned} \tag{C.66}$$

Differentiating a second time gives

$$H_{ijk} \;=\; \alpha \Big(B_{ijk} + B_{ikj} \Big), \tag{C.67}$$

so that at $\mathbf{x}^\star = \mathbf{1}_n$,

$$T_2[i] \;=\; \tfrac{1}{2}\sum_{j,k} H_{ijk} \;=\; \tfrac{\alpha}{2}\sum_{j,k}\Big(B_{ijk} + B_{ikj}\Big) \;=\; \alpha\sum_{j,k} B_{ijk} \;=\; -\alpha, \tag{C.68}$$

where the penultimate equality uses the relabeling $j \leftrightarrow k$, and the last equality uses the slice-sum constraint in Eq. C.14. Both $T_1[i]$ and $T_2[i]$ are independent of i, so averaging their absolute values over species gives, for $\alpha \in [0, 1]$,

$$P \;=\; 1 + \alpha, \qquad Q \;=\; \alpha, \tag{C.69}$$

and substituting into Eq. (C.34) yields the closed form equivalence between α and α_{eff}^{Taylor} in Eq. (C.35).

C.10 Regimes in Gibbs et. al (2024)

Here we describe in detail the parameterizations used for the robustness check, which are the same used by Gibbs et al. All parameterizations use $S = 20$ species.

Regime Q1 (Dirichlet-constrained HOIs, varying pairwise strength). Off-diagonal entries of A are drawn from Normal(μ_A, σ_A) with self-regulation fixed at $A_{ii} = 1$. Two parameter sweeps are combined: (i) $\mu_A \in [-0.75, 0.25]$ with $\sigma_A \in \{0, 0.1\}$; (ii) $\mu_A \in \{-1/S, 0, 1/S\}$ with $\sigma_A \in [0.7/\sqrt{S}, 1.6/\sqrt{S}]$. The target equilibrium is $\mathbf{x}^\star = (R_1/A_{11})\,\mathbf{1}$ (unit carrying capacity when $R_i = A_{ii} = 1$). HOI coefficients B_{ijk} are determined by distributing the per-species residual $R_i - \sum_j A_{ij}x_j^\star$ across distinct pairs (j, k) with $j \neq i$, $k \neq i$ using symmetric Dirichlet weights, so that all B_{ijk} share the sign of the residual. When pairwise interactions are net facilitative this yields non-negative (competitive) HOIs, corresponding to the high-stability region identified in Fig. 2 of Gibbs et al.

Regime Q2 (varying target abundances). Two sub-grids are combined. (i) *Specified abundance*: $\mu_A \in \{-0.5/S,\, 0.5/S\}$, $\sigma_A = 0.15$, and the target equilibrium is a constant vector $\mathbf{x}^\star = x_0\,\mathbf{1}$ with $x_0 \in [0.01,\, 1.99,\, 10]$; HOI coefficients are sampled via the same Dirichlet construction as Q1. (ii) *Noisy carrying capacity*: $\mu_A = 0.5/S$, $\sigma_A \in \{0,\, 1/\sqrt{S}\}$, and $\mathbf{x}^\star$ is drawn near the carrying capacity R_i/A_{ii} with additive Gaussian noise of standard deviation $\eta \in \text{linspace}(0,\, 0.75,\, 10)$, clipped to a minimum of 0.01 and rescaled to preserve the mean; HOI coefficients use a non-equal-abundance Dirichlet construction in which each weight is divided by $x_j^\star x_k^\star$. In both sub-grids, $A_{ii} = 1$ and HOI coefficients can take either sign, corresponding to the moderate-stability region in Fig. 3 of Gibbs et al.

Regime Q3 (correlation-stabilized, strong interactions). Off-diagonal entries of A are drawn with $\mu_A \in \{-0.5/S,\, 0,\, 0.5/S\}$ and $\sigma_A \in \text{linspace}(0.5,\, 1.5,\, 3)$, allowing strong pairwise interactions. The aggregated HOI effect matrix $\tilde{B}_{ij} = \sum_k (B_{ijk} + B_{ikj}) x_k^\star$ is constructed as

$$\tilde{B}_{ij} = -p\, A_{ij} + (1-p)\, Y_{ij}, \tag{C.70}$$

where the random component Y_{ij} is initialized from $\text{Uniform}(0, 1/S)$ and then adjusted to satisfy the row-sum constraint $\sum_j \tilde{B}_{ij} = 2(R_i - \sum_j A_{ij})$, with anti-correlation strength $p \in \text{linspace}(0.1,\, 1.0,\, 10)$. This ensures that the HOI and pairwise contributions to the Jacobian have opposing sign structure—a mechanism that confers near-certain stability even with strong interactions (Fig. 4c of Gibbs et al.). The full tensor B_{ijk} is obtained by distributing $\tilde{B}_{ij}$ across the k-indices.

C.11 Pseudocode of main pipeline

Here we describe with pseudocode the main pipeline use in the manuscript covering the four stages: model bank generation, boundary scan, post-boundary dynamics, and backtrack

analysis.

Algorithm C.1 Tipping-point pipeline for GLV+HOI communities. Each stage reads and enriches the same per-model record $\mathcal{M}$.

Require: dimensions n, models per n (N_{mod}), ray count N_{dir}, interaction means (μ_A, μ_B), base seed s_0, grid $\mathcal{A} \subset [0, 1]$, $\delta_{\max}$, $\eta \in (0, 1)$

for each (n, m) with $m = 1, \ldots, N_{\text{mod}}$ **do**

  $\mathcal{M} \leftarrow \textsc{GenerateBank}(n, s_0 + m, \mu_A, \mu_B, N_{\text{dir}})$ ▷ Stage 1

  $\mathcal{M} \leftarrow \textsc{BoundaryScan}(\mathcal{M}, \mathcal{A}, \delta_{\max}, \eta)$ ▷ Stage 2

  $\mathcal{M} \leftarrow \textsc{PostBoundaryDynamics}(\mathcal{M}, 2 - \eta)$ ▷ Stage 3

  $\mathcal{M} \leftarrow \textsc{BacktrackPerturbation}(\mathcal{M})$ ▷ Stage 4

end for

Algorithm C.2 GENERATEBANK — sample one stable GLV+HOI system with planted equilibrium $x^\star = \mathbf{1}$ and N_{dir} uniform rays on S^{n-1}.

Require: n, seed s, (μ_A, μ_B), N_{dir}

repeat

  $A_0 \sim \mu_A + \mathcal{N}(0, 1/n)^{n\times n}$; set $A_0[i,i] \leftarrow -\sum_{j\neq i} A_0[i,j]$

  $S_A \leftarrow \frac{1}{2}(A_0 + A_0^\top)$

  if $\mu_A > 0$ **then** $\delta_A \leftarrow \lambda_{\max}\big(S_A - \mathbb{E}[S_A]\big)$

  else $\delta_A \leftarrow \lambda_{\max}(S_A)$

  end if

  $A \leftarrow A_0/\delta_A - I$ ▷ row sums $= -1$

  $B_0 \sim \mu_B + \mathcal{N}(0, 1/n^2)^{n\times n\times n}$; set $B_0[i,i,i] \leftarrow -\sum_{j,k\neq(i,i)} B_0[j,k,i]$

  Form $\widehat{B}_0[i,j] = \sum_k (B_0[j,k,i] + B_0[k,j,i])$; $\widetilde{S} \leftarrow \widehat{B}_0 + \widehat{B}_0^\top$

  $\delta_B \leftarrow \lambda_{\max}(\widetilde{S})/4$ (centred when $\mu_B > 0$)

  $B \leftarrow B_0/\delta_B$; $B[i,i,i] -= 1$

until $\lambda_{\max}\big(\frac{A+A^\top}{2}\big) < 0$ **and** $\lambda_{\max}\big(\frac{\widehat{B}+\widehat{B}^\top}{2}\big) < 0$

$r \leftarrow \mathbf{1}$ ▷ so $f_i(\mathbf{1}) = 0$ for every α

Sample $U \in \mathbb{R}^{n\times N_{\text{dir}}}$, columns i.i.d. uniform on S^{n-1}

return $\mathcal{M} = (n, r, A, B, U, x^\star = \mathbf{1})$

Algorithm C.3 BoundaryScan — for each (α, u) continue the equilibrium branch of $f_i(x;\, r_0 + \delta u) = r_i + (1-\alpha)(Ax)_i + \alpha(Bxx)_i = 0$ along the ray until an exit event.

Require: $\mathcal{M}$, grid $\mathcal{A}$, $\delta_{\max}$, pre-boundary fraction η

for $\alpha \in \mathcal{A}$ **do**
  Build polynomial system $F_\alpha(x; p) = f(x;\, r_0 + p)$ with parameters $p \in \mathbb{R}^n$
  for u in columns of U **do**
    $p_{\text{tgt}} \leftarrow \delta_{\max}\, u$; initialise tracker at $(x^\star,\, p = 0)$
    while tracking **do**
      step the parameter homotopy $p(t) = (1-t)p_{\text{start}} + t\, p_{\text{tgt}}$
      if $\min_i x_i(t) \le \epsilon_{>0}$ **then return** *event* = negative
      else if $\lambda_{\max}\big(\operatorname{diag}(x)\, J_f(x;p)\big) > \lambda_{\text{tol}}$ **then return** *event* = unstable
      else if tracker reports turning point **then return** *event* = fold
      end if
    end while
    Bisect on t (depth $\le K$, tol τ) to refine t_c
    $\delta r_c \leftarrow (1 - t_c)\, p_{\text{tgt}}$; $\delta_c \leftarrow \|\delta r_c\|$
    $x_{\text{pre}} \leftarrow$ track from $x^\star$ to $p = \eta\, \delta r_c$
    Store $\{event, \delta_c, \delta r_c, x_{\text{pre}}, x_c\}$
  end for
end for
▷ $\alpha = 0$ (pairwise) uses the closed-form linear fallback $x(\delta) = x^\star - \delta A^{-1} u$ with the same bisection.
return $\mathcal{M}$ enriched with `scan_results`

Algorithm C.4 PostBoundaryDynamics — integrate the GLV+HOI ODE just past the boundary and snap onto the resulting attractor.

Require: $\mathcal{M}$ with `scan_results`; post-boundary fraction $\rho > 1$

for each row $(\alpha, u, \delta_c, x_{\text{pre}})$ in `scan_results` **do**

  $\delta_{\text{post}} \leftarrow \rho\,\delta_c$; $r_{\text{post}} \leftarrow r_0 + \delta_{\text{post}}\,u$

  Solve $\dot{x}_i = x_i\Big(r_i + (1-\alpha)(Ax)_i + \alpha(Bxx)_i\Big)$ with $x(0) = x_{\text{pre}}$, $r = r_{\text{post}}$, solver `Tsit5`

  extinction callback: whenever $x_i < \epsilon_{\text{ext}}$, set $x_i \leftarrow 0$

  stop once every surviving species has $|f_i| < \tau_{\text{rate}}$

  if no extinction by $T_{\max}$ **then** extend window once to $2T_{\max}$

  end if

  $x_{\text{post}} \leftarrow$ final state, with $x_i < \tau_+$ clamped to 0

  Store $\{x_{\text{post}}, n_{\text{lost}}, \textit{snap_reason}\}$

end for

return $\mathcal{M}$ enriched with `post_dynamics_results`

Algorithm C.5 BacktrackPerturbation — homotopy-continue the post-boundary attractor back toward $\delta = 0$ to test reversibility.

Require: $\mathcal{M}$ with `post_dynamics_results`

for each row $(\alpha, u, \delta_{\text{post}}, x_{\text{post}})$ **do**

  $S \leftarrow \{i : x_{\text{post},i} > \tau_+\}$ ▷ active support

  Restrict (r_0, A, B, u) to S; build F_α^S

  $p_{\text{start}} \leftarrow \delta_{\text{post}}\, u_S$; $\quad p_{\text{tgt}} \leftarrow 0$

  Track from $x_{\text{post}}|_S$ along $p(t)$, monitoring:

  (i) **stability** of restricted Jacobian ($\lambda_{\max} > \lambda_{\text{tol}}$),

  (ii) **invasion** by some $j \notin S$ ($f_j(x;\, r_0 + \delta u) > \tau_{\text{inv}}$),

  (iii) **negativity** ($\min_i x_i < \epsilon_{>0}$)

  if tracker reaches $p = 0$ without event **then**

    class $\leftarrow$ success_to_zero; $\delta_{\text{return}} \leftarrow 0$

  else

    Bisect to localise δ_{event}; $\delta_{\text{probe}} \leftarrow \delta_{\text{event}} - \delta_s$

    Build seeded state: $x_{\text{seed}} \leftarrow x_{\text{pre}}|_S$, add small invasion amplitude on S^c

    Integrate ODE at $r_0 + \delta_{\text{probe}} u$ with extinction callback

    Classify outcome: returned_n if all n species alive, else boundary_persist or other_attractor

    $\delta_{\text{return}} \leftarrow \delta_{\text{post}}$ if returned_n, else δ_{probe}

  end if

  $rev \leftarrow \text{clamp}\Big((\delta_{\text{post}} - \delta_{\text{return}})/\delta_{\text{post}},\, 0,\, 1\Big)$

  Store $\{\mathit{class}, \delta_{\text{return}}, \mathit{rev}\}$ ▷ hysteresis $\Leftrightarrow$ $rev < 1$

end for

return $\mathcal{M}$ enriched with `backtrack_results`

C.12 Full simulation results figures

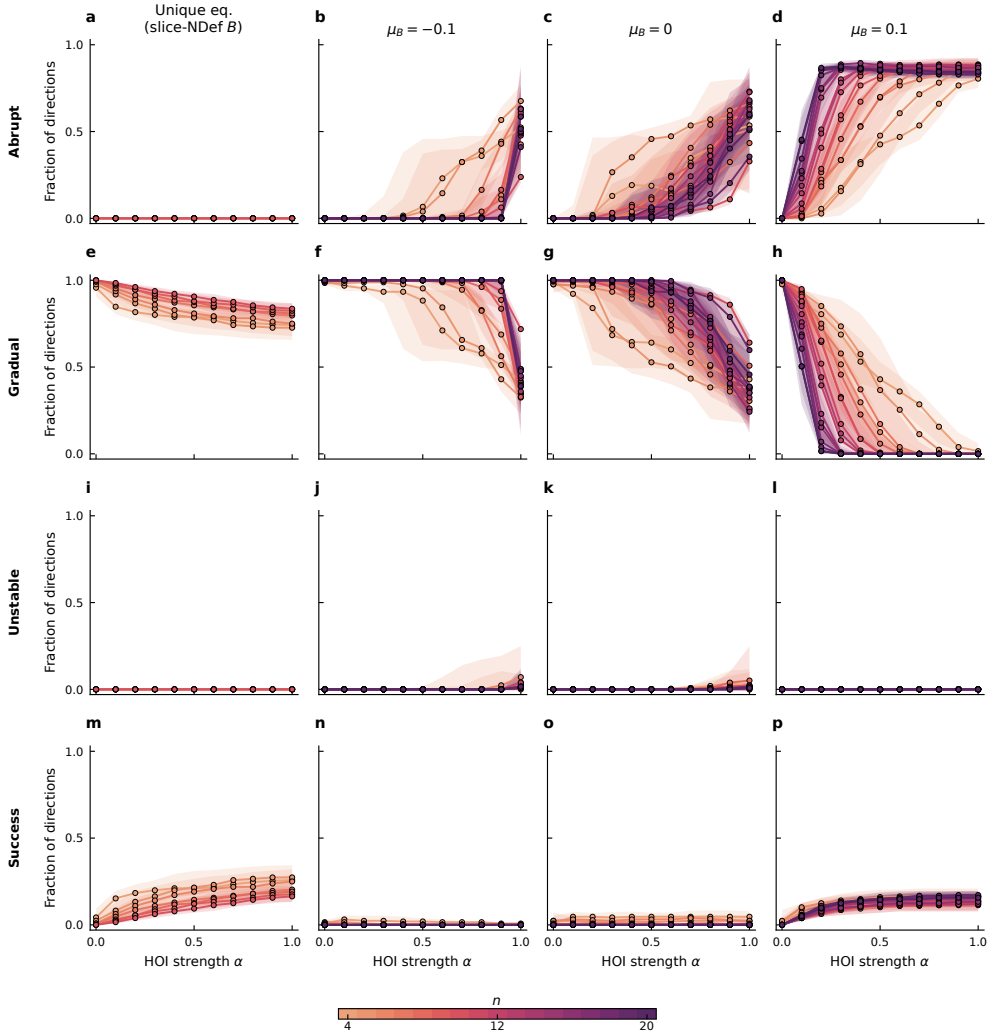

Figure C.9: **Boundary-type prevalence as a function of HOI strength across four simulation banks.** Fraction of perturbation directions leading to each boundary type as a function of HOI strength α, across community sizes $n = 4$–20. Columns correspond to four simulation banks: unique equilibrium parameterization, $\mu_B = -0.1$, $\mu_B = 0$, and $\mu_B = 0.1$. Rows show the fraction of directions classified as abrupt (**a**–**d**), gradual (**e**–**h**), unstable (**i**–**l**), and successful (**m**–**p**). Lines indicate medians across model replicates; shaded bands span the interquartile range. Colours encode community size n. As α increases, the fraction of abrupt boundaries grows while gradual boundaries decline, with the transition sharpening for larger n and positive μ_B. The successful-direction fraction increases monotonically with α and n for the unique equilibrium and facilitative parameterizations, while it remains very low for the competitive and mixed parameterizations.

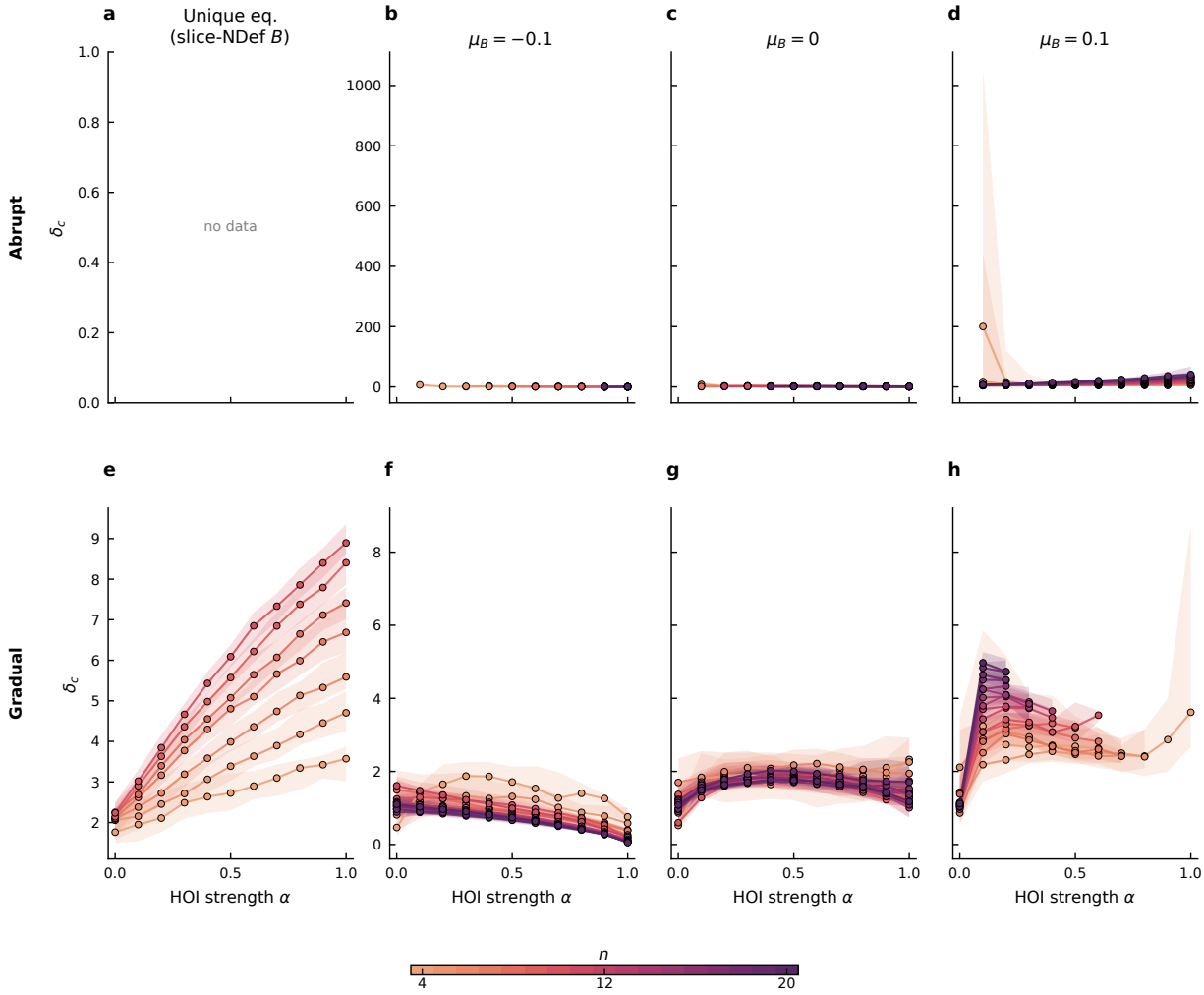

Figure C.10: **Critical perturbation magnitude δ_c across HOI strength and four simulation banks.** δ_c is shown as a function of HOI strength α, across community sizes $n = 4$–20. Columns correspond to four simulation banks: unique equilibrium, $\mu_B = -0.1$, $\mu_B = 0$, and $\mu_B = 0.1$. Rows show δ_c for abrupt (**a**–**d**) and gradual (**e**–**h**) boundary types. Lines indicate medians across model replicates; shaded bands span the interquartile range. Colours encode community size n. Panel **a** display "no data" because the abrupt boundary type is absent for the unique equilibrium parameterization.

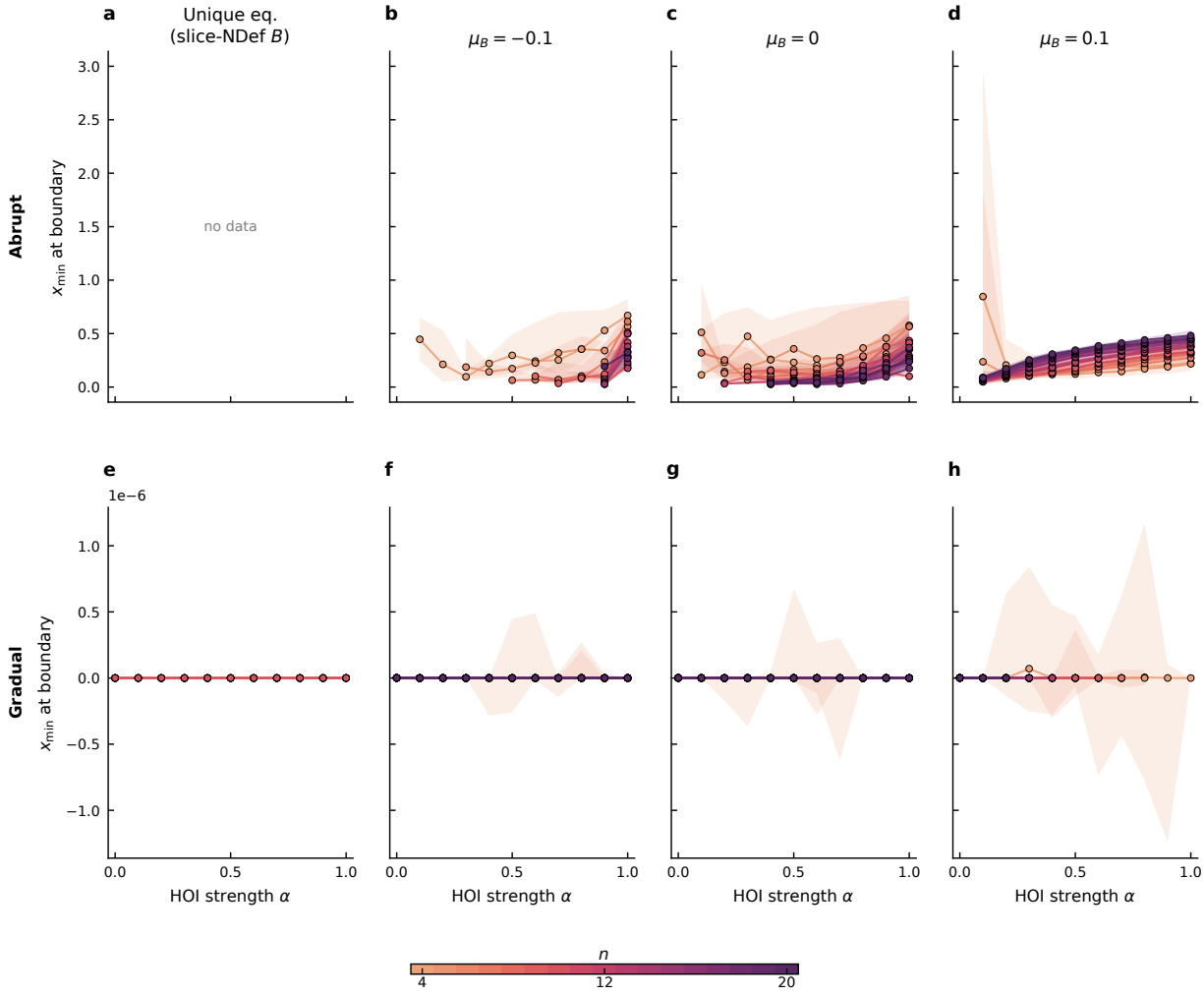

Figure C.11: **Minimum species abundance $x_{\min}$ at the boundary across HOI strength and four simulation banks.** $x_{\min}$ at the tipping boundary is shown as a function of HOI strength α, across community sizes $n = 4$–20. Columns correspond to four simulation banks: unique equilibrium, $\mu_B = -0.1$, $\mu_B = 0$, and $\mu_B = 0.1$. Rows show $x_{\min}$ for abrupt (**a**–**d**) and gradual (**e**–**h**) boundary types. Lines indicate medians across model replicates; shaded bands span the interquartile range. Colours encode community size n. For abrupt boundaries, $x_{\min}$ remains strictly positive, confirming that species abundances have not yet reached zero when the fold bifurcation occurs. For gradual boundaries, $x_{\min}$ is effectively zero ($\sim 10^{-6}$), consistent with the boundary being defined by a species abundance crossing zero.

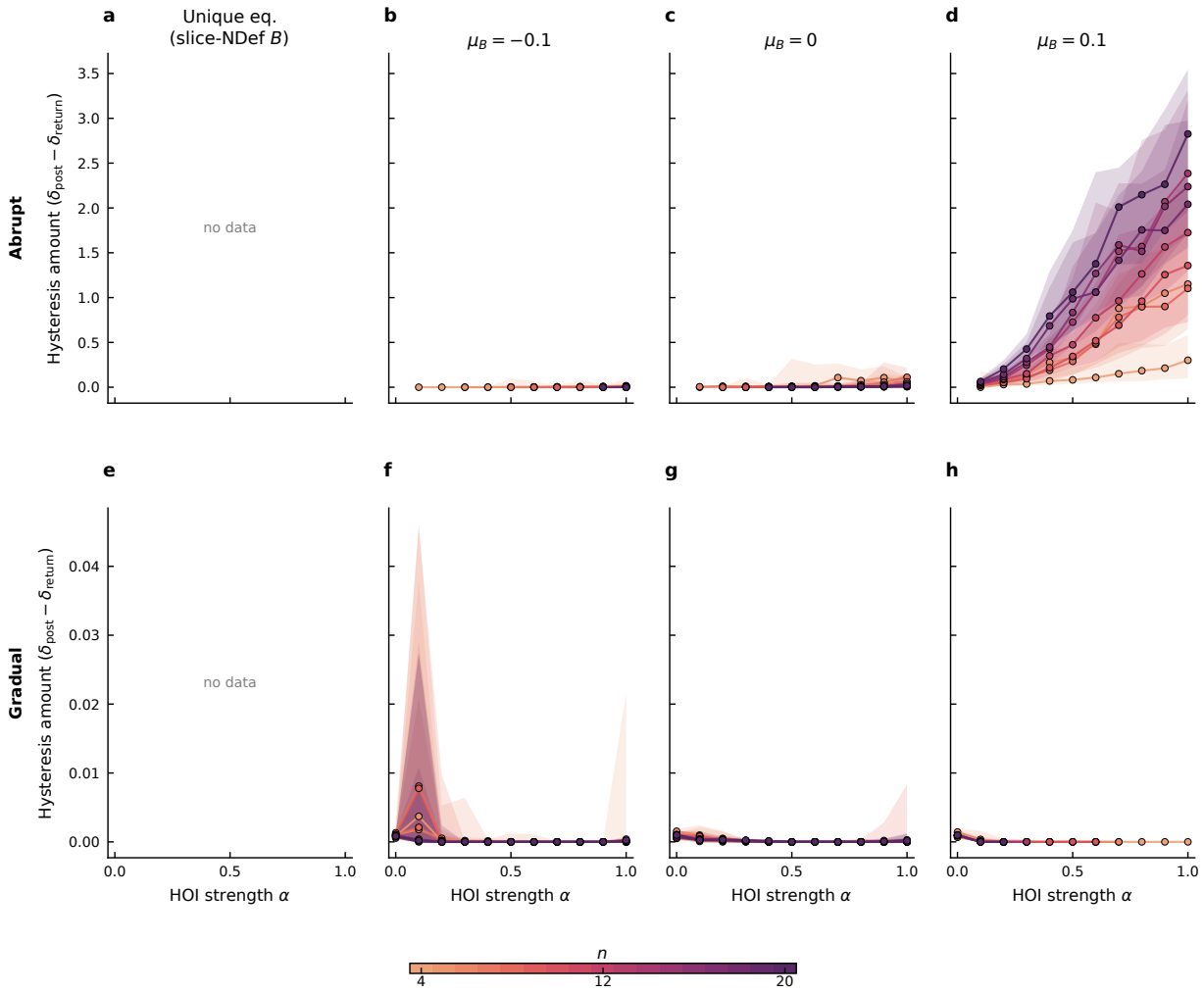

Figure C.12: **Hysteresis amount** ($\delta_c - \delta_{\text{recover}}$) **across HOI strength and four simulation banks.** The hysteresis amount is shown as a function of HOI strength α, across community sizes $n = 4$–20. Columns correspond to four simulation banks: unique equilibrium, $\mu_B = -0.1$, $\mu_B = 0$, and $\mu_B = 0.1$. Rows show hysteresis for abrupt (**a**–**d**) and gradual (**e**–**h**) boundary types. The hysteresis amount measures the difference between the forward critical perturbation and the perturbation at which the system returns to its original state upon reversal. Lines indicate medians across model replicates; shaded bands span the interquartile range. Colours encode community size n. Abrupt boundaries exhibit hysteresis while gradual ones do not, consistent with the irreversibility expected from fold bifurcations.

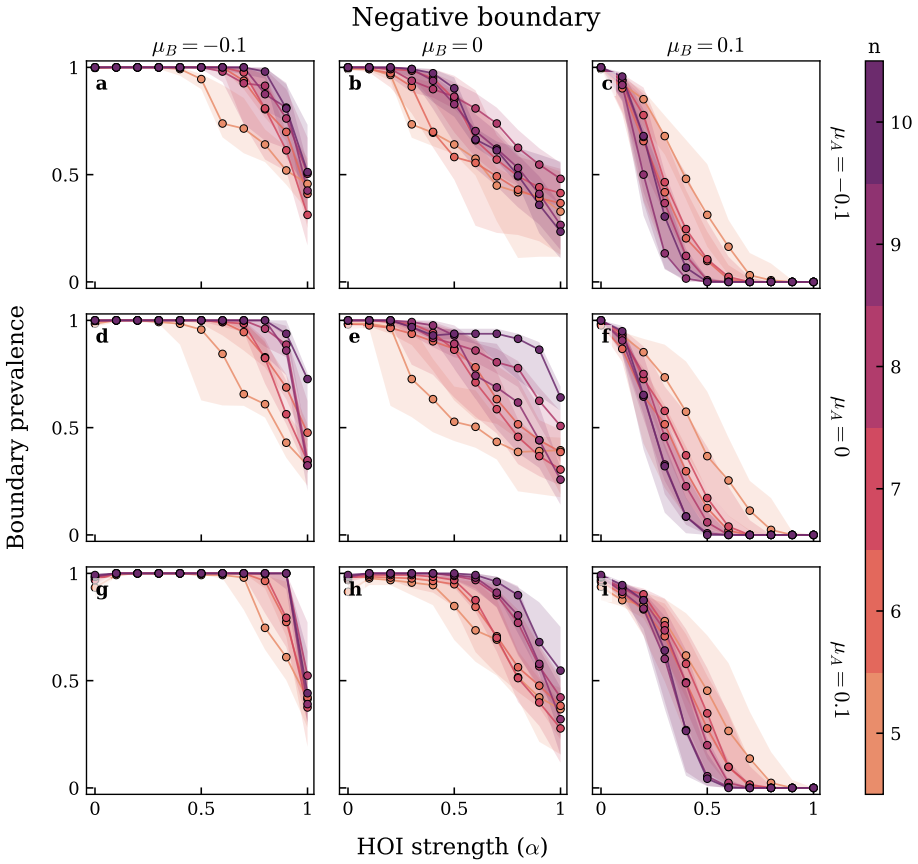

Figure C.13: **Gradual (negative-transcritical) boundary prevalence across the (μ_A, μ_B) plane.** Each panel shows the fraction of perturbation directions terminating at a gradual boundary as a function of HOI strength α, for community sizes $n = 5$–10 (colours). Columns vary the mean higher-order interaction $\mu_B \in \{-0.1, 0, 0.1\}$; rows vary the mean pairwise interaction $\mu_A \in \{-0.1, 0, 0.1\}$. Points are medians across 50 community replicates at each (n, α) condition; shaded bands span the interquartile range. Companion to Fig. C.3 for the gradual boundary class.

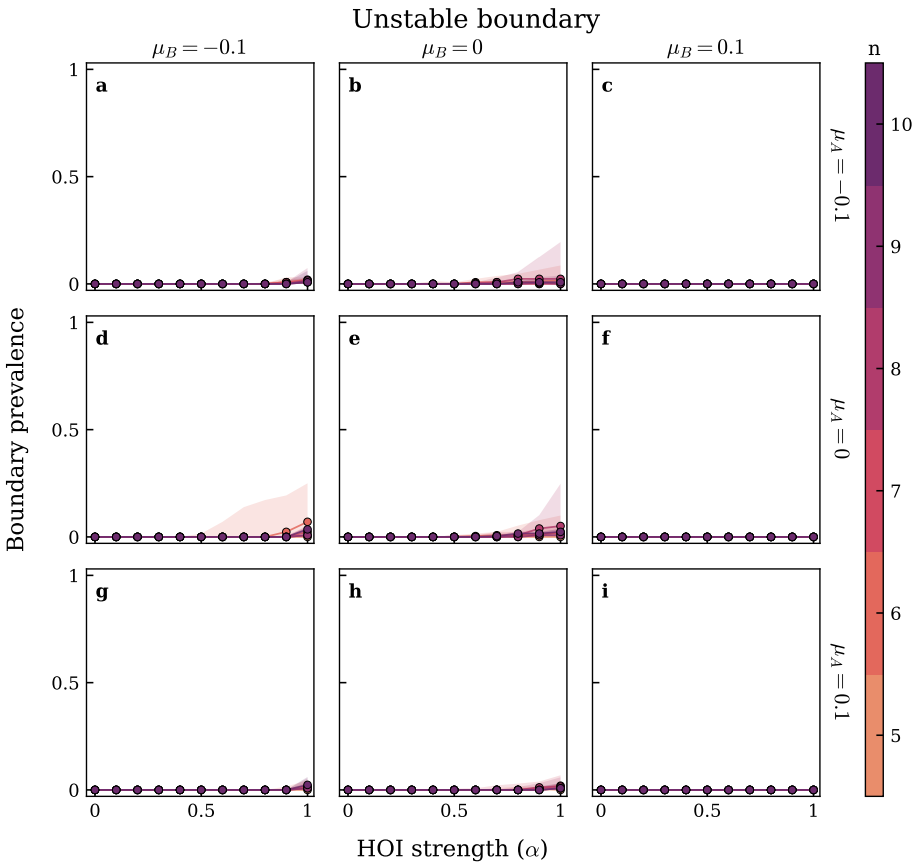

Figure C.14: **Unstable-boundary prevalence across the (μ_A, μ_B) plane.** Each panel shows the fraction of perturbation directions terminating at an unstable (Hopf-type) boundary as a function of HOI strength α, for community sizes $n = 5$–10 (colours). Columns vary the mean higher-order interaction $\mu_B \in \{-0.1, 0, 0.1\}$; rows vary the mean pairwise interaction $\mu_A \in \{-0.1, 0, 0.1\}$. Points are medians across 50 community replicates at each (n, α) condition; shaded bands span the interquartile range. Companion to Fig. C.3 for the unstable-boundary class.

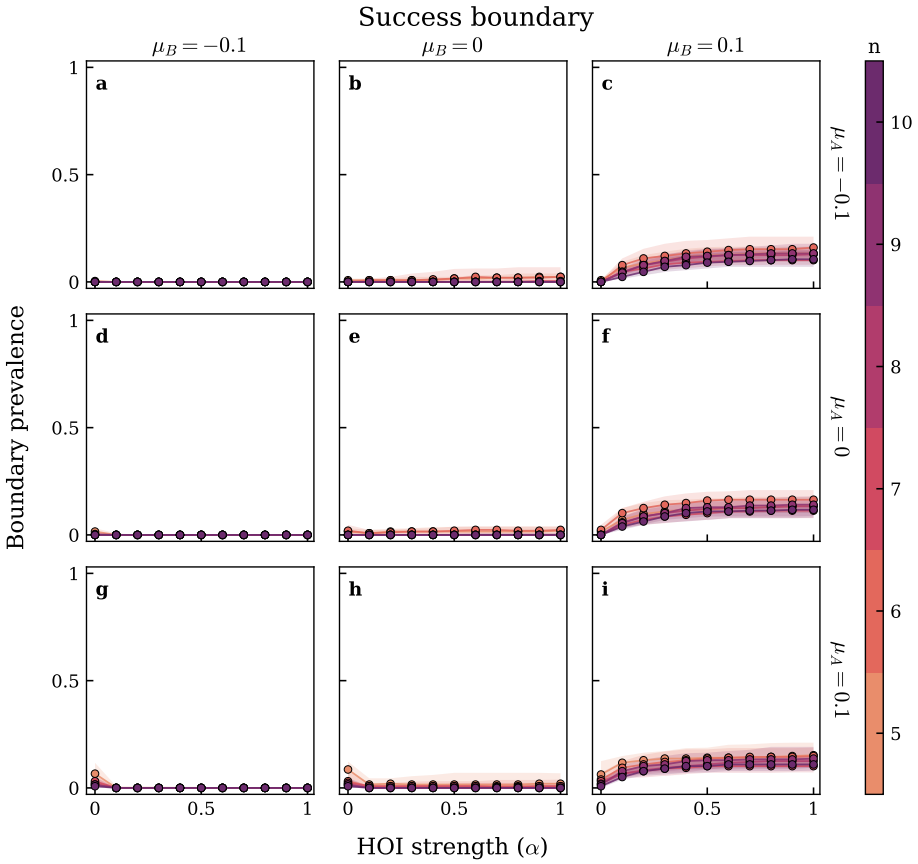

Figure C.15: **Successful-direction prevalence across the (μ_A, μ_B) plane.** Each panel shows the fraction of perturbation directions classified as successful (no boundary reached within the sampled δ range) as a function of HOI strength α, for community sizes $n = 5$–10 (colours). Columns vary the mean higher-order interaction $\mu_B \in \{-0.1, 0, 0.1\}$; rows vary the mean pairwise interaction $\mu_A \in \{-0.1, 0, 0.1\}$. Points are medians across 50 community replicates at each (n, α) condition; shaded bands span the interquartile range. Companion to Fig. C.3 for the successful-direction class.

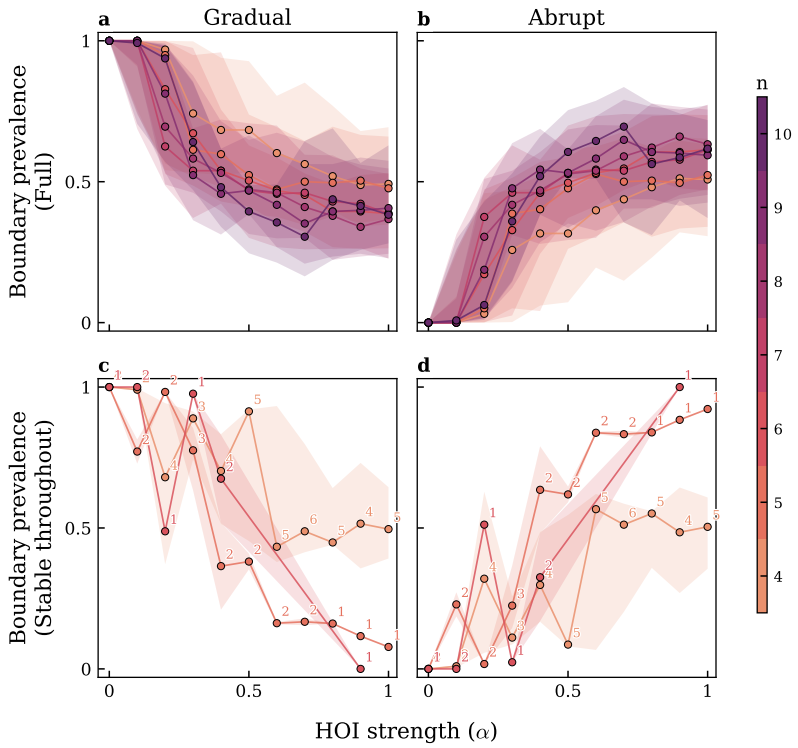

Figure C.16: **Boundary-type prevalence under the purely competitive parameterization.** Each panel shows the fraction of perturbation directions terminating at a given boundary type as a function of HOI strength α, for community sizes $n = 4$–10 (colours). Columns correspond to abrupt (fold) and gradual (negative-transcritical) boundaries. **Top row:** full bank, containing every replicate with a feasible equilibrium at $\alpha = 0$, including those that later lose stability as α increases. **Bottom row:** stable-throughout subset, restricted to replicates whose coexistence equilibrium $\mathbf{x}^\star = \mathbf{1}$ remains locally stable across the entire α grid, matching the stability condition imposed by construction in the main-text protocol. Points are medians across replicates; bars span the interquartile range. Numerals in the bottom row report the replicate count contributing to each point. In both subsets, fold prevalence rises monotonically with α while gradual-boundary prevalence falls, matching the qualitative pattern of the main text and of Fig. C.3. The signature therefore persists in a sampling protocol that removes both the zero-sum-diagonal construction and the spectral rescaling used in the main text, retaining only a planted equilibrium for a purely competitive community.

REFERENCES

[1] Stefano Allesina. One Hundred Years of Lotka–Volterra Models. *Annual Review of Ecology, Evolution, and Systematics*, September 2026. doi:10.1146/annurev-ecolsys-102924-040829.

[2] Richard Levins. The Strategy of Model Building in Population Biology. *American Scientist*, 54(4):421–431, 1966.

[3] Peter A. Abrams. Arguments in Favor of Higher Order Interactions. *The American Naturalist*, 121(6):887–891, 1983. ISSN 0003-0147.

[4] Andrew D. Letten and Daniel B. Stouffer. The mechanistic basis for higher-order interactions and non-additivity in competitive communities. *Ecology Letters*, 22(3): 423–436, 2019. ISSN 1461-0248. doi:10.1111/ele.13211.

[5] Andrew R. Kleinhesselink, Nathan J. B. Kraft, Stephen W. Pacala, and Jonathan M. Levine. Detecting and interpreting higher-order interactions in ecological communities. *Ecology Letters*, 25(7):1604–1617, 2022.

[6] Alfred J. Lotka. Analytical note on certain rhythmic relations in organic systems. *Proceedings of the National Academy of Sciences*, 6(7):410–415, July 1920. ISSN 1091-6490. doi:10.1073/pnas.6.7.410. URL http://dx.doi.org/10.1073/pnas.6.7.410.

[7] VITO VOLTERRA. Fluctuations in the abundance of a species considered mathematically. *Nature*, 118(2972):558–560, October 1926. ISSN 1476-4687. doi:10.1038/118558a0. URL http://dx.doi.org/10.1038/118558a0.

[8] John H. Vandermeer. The Competitive Structure of Communities: An Experimental Approach with Protozoa. *Ecology*, 50(3):362–371, 1969. ISSN 1939-9170. doi:10.2307/1933884.

[9] Jonathan M. Levine, Jordi Bascompte, Peter B. Adler, and Stefano Allesina. Beyond pairwise mechanisms of species coexistence in complex communities. *Nature*, 546 (7656):56–64, June 2017.

[10] Michael Shub and Steve Smale. Complexity of Bezout's Theorem II Volumes and Probabilities. In *Computational Algebraic Geometry*, pages 267–285. Birkhäuser Boston, 1993. doi:10.1007/978-1-4612-2752-6_19.

[11] Andrew J Sommese and Charles W Wampler. *The Numerical Solution of Systems of Polynomials Arising in Engineering and Science*. WORLD SCIENTIFIC, March 2005.

[12] Robert M. May. Will a Large Complex System be Stable? *Nature*, 238(5364):413–414, August 1972. ISSN 1476-4687. doi:10.1038/238413a0.

[13] Alan Edelman and Eric Kostlan. How many zeros of a random polynomial are real? *Bulletin of the American Mathematical Society*, 32(1):1–37, 1995. doi:10.1090/s0273-0979-1995-00571-9.

[14] Josef Hofbauer and Karl Sigmund. *Evolutionary Games and Population Dynamics*. Cambridge University Press, 1 edition, May 1998. ISBN 978-0-521-62365-0 978-0-521-62570-8 978-1-139-17317-9. doi:10.1017/CBO9781139173179.

[15] Jurij A. Kuznetsov. *Elements of applied bifurcation theory*. Number 112 in Applied mathematical sciences. Springer, New York Berlin Heidelberg, third edition edition, 2004.

[16] ALAN ROBERTS. The stability of a feasible random ecosystem. *Nature*, 251(5476): 607–608, October 1974. ISSN 1476-4687. doi:10.1038/251607a0. URL http://dx.doi.org/10.1038/251607a0.

[17] B.S. Goh and L.S. Jennings. Feasibility and stability in randomly assembled lotka-volterra models. *Ecological Modelling*, 3(1):63–71, February 1977. ISSN 0304-3800. doi:10.1016/0304-3800(77)90024-2. URL http://dx.doi.org/10.1016/0304-3800(77)90024-2.

[18] Lewi Stone. The feasibility and stability of large complex biological networks: A random matrix approach. *Scientific Reports*, 8(1):8246, May 2018. ISSN 2045-2322. doi:10.1038/s41598-018-26486-2.

[19] Pierre Bizeul and Jamal Najim. Positive solutions for large random linear systems. *Proceedings of the American Mathematical Society*, 149(6):2333–2348, March 2021. ISSN 0002-9939, 1088-6826. doi:10.1090/proc/15383.

[20] Maxime Clenet, Hafedh El Ferchichi, and Jamal Najim. Equilibrium in a large lotka–volterra system with pairwise correlated interactions. *Stochastic Processes and their Applications*, 153:423–444, November 2022. ISSN 0304-4149. doi:10.1016/j.spa.2022.08.004. URL http://dx.doi.org/10.1016/j.spa.2022.08.004.

[21] V. L. Girko. Elliptic law. *Theory of Probability & Its Applications*, 30(4):677–690, December 1986. ISSN 1095-7219. doi:10.1137/1130089. URL http://dx.doi.org/10.1137/1130089.

[22] Stefano Allesina and Si Tang. Stability criteria for complex ecosystems. *Nature*, 483 (7388):205–208, March 2012. ISSN 1476-4687. doi:10.1038/nature10832.

[23] Niels Henrik Abel. Mémoire sur les equations algébriques, où l'on démontre l'impossibilité de la résolution de l'équation générale du cinquième degré. In L. Sylow and S.Editors Lie, editors, *Oeuvres Complètes de Niels Henrik Abel: Nouvelle Édition*, volume 1 of *Cambridge Library Collection - Mathematics*, pages 28–33. Cambridge University Press, 2012. doi:10.1017/CBO9781139245807.004.

[24] Ian Stewart. *Galois theory*. Chapman & Hall/CRC, Boca Raton, 2nd ed edition, 1998.

[25] David A. Cox, John B. Little, and Donal O'Shea. *Ideals, varieties, and algorithms: an introduction to computational algebraic geometry and commutative algebra*. Springer, Cham Heidelberg New York Dordrecht London, fourth edition edition, 2018.

[26] Joe Harris. Galois groups of enumerative problems. *Duke Mathematical Journal*, 46 (4):685–724, 1979. doi:10.1215/S0012-7094-79-04635-0.

[27] Robert Macarthur and Richard Levins. The limiting similarity, convergence, and divergence of coexisting species. *The American Naturalist*, 101(921):377–385, September 1967. ISSN 1537-5323. doi:10.1086/282505. URL http://dx.doi.org/10.1086/282505.

[28] Peter Chesson. General theory of competitive coexistence in spatially-varying environments. *Theoretical Population Biology*, 58(3):211–237, November 2000. ISSN 0040-5809. doi:10.1006/tpbi.2000.1486. URL http://dx.doi.org/10.1006/tpbi.2000.1486.

[29] MICHAEL E. GILPIN. Stability of feasible predator-prey systems. *Nature*, 254(5496): 137–139, March 1975. ISSN 1476-4687. doi:10.1038/254137a0. URL http://dx.doi.org/10.1038/254137a0.

[30] Lewi Stone. *Some problems of community ecology: processes, patterns and species persistence in ecosystems*. PhD thesis, Monash University, 1988.

[31] Lewi Stone. The Google matrix controls the stability of structured ecological and biological networks. *Nature Communications*, 7(1):12857, September 2016. ISSN 2041-1723. doi:10.1038/ncomms12857.

[32] Carlos A. Serván, José A. Capitán, Jacopo Grilli, Kent E. Morrison, and Stefano Allesina. Coexistence of many species in random ecosystems. *Nature Ecology & Evolution*, 2(8):1237–1242, August 2018. ISSN 2397-334X. doi:10.1038/s41559-018-0603-6.

[33] Jacopo Grilli, Matteo Adorisio, Samir Suweis, György Barabás, Jayanth R. Banavar, Stefano Allesina, and Amos Maritan. Feasibility and coexistence of large ecological communities. *Nature Communications*, 8(1):14389, February 2017. ISSN 2041-1723. doi:10.1038/ncomms14389.

[34] Robert M. May. Thresholds and breakpoints in ecosystems with a multiplicity of stable states. *Nature*, 269(5628):471–477, October 1977.

[35] Marten Scheffer, Steve Carpenter, Jonathan A. Foley, Carl Folke, and Brian Walker. Catastrophic shifts in ecosystems. *Nature*, 413(6856):591–596, October 2001.

[36] J. Jelle Lever, Egbert H. van Nes, Marten Scheffer, and Jordi Bascompte. The sudden collapse of pollinator communities. *Ecology Letters*, 17(3):350–359, 2014.

[37] Vasilis Dakos and Jordi Bascompte. Critical slowing down as early warning for the onset of collapse in mutualistic communities. *Proceedings of the National Academy of Sciences*, 111(49):17546–17551, December 2014.

[38] Helmut Hillebrand, Ian Donohue, W. Stanley Harpole, Dorothee Hodapp, Michal Kucera, Aleksandra M. Lewandowska, et al. Thresholds for ecological responses to global change do not emerge from empirical data. *Nature Ecology & Evolution*, 4(11): 1502–1509, November 2020.

[39] Sonia Kéfi, Camille Saade, Eric L. Berlow, Juliano S. Cabral, and Emanuel A. Fronhofer. Scaling up our understanding of tipping points. *Philosophical Transactions of the Royal Society B: Biological Sciences*, 377(1857):20210386, June 2022.

[40] Rudolf P. Rohr, Serguei Saavedra, and Jordi Bascompte. On the structural stability of mutualistic systems. *Science*, 345(6195):1253497, July 2014.

[41] Marten Scheffer, Stephen R. Carpenter, Timothy M. Lenton, Jordi Bascompte, William Brock, Vasilis Dakos, et al. Anticipating Critical Transitions. *Science*, 338(6105):344–348, October 2012.

[42] P Abrams. The theory of limiting similarity. *Annual Review of Ecology and Systematics*, 14(1):359–376, November 1983. ISSN 0066-4162. doi:10.1146/annurev.es.14.110183.002043. URL http://dx.doi.org/10.1146/annurev.es.14.110183.002043.

[43] P. Yodzis. The stability of real ecosystems. *Nature*, 289(5799):674–676, February 1981. ISSN 1476-4687. doi:10.1038/289674a0. URL http://dx.doi.org/10.1038/289674a0.

[44] György Barabás, Matthew J. Michalska-Smith, and Stefano Allesina. Self-regulation and the stability of large ecological networks. *Nature Ecology & Evolution*, 1(12): 1870–1875, October 2017. ISSN 2397-334X. doi:10.1038/s41559-017-0357-6. URL http://dx.doi.org/10.1038/s41559-017-0357-6.

[45] György Barabás, Rafael D'Andrea, and Simon Maccracken Stump. Chesson's coexistence theory. *Ecological Monographs*, 88(3):277–303, May 2018. ISSN 1557-7015. doi:10.1002/ecm.1302. URL http://dx.doi.org/10.1002/ecm.1302.

[46] Chuliang Song, Rudolf P. Rohr, and Serguei Saavedra. A guideline to study the feasibility domain of multi-trophic and changing ecological communities. *Journal of Theoretical Biology*, 450:30–36, August 2018. ISSN 0022-5193. doi:10.1016/j.jtbi.2018.04.030. URL http://dx.doi.org/10.1016/j.jtbi.2018.04.030.

[47] Mohammad AlAdwani and Serguei Saavedra. Feasibility conditions of ecological models: Unfolding links between model parameters. *Ecological Modelling*, 466:109900, April 2022. ISSN 0304-3800. doi:10.1016/j.ecolmodel.2022.109900.

[48] Fernando Lucas Metz, Izaak Neri, and Tim Rogers. Spectral theory of sparse non-hermitian random matrices. *Journal of Physics A: Mathematical and Theoretical*, 52 (43):434003, October 2019. ISSN 1751-8121. doi:10.1088/1751-8121/ab1ce0. URL http://dx.doi.org/10.1088/1751-8121/ab1ce0.

[49] Lyle Poley, Tobias Galla, and Joseph W. Baron. Eigenvalue spectra of finely structured random matrices. *Physical Review E*, 109(6), June 2024. ISSN 2470-0053. doi:10.1103/physreve.109.064301. URL http://dx.doi.org/10.1103/physreve.109.064301.

[50] Xiaoyuan Liu, George W. A. Constable, and Jonathan W. Pitchford. Feasibility and stability in large Lotka Volterra systems with interaction structure. *Physical Review E*, 107(5):054301, May 2023. ISSN 2470-0045, 2470-0053. doi:10.1103/PhysRevE.107.054301.

[51] Stav Marcus, Ari M. Turner, and Guy Bunin. Extinctions as a vestige of instability: The geometry of stability and feasibility. *Journal of Theoretical Biology*, 608:112141, July 2025. ISSN 0022-5193. doi:10.1016/j.jtbi.2025.112141. URL http://dx.doi.org/10.1016/j.jtbi.2025.112141.

[52] S. Smale. On the differential equations of species in competition. *Journal of Mathematical Biology*, 3(1):5–7, 1976. ISSN 1432-1416. doi:10.1007/bf00307854. URL http://dx.doi.org/10.1007/bf00307854.

[53] J A Vano, J C Wildenberg, M B Anderson, J K Noel, and J C Sprott. Chaos in low-dimensional lotka–volterra models of competition. *Nonlinearity*, 19(10):2391–2404, September 2006. ISSN 1361-6544. doi:10.1088/0951-7715/19/10/006. URL http://dx.doi.org/10.1088/0951-7715/19/10/006.

[54] Carlos A. Serván and Stefano Allesina. Tractable models of ecological assembly. *Ecology Letters*, 24(5):1029–1037, March 2021. ISSN 1461-0248. doi:10.1111/ele.13702. URL http://dx.doi.org/10.1111/ele.13702.

[55] Alfred J. Lotka. *Elements of Physical Biology*. Williams & Wilkins, Baltimore, 1925.

[56] Vito Volterra. *Leçons sur la théorie mathématique de la lutte pour la vie*. Gauthier-Villars, Paris, 1931.

[57] Johannes Alt and Torben Krüger. Local elliptic law. *Bernoulli*, 28(2), May 2022. ISSN 1350-7265. doi:10.3150/21-bej1370. URL http://dx.doi.org/10.3150/21-bej1370.

[58] Michaël Dougoud, Laura Vinckenbosch, Rudolf P. Rohr, Louis-Félix Bersier, and Christian Mazza. The feasibility of equilibria in large ecosystems: A primary but neglected concept in the complexity-stability debate. *PLOS Computational Biology*, 14(2):e1005988, February 2018. ISSN 1553-7358. doi:10.1371/journal.pcbi.1005988.

[59] Susanne Pettersson, Van M. Savage, and Martin Nilsson Jacobi. Stability of ecosystems enhanced by species-interaction constraints. *Physical Review E*, 102(6), December 2020. ISSN 2470-0053. doi:10.1103/physreve.102.062405. URL http://dx.doi.org/10.1103/physreve.102.062405.

[60] Ian D. Rozdilsky and Lewi Stone. Complexity can enhance stability in competitive systems. *Ecology Letters*, 4(5):397–400, August 2001. ISSN 1461-0248. doi:10.1046/j.1461-0248.2001.00249.x. URL http://dx.doi.org/10.1046/j.1461-0248.2001.00249.x.

[61] Robert MacArthur. Species packing and competitive equilibrium for many species. *Theoretical Population Biology*, 1(1):1–11, May 1970. ISSN 0040-5809. doi:10.1016/0040-5809(70)90039-0. URL http://dx.doi.org/10.1016/0040-5809(70)90039-0.

[62] Carlos A. Serván, José A. Capitán, Zachary R. Miller, and Stefano Allesina. Effects of phylogeny on coexistence in model communities. *The American Naturalist*, 205(2): E34–E48, February 2025. ISSN 1537-5323. doi:10.1086/733415. URL http://dx.doi.org/10.1086/733415.

[63] David Tilman. Resource competition between plankton algae: An experimental and theoretical approach. *Ecology*, 58(2):338–348, March 1977. ISSN 1939-9170. doi:10.2307/1935608. URL http://dx.doi.org/10.2307/1935608.

[64] Ray Dybzinski and David Tilman. Resource use patterns predict long-term outcomes of plant competition for nutrients and light. *The American Naturalist*, 170(3):305–318, September 2007. ISSN 1537-5323. doi:10.1086/519857. URL http://dx.doi.org/10.1086/519857.

[65] Amanda Burson, Maayke Stomp, Lisette Mekkes, and Jef Huisman. Stable coexistence of equivalent nutrient competitors through niche differentiation in the light spectrum. *Ecology*, 100(12), September 2019. ISSN 1939-9170. doi:10.1002/ecy.2873. URL http://dx.doi.org/10.1002/ecy.2873.

[66] Leonora S. Bittleston, Matti Gralka, Gabriel E. Leventhal, Itzhak Mizrahi, and Otto X. Cordero. Context-dependent dynamics lead to the assembly of functionally distinct microbial communities. *Nature Communications*, 11(1), March 2020. ISSN 2041-1723. doi:10.1038/s41467-020-15169-0. URL http://dx.doi.org/10.1038/s41467-020-15169-0.

[67] Chang-Yu Chang, Djordje Bajić, Jean C. C. Vila, Sylvie Estrela, and Alvaro Sanchez. Emergent coexistence in multispecies microbial communities. *Science*, 381(6655): 343–348, July 2023. ISSN 1095-9203. doi:10.1126/science.adg0727. URL http://dx.doi.org/10.1126/science.adg0727.

[68] Kiseok Keith Lee, Siqi Liu, Kyle Crocker, Jocelyn Wang, David R. Huggins, Mikhail Tikhonov, Madhav Mani, and Seppe Kuehn. Functional regimes define soil microbiome

response to environmental change. *Nature*, 644(8078):1028–1038, July 2025. ISSN 1476-4687. doi:10.1038/s41586-025-09264-9. URL http://dx.doi.org/10.1038/s41586-025-09264-9.

[69] Gregor F. Fussmann, Stephen P. Ellner, Kyle W. Shertzer, and Nelson G. Hairston Jr. Crossing the hopf bifurcation in a live predator-prey system. *Science*, 290(5495): 1358–1360, November 2000. ISSN 1095-9203. doi:10.1126/science.290.5495.1358. URL http://dx.doi.org/10.1126/science.290.5495.1358.

[70] Takehito Yoshida, Laura E. Jones, Stephen P. Ellner, Gregor F. Fussmann, and Nelson G. Hairston. Rapid evolution drives ecological dynamics in a predator–prey system. *Nature*, 424(6946):303–306, July 2003. ISSN 1476-4687. doi:10.1038/nature01767. URL http://dx.doi.org/10.1038/nature01767.

[71] Lutz Becks, Frank M. Hilker, Horst Malchow, Klaus Jürgens, and Hartmut Arndt. Experimental demonstration of chaos in a microbial food web. *Nature*, 435(7046): 1226–1229, June 2005. ISSN 1476-4687. doi:10.1038/nature03627. URL http://dx.doi.org/10.1038/nature03627.

[72] Lutz Becks and Hartmut Arndt. Transitions from stable equilibria to chaos, and back, in an experimental food web. *Ecology*, 89(11):3222–3226, November 2008. ISSN 1939-9170. doi:10.1890/07-1988.1. URL http://dx.doi.org/10.1890/07-1988.1.

[73] Elisa Benincà, Jef Huisman, Reinhard Heerkloss, Klaus D. Jöhnk, Pedro Branco, Egbert H. Van Nes, Marten Scheffer, and Stephen P. Ellner. Chaos in a long-term experiment with a plankton community. *Nature*, 451(7180):822–825, February 2008. ISSN 1476-4687. doi:10.1038/nature06512. URL http://dx.doi.org/10.1038/nature06512.

[74] Bernd Blasius, Lars Rudolf, Guntram Weithoff, Ursula Gaedke, and Gregor F. Fussmann. Long-term cyclic persistence in an experimental predator–prey system. *Nature*, 577(7789):226–230, December 2019. ISSN 1476-4687. doi:10.1038/s41586-019-1857-0. URL http://dx.doi.org/10.1038/s41586-019-1857-0.

[75] Jiliang Hu, Daniel R. Amor, Matthieu Barbier, Guy Bunin, and Jeff Gore. Emergent phases of ecological diversity and dynamics mapped in microcosms. *Science*, 378(6615): 85–89, October 2022. ISSN 1095-9203. doi:10.1126/science.abm7841. URL http://dx.doi.org/10.1126/science.abm7841.

[76] Matthieu Barbier. Fingerprints of High-Dimensional Coexistence in Complex Ecosystems. *Physical Review X*, 11(1), 2021. doi:10.1103/PhysRevX.11.011009.

[77] Pablo Lechón-Alonso, Srilena Kundu, Paula Lemos-Costa, José A. Capitán, and Stefano Allesina. Robust coexistence in competitive ecological communities. *Nature Communications*, 17(1):2637, February 2026. ISSN 2041-1723. doi:10.1038/s41467-026-69151-3.

[78] Stuart Nattrass, Stephen Baigent, and David J. Murrell. Quantifying the Likelihood of Co-existence for Communities with Asymmetric Competition. *Bulletin of Mathematical Biology*, 74(10):2315–2338, October 2012. ISSN 1522-9602. doi:10.1007/s11538-012-9755-8.

[79] Serguei Saavedra, Rudolf P. Rohr, Jordi Bascompte, Oscar Godoy, Nathan J. B. Kraft, and Jonathan M. Levine. A structural approach for understanding multispecies coexistence. *Ecological Monographs*, 87(3):470–486, August 2017. ISSN 0012-9615, 1557-7015. doi:10.1002/ecm.1263.

[80] Chuliang Song and Serguei Saavedra. Will a small randomly assembled community be feasible and stable? *Ecology*, 99(3):743–751, 2018. ISSN 1939-9170. doi:10.1002/ecy.2125.

[81] Matteo Detto, Jonathan M. Levine, and Stephen W. Pacala. Maintenance of high diversity in mechanistic forest dynamics models of competition for light. *Ecological Monographs*, 92(2):e1500, 2022. ISSN 1557-7015. doi:10.1002/ecm.1500.

[82] Andrea Aparicio, Tong Wang, Serguei Saavedra, and Yang-Yu Liu. Feasibility in MacArthur's consumer-resource model. *Theoretical Ecology*, 16(3):225–238, September 2023. ISSN 1874-1746. doi:10.1007/s12080-023-00566-0.

[83] Pablo Lechón-Alonso, Zachary R. Miller, Armun Liaghat, Paul Breiding, Mercedes Pascual, and Stefano Allesina. Tipping points are typical in ecosystems with higher-order interactions, April 2026.

[84] Brent J. Danielson. Communities in a Landscape: The Influence of Habitat Heterogeneity on the Interactions between Species. *The American Naturalist*, 138(5):1105–1120, 1991. ISSN 0003-0147.

[85] Larry B. Crowder and William E. Cooper. Habitat Structural Complexity and the Interaction Between Bluegills and Their Prey. *Ecology*, 63(6):1802–1813, 1982. ISSN 0012-9658. doi:10.2307/1940122.

[86] Iacopo Iacopini, Jennifer R. Foote, Nina H. Fefferman, Elizabeth P. Derryberry, and Matthew J. Silk. Not your private tête-à-tête: Leveraging the power of higher-order networks to study animal communication. *Philosophical Transactions of the Royal Society B: Biological Sciences*, 379(1905):20230190, July 2024. ISSN 0962-8436, 1471-2970. doi:10.1098/rstb.2023.0190.

[87] Henry M. Wilbur. Competition, Predation, and the Structure of the Ambystoma-Rana Sylvatica Community. *Ecology*, 53(1):3–21, 1972. ISSN 0012-9658. doi:10.2307/1935707.

[88] Andrew P. Beckerman, Maria Uriarte, and Oswald J. Schmitz. Experimental evidence for a behavior-mediated trophic cascade in a terrestrial food chain. *Proceedings of the National Academy of Sciences*, 94(20):10735–10738, September 1997. doi:10.1073/pnas.94.20.10735.

[89] Scott D. Peacor and Earl E. Werner. The contribution of trait-mediated indirect effects to the net effects of a predator. *Proceedings of the National Academy of Sciences*, 98 (7):3904–3908, March 2001. doi:10.1073/pnas.071061998.

[90] Geoffrey C. Trussell, Patrick J. Ewanchuk, and Mark D. Bertness. Field evidence of trait-mediated indirect interactions in a rocky intertidal food web. *Ecology Letters*, 5 (2):241–245, 2002. ISSN 1461-0248. doi:10.1046/j.1461-0248.2002.00304.x.

[91] Harry Mickalide and Seppe Kuehn. Higher-Order Interaction between Species Inhibits Bacterial Invasion of a Phototroph-Predator Microbial Community. *Cell Systems*, 9 (6):521–533.e10, December 2019. ISSN 2405-4712. doi:10.1016/j.cels.2019.11.004.

[92] Eric D. Kelsic, Jeffrey Zhao, Kalin Vetsigian, and Roy Kishony. Counteraction of antibiotic production and degradation stabilizes microbial communities. *Nature*, 521 (7553):516–519, May 2015. ISSN 1476-4687. doi:10.1038/nature14485.

[93] Hao Ran Lai, Kwek Yan Chong, Alex Thiam Koon Yee, Margaret M. Mayfield, and Daniel B. Stouffer. Non-additive biotic interactions improve predictions of tropical tree growth and impact community size structure. *Ecology*, 103(2):e03588, 2022. ISSN 1939-9170. doi:10.1002/ecy.3588.

[94] William J. Grenney, David A. Bella, and Herbert C. Curl. A Theoretical Approach to Interspecific Competition in Phytoplankton Communities. *The American Naturalist*, 107(955):405–425, 1973. ISSN 0003-0147.

[95] Kalin Vetsigian. Diverse modes of eco-evolutionary dynamics in communities of antibiotic-producing microorganisms. *Nature Ecology & Evolution*, 1(7):1–9, June 2017. ISSN 2397-334X. doi:10.1038/s41559-017-0189.

[96] Theo L. Gibbs, Zachary J. Gold, Haylee Oyler, Jonathan M. Levine, and Nathan J. B. Kraft. Spatial clustering modifies competition in a diverse annual plant community. *Proceedings of the National Academy of Sciences*, 123(3):e2516084123, January 2026. ISSN 0027-8424, 1091-6490. doi:10.1073/pnas.2516084123.

[97] William E. Neill. The Community Matrix and Interdependence of the Competition Coefficients. *The American Naturalist*, 108(962):399–408, 1974. ISSN 0003-0147.

[98] John Vandermeer. A Further Note on Community Models. *The American Naturalist*, 117(3):379–380, March 1981. ISSN 0003-0147, 1537-5323. doi:10.1086/283716.

[99] Mark J. Pomerantz. Do "Higher Order Interactions" in Competition Systems Really Exist? *The American Naturalist*, 117(4):583–591, 1981. ISSN 0003-0147.

[100] Wade B. Worthen and Jennifer L. Moore. Higher-Order Interactions and Indirect Effects: A Resolution Using Laboratory Drosophila Communities. *The American Naturalist*, 138(5):1092–1104, 1991. ISSN 0003-0147.

[101] Erik T. Aschehoug and Ragan M. Callaway. Diversity Increases Indirect Interactions, Attenuates the Intensity of Competition, and Promotes Coexistence. *The American Naturalist*, 186(4):452–459, October 2015. ISSN 0003-0147. doi:10.1086/682901.

[102] Margaret M. Mayfield and Daniel B. Stouffer. Higher-order interactions capture unexplained complexity in diverse communities. *Nature Ecology & Evolution*, 1(3):1–7, February 2017. ISSN 2397-334X. doi:10.1038/s41559-016-0062.

[103] Babak Momeni, Li Xie, and Wenying Shou. Lotka-Volterra pairwise modeling fails to capture diverse pairwise microbial interactions. *eLife*, 6:e25051, March 2017. ISSN 2050-084X. doi:10.7554/eLife.25051.

[104] J. Christopher D. Terry, Rebecca J. Morris, and Michael B. Bonsall. Interaction modifications lead to greater robustness than pairwise non-trophic effects in food webs. *Journal of Animal Ecology*, 88(11):1732–1742, 2019. ISSN 1365-2656. doi:10.1111/1365-2656.13057.

[105] Alicia Sanchez-Gorostiaga, Djordje Bajić, Melisa L. Osborne, Juan F. Poyatos, and Alvaro Sanchez. High-order interactions distort the functional landscape of microbial consortia. *PLOS Biology*, 17(12):e3000550, December 2019. ISSN 1545-7885. doi:10.1371/journal.pbio.3000550.

[106] Deepika Sundarraman, Edouard A. Hay, Dylan M. Martins, Drew S. Shields, Noah L. Pettinari, and Raghuveer Parthasarathy. Higher-Order Interactions Dampen Pairwise Competition in the Zebrafish Gut Microbiome. *mBio*, 11(5):10.1128/mbio.01667–20, October 2020. doi:10.1128/mbio.01667-20.

[107] Junli Xiao, Yuanzhi Li, Chengjin Chu, Youshi Wang, Scott J. Meiners, and Daniel B. Stouffer. Higher-order interactions mitigate direct negative effects on population dynamics of herbaceous plants during succession. *Environmental Research Letters*, 15(7): 074023, June 2020. ISSN 1748-9326. doi:10.1088/1748-9326/ab8a88.

[108] Yuanzhi Li, Margaret M Mayfield, Bin Wang, Junli Xiao, Kamil Kral, David Janik, Jan Holik, and Chengjin Chu. Beyond direct neighbourhood effects: Higher-order interactions improve modelling and predicting tree survival and growth. *National Science Review*, 8(5):nwaa244, May 2021. ISSN 2095-5138. doi:10.1093/nsr/nwaa244.

[109] Milton Barbosa, Geraldo Wilson Fernandes, and Rebecca Jane Morris. Experimental evidence for a hidden network of higher-order interactions in a diverse arthropod community. *Current Biology*, 33(2):381–388.e4, January 2023. ISSN 0960-9822. doi:10.1016/j.cub.2022.11.057.

[110] Jeremy W. Fox. The existence and strength of higher order interactions is sensitive to environmental context. *Ecology*, n/a(n/a):e4156, 2023. ISSN 1939-9170. doi:10.1002/ecy.4156.

[111] Eyal Bairey, Eric D. Kelsic, and Roy Kishony. High-order species interactions shape ecosystem diversity. *Nature Communications*, 7(1):12285, August 2016. ISSN 2041-1723. doi:10.1038/ncomms12285.

[112] Jacopo Grilli, György Barabás, Matthew J. Michalska-Smith, and Stefano Allesina. Higher-order interactions stabilize dynamics in competitive network models. *Nature*, 548(7666):210–213, August 2017. ISSN 0028-0836, 1476-4687. doi:10.1038/nature23273.

[113] Mohammad AlAdwani and Serguei Saavedra. Is the addition of higher-order interactions in ecological models increasing the understanding of ecological dynamics? *Mathematical Biosciences*, 315:108222, September 2019. ISSN 0025-5564. doi:10.1016/j.mbs.2019.108222.

[114] Mohammad AlAdwani and Serguei Saavedra. Ecological models: Higher complexity in, higher feasibility out. *Journal of The Royal Society Interface*, 17(172):20200607, November 2020. doi:10.1098/rsif.2020.0607.

[115] Theo Gibbs, Simon A. Levin, and Jonathan M. Levine. Coexistence in diverse communities with higher-order interactions. *Proceedings of the National Academy of Sciences*, 119(43):e2205063119, October 2022. doi:10.1073/pnas.2205063119.

[116] Violeta Calleja-Solanas, Santiago Lamata-Otín, Carlos Gómez-Ambrosi, Jesús Gómez-Gardeñes, and Sandro Meloni. Higher-order interactions in ecology can be hidden in plain sight, May 2026.

[117] Manh Hong Duong and The Anh Han. Random evolutionary games and random polynomials. *Proceedings of the Royal Society A: Mathematical, Physical and Engineering Sciences*, 481(2319):20240911, August 2025. doi:10.1098/rspa.2024.0911.

[118] Federico Dalmao. Asymptotic variance and CLT for the number of zeros of Kostlan Shub Smale random polynomials. *Comptes Rendus Mathematique*, 353(12):1141–1145, December 2015. doi:10.1016/j.crma.2015.09.016.

[119] Chaitanya S. Gokhale and Arne Traulsen. Higher-order equivalence of Lotka-Volterra and replicator dynamics, April 2025.

[120] Stefano Allesina. Global stability of ecological and evolutionary dynamics via equivalence. *Proceedings of the National Academy of Sciences*, 123(13):e2534915123, March 2026. doi:10.1073/pnas.2534915123.

[121] Türkü Özlüm Çelik, Vincenzo Antonio Isoldi, Irem Portakal, and Giulio Zucal. Stable Coexistence in Ecologies and Games, September 2026.

[122] Andrew McLennan. The Expected Number of Nash Equilibria of a Normal Form Game. *Econometrica*, 73(1):141–174, January 2005. ISSN 0012-9682, 1468-0262. doi:10.1111/j.1468-0262.2005.00567.x.

[123] Andrew McLennan and Johannes Berg. Asymptotic expected number of Nash equilibria of two-player normal form games. *Games and Economic Behavior*, 51(2):264–295, May 2005. ISSN 0899-8256. doi:10.1016/j.geb.2004.10.008.

[124] The Anh Han, Arne Traulsen, and Chaitanya S. Gokhale. On equilibrium properties of evolutionary multi-player games with random payoff matrices. *Theoretical Population Biology*, 81(4):264–272, June 2012. ISSN 0040-5809. doi:10.1016/j.tpb.2012.02.004.

[125] Paul Breiding and Sascha Timme. HomotopyContinuation.jl: A Package for Homotopy Continuation in Julia. In James H. Davenport, Manuel Kauers, George Labahn, and Josef Urban, editors, *Mathematical Software – ICMS 2018*, pages 458–465, Cham, 2018. Springer International Publishing. ISBN 978-3-319-96418-8. doi:10.1007/978-3-319-96418-8_54.

[126] Chaitanya S. Gokhale and Arne Traulsen. Evolutionary games in the multiverse. *Proceedings of the National Academy of Sciences*, 107(12):5500–5504, March 2010. ISSN 0027-8424, 1091-6490. doi:10.1073/pnas.0912214107.

[127] R.W. Newcomb. Nonlinear differential systems: A canonic, multivariable theory. *Proceedings of the IEEE*, 65(6):930–935, 1977. ISSN 0018-9219. doi:10.1109/PROC.1977.10590.

[128] Oscar Godoy, Ignasi Bartomeus, Rudolf P. Rohr, and Serguei Saavedra. Towards the Integration of Niche and Network Theories. *Trends in Ecology & Evolution*, 33(4): 287–300, April 2018.

[129] Simone Cenci and Serguei Saavedra. Structural stability of nonlinear population dynamics. *Physical Review E*, 97(1):012401, January 2018.

[130] Zachary R. Miller and Stefano Allesina. Metapopulations with habitat modification. *Proceedings of the National Academy of Sciences*, 118(49):e2109896118, December 2021.

[131] Hsun-Yi Hsieh, John Vandermeer, and Ivette Perfecto. Surprising effects of cascading higher order interactions. *Scientific Reports*, 12(1):19378, November 2022.

[132] Yuanzhi Li, Junli Xiao, Yuan Jiang, Stuart Joseph Wright, Margaret M. Mayfield, Oscar Godoy, et al. Higher-order interactions enhance the latitudinal tree diversity gradient. *Nature*, pages 1–6, April 2026.

[133] Max Rietkerk, Stefan C. Dekker, Peter C. de Ruiter, and Johan van de Koppel. Self-Organized Patchiness and Catastrophic Shifts in Ecosystems. *Science*, 305(5692):1926–1929, September 2004.

[134] Marten Scheffer, Stephen R. Carpenter, Vasilis Dakos, and Egbert H. van Nes. Generic Indicators of Ecological Resilience: Inferring the Chance of a Critical Transition. *Annual Review of Ecology, Evolution, and Systematics*, 46(Volume 46, 2015):145–167, December 2015.

[135] Pablo Moreno-Spiegelberg, Max Rietkerk, and Damià Gomila. How spatiotemporal dynamics can enhance ecosystem resilience. *Proceedings of the National Academy of Sciences*, 122(11):e2412522122, March 2025.

[136] Peter J. Mumby, Alan Hastings, and Helen J. Edwards. Thresholds and the resilience of Caribbean coral reefs. *Nature*, 450(7166):98–101, November 2007.

[137] Junjie Jiang, Zi-Gang Huang, Thomas P. Seager, Wei Lin, Celso Grebogi, Alan Hastings, et al. Predicting tipping points in mutualistic networks through dimension reduction. *Proceedings of the National Academy of Sciences*, 115(4):E639–E647, January 2018.

[138] Vadim A. Karatayev, Marissa L. Baskett, and Egbert H. van Nes. The Potential for Alternative Stable States in Food Webs Depends on Feedback Mechanism and Trait Diversity. *The American Naturalist*, 202(3):260–275, September 2023.

[139] Jordi Bascompte and Marten Scheffer. The Resilience of Plant–Pollinator Networks. *Annual Review of Entomology*, 68(Volume 68, 2023):363–380, January 2023.

[140] J. Jelle Lever, Ingrid A. van de Leemput, Els Weinans, Rick Quax, Vasilis Dakos, Egbert H. van Nes, et al. Foreseeing the future of mutualistic communities beyond collapse. *Ecology Letters*, 23(1):2–15, 2020.

[141] Marc Duran-Sala, Sandro Meloni, and Violeta Calleja-Solanas. Towards a less spherical cow: Species differences dilute the stabilizing effect of higher-order interactions, October 2025.

[142] Paul Breiding, Bernd Sturmfels, and Sascha Timme. 3264 Conics in a Second, 2019.

[143] B. S. Goh. Global stability in many-species systems. *The American Naturalist*, 111 (977):135–143, January 1977. ISSN 1537-5323. doi:10.1086/283144. URL http://dx.doi.org/10.1086/283144.

[144] Michael P. Mustri, Quqiming Duan, and Samraat Pawar. Accuracy of the Lotka-Volterra model fails in strongly coupled microbial consumer-resource systems. *PLOS Computational Biology*, 21(12):e1013719, December 2025.

[145] Theo L. Gibbs, Gabriel Gellner, Simon A. Levin, Kevin S. McCann, Alan Hastings, and Jonathan M. Levine. When can higher-order interactions produce stable coexistence? *Ecology Letters*, 27(6):e14458, 2024.

[146] Akihiko Mougi. Ecosystem engineering and food web stability. *Scientific Reports*, 14 (1):19400, August 2024.

[147] Guim Aguadé-Gorgorió, Jean-François Arnoldi, Matthieu Barbier, and Sonia Kéfi. A taxonomy of multiple stable states in complex ecological communities. *Ecology Letters*, 27(4):e14413, 2024.

[148] Daniel B. Stouffer and Jordi Bascompte. Understanding food-web persistence from local to global scales. *Ecology Letters*, 13(2):154–161, 2010.

[149] Tong Wang, Ashish B. George, and Sergei Maslov. Higher-order interactions in auxotroph communities enhance their resilience to resource fluctuations. *Cell Systems*, 17 (3), March 2026.

[150] J. Jelle Lever, Egbert H. Van Nes, Marten Scheffer, and Jordi Bascompte. Five fundamental ways in which complex food webs may spiral out of control. *Ecology Letters*, 26(10):1765–1779, 2023.

[151] Yuguang Yang, György Barabás, Serguei Saavedra, and Aming Li. Catalysts and inhibitors of critical transitions in ecological systems. *Proceedings of the National Academy of Sciences*, 123(2):e2516856122, January 2026.

[152] Federico Battiston, Enrico Amico, Alain Barrat, Ginestra Bianconi, Guilherme Ferraz de Arruda, Benedetta Franceschiello, et al. The physics of higher-order interactions in complex systems. *Nature Physics*, 17(10):1093–1098, October 2021.

[153] Guilherme Ferraz de Arruda, Alberto Aleta, and Yamir Moreno. Contagion dynamics on higher-order networks. *Nature Reviews Physics*, 6(8):468–482, August 2024.

[154] Iacopo Iacopini, Giovanni Petri, Alain Barrat, and Vito Latora. Simplicial models of social contagion. *Nature Communications*, 10(1):2485, June 2019.

[155] Ana P. Millán, Joaquín J. Torres, and Ginestra Bianconi. Explosive Higher-Order Kuramoto Dynamics on Simplicial Complexes. *Physical Review Letters*, 124(21):218301, May 2020.

[156] Leonie Neuhäuser, Andrew Mellor, and Renaud Lambiotte. Multibody interactions and nonlinear consensus dynamics on networked systems. *Physical Review E*, 101(3): 032310, March 2020.

[157] Mateusz Michałek and Bernd Sturmfels. *Invitation to Nonlinear Algebra*, volume 211. American Mathematical Soc., 2021.

[158] Daniel R. Grayson and Michael E. Stillman. Macaulay2, a software system for research in algebraic geometry. Available at http://www2.macaulay2.com.

[159] Paul Breiding, John Cobb, Aviva K. Englander, Nayda Farnsworth, Jonathan D. Hauenstein, Oskar Henriksson, et al. Elimination Without Eliminating: Computing Complements of Real Hypersurfaces Using Pseudo-Witness Sets, January 2026.

[160] Longquan Yong. Nonlinear Complementarity Problem and Solution Methods. In Fu Lee Wang, Hepu Deng, Yang Gao, and Jingsheng Lei, editors, *Artificial Intelligence and Computational Intelligence*, volume 6319, pages 461–469. Springer Berlin Heidelberg, Berlin, Heidelberg, 2010.

[161] Josef Hofbauer and Sebastian J. Schreiber. Permanence via invasion graphs: incorporating community assembly into modern coexistence theory. *Journal of Mathematical Biology*, 85(5), October 2022. ISSN 1432-1416. doi:10.1007/s00285-022-01815-2. URL http://dx.doi.org/10.1007/s00285-022-01815-2.

[162] Guy Bunin. Ecological communities with lotka-volterra dynamics. *Physical Review E*, 95(4), April 2017. ISSN 2470-0053. doi:10.1103/physreve.95.042414. URL http://dx.doi.org/10.1103/physreve.95.042414.

[163] Pablo Lechón-Alonso, Tom Clegg, Jacob Cook, Thomas P. Smith, and Samraat Pawar. The role of competition versus cooperation in microbial community coalescence. *PLOS Computational Biology*, 17(11):e1009584, November 2021. ISSN 1553-7358. doi:10.1371/journal.pcbi.1009584.

[164] Robert Marsland, III, Wenping Cui, Joshua Goldford, Alvaro Sanchez, Kirill Korolev, and Pankaj Mehta. Available energy fluxes drive a transition in the diversity, stability, and functional structure of microbial communities. *PLOS Computational Biology*, 15 (2):e1006793, February 2019. ISSN 1553-7358. doi:10.1371/journal.pcbi.1006793.

[165] Joshua E. Goldford, Nanxi Lu, Djordje Bajić, Sylvie Estrela, Mikhail Tikhonov, Alicia Sanchez-Gorostiaga, Daniel Segrè, Pankaj Mehta, and Alvaro Sanchez. Emergent simplicity in microbial community assembly. *Science*, 361(6401):469–474, August 2018. doi:10.1126/science.aat1168.

[166] Tim A. Hoek, Kevin Axelrod, Tommaso Biancalani, Eugene A. Yurtsev, Jinghui Liu, and Jeff Gore. Resource Availability Modulates the Cooperative and Competitive Nature of a Microbial Cross-Feeding Mutualism. *PLOS Biology*, 14(8):e1002540, August 2016. ISSN 1545-7885. doi:10.1371/journal.pbio.1002540.

[167] Tom Clegg and Thilo Gross. Cross-feeding creates tipping points in microbiome diversity. *Proceedings of the National Academy of Sciences*, 122(19):e2425603122, May 2025. doi:10.1073/pnas.2425603122.

[168] Theo Gibbs, Yifan Zhang, Zachary R. Miller, and James P. O'Dwyer. Stability criteria for the consumption and exchange of essential resources. *PLOS Computational Biology*, 18(9):e1010521, September 2022. ISSN 1553-7358. doi:10.1371/journal.pcbi.1010521.

[169] John H. Vandermeer and Douglas H. Boucher. Varieties of mutualistic interaction in population models. *Journal of Theoretical Biology*, 74(4):549–558, October 1978. ISSN 0022-5193. doi:10.1016/0022-5193(78)90241-2.

[170] Stefan Vet, Lendert Gelens, and Didier Gonze. Mutualistic cross-feeding in microbial systems generates bistability via an Allee effect. *Scientific Reports*, 10(1):7763, May 2020. ISSN 2045-2322. doi:10.1038/s41598-020-63772-4.

[171] Ted J. Case and Richard G. Casten. Global stability and multiple domains of attraction in ecological systems. *The American Naturalist*, 113(5):705–714, 1979. ISSN 0003-0147.

[172] Thomas Louis-Sarrola and Valentina Ros. Fragile vs robust multiple equilibria phases in generalized Lotka-Volterra model with non-reciprocal interactions, February 2026.

[173] Valentina Ros, Felix Roy, Giulio Biroli, Guy Bunin, and Ari M. Turner. Generalized Lotka-Volterra equations with random, nonreciprocal interactions: The typical number of equilibria. *Physical Review Letters*, 130(25):257401, June 2023. doi:10.1103/PhysRevLett.130.257401.

[174] Giulio Biroli, Guy Bunin, and Chiara Cammarota. Marginally stable equilibria in critical ecosystems. *New Journal of Physics*, 20(8):083051, August 2018. ISSN 1367-2630. doi:10.1088/1367-2630/aada58.

[175] Marco Zenari, Francesco Ferraro, Sandro Azaele, Amos Maritan, and Samir Suweis. Generalized Lotka-Volterra systems with quenched random interactions and saturating nonlinear response. *Physical Review E*, 113(2):024206, February 2026. doi:10.1103/hyxm-vxgy.

[176] Nirbhay Patil and Ada Altieri. The role of nestedness and saturating feedback in bipartite ecological systems, September 2026.

[177] W. E. Arnoldi. The principle of minimized iterations in the solution of the matrix eigenvalue problem. *Quarterly of Applied Mathematics*, 9(1):17–29, April 1951. ISSN 0033-569X. doi:10.1090/qam/42792. URL http://dx.doi.org/10.1090/qam/42792.

[178] Hoi H. Nguyen and Sean O'Rourke. The elliptic law. *International Mathematics Research Notices*, 2015(17):7620–7689, October 2014. ISSN 1687-0247. doi:10.1093/imrn/rnu174. URL http://dx.doi.org/10.1093/imrn/rnu174.

[179] Sean O'Rourke and David Renfrew. Low rank perturbations of large elliptic random matrices. *Electronic Journal of Probability*, 19(none), January 2014. ISSN 1083-6489. doi:10.1214/ejp.v19-3057. URL http://dx.doi.org/10.1214/ejp.v19-3057.

[180] Peter Hall. On the rate of convergence of normal extremes. *Journal of Applied Probability*, 16(2):433–439, June 1979. ISSN 1475-6072. doi:10.2307/3212912. URL http://dx.doi.org/10.2307/3212912.

[181] Alan Genz and Koon-Shing Kwong. Numerical evaluation of singular multivariate normal distributions. *Journal of Statistical Computation and Simulation*, 68(1):1–21, 2000.

[182] LÁSZLÓ ERDŐS, TORBEN KRÜGER, and DOMINIK SCHRÖDER. Random matrices with slow correlation decay. *Forum of Mathematics, Sigma*, 7, 2019. ISSN 2050-5094. doi:10.1017/fms.2019.2. URL http://dx.doi.org/10.1017/fms.2019.2.

[183] Oskari Ajanki, László Erdős, and Torben Krüger. Quadratic vector equations on complex upper half-plane. *Memoirs of the American Mathematical Society*, 261(1261), November 2019. ISSN 0065-9266. doi:10.1090/memo/1261. URL http://dx.doi.org/10.1090/memo/1261.

[184] F Roy, G Biroli, G Bunin, and C Cammarota. Numerical implementation of dynamical mean field theory for disordered systems: application to the lotka–volterra model of ecosystems. *Journal of Physics A: Mathematical and Theoretical*, 52(48):484001, November 2019. ISSN 1751-8121. doi:10.1088/1751-8121/ab1f32. URL http://dx.doi.org/10.1088/1751-8121/ab1f32.

[185] D. Armentano, J.-M. Azaïs, F. Dalmao, and J. León. Asymptotic variance of the number of real roots of random polynomial systems. *Proceedings of the American Mathematical Society*, 146(12):5437–5449, September 2018. doi:10.1090/proc/14215.

[186] Michael Shub and Steve Smale. Complexity of Bézout's theorem. I. Geometric aspects. *Journal of the American Mathematical Society*, 6(2):459–501, 1993. doi:10.1090/s0894-0347-1993-1175980-4.

[187] Mario Wschebor. On the Kostlan–Shub–Smale model for random polynomial systems. Variance of the number of roots. *Journal of Complexity*, 21(6):773–789, December 2005. doi:10.1016/j.jco.2005.05.005.

[188] J. Maurice Rojas. On the Average Number of Real Roots of Certain Random Sparse Polynomial Systems. *Lectures in Applied Mathematics-American Mathematical Society*, 32:689–700, 1996.

[189] Ralph Howard. The kinematic formula in Riemannian homogeneous spaces. *Memoirs of the American Mathematical Society*, 106(509), 1993. ISSN 1947-6221, 0065-9266. doi:10.1090/memo/0509.

[190] Peter Bürgisser and Antonio Lerario. Probabilistic Schubert Calculus, December 2016.

[191] Yan V. Fyodorov, Antonio Lerario, and Erik Lundberg. On the number of connected components of random algebraic hypersurfaces. *Journal of Geometry and Physics*, 95: 1–20, September 2015. ISSN 03930440. doi:10.1016/j.geomphys.2015.04.006.

[192] Léo Mathis. Real Gaussian exponential sums via a real moment map, April 2025.

[193] C. S. Holling. The Components of Predation as Revealed by a Study of Small-Mammal Predation of the European Pine Sawfly. *The Canadian Entomologist*, 91(5):293–320, May 1959.

[194] Richard J. Williams and Neo D. Martinez. Simple rules yield complex food webs. *Nature*, 404(6774):180–183, March 2000.

[195] M. R. Leadbetter. Extremes and local dependence in stationary sequences. *Zeitschrift für Wahrscheinlichkeitstheorie und Verwandte Gebiete*, 65(2):291–306, December 1983.